

**Design, synthesis, and biological evaluation
of PqsR antagonists guided by classic hit-to-
lead optimisation process and fragment-
based methods for the treatment of
Pseudomonas aeruginosa infections**

Thesis submitted to the University of Nottingham

for the degree of Doctor of Philosophy

2021

Rui Ling Liu

Faculty of Science, School of Pharmacy

Acknowledgment

Firstly, I would like to express my special gratitude to my parents, Xianquan Liu and Ping Li, who have been very generous and supportive.

Next, I would like to express my utmost gratitude to my supervisors. Firstly, Dr. Michael Stocks who is a very kind, super sweet and of course very intelligent person. He has been incredibly supportive, and it has been a great honour and privilege to be supervised by him. Dr. Shailesh Mistry, who is not only full of knowledge but also genuinely a very kind and sweet person. Dr. Shailesh Mistry has been very supportive throughout my PhD and I could never thank him enough.

I would like to thank Dr. Sarah Mistry who is a very sweet and nice person and helped me to build the very first column in my life. She has the most standard and strict experimental protocols, which I have been secretly using them ever since. I would like to thank Dr. Christophe Fromont for his very kind help on the LCMS and Dr. Nicholas Kindon for his helpful chemistry advices. I would like to thank Dr. Divneet Kaur for her precious friendship and Dr. Weng Chan for his delightful conversations. I would like to thank Dr. Miguel Camara for his insightful suggestions and Dr. Jonas Emsley for his generous support. I would also like to thank Professor Chunhao Yang for his inspiring suggestions and Professor Zaiyou Tan for his generous support.

I would like to thank William Richard for his very generous help on ITC, TSA, and X-ray crystallography experiments. I have learned a lot of knowledge from him and it has been a great and successful collaboration.

I would like to thank our C30 members for their very delightful support and it was my pleasure to be friend with all of them. I would like to thank Jack Ayre and Scott

Grossman for their very kind and nice support, and it has been very delightful 4 years. I would like to thank Eleonora Comeo who is the most warm-hearted person I have ever seen and Dr. Aimie Garces who I built special friendship with during this Pandemic. Of course, I would like to thank Alaa Mashabi, Bianca Casella, Matthew Allison, Dr. Fadi Soukarieh and Anas buzrieda for their very kind support.

I would like to thank all my incredible chinses friends who have been very kind and supportive. I would like to thank Lei Yang who has been very patient and supportive during the painful thesis writing period. I would like to thank Wanshan Feng, Chaolong Qin, Tachi Su, Lili Sheng, Chen Liu for their precious friendship and my PhD life would be so different without them.

Abstract

Pseudomonas aeruginosa (*P. aeruginosa*) a nosocomial pathogen, has become a serious public health threat due to its high mortality rates and serious antibiotic resistance issue.^{1,2,3,4} The *Pseudomonas* quinolone signal (*pqs*) system of *P. aeruginosa* is essential in regulating the biosynthesis of virulence factors.⁵⁻⁹ The transcriptional regulator of *pqs* system PqsR has been regarded as an interesting research topic for the treatment of *P. aeruginosa* infections.^{10,11,12} This thesis is focused on using multiple hit-to-lead optimization methods to find novel PqsR antagonists to overcome *P. aeruginosa* infections.

Chapter 1 provides background information about *P. aeruginosa* pathogenicity, the *pqs* system and current progress towards finding PqsR antagonists. An overview of fragment-based lead discovery (FBLD) including hit identification, fragment library construction, biophysical methods and hit-to-lead evolution methods is also provided.

Chapter 2 describes a classic hit-to-lead optimisation process starting from the virtual screening of an in-house compound library against PqsR protein to obtain **19**. Compound **19** displayed good hit likeness and was subjected to hit-to-lead optimization to achieve a potent drug sized PqsR antagonist **69** with IC₅₀ values of 0.25 μ M and 0.34 μ M in PAO1-LmCTX::*PpqsA-lux* and PA14mCTX::*PpqsA-lux* reporter assays respectively (**Figure 1**). The X-ray crystal structure of the **69**-PqsR LBD complex was also obtained, which provides insights into specific ligand-target interactions.

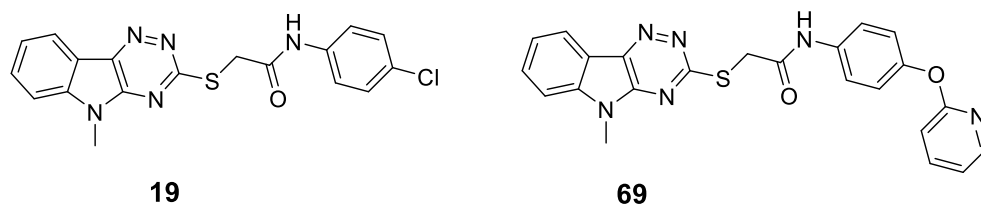


Figure 1. The structures of compounds **19** and **69**.

Chapter 3 focuses on fragment-based methods in the discovery of PqsR antagonists. Assisted by *in silico* methods, five fragment libraries were screened against PqsR protein and the high scoring fragments were subjected to a thermal shift assay (TSA) to give fragment hits **106**, **107**. Through hit exploration study, fragments **106**, **107** were optimised and led to the identification of fragments **145a**, **145c** and **146b** displaying improved biophysical profiles and these fragments can act as good starting points for the identification drug-sized PqsR antagonists ($350 < \text{MWt} < 500$).

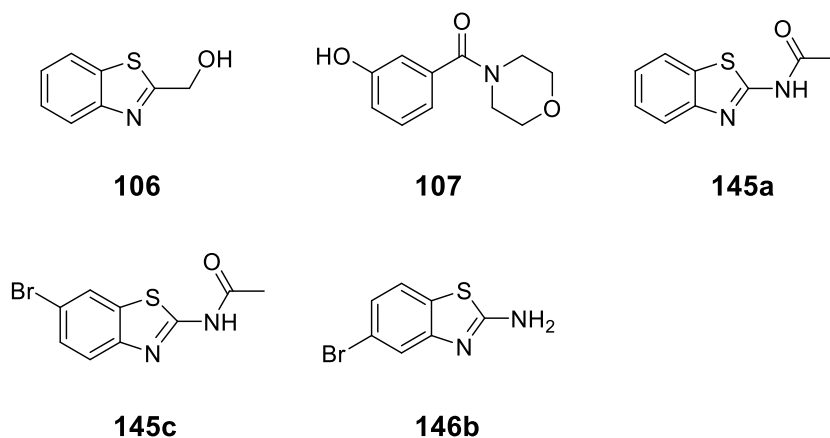


Figure 2. Structures of **106**, **107**, **145a**, **145c**, **146b**.

Chapter 4 demonstrates the evolution of fragment hits **106**, **149**, **145a**, **145c** and **146b** to drug-sized molecules through fragment linking, merging, and growing methods. Applying a fragment growing method on **106** led to the discovery of **148b** and **148c** displaying *pqs* inhibition observed as remaining activity (RA%) values of 60% and 63%

at 50 μM screening concentration in PAO1-LmCTX::*PpqsA-lux* reporter assays, respectively. Linking fragment **146b** and **152a** led to the discovery of compound **154b** showing a RA% value of 34% at 10 μM screening concentration (**Figure 3**). It was hypothesized that two fragments bound to the PqsR LBD in different sub-pockets can functionalize as synergistic combinations observed as the fragment cocktails displaying a greater effect in bioreporter assay and biophysical experiments than the single fragments. A synergistic exploration experiment was designed assisted by TSA and mCTX::*PpqsA-lux* based bioreporter assay and led to the identification of two pairs of synergistic combinations (**81** and **108**, **81** and **105**) showing improved *in vitro* or biophysical profiles in combination than in single fragments.

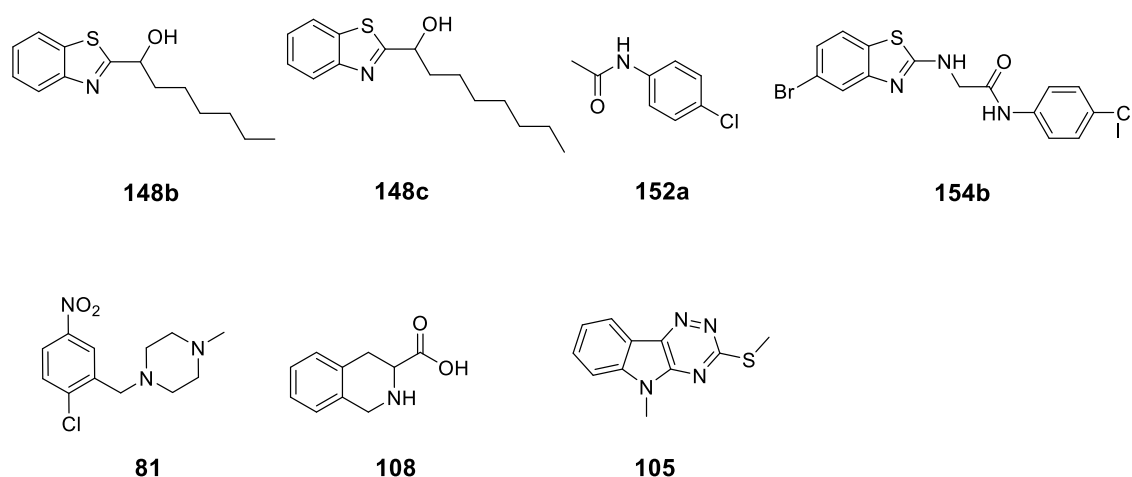


Figure 3. Ligand scaffold for **148b**, **148c**, **152a**, **154b**, **81**, **108**, and **105**.

List of abbreviation

Als	Autoinducers
CDC	Centre of Disease Control and Prevention
C4HSL	Butanoyl homoserine lactone
cLogP	Calculated partition coefficient
DCM	dichloromethane
DMAP	4-(dimethylamino)pyridine
DSF	Differential scanning fluorimetry
eDNA	Extracellular DNA
EPS	Extracellular polymeric substance
EPS	Extracellular polymeric matrix
Et ₃ N	<i>t</i> -butyl-2-bromoacetate, Triethylamine
EWGs	electron withdrawing groups
FBLD	Fragment-based lead discovery
ΔG	Gibbs free energy change
Gln	Glutamine
ΔH	Enthalpy change
HAQs	4-Hydroxy-2-alkylquinolines
HATU	<i>N</i> -Boc-piperazine, 1-[<i>bis</i> (dimethylamino)methylene]-1 <i>H</i> -1,2,3-triazolo[4,5- <i>b</i>]pyridinium-3-oxide hexafluorophosphate
HBA	Hydrogen bond acceptor
HBD	Hydrogen bond donor
HTS	High-throughput screening
HTVS	High-throughput virtual screening
Ile	Isoleucine
ITC	Isothermal titration calorimetry
K_d	Dissociation constant
LBD	Ligand binding domain
LC-MS	Liquid chromatography–mass spectrometry
Leu	Leucine
LPS	Lipopolysaccharide

MCCC	University of Nottingham Medicinal Chemistry Compound Collection
MvfR	Multiple virulence factor regulator
MWt.	Molecular weight
<i>N</i>	Binding stoichiometry
NMP	<i>N</i> -methylpyrrolidone
NMR	Nuclear magnetic resonance
3OC12-HSL	3-Oxo-C12-homoserine lactone
PDB	Protein Data Bank
PPIs	Target protein-protein interactions
PQS	2-Heptyl-3-hydroxy-4-quinolone signal
<i>pqs</i> system	<i>Pseudomonas</i> Quinolone Signal system
QS	Quorum sensing
RA%	Remaining Activity
Ro3	Rule of three
SAR study	Structure activity relationship study
ΔS	Entropy change
SD	Standard deviation
SPR	Surface plasmon resonance
TLC	Thin-layer chromatography
<i>T_m</i>	Melting temperature
tPSA	topological polar surface area
TSA	Thermal shift assay
Tyr	Tyrosine

Table of Contents

Acknowledgment	I
Abstract	III
List of abbreviation	VI
Chapter 1: Introduction	1
Developing novel antivirulence strategies targeting the pqs system for the treatment of <i>Pseudomonas aeruginosa</i> infections	1
1. 1 <i>Pseudomonas aeruginosa</i> pathogenicity and its antibiotic resistance situation	1
1. 2 The <i>P. aeruginosa</i> quorum sensing system, a promising antivirulence target for the treatment of <i>P. aeruginosa</i> infections	4
1. 2. 1 Quorum sensing in <i>P. aeruginosa</i>	4
1. 2. 2 Targeting the <i>pqs</i> system.....	10
Current perspectives in fragment-based lead discovery	12
1.3 Concepts and an overview of fragment-based lead discovery (FBLD).....	12
1.4 General approaches to fragment-based lead discovery	15
1.5 General considerations for fragment library construction and evaluation	18
1. 5. 1 The physicochemical properties of fragments	18
1.5.2 Fragment library construction and preselection and general considerations	19
1.6 Biophysical methods in FBLD	21
1. 6. 1 Isothermal titration calorimetry (ITC).....	22
1. 6. 2 Thermal shift assay (TSA)	24
1. 6. 3 Surface plasmon resonance (SPR), NMR and X-ray crystallography	27
1. 6. 4 Computational methods	29
1.7 Fragment evolution methods	29
1.8 Using a fragment-based approach to find <i>pqs</i> inhibitors	31
1.9 Aims and hypothesis.....	32
Chapter II: Hit to lead optimization of new potent PqsR antagonists as inhibitors of quorum sensing in <i>Pseudomonas aeruginosa</i>	35
2.1 Introduction and project aims.....	35
2.2 Hit-to-lead optimisation process	39
2.2.1 The first SAR study around 19.....	39
2.2.2 The second SAR study around the tail group to improve analogues' <i>pqs</i> inhibition	47

2.2.3 The design of compound 79 to improve solubility	53
2.2.4 Investigation of the pharmacophore model based on an SAR exploration around the 5-methyl-5 <i>H</i> -[1,2,4]triazino[5,6- <i>b</i>]indole analogues	57
2.2.5 Concept validation investigation for the three essential structure features and their effects on <i>pqs</i> inhibition	61
2.3 Conclusion	63
Chapter III: Using <i>in silico</i>, <i>in vitro</i> and biophysical methods for the fragment-based hit identification and optimization for PqsR inhibition	65
3.1 Introduction and project aim	65
3.2 Using an <i>in silico</i> method for fragment screening against PqsR LBD	66
3.2.1 Selection of five fragment libraries for virtual screening	67
3.2.2 Selection of optimal fragment starting points based on the virtual screening results.....	68
3.3 Using bioreporter assay and biophysical methods for the secondary screening on the selected fragments (106-112 and 29).....	72
3.3.1 Bioreporter assay and TSA screening results on the selected fragments	72
3.3.2 ITC experiment on 106 and 108	74
3.4 Hit optimization I: fragment hit 107 exploration.....	78
3.4.1 The design of hit exploration study for fragment 107	78
3.4.2 The synthesis of designed analogues.....	79
3.4.2 The results for the hit exploration study around 107	81
3.5 Hit optimization II: hit exploration around fragment 106	84
3.5.1 The synthesis of designed analogues.....	85
3.5.2 The results for the hit exploration study around 106.....	86
3.6 Conclusion	92
Chapter IV: Using fragment-based method for the discovery of novel PqsR antagonists for the treatment of <i>P. aeruginosa</i> infections.....	94
4.1 Introduction and aim	94
4.2 Advancing 106 through a fragment growing method	96
4.2.1 The synthesis of designed analogues 143, 148a-d	97
4.2.2 Bioreporter assay and TSA screening results for designed analogues 143 and 148a-d.....	98

4.3 Extract fragments from the 5-methyl-5 <i>H</i> -[1,2,4]triazino[5,6- <i>b</i>]indol-3-yl)thiol analogues	100
4.3.1 The synthesis of designed fragments 152a-c	101
4.3.2 The screening of fragments 152a-d, 81 and 82 using TSA	101
4.3.3 Determination of the thermodynamic parameters of 152a using ITC	103
4.4 Applying fragment linking and merging methods between strong PqsR fragment binders benzothiazole analogues (145a and 146b) and 152a.....	104
4.4.1 The synthesis of designed compounds 154a and 154b.....	106
4.4.2 The biophysical and <i>in vitro</i> profiles of compounds 154a-b	107
4.5 Fragment linking strategy between a weak binder 144 and a strong binder 152a	107
4.5.1 The synthesis of designed compound 156a-c	109
4.5.2 The bioreporter assay screening results for compound 156a-c.....	109
4.6 Exploration of synergistic combinations assisted by the mCTX::PpqsA-lux-based bioreporter assay and TSA	110
4.7 Conclusion	113
Chapter V: Conclusions and future work.....	115
5.1 Conclusions	115
5.1.1 A classic hit-to-lead optimization process to find PqsR antagonists	115
5.1.2 PqsR antagonist fragment hit identification and optimisation	118
5.1.3 Using fragment growing, linking, and merging methods advancing PqsR antagonist fragment hits.....	121
5.2 Future work.....	123
5.2.1 Further modification on compound 154b	123
5.2.2 Further modification on 148d	124
5.2.3 Advancing synergistic pairs	125
5.2.4 Finding dual PqsA/R or PqsA inhibitors through fragment-based methods	126
Experimental.....	128
6.1 Microbiological Experiments	128
6.1.1 PqsR bioreporter assay	128

6.2 Biophysical experiments	130
6.2.1 Thermal shift assay (TSA)	130
6.2.2 Isothermal titration calorimetry (ITC).....	131
6.3 Molecular Docking	131
6.3.1 Protein structure preparation	131
6.3.2 Grid generation	132
6.3.3 Ligand preparation	132
6.3.4 Molecular Docking	132
6.4 Chemistry experimental section.....	133
6.4.1 General chemistry	133
6.4.2 Synthesis	134
Reference	195

Chapter 1: Introduction

Developing novel antivirulence strategies targeting the pqs system for the treatment of *Pseudomonas aeruginosa* infections

1. 1 *Pseudomonas aeruginosa* pathogenicity and its antibiotic resistance situation

Pseudomonas aeruginosa (*P. aeruginosa*) is a Gram-negative bacterium, which was initially discovered in the late 19th century.¹⁴ This opportunistic pathogen is able to infect almost any site in the human body and causes serious tissue damage, blood stream invasion, and systemic dissemination.^{15, 16, 17} *P. aeruginosa* is particularly devastating for immunocompromised patients and most often targets epithelial tissues. It is now becoming the leading cause of death in cystic fibrosis patients.^{18, 19}

The pathogenicity of *P. aeruginosa* stems from biofilm formation and biosynthesis and secretion of a wide range of virulence factors, which are bacteria-associated extracellular products released by bacteria^{20,21} to invade the host and cause diseases, including siderophores, pyocyanin.²² Siderophores are organic compounds secreted by bacteria for iron chelation where iron is an essential nutrient acting as catalyst in bacteria metabolism and biofilm formation.²³⁻²⁵ Pyocyanin is a redox-active molecule secreted by *P. aeruginosa* to inhibit the growth of other competing microbes and damage mammalian cells.²⁶⁻²⁸

When bacteria attach to a surface, they grow in a community defined as a biofilm (**Figure 4**), which is characterized by the formation of highly hydrated extracellular

polymeric substance (EPS) and provides protection from antimicrobial treatments.²⁹ Additionally, biofilms commonly attach to extracellular DNA (eDNA) that provides a breeding platform for mutations. It has been reported that bacteria within biofilms are commonly 10-1000 times more tolerant to antibiotics than planktonic cells.³⁰ *P. aeruginosa* is more susceptible to antimicrobial treatments when the bacteria are dispersed or removed from the biofilm and antibiotic therapy alone barely cures the infections when the bacteria grow within the biofilm.³¹ It has been reported that chronic infections are almost impossible to eradicate when *P. aeruginosa* grows in biofilms especially for cystic fibrosis patients.²⁹ For multidrug-resistant *P. aeruginosa* strains, removing the biofilm helps restore antibiotic sensitivity.^{16, 32, 33}

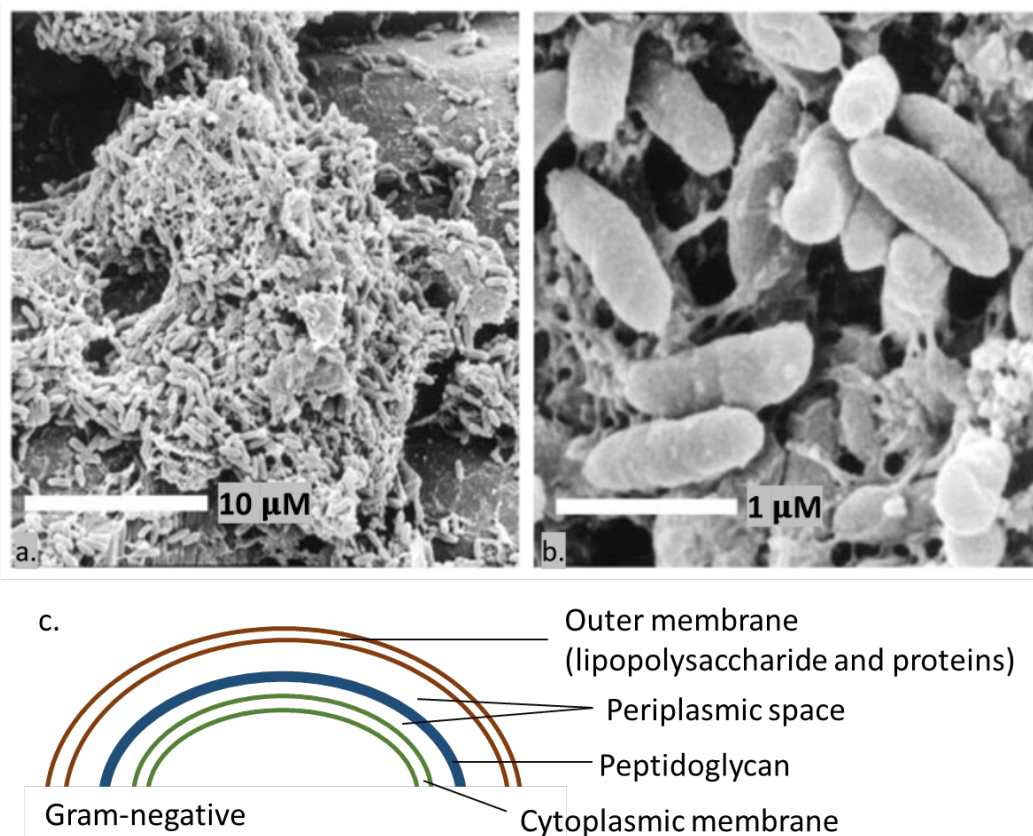


Figure 4. (a and b) Scanning electron micrographs of a *P. aeruginosa* PAO1 strain biofilm. a) A biofilm on the surface of a pebble. b) high magnification of *P. aeruginosa* embedded in an extracellular polymeric (EPS) matrix.³³ (c) Gram-negative cell wall diagram. The outer membrane consists of a lipid bilayer anchored with lipopolysaccharide (LPS) which is consisted of three components: O-polysaccharide, core polysaccharide and lipid A. LPS has multiple functions for the bacteria including

stabilizing the outer membrane, providing a physical protection for the bacteria, and acting as toxin causing pathogenicity such as fever. Peptidoglycan is the polymer of sugar and amino acids and formed the overall structure of the bacteria cell wall. The periplasmic space stores macromolecules including amino acids, iron, and enzymes, which is vital for bacteria nutrition.

The primary treatment for *P. aeruginosa* infection is antibiotic therapy, which is becoming less effective due to the increasing level of resistance to many clinically employed antibiotics.³¹ There are multiple mechanisms underlying *P. aeruginosa* antibiotic resistance. *P. aeruginosa* possesses a markedly large and complex genome (6.3 million base pairs), which gives huge potential for high adaptability to diverse environments and developing antimicrobial resistance.³⁴ These resistance genes can be further transferred through horizontal transfer to non-resistant strains.³¹ The intrinsic resistance mechanisms also include low cell permeability of its outer membrane^{35–37}, various efflux systems and biofilm natural protection.¹⁵ Overexpressed efflux systems and the additional outer membrane barrier limit the penetration rate of drugs³⁸, whilst biofilm serves as a diffusion barrier to also decrease antibiotic entry into bacterial cells.³¹

In 2013, the Centre of Disease Control and Prevention (CDC) announced that *P. aeruginosa* was a severe threat to public health because of emerging antibiotic resistance.³⁹ There are approximately 50,000 *P. aeruginosa* infection cases in the USA every year and around 13% are multidrug-resistant *P. aeruginosa* infections that have proved to be resistant to nearly all antibiotics, including aminoglycosides, cephalosporins, fluoroquinolones and even carbapenem.^{40, 39, 41, 42}

1. 2 The *P. aeruginosa* quorum sensing system, a promising antivirulence target for the treatment of *P. aeruginosa* infections

P. aeruginosa recruits quorum-sensing (QS) systems to regulate virulence mechanisms which makes QS an attractive antivirulence target.^{19, 15, 43, 44, 45, 46} Antivirulence therapy has been regarded as a promising alternative to antibiotics. The overall strategy is to disarm the pathogen, and in doing so not disturb bacteria growth or cause bacteria cell death which could lead to antibiotic resistance.^{40, 45} Antivirulence agents have several advantages over traditional antibiotics. Firstly, they specifically target the pathogens without disturbing the healthy microbiome, which is essential for the overall health of the human body. Secondly, inhibition of virulence factors is not vital for bacteria survival and therefore decreases the chances of selective pressure for development and therefore resistance. Therefore, antivirulence agents have been regarded as a promising strategy to be used alone or in combination with antibiotic therapy.^{47, 39, 43}

1. 2. 1 Quorum sensing in *P. aeruginosa*

Quorum sensing is a cell-to-cell communication system that allows bacteria to coordinate gene expression in response to local population density. This process relies on the production, detection and response to extracellular signalling molecules called autoinducers (AIs). AIs are chemically diverse, and include a range of small peptides and organic molecules.¹¹ At low cell density, AIs diffuse freely out of the cell and accumulate in the extracellular environment, but the overall concentration of AIs is below the threshold required for detection. When bacteria population density increases, AIs accumulate and lead to a locally high concentration that enables

bacteria to detect and respond. In this case, accumulated AIs are able to interact with cognate receptors and lead collectively to gene expression alteration.^{48, 49, 50}

Many Gram-negative bacteria employ QS to regulate the expression of certain genes and the QS system in *P. aeruginosa* is an intricate regulatory network. There are some detailed mechanisms of the QS systems that still remain unknown. In general, QS signals acting as multifunctional signals regulate the organism's behaviour and virulence mechanisms. The genes controlled by QS can be classified into four categories based on their functions: cell maintenance and proliferation (siderophore production), cell behaviours (biofilm formation), horizontal gene transfer and interactions between host and other microbes (virulence factors secretion).⁵¹ Disturbing the QS cascade enables inhibition of almost all the virulence mechanisms including biofilm formation, iron scavenging, cytotoxicity, and even antibiotic resistance without triggering resistance.⁵² A significant number of QS signalling molecules have been found at the sites of infection *in vivo*, which also suggests QS is an attractive therapeutic area to target for *P. aeruginosa* infections.^{19, 15, 44, 46,45}

1. 2. 1. 1 Two *N*-acylhomoserine lactone (AHL)-dependent QS Systems

There are three QS systems in *P. aeruginosa*: two *N*-acylhomoserine lactone (AHL)-dependent QS Systems (the *las* and *rhl* systems) and one *Pseudomonas* Quinolone Signal (*pqs*) system. The three QS systems in *P. aeruginosa* are highly interconnected and complex (**Figure 5**).

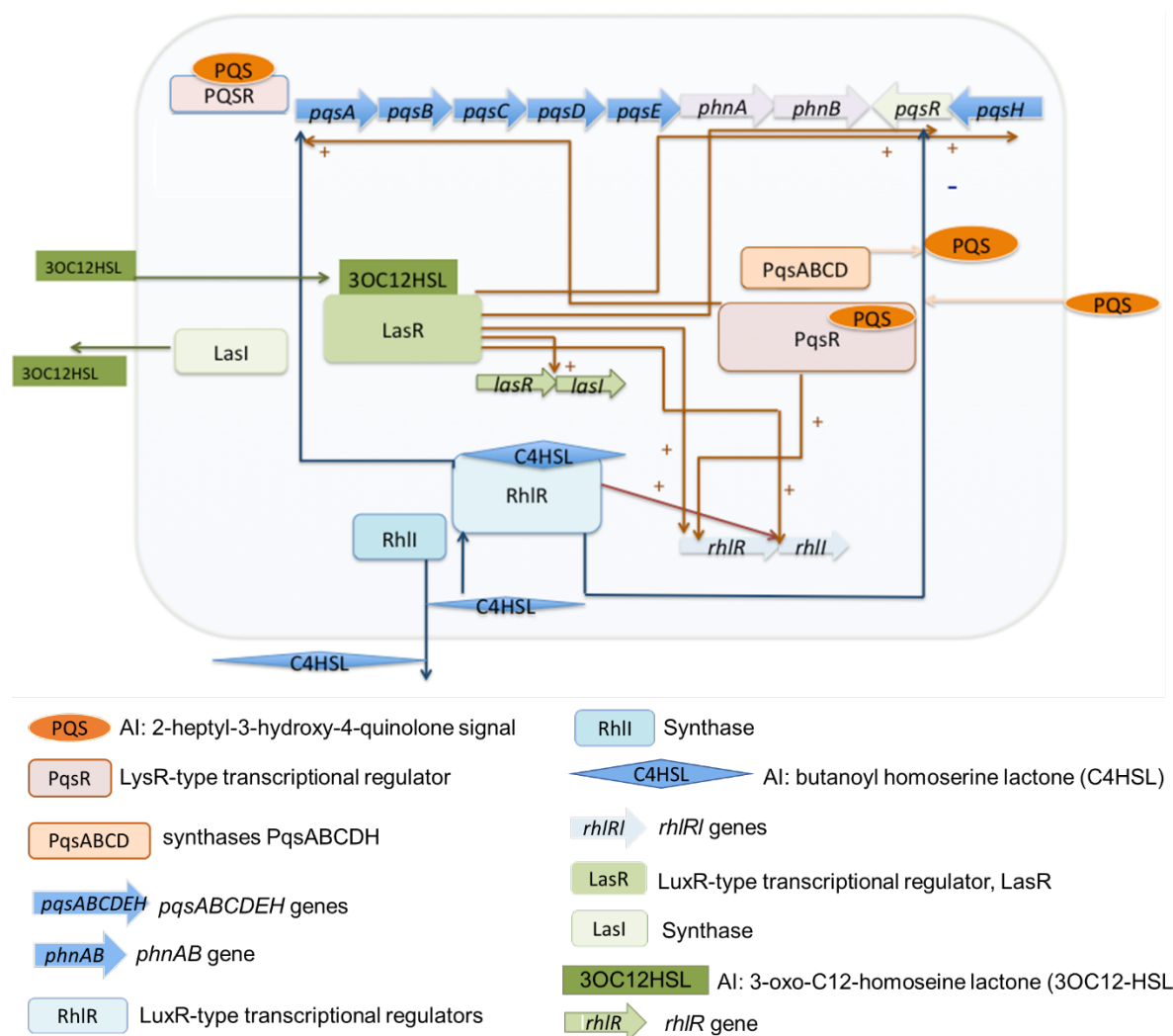
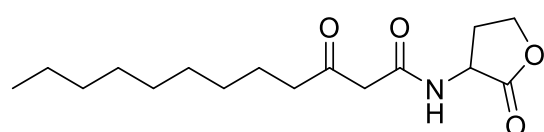


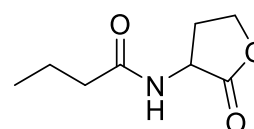
Figure 5. The three QS systems in *P. aeruginosa* are highly interconnected. (-) represents down regulation. (+) represents up regulation. The *las* system is the dominant system and it positively controls *pqs* and *rhl* system through regulating the transcription of *pqsH* and *pqsR*. *rhl* system negatively regulate the *pqs* system through inhibition the transcription of *pqsR* and *pqsA* promoter region. The *pqs* system involves with *rhl* system regulation. The three QS systems in *P. aeruginosa* are highly interconnected. The PqsR-PQS complex is able to activate *rhIR* the same as the LasR-3OC12HSL complex. The *las* and *rhl* quorum sensing systems control the production of PQS through determining the expression of *pqsABCDE*. The LasR-3-OC12-HSL complex positively controls the transcription of *pqsR*, while RhIR-C4HSL suppresses this transcription.^{19, 53} Additionally, RhIR are able to bind to the promoter region of *pqsR* and *pqsA* and LasR is able to bind to the promoter region of *pqsR* and *pqsH*.^{54, 55} PQS inhibits the expression of *rhII*⁵³ however is required for the expression of *rhl*-dependent phenotypes.¹⁹

The AHL system in *P. aeruginosa* contains two LuxR-type transcriptional regulators (LasR and RhIR) and two LuxI homologs (LasI and RhII). Together they regulate over 200 genes⁵⁶. LasI and RhII synthesize 3-oxo-C12-homoserine lactone (3OC12-HSL)

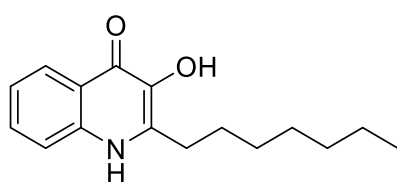
and butanoyl homoserine lactone (C4HSL) respectively (**Figure 6**). 3OC12HSL and C4HSL acting as AIs bind to and stabilize LuxR-type transcriptional regulators LasR and RhIR respectively. LasR-3OC12-HSL and RhIR-C4HSL complexes are then able to bind to the promoter region of target genes and initiate gene transcription.^{46, 52} For example, 3OC12HSL binds to the transcriptional regulator LasR and results in the LasR hydrophobic core folding and dimerizing, which then activates the transcription of the target genes. Through this process, the *las* system controls the production of a wide range of virulence factors, including exotoxin, and biofilm.^{19, 55} The LasR-3OC12HSL complex is also involved in regulating the *rhl* and *pqs* systems^{48, 55}. The *las* system is the dominant QS system in *P. aeruginosa*, however shutting down the *las* system in *P. aeruginosa* does not stop the transcription of virulence factor related genes, an observation which led to the discovery of the *pqs* system.⁵⁷

**1**

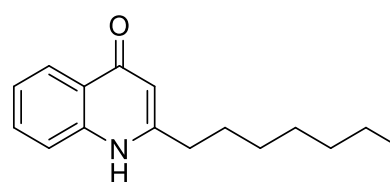
3-oxo-C12-homoserine lactone (3OC12HSL)

**2**

butanoyl homoserine lactone (C4HSL)

**3**

2-heptyl-3,4-dihydroxyquinoline (PQS)

**4**

4-hydroxy-2-heptylquinoline (HHQ)

Figure 6. Examples of autoinducer structures of *P. aeruginosa* quorum sensing systems

When C4HSL binds to RhIR, the *rhl* signaling cascade is initiated and the RhIR-C4HSL complex activates the transcription of target genes. The *rhl* system is upregulated by the *las* system directly through interaction between the LasR-3OC12HSL complex and

rhlI and *rhlR*.^{19, 55, 56} The *rhl* system also plays an important role in regulating virulence factors biosynthesis, such as pyocyanin and siderophores.^{58,59}

1. 2. 1. 2 The *pqs* system

The *pqs* system is unique to *P. aeruginosa*, which employs a LysR-type transcriptional regulator MvfR (Multiple virulence factor regulator, also known as PqsR), synthesizes PqsABCDH and Als especially 2-heptyl-3,4-dihydroxyquinoline (PQS, Pseudomonas quinolone signal) and 4-hydroxy-2-heptylquinoline (HHQ) (**Figure 6**). The synthases PqsABCDH are in charge of biosynthesis of PQS and its precursor HHQ. PQS and HHQ bind to their cognate receptor PqsR and enhance DNA-binding of PqsR to the *pqsA-E* promoter, which leads to the transcription of *pqsA-E* and *phnAB* genes.^{60, 61}

The transcription regulator PqsR belongs to LysR-type transcription regulators (LTTR) family encoded by *pqsR*, and controls *pqsABCDE* gene transcription to PqsABCDH synthases.^{62, 63} PqsR contains a highly conserved N-terminal DNA binding domain, a large C-terminal ligand binding domain (LBD) and a hinge region that connects the two sub-domains. The small cognate autoinducers, such as PQS and HHQ are able to bind to the C-termini LBD and leads to a conformation change on PqsR. The helix-turn-Helix DNA binding domain in PqsR is then activated and able to bind to the *pqsA* promoter region⁵⁴ and therefore initiates transcription of *pqsABCDE*, *phnAB* and regulates a wide range of virulence factors, such as pyocyanin, hydrogen cyanide and 4-hydroxy-2-alkylquinolines (HAQs).^{60, 18}

The biosynthesis of HHQ and PQS is controlled by the PqsR-regulated operons *pqsABCDH* and *phnAB* (**Figure 7**).⁶⁰ PhnAB enzymes encoded by *phnAB* genes are responsible for conversion of shikimic acid to anthranilic acid, while PqsABCDH enzymes encoded by *pqsABCDH* catalyze the biosynthesis of PQS and HHQ from

anthranilic acid.^{65, 56} PqsH controls the last synthesis step oxidizing HHQ to PQS, which is limited by oxygen,⁶⁶ whilst the specific function of PqsE is unknown. It has been proven that PqsE is not involved in HHQ and PQS biosynthesis but is able to positively regulate virulence genes in the absence of PQS and HHQ.^{64, 11} Mutations in *pqsA* or *pqsE* led to a significant decrease of virulence factor production *in vivo*, indicating the importance of PqsA and PqsE in this process.⁴² HHQ alone is able to activate PqsR-dependent gene transcription⁵⁵ but PQS is more potent than HHQ in terms of PqsR binding and activation.⁶⁰ HHQ and PQS are released into the extracellular medium that allows them to be taken up by neighbouring cells.⁵⁵

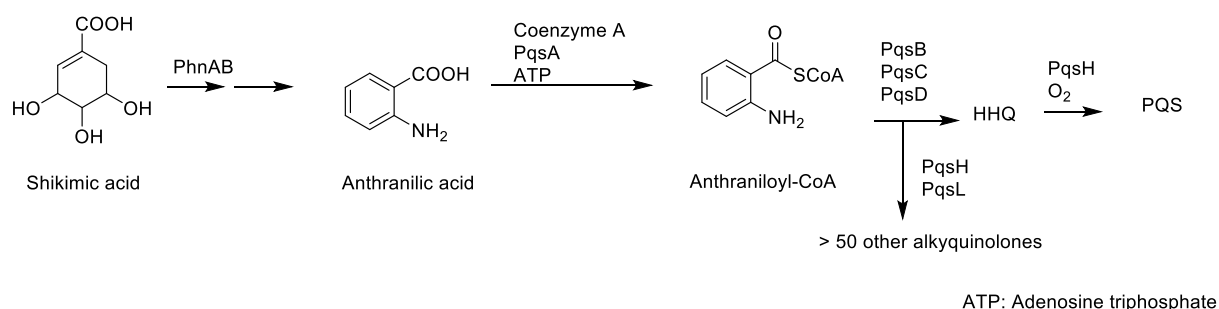


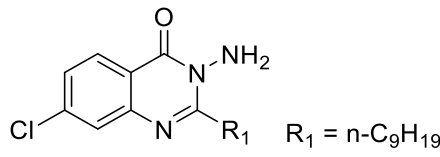
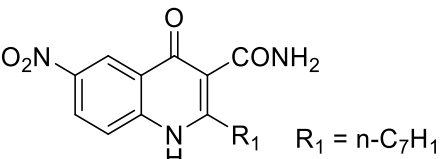
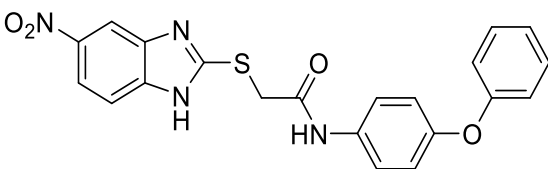
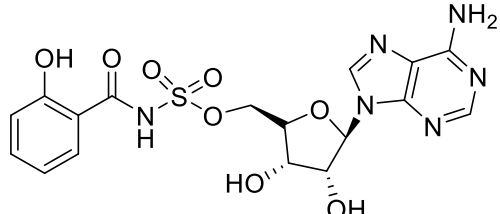
Figure 7. Biosynthesis of HHQ and PQS involves PqsABCDH enzymes and is an auto-induced feedback loop. Anthranilic acid can be synthesized from shikimic acid pathway. PqsABCDH enzymes then catalyse the biosynthesis of PQS from anthranilic acid. PqsR in complex with PQS or HHQ is then activate the transcription of *pqsABCDE* and then initiate the transcription of *phnAB* and *pqsR*, which in turn activates the biosynthesis of anthranilic acid through shikimic acid pathway.

PQS is an essential AI for *P. aeruginosa* pathogenicity. PQS, and not HHQ, is able to activate the *phzA1-phzG1*, which is responsible for pyocyanin biosynthesis.⁵⁵ PQS is found in infection sites in cystic fibrosis patients⁶⁵ and in wild type *P. aeruginosa*, provision of exogenous PQS leads to significant increase in virulence secretion including pyocyanin and biofilm.⁵⁴ Loss of PQS signalling can result in reduction of pyocyanin production.¹⁹ With the 3-OH group, PQS can also act as iron chelator and inhibit other species take up irons in the same environment.^{67,68,69}

1. 2. 2 Targeting the *pqs* system

There have been several attempts to target the *pqs* system in *P. aeruginosa* as shown in **Table 1**. Shutting down the *las* system does not stop virulence factors biosynthesis⁵⁷ and clinically isolated *P. aeruginosa* strains frequently contain *las* system mutations, which limits the therapeutic use of LasR inhibitors.⁷⁰ Disturbing the *rhl* system alone does not have a significant impact on virulence factor biosynthesis.^{58,59} Lack of RhlR and RhlI protein structures also hinders the development of *rhl* inhibitors.

Table 1. Examples of *pqs* inhibitors. ^{11,71,72,52,61}

No.	Structure	Biological target	IC ₅₀
5		PqsR	5.0 ± 1.6 μM
6		PqsR	404 μM
7 (M64)		PqsR	0.32 ± 0.14 μM
8		PqsA	88 ± 12 nM

The *pqs* system is crucial for *P. aeruginosa* pathogenicity and finding novel PQS inhibitors has been regarded as a promising research area for overcoming *P. aeruginosa* infection and antibiotic resistance. The crystal structures for PqsR, PqsA, PqsD, PqsBC have been published and there have been some recent advances towards finding new inhibitors of *pqs*, especially for PqsR (**Table 1**).

Some PqsR antagonists were discovered based on the structural modification of native agonists 4-hydroxy-2-alkylquinolines (HAQs) such as compounds **5** and **6** in **Table 1**. Some other PqsR antagonists have unique structures such as compound **7** in **Table 1**. The crystal structure of PqsR in complex with **7** revealed that **7** and PQS bind in the same binding pocket. The sulfur atom in **7** helps the compound bend in a particular conformation that allows the compound to fit into the ligand-binding domain. The amide bond, acting as a hydrogen bond acceptor (HBA), interacts with Gln¹⁹⁴ while the Tyr²⁵⁸ is involved in a π - π interaction with the aromatic moiety on **7** (**Figure 8**).^{61, 73}

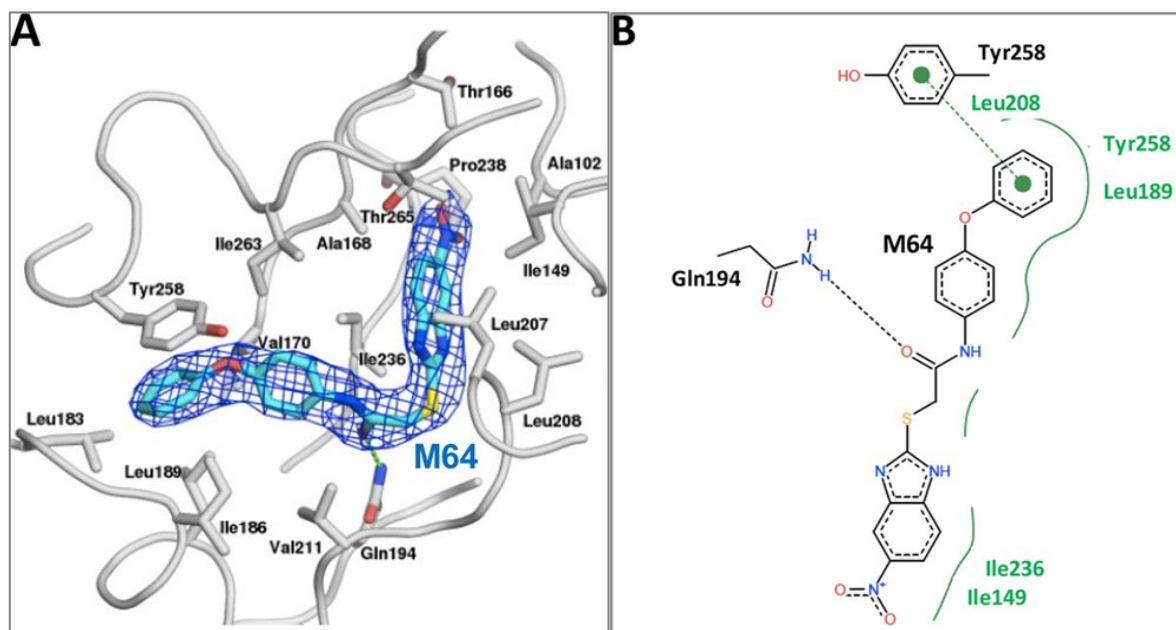


Figure 8. Schematic presentation of **7** (named as **M64** on literature) binding to the hydrophobic ligand binding pockets of PqsR.⁶¹ (A) Crystal structure of MvfR in complex with M64. (B) Two-dimensional diagram of **7** in complex with PqsR LBD. Green dash line indicates π interactions. Black dash line indicates hydrogen bonding and green solid line indicates hydrophobic effect.

Current perspectives in fragment-based lead discovery

1.3 Concepts and an overview of fragment-based lead discovery (FBLD)

Traditional high-throughput screening (HTS) methods start from screening of compound libraries against interested biological targets where HTS libraries normally contain several hundreds of thousands or even millions of compounds with molecular weight (MWt.) in a range from 300 Da to 550 Da (**Figure 9**). Screening such a large compound library is time-consuming and requires a high financial investment.^{74,75,76} For allosteric sites or protein-protein interaction targets, HTS of compound libraries with molecular weight (MWt.) in a range from 300 Da to 550 Da can provide a low hit rate.^{77, 78, 79}

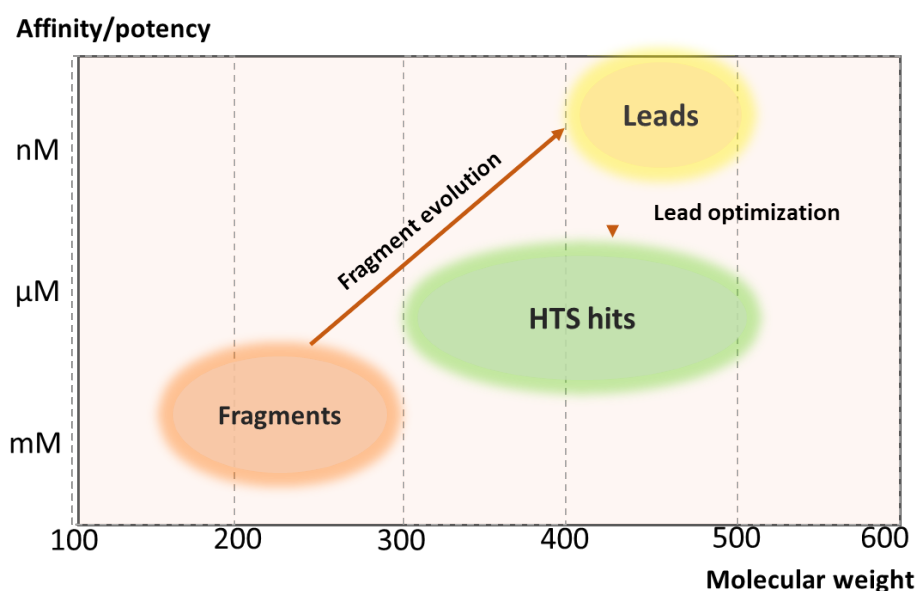


Figure 9. Comparison between fragment-based and HTS hit-based lead discovery process. Fragment hits are smaller (molecular weight 150 <MWt < 300 Da) and weakly bind to their targets with affinity in a μM-mM range, whilst HTS hits (molecular weight 300 <MWt < 550 Da) are larger with stronger affinity to the biological targets. In FBLD, the approach used is to screen much smaller compound libraries, normally containing a few hundred to a thousand fragments (molecular weight 150 <MWt < 300 Da) against biological targets of interest using either biophysical or biochemical methods to identify

chemical starting points,⁸⁰ and tend to achieve higher hit rates compared with HTS.⁸¹ The resulting fragment hits are smaller and less lipophilic compared with HTS hits and therefore provide greater opportunity for structure modification in order to optimize physicochemical properties and biological activity.⁸² FBLD approaches have been regarded as powerful methods in structural characterization of orthosteric and allosteric binding sites providing new starting points even for well characterized targets.⁸⁰

In FBLD approaches, fragments are defined as small, low molecular weight compounds (normally below 300 Da). By reducing structure complexity, fragments are more likely to occupy a single pocket or multiple pockets in the biomacromolecule of interest. Some fragments can bind to and produce weak but measurable binding or inhibitory events observed using biophysical or pharmacological methods. If these active fragments have the desired physicochemical properties and pharmacological activities, they can be defined as fragment hits and act as chemical starting points for the hit-to-lead process (**Figure 10**).⁸⁰ Additionally, combined with biophysical methods such as X-ray crystallography or protein-observed NMR, it is possible to identify functional portions of the molecules that are key in ligand binding and resolve detailed binding mechanisms. In addition, fragments tend to be weak but efficient binders (as measured by ligand efficiency metrics).^{80, 82, 83}

FBLD methods aim to provide fewer lipophilic hits⁸⁴ and address a common issue of low hit rates in traditional HTS methods, especially for difficult targets or new classes of biological targets classes.^{81, 82, 85} FBLD methods have been regarded as an alternative to traditional HTS based lead discovery and an important lead discovery technique for both well-characterized or new drug targets in the last 20 years.^{86,81, 87,}

88, 89

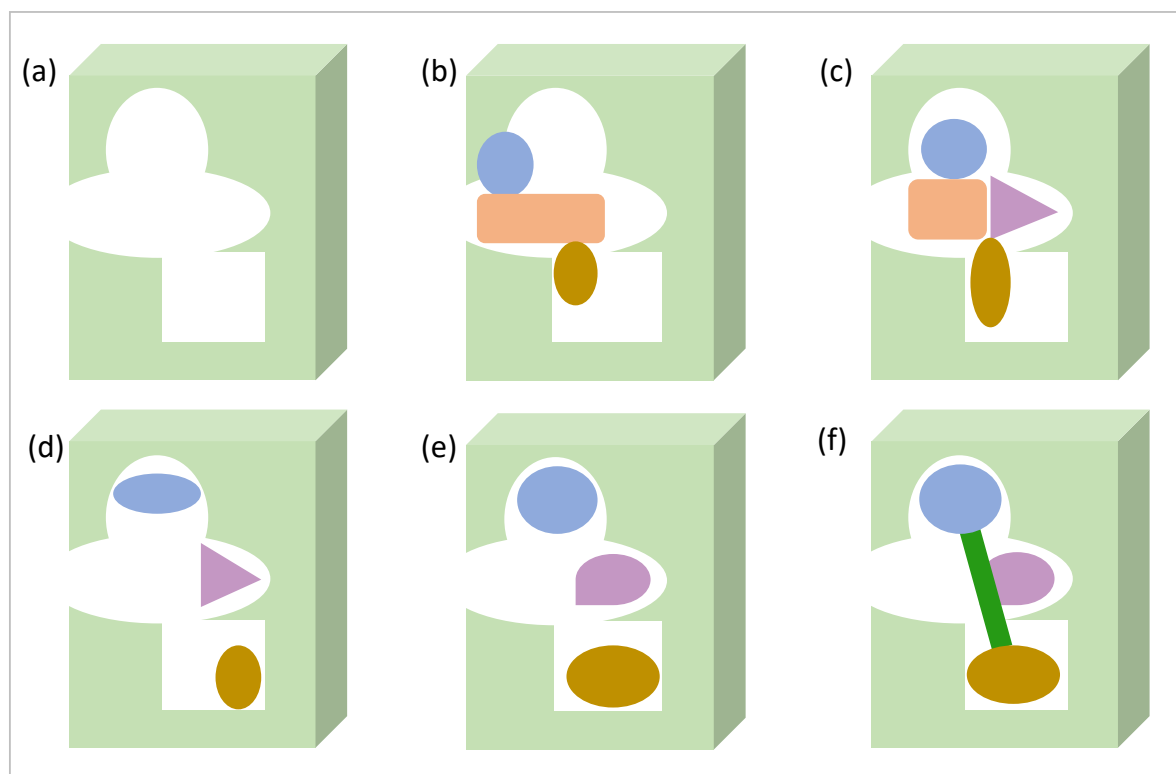


Figure 10. Schematic representation of drug-sized HTS hits and fragment hits as starting points followed by structure modification. **(a)** Representation of the active site of interest in a biomacromolecule, in which there are three main sub-pockets available within the active site. **(b)** Representation of a drug-sized hit compound from high-throughput screening (HTS). The hit compound can be active in pharmacological assays, but the compound is functionally complex. Some parts of the molecule can have unfavoured clashes within the binding site and the ligand efficiency can be quite low. **(c)** Representation of a lead compound obtained from the hit from **(b)** after SAR study. Lead compounds can have better shape complementarity with the active site by either removing unfavoured clashes with residues within the binding site or by occupying unexplored regions in the binding site. However, synthetic complexity and poor physicochemical properties, including high lipophilicity, low solubility and poor metabolic stability can arise with a significant increase in structure complexity and molecule size. **(d)** Representation of fragments binding to different sub-pockets in the active site of biological targets. Fragments are small and more likely to fit into regions of the binding pocket that are often hard to target with larger molecules. **(e)** Representation of SAR study around fragments. SAR studies around original fragment hits are essential to probe or optimise interactions between fragments and the binding sites. **(f)** Representation of a lead compound driven from the hit from **(e)**. The new lead compound can have less structure complexity compared with **(c)**, which provides more opportunity to further modify the compound's structure and improve drug-likeness. Besides, fragments can occupy unexplored regions and the resulting compound **(f)** can have either improved activity or affinity.

1.4 General approaches to fragment-based lead discovery

The general procedures for FBLD method have been well established and summarized as shown in **Figure.11**. Fragment library design and selection requires a manual inspection step where the diversity and quality of fragments needs to be considered.^{79,90,91} X-ray crystal structure of protein-fragment complexes are also essential for the guidance of fragment evolution.^{92,93}

Fragments are small molecules with affinity generally in the range from micromolar (μM) to millimolar (mM). Therefore, the selection of the appropriate fragment screening method is an important consideration in the FBLD project. An inappropriate screening method can lead to either false positives or a low hit rate. Pharmacological assays, *in silico* screening methods and more importantly biophysical methods are all widely used and, in order to obtain more accurate and reliable results, it is common to cross validate results through different methods.⁸⁵

After fragment screening, a manual inspection step is required where medicinal chemists evaluate and select fragment hits for further hit-to-lead optimization. In this step, physicochemical properties, synthetic complexity as well as the chemical evolution potential of fragments need be carefully considered. Once initial fragment hits have been chosen, a structure activity relationship (SAR) study should be conducted around hits to probe and/or optimize binding interactions. This activity has been recently named “SAR by catalog”.⁹⁴ In order to exclude non-specific binding, the fragment binding mode or site should be confirmed and the most informative method to achieve this is X-ray crystallography.^{95, 96}

There are three main fragment evolution methods, which are fragment growing, fragment linking and fragment merging. Each of these will be discussed in detail later. Fragments are grown to form new interactions or occupy new pockets guided by rational structure-based design using either computer-assisted methods or high-quality X-ray crystallography data. The fragment evolution step is an iterative cycle and the resulting lead compounds should expect at least a 10 times increase in potency and/or affinity.⁹⁰

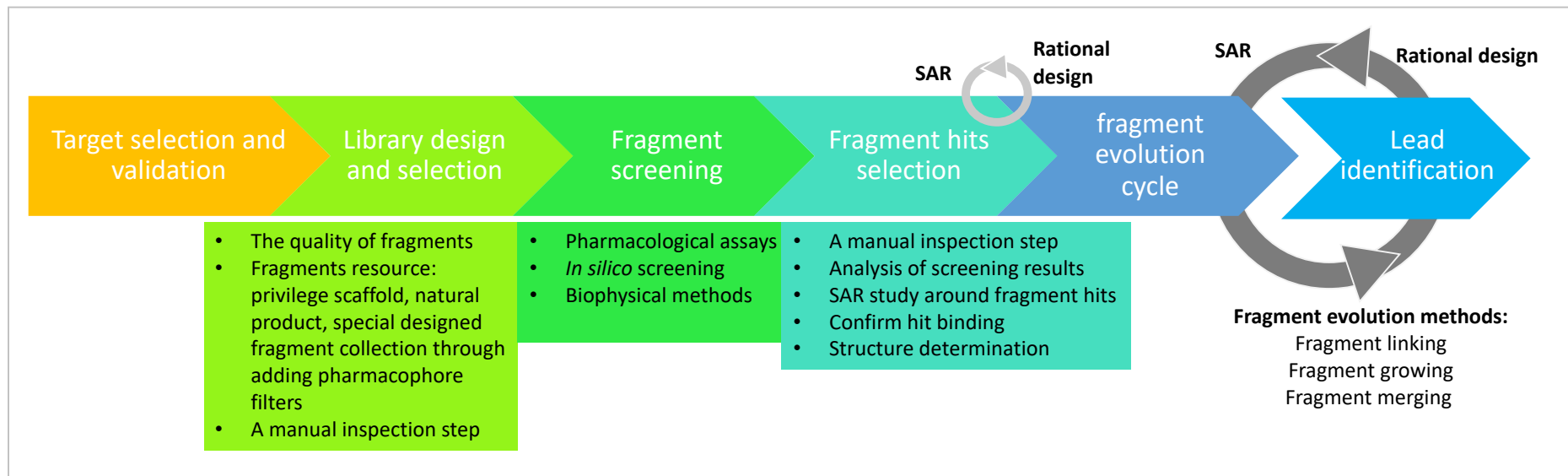


Figure 11. General workflow of the fragment-based lead discovery approach. Structure active relationship (SAR) study indicates the relationship between chemical groups and its biological effects.

1.5 General considerations for fragment library construction and evaluation

The selection of good quality fragments as chemical starting points for the hit-to-lead optimization process is fundamental to the FBLD approach. There are several considerations in the construction of the fragment library and hit selection.

1.5.1 The physicochemical properties of fragments

Physicochemical properties are key in fragment selection and evaluation. Starting with fragments possessing good physicochemical properties can reduce attrition rates in later hit-to-lead optimisation.⁸⁴

1.5.1.1 Fragment rule of three

Similar to drug-like compounds with a “rule of five” to indicate the desired physicochemical properties,^{97, 98, 99} there is the “rule of three” (Ro3) to describe fragment-like properties, which include: molecular weight less than 300, the number of HBA or the number of hydrogen bond donors (HBD) less than 3 and the calculated partition coefficient (cLogP) no more than 3. It also suggests that the number of rotatable bonds (below 3) and polar surface area (below 60 Å²) should be considered to minimise the entropic energy penalty and facilitate better oral bioavailability. In general, fragments should be simple enough to minimize steric hinderance or electrostatic repulsion in target binding sites yet have sufficient complexity to hold enough chemical elaboration points.¹⁰⁰ Ro3 rules describe desirable physicochemical properties for fragments and also limit molecular complexity, which is key in fragment library construction and fragment evaluation.^{2, 83, 101, 102, 103, 104}

1.5.2 Fragment library construction and preselection and general considerations

Fragment libraries need to cover a wide and diverse chemical space and there are two main considerations in assembling fragment libraries: the quality of fragments and the balance between fragment diversity and size.⁸⁰

1.5.2.1 Fragment library assembly and preselection

Fragments originate from different sources including natural products, privileged scaffolds and approved drugs.¹⁰⁵ Privileged scaffolds from drugs are commonly introduced to fragment libraries and these libraries tend to have higher hit rates. Some fragment libraries are carefully built based on biological target structural features. Structure deconstruction and extraction from potent compounds for a specific target followed by synthesis or purchasing of interested fragments and their analogues are also common approaches in fragment library construction.¹⁰⁶

It has been widely accepted that introducing sp^3 carbon atoms into fragments enable more “natural product-like” features and provide improved three-dimensional shape.^{107, 108} These fragments are often designed to target protein-protein interactions (PPIs) or new biological target classes. This may result from the assumption that PPI targets require more three-dimensionality in compounds compared with other protein targets.¹⁰⁹ Common fragment libraries tend to have more flat topographies and lead to lower hit rates against PPIs and new biological target classes. However, synthetic difficulties and the increase in fragment size should be considered when design sp^3 carbon rich fragments.¹¹⁰

Another feature for FBLD is that a high-quality fragment library can be used to screen against different biological targets and the outcome fragment screening results can be similar. Therefore, the final selection of fragment hits normally requires a manual inspection step where medicinal chemists need to assess fragment hits and decide how to optimize them. This step is one of the most important steps in fragment-to-lead optimization process.

1. 5. 2. 2 Stability and solubility of fragments

Fragments are normally stored and screened at a relatively high concentration for a significant length of time, depending on the size of fragment library and screening methods. Therefore, fragment properties in terms of purity, stability and solubility should be regularly checked.

In primary screening, fragment screening concentrations can be above 500 μM and up to 1 mM allowing the detection of weak binders.⁷⁸ Therefore, fragments should be soluble at these high concentrations in dimethylsulfoxide (DMSO) and phosphate buffered saline. Additionally, the purity of fragment samples should be checked as even minor impurities at high concentrations could lead to false positive results, e.g. a 1% impurity in 1 mM fragment solution can lead to 10 μM contaminant.^{111, 102} The analysis of molecular purity and solubility is commonly carried out using analytical methods such as liquid chromatography–mass spectrometry (LC-MS) and nuclear magnetic resonance (NMR).

The most commonly used solvent for stock solution preparation is DMSO, which is a mild oxidant and is also hygroscopic. Fragment library screening can take a significant length of time and fragments need to have long term stability in DMSO or aqueous

solution.^{112,111} Therefore, fragments are stored either as solids and dissolved into media buffer immediately before use or are solubilized in DMSO and stored under an inert, dry atmosphere to maintain their integrity.

Another important concern in fragment library construction and hit selection stages is the exclusion of highly reactive chemical functionalities such as acyl chlorides and Michael acceptors to avoid instability and reactivity issues. These functional groups can non-specifically bind to proteins and cause proteins or fragment precipitation and aggregation, which influences the accuracy of screening results.^{78, 85, 111}

In general, screening of a relatively small but diverse fragment library enables coverage of a large chemical space. According to Reymond's group, addition of one heavy atom to fragments increases the chemical space approximately 8.3-fold. A fragment library containing 1000 fragments with molecular weight around 190 Da covers a similar chemical space as 10^{18} compounds with molecular weight around 450 Da.¹¹² Therefore, FBLD approaches tend to require lower investment and achieve higher hit rates compared with the traditional methods.^{81, 102}

1.6 Biophysical methods in FBLD

Fragments generally have weak but highly efficient binding to the biological targets. Therefore, the selection of an appropriate method to detect and measure fragment binding is essential. Bioactivity assays are widely used in HTS, however much higher concentrations are required in fragment screening and sometimes these methods, such as radio-ligand binding or outputs from reporter gene assays will give false positive results because of potential precipitation and aggregation of the fragments.^{103,}

¹¹³ Sensitive biophysical methods are commonly used for primary fragment screening

including isothermal titration calorimetry (ITC), thermal shift assay (TSA), surface plasmon resonance (SPR), ligand-observed and protein-observed NMR and X-ray crystallography.¹¹⁴ These biophysical methods have different sensitivity range shown in **Figure 12** and the selection of an appropriate method for fragment screening is key in hit identification and optimization.

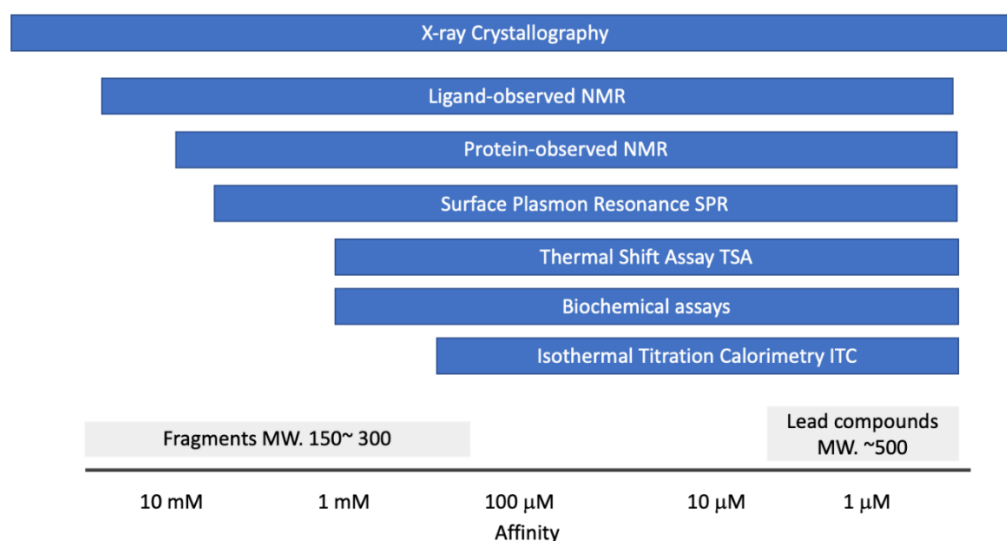


Figure 12. A representation of affinity range of different biophysical methods.

1. 6. 1 Isothermal titration calorimetry (ITC)

Isothermal titration calorimetry (ITC) is a sensitive biophysical method that accurately determines thermodynamic parameters of ligand-protein interactions. A calorimeter consists of a reference cell containing buffer or water as a control and a sample cell where binding partners are mixed.¹¹⁵ The common experimental set up is ligand samples in higher concentrations are titrated into protein solutions in lower concentration in the sample cell. However, if a ligand suffers poor solubility, the components can be reversed.¹¹⁶

When binding components are mixed in the sample cell, heat can be released or absorbed. Through measuring the differential power required to maintain a zero-

temperature difference between reference and sample cell, the calorimeter is able to monitor ligand-protein interactions and determine thermodynamic parameters including the enthalpy change (ΔH_{obs}), binding stoichiometry (N), and binding affinity (K_d)¹¹⁵. The entropy change (ΔS) and Gibbs free energy change (ΔG) can be further calculated using the equations (1) and (2). It should be noticed that the ITC experiment is very sensitive and the buffers for dissolving ligands and protein should be matched in order to avoid the heat of dilution from titrating two different buffers.^{112, 79, 117, 118}

$$\Delta G = - RT \ln K_d \quad (1)$$

$$\Delta G = \Delta H - T\Delta S \quad (2)$$

Where ΔG indicates Gibbs free energy; ΔH indicates enthalpy; ΔS indicates entropy; R is the gas constant ($1.985 \text{ cal K}^{-1}\text{mol}^{-1}$); T is the temperature in Kelvin; K_d indicates affinity.

Through ITC experiments, thermodynamic parameters for ligand-protein interactions are determined. However, ITC experiments cannot provide detailed ligand binding modes. In order to confirm ligand binding site interactions, a competitive displacement ITC experiment can be conducted in which protein samples are mixed with a known competitive ligand and you then titrate in the fragment of interest. The main limitations for ITC methods are the large consumption of protein sample and high solubility requirement for ligands. ITC experiments are also time-consuming as a single experiment can take approximately 90 minutes and therefore this approach is not suitable for fragment library screening.^{119, 120}

1. 6. 2 Thermal shift assay (TSA)

Thermal shift assay, also known as differential scanning fluorimetry (DSF) is an effective biophysical method to monitor protein denaturation and can be used in a parallel format. It has been widely used in fragment library screening and protein buffer optimization for storage or crystallization.¹²¹

In a TSA experiment, protein samples are dissolved in aqueous-based buffer with addition of an environmental sensitive fluorescent dye, such as SYPRO™ Orange. Proteins are in a denatured equilibrium between folded and unfolded states (Native \rightleftharpoons Denatured) and the energy changes of the environment, such as temperature or pressure or the addition of ligands/denaturants would change the equilibrium towards one side.¹²² When the protein unfolds, the dye is able to bind to the protein hydrophobic core and this leads to a large increase in fluorescence.¹²³ Through monitoring the fluorescent change during the protein-unfolding transition process, a sigmoidal curve can be obtained (**Figure 13**) and this allows determination of the melting temperature (T_m), defined as the temperature where 50% of protein sample is unfolded.

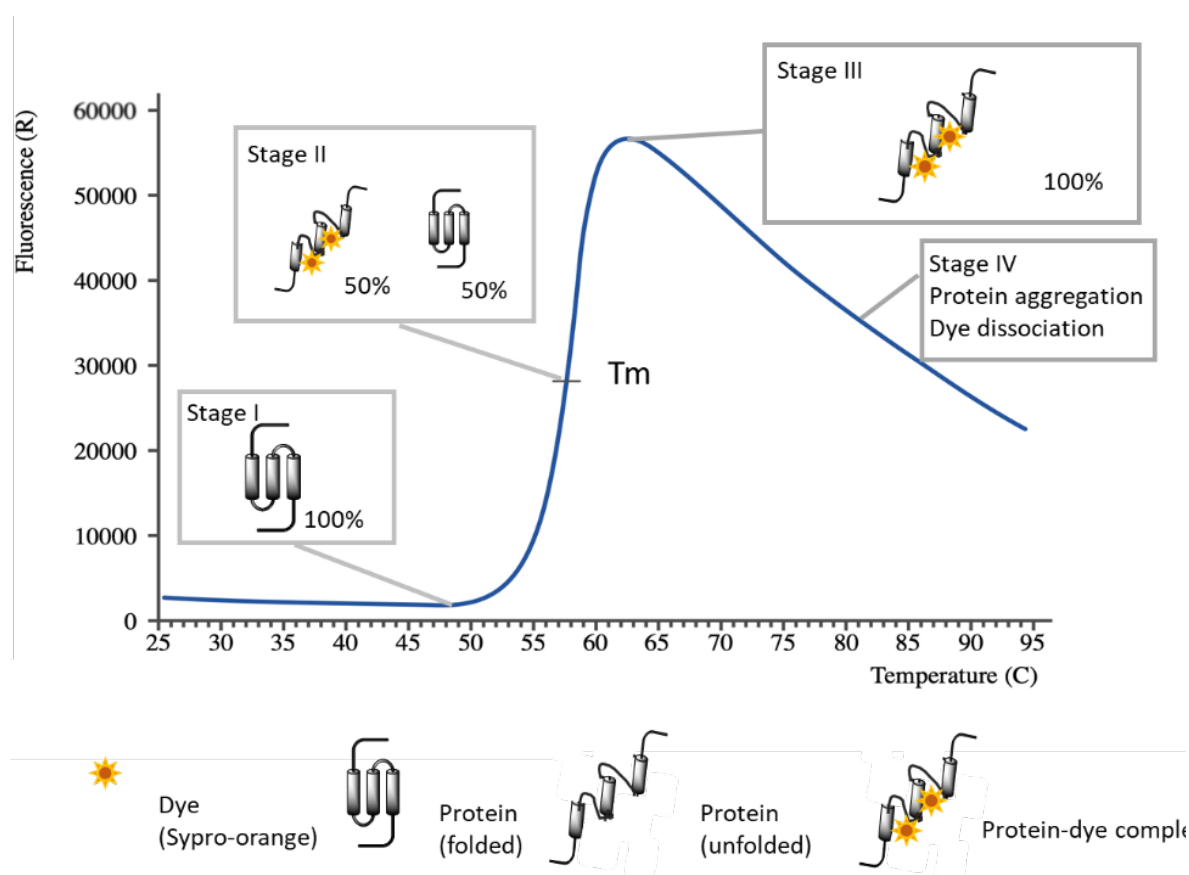


Figure 13. A protein thermal denaturation curve. In stage I, protein samples are all in the folded form and the dye (sypro-orange) is quenched by aqueous buffer. With temperature increase, proteins start to unfold, which allows sypro-orange to bind to the hydrophobic core and gives a fluorescence signal. When 50% of the proteins are melted in stage II, the temperature is defined as T_m . With the temperature continues increasing, the percentage of protein samples in unfolded form is also increasing till the fluorescence signal reach to the peak where the proteins are all in complex with the dye (stage III). After that, protein started to aggregate with dye dissociation reflecting as fluorescence signal decrease (Stage IV).

With the addition of ligand samples, the protein thermodynamic equilibrium ($\text{Native} \rightleftharpoons \text{Denatured}$) is moved towards one side with the ligand binding equilibrium ($\text{protein} + \text{ligand} \rightleftharpoons \text{Protein-ligand complex}$). If ligands stabilize the protein, it manifests as an increasing of $T_{m_{\text{ligand}}}$ with a positive ΔT_m value. The calculation of ΔT_m is calculated using the equation (5) shown below:

$$\Delta T_m = T_{m_{\text{ligand}}} - T_{m_{\text{DMSO control}}} \quad (3)$$

Where, $T_{m_{\text{ligand}}}$ is the protein melting point with the addition of ligand sample. $T_{m_{\text{DMSO control}}}$ is the protein melting point with the addition of DMSO as control.

It has been accepted that ΔT_m values correlated with hit-likeness shown below¹²⁴:

- **For more druggable ligand binding site:**

$\Delta T_m > 2.5$ °C: strong hit

1 °C $< \Delta T_m < 2.5$ °C: medium hit

0.5 °C $< \Delta T_m < 1$ °C: weak hit

- **For less druggable ligand binding site:**

$\Delta T_m > 1.5$ °C: strong hit

0.5 °C $< \Delta T_m < 1$ °C: medium hit

0.2 °C $< \Delta T_m < 0.5$ °C: weak hit

The TSA experiment requires less protein compared with ITC experiment and is able to work on a 96-well plate format with approximately 90 minutes per run on a q-PCR instrument.¹²⁵ Therefore, TSA is suitable for fragment libraries screening. However, TSA is not as accurate as an ITC experiment and cannot provide thermodynamic parameters such as K_D or ΔH values. Proteins or the dye aggregation can lead to false positive or negative results and therefore TSA is more accurate in detecting strong hits with affinity in the range of 1 nM- 100 μ M. Fragment hits selected from TSA tend to require a cross validation using another biophysical method to exclude false positives.^{124, 126,127}

1. 6. 3 Surface plasmon resonance (SPR), NMR and X-ray crystallography

There are some other biophysical methods commonly used in detecting fragment binding interactions, such as SPR and ligand- or protein- observed NMR. Surface plasmon resonance (SPR) is a very sensitive biophysical method measuring changes in molecular weight in real time. The SPR biosensor contains a glass prism with a biocompatible coated gold film with one of the components (either protein or ligand) immobilised to it through different kits such as histidine tagging whilst another binding component in solution is passed over. When an optical beam is directed at the gold surface, the change in the angle or intensity of reflection index can be used to determine the compound binding interactions shown in **Figure 14**.^{128, 119}

SPR is a very powerful screening method, which is able to determine both drug-sized and fragment-sized ligand binding and provides affinity (K_d) and kinetic measurements (the association rate constant K_{on} , and the dissociation rate constant K_{off}). SPR experiments are suitable for fragment library screening as up to 8 samples can be screened at the same time with each run taking 3-10 mins.^{128, 129} However, SPR method does not provide detailed molecular binding mode or thermodynamic parameters, such as ΔG or ΔH . The detection of fragments binding to the protein targets can also be difficult due to the large molecular size differences.

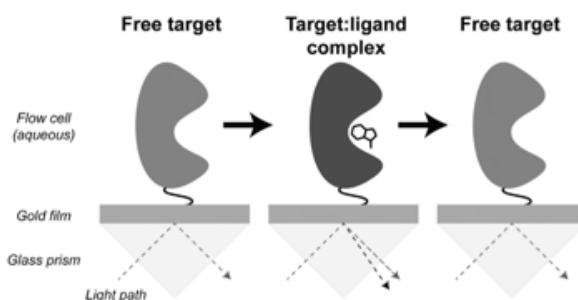


Figure 14. SPR interaction sensor scheme.¹²⁸

NMR methods are highly recommended in fragment screening as they are sensitive enough to detect weak binding with an affinity range from 100 nM to 1 mM¹²⁹ and both ligand-observed and protein-observed NMR are widely used. Ligand-observed NMR detects the changes of ligand signal in terms of intensity, sign and relaxation. It requires tens of milligrams of unlabelled protein and is able to maintain protein and ligand sample integrity. The main limitation for ligand-observed NMR is the limited structure information obtained, i.e. it cannot provide detailed information on ligand-protein binding mode.^{130, 131}

Protein-observed NMR detects the changes of isotopically labelled protein signals and generally requires 2D ¹H-¹⁵N HSQC (heteronuclear signal-quantum correlation/coherence) experiments. In ¹H-¹⁵N HSQC spectrum, each amide on the backbone of the protein sample yields a peak and is sensitive to local chemical environment, especially to ligand binding.^{128,130} Detailed structure binding information can be obtained from the sequence-specific assignments of the protein¹³², which is useful in detecting fragments binding in allosteric sites. However, the size of the protein should be less than 40 kDa otherwise the amide signals can be very broad due to slower tumbling time.¹¹⁹

X-ray crystallography is a very informative method and provides detailed binding modes of fragment hits despite low binding affinity. It allows rapid assessment to decide which fragment is able to progress into hit-to-lead chemistry. There are two main methods to obtain crystals of protein-ligand complexes, which are soaking and co-crystallization.¹³³ The co-crystallization method requires the exposure of ligands to protein solutions allowing the ligand-protein complex crystallized. The soaking method

is more commonly used which requires the exposure of pre-manufactured protein crystals to ligand solutions.^{133–136}

1.6.4 Computational methods

Well-developed biophysical and biochemical experimental techniques are able to confirm ligand-protein binding interactions but are very expensive and time-consuming, particularly in fragment library screening where hundreds of fragments need to be tested. In contrast, *in silico* methods significantly decrease financial and time investment and are now widely applied in the FBLD process.^{111,137,138}

Taking the advantages of the protein three-dimensional structural information in the Protein Data Bank (PDB), computational methods are applied in fragment library virtual screening and fragment evolution simulation.¹³⁹ In these experiments, fragments can be docked into selected regions on the macromolecule and ranked according to docking scores. It should be noticed that grid-based algorithms tend to lack the description about protein flexibility and thermodynamic parameter calculations, which lower accuracy of the docking results.^{140, 95,141–146} It is common to use biophysical and/or biochemical experiment after *in-silico* experiments to cross validate those fragments with a high docking score.^{142,144,147}

1.7 Fragment evolution methods

Once the fragment hits have been selected, there are three main fragment evolution methods, which are fragment growing, linking, and merging. As the name suggests, fragment growing methods involve using structure-based approaches to guide fragment size increase to obtain new binding interactions and/or occupy new pockets. The fragment growing method is the most used strategy. To date, there are in total 46

clinical candidates or drugs which have their origins from fragment-based approaches and used fragment growing methods.¹⁴⁸ The fragment linking method describes joining two non-competitive fragments through a linker. Fragment linking methods are the most attractive method as the resulting compound normally shows a significant enhancement in potency and affinity. However, the design of an appropriate linker can be quite challenging and generally requires structure characterization of the target protein.

Fragment merging methods describes combining two fragment hits together, which are partially overlapping in terms of their ligand binding sites. This method strongly relies on high quality crystal structures and careful structure based design⁸⁰ and there is only one clinical candidate (**14, AZD5991**) acting as a myeloid cell leukemin-1 (Mcl-1) inhibitor using a fragment merging method to guide the hit-to-lead optimization process (**Figure 15**).^{149, 150}

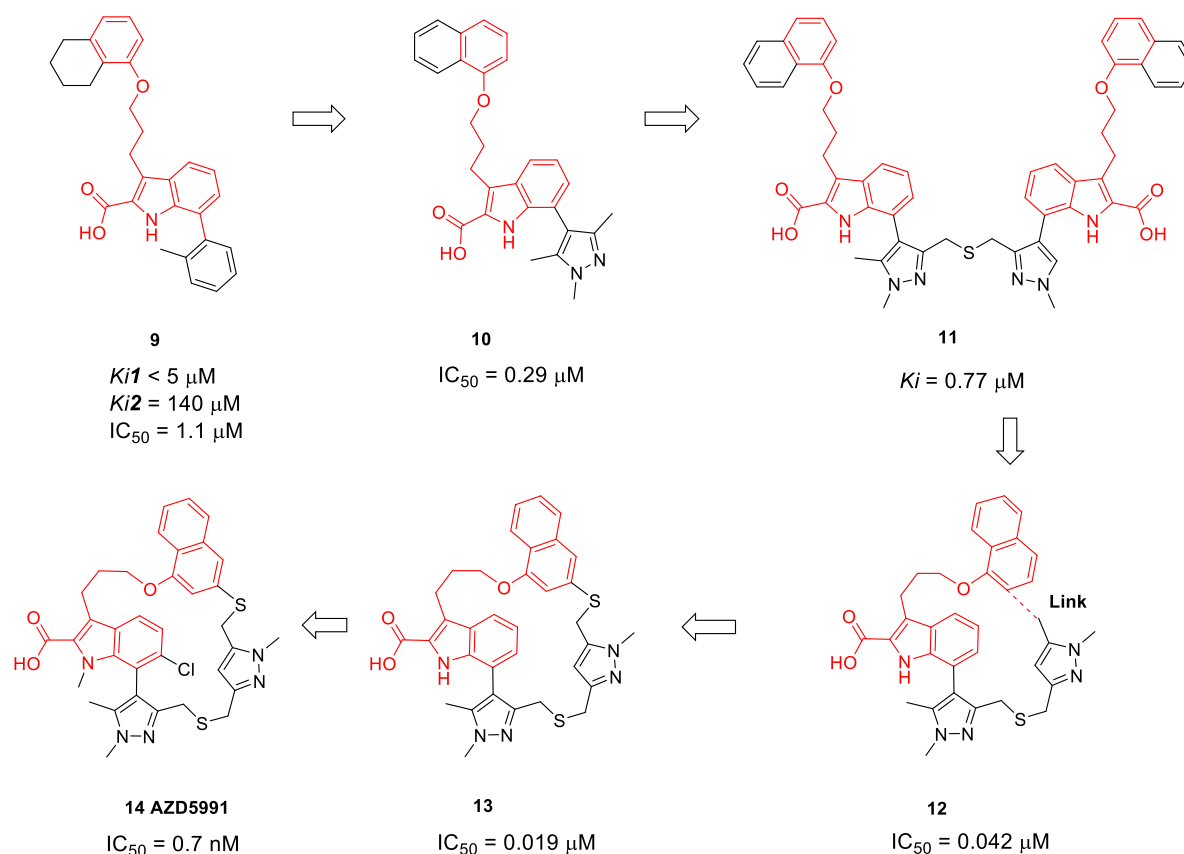


Figure 15. Development of a microcyclic Myeloid cell leukemin-1 inhibitor, **AZD5991** from fragment **16-Mcl-1** and **17 Mcl-1**. **9** was initially found as an active lead compound for the project of finding Mcl-1 inhibitor from AstraZeneca. The crystallography experiment revealed that myeloid cell leukemin-1 (Mcl-1) bound with two molecules of **9** in the same binding pocket but different sites. One of the **9** molecule enlarged the binding pocket that allowed the second **9** to fit into the pocket. This finding suggested that the hybrid compound from merging the two molecules of **9** can show improved potency because of better occupancy of the binding pockets. Compound **10** showed better physicochemical properties than **9**, was selected as the monomer and built into a hybrid compound **11**. The hybrid compound **11** didn't show improved potency compared with **10**, however, the by-product **12** showed improved Mcl-1 inhibition. The crystallography data revealed that the tethered ring enlarged the binding pocket, which was similar to the previous **9**. **13** showed improved affinity and finally lead to the identification of clinical candidate **14**, AZD5991.^{150, 149, 151}

1.8 Using a fragment-based approach to find *pqs* inhibitors

Finding novel *pqs* inhibitors for the treatment of *P. aeruginosa* infections has been a focus of current research. There is only one publication to date that describes using fragment growing methods to find *pqs* inhibitors shown in **Figure 16**.¹⁵²

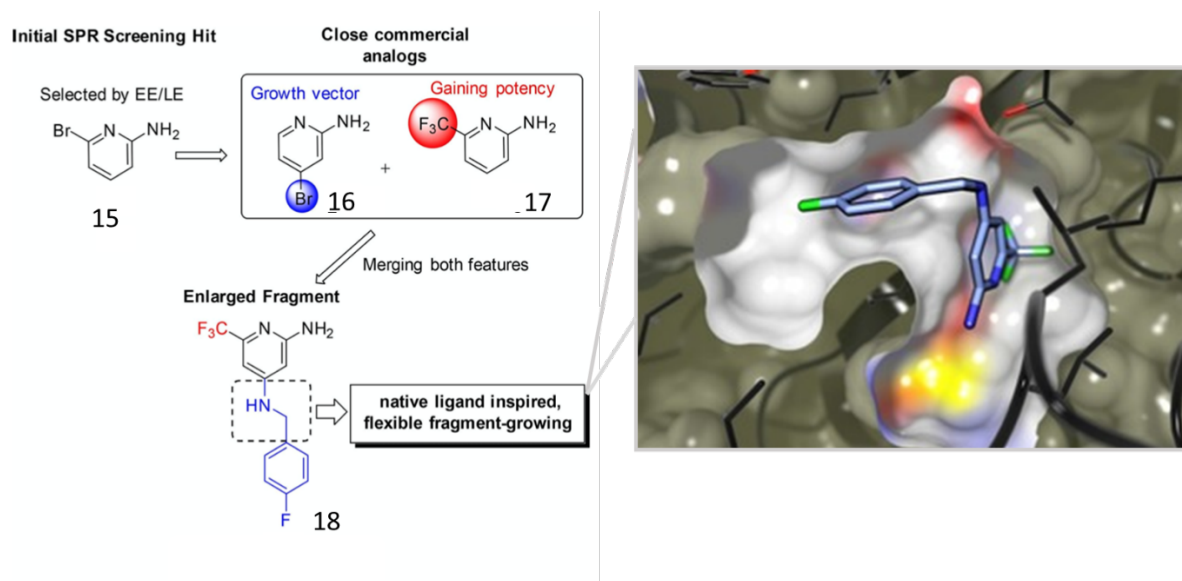


Figure 16. Schematic description of hit-to-lead optimisation starting from fragment **15** to final active inhibitor **18** and crystal structure of **18** in complex with PqsR LBD.¹⁵²

In this work, different biophysical screening methods (SPR and ITC) were used to detect and confirm fragment binding. Based on LE and EE values (based on ITC experiments), the low affinity compound **15** was selected as the hit. SAR studies were then conducted around fragment **15** and fragment growing methods were used to guide hit-to-lead optimization giving compound **18** as a potent PqsR inhibitor ($IC_{50}=5.9 \mu\text{M}$).¹⁵² This work provide confidence for the focus of this thesis, which is to use fragment-based approaches to discover novel *pqs* inhibitors.

1.9 Aims and hypothesis

P. aeruginosa infections and the associated multidrug resistance issue has become a serious public health threat and *pqs* inhibitors acting as anti-virulence agents are able to cure *P. aeruginosa* infections and relieve antibiotic resistance situation.^{31,153} In this work, different hit-to-lead discovery and optimisation methods were attempted for the identification of novel PqsR antagonists to overcome *P. aeruginosa* infections.

In previous work from our group, compound **19** was identified through a virtual screening of an in-house compound library against PqsR ligand binding domain (LBD) followed by an *in vitro* PAO1-PpqsA-lux reporter gene assay ($IC_{50} = 0.98 \mu\text{M}$). Compound **19** displaying good hit-likeness was selected as hit compound and can act as the starting point for the hit-to-lead optimisation process (**Figure 17**).

The protocols for the purification and crystallization of PqsR LBD were published, which provides opportunities to investigate compound binding modes through ligand-protein complex crystals.

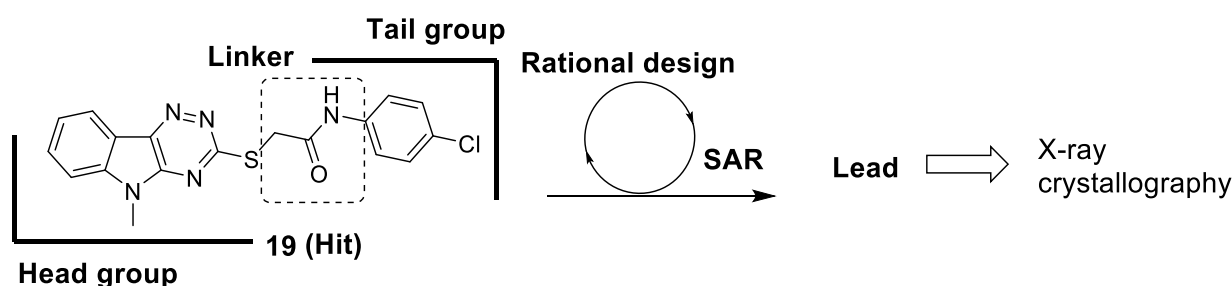


Figure 17. The proposed workflow of the hit-to-lead optimisation workflow starting from compound **19**.

Fragment-based methods was then applied for identification of novel PqsR antagonists inspired by literature compound **18**. *In silico* method was introduced for fragment libraries screening against PqsR LBD and the resulting fragment hits can be validated using bioreporter assay and biophysical methods, such as TSA and ITC. Through hit exploration studies around the initial hits, chemistry starting points can be confirmed for later fragment evolution. The ultimate aim in this fragment-based method guided project was to advance fragment hits using fragment growing, linking and merging methods into drug-sized PqsR antagonists ($300 < \text{Mwt.} < 500$) (**Figure 18**).

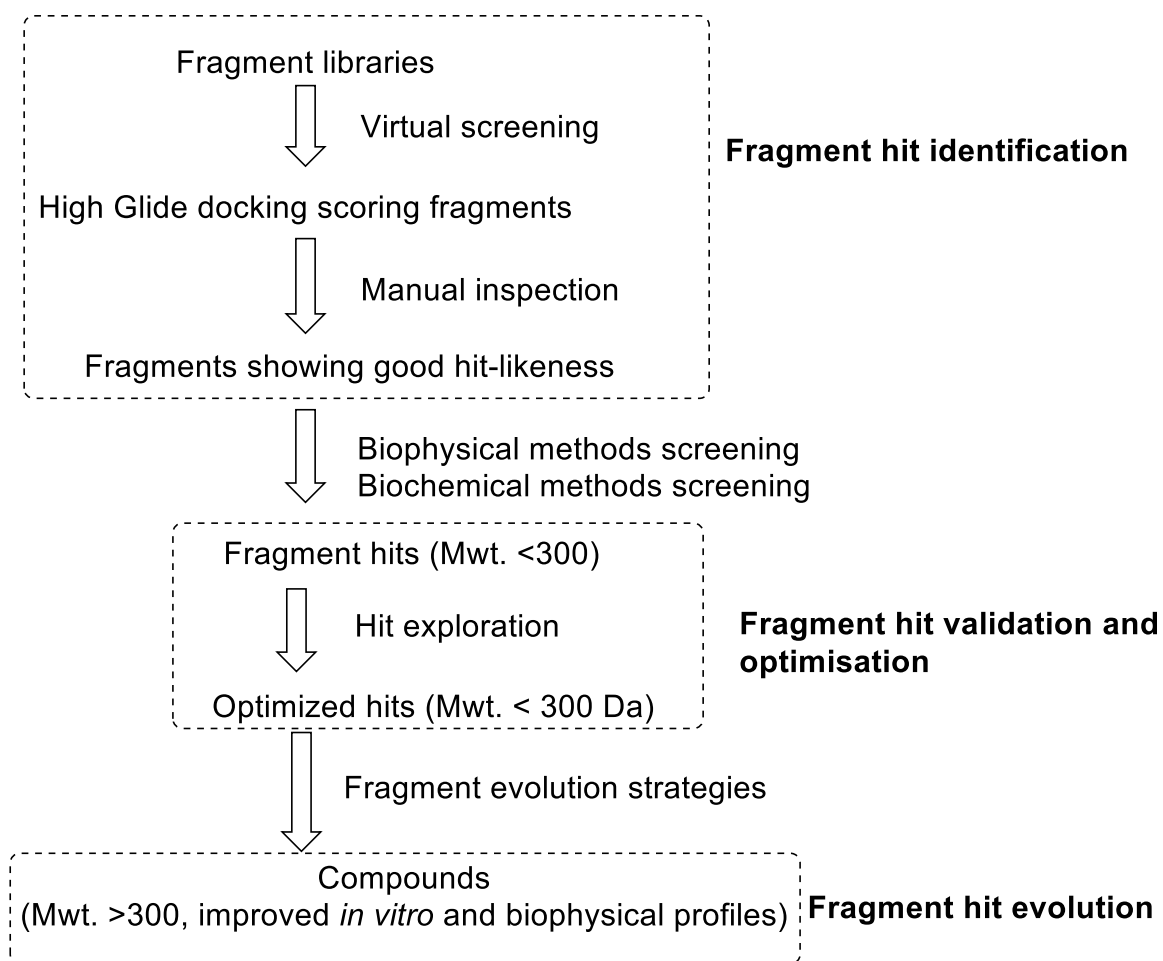


Figure 18. Proposed workflow of the fragment-based lead discovery approach starting from virtual screening of fragment libraries against PqsR LBD.

Chapter II: Hit to lead optimization of new potent PqsR antagonists as inhibitors of quorum sensing in *Pseudomonas aeruginosa*

2.1 Introduction and project aims

In previous work, a virtual screen on the PqsR ligand binding domain against the University of Nottingham Medicinal Chemistry Compound Collection (MCCC) - an in-house compound library containing approximately 80,000 compounds was conducted by Dr. Fadi Soukarieh using Glide HTVS (high throughput virtual screening). The cut-off filter docking score was set as -9.0 where the GlideScore is a scoring function to predict compounds affinity and the virtual hits satisfying these criteria were subjected to a PAO1-L mCTX::P_{pqsA}-lux luminescence-based bioreporter assay, which led to the discovery of **19** a moderate PqsR antagonist (IC₅₀ = 0.98 μM) (**Figure 19**).

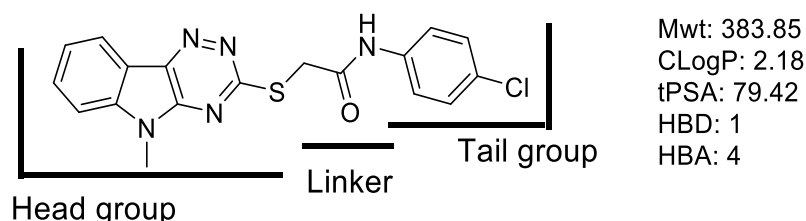


Figure 19. The structure of hit compound **19**.

The mCTX::P_{pqsA}-lux-based bioreporter was used in both the parent strain of *P. aeruginosa* (PAO1-L) and the more clinically relevant PA14 strain for the evaluation of the compound *pqs* inhibition in this thesis. PAO1-L strain is a derivative of the original Australian PAO isolate, whilst PA14 is a hypervirulent strain isolated from a patient with burn infection.¹⁵⁴ It has been shown that *P. aeruginosa* strain PA14 is more virulent than PAO1-L in diverse infection models, which could result from horizontal

gene transfer of the two pathogenicity islands, PAPI-1 and PAPI-2.¹⁵⁵ The whole-cell based bioreporter assay was designed through the insertion of miniCTX::*PpqsA::luxCDABE* bioreporter into the chromosome of the *pqsA* mutant PAO1-L and PA14 strains. The activation of *pqs* system initiates the transcription of *pqsA::luxCDABE* and leads to the expression of the LuxCDABE protein, which produces the bioluminescent luciferase. The growth and bioluminescence of the strains can be monitored using microplate readers and compound *pqs* inhibitory activity was evaluated through the remaining activity (RA%), which is the ratio of Δ luminescence (the detected luminescence of compound minus the DMSO control) over OD600 (the strains optical density at 600 nm).^{156–159}

Through the miniCTX::*PpqsA::luxCDABE* based bioreporter assay, the activation or inhibition of the *pqs* system can be monitored. In this work, PAO1-L and PA14 strains were treated with a 10 μ M compound solution and compounds showing a *pqs* activity reduction greater than 50% (i.e. RA% < 50%) were regarded as being active. Compound **19** was active against PAO1-L with a IC₅₀ value of 0.98 μ M, whilst it was inactive against PA14 strain (RA% = 73%). Due to solubility limitation, binding affinity of compound **19** against PqsR LBD cannot be obtained through ITC method. However, the initial virtual screening was conducted against PqsR LBD and the later TSA and X-ray crystallography experiments proved the binding of the 5-methyl-5*H*-[1,2,4]triazino[5,6-*b*]indol-3-yl)thiol analogues to PqsR LBD. These results suggested that the 5-methyl-5*H*-[1,2,4]triazino[5,6-*b*]indol-3-yl)thiol analogues can function as PqsR antagonists.

Compound **19**, contains a (5-methyl-5*H*-[1,2,4]triazino[5,6-*b*]indol-3-yl)thiol head group, a 4-chlorophenyl substituted tail group, and an acetamide linker. It displays

good physicochemical properties including moderate lipophilicity reflected as calculated partition coefficient, (ClogP), topological polar surface area (tPSA) and hydrogen bond donor/acceptor (HBD/HBA) values (**Figure 19**). According to the 'Lipinski rule of five' (Ro5), which is commonly used for the evaluation of molecules optimal physicochemical properties⁹⁹, **19** shows good hit-likeness and was subsequently selected as a hit.

Docking studies were conducted to predict the binding mode of **19** against the PqsR LBD using Glide SP (standard precision) (force field: OPLS3e; PDB: 4JVD). According to the docking study, **19** can occupy the PqsR LBD with two potential binding modes with flipped orientations (**Figure 20B** and **C**). The X-ray crystal of the 5-methyl-5*H*-[1,2,4]triazino[5,6-*b*]indol-3-yl)thiol analogue compound **69** in complex with PqsR LBD was obtained (**Figure 20A**), which will discuss in details in later in this chapter. Comparing the predicted binding mode of **19** with the **69**-PqsR LBD crystal complex, it was noticed that the 5-methyl-5*H*-[1,2,4]triazino[5,6-*b*]indol-3-yl)thiol head groups of compound **19** and **69** were pointing towards different direction (**Figure 20A** and **B**). This finding suggested that the docking study of compound **19** may not be accurate for the prediction of ligand binding modes, whilst docking study can still be a powerful method to guide analogues SAR study design.

In this work, a hit-to-lead optimisation workflow was presented including design, synthesis, and biological evaluation of a series of novel PqsR inhibitors and was published in *Frontiers Chemistry* 04 May 2020 (doi.org/10.3389/fchem.2020.00204).¹³

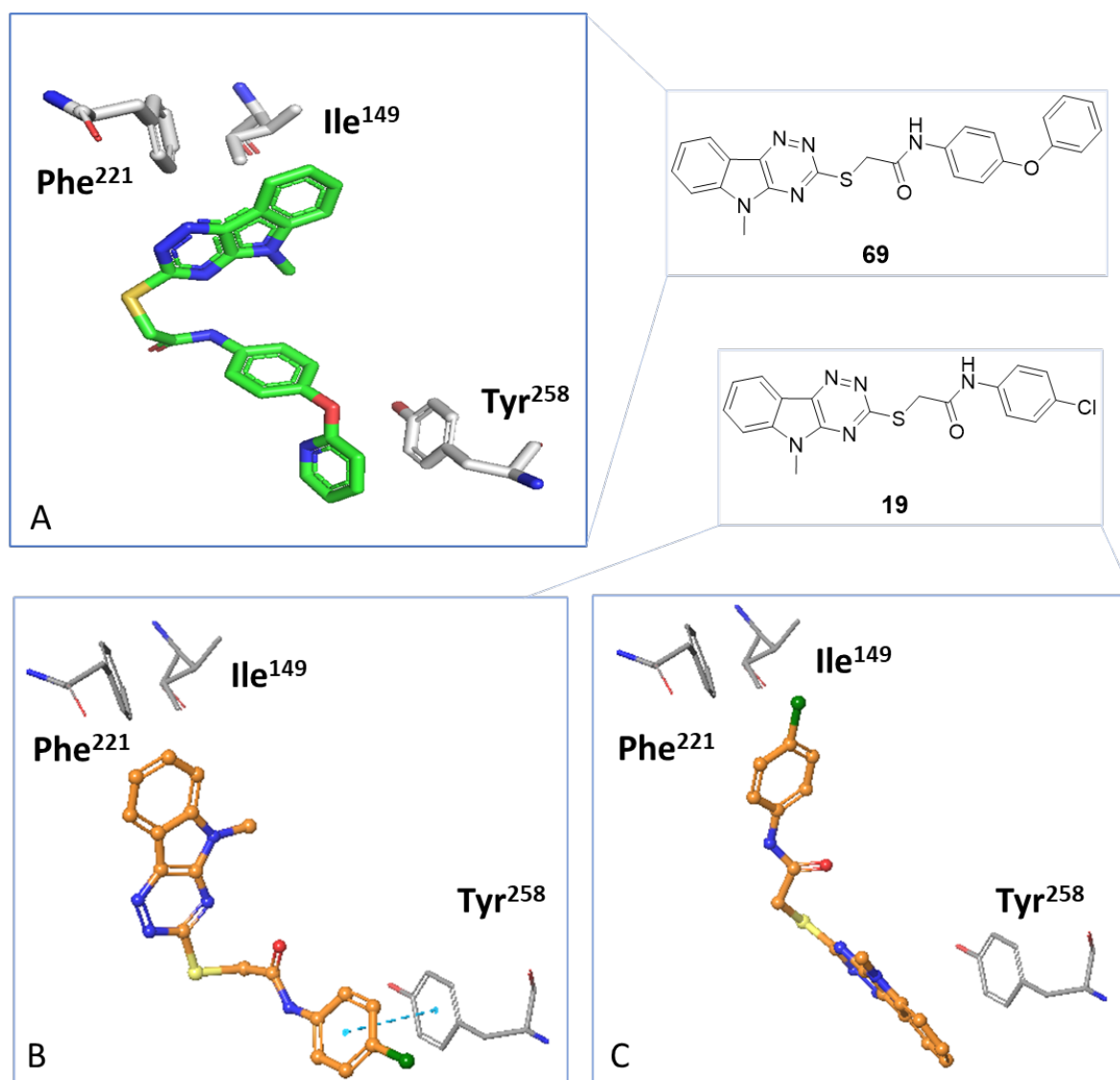


Figure 20. (A) The X-ray crystallography data of **69** in complex with PqsR LBD. (B and C) Three-dimensional diagram of predicted binding mode for **19** against PqsR LBD (PDB 4JVD). The docking shows that **5d** can fit into the PqsR LBD in two possible modes. (B) The head group inserts deeply in the binding site, whilst the terminal aryl group points outside of the pocket π -stacking with Tyr²⁵⁸. (C) The aryl tail group inserts deeply in the binding pocket and the head group points outside the pocket π -stacking with Tyr²⁵⁸. The scaffold structure of **19** is represented in orange. The scaffold structure of **69** is represented in green. The blue dashed line indicates a π -stacking interaction.

2.2 Hit-to-lead optimisation process

2.2.1 The first SAR study around **19**

2.2.1.1 The design of the first SAR study around **19**

Compound **19** showing moderate *pqs* inhibition against PAO1-L and good hit-likeness was selected as a hit and advanced to the hit-to-lead optimisation process. According to docking studies, **19** binds to the PqsR ligand-binding site and leaves significant empty space allowing further modification around **19** (**Figure 21**). Increasing the ligand binding pocket occupancy by introducing substituents on **19** may lead to a more favourable shape complementarity or allow it to probe new binding interactions. Based on this hypothesis, the first SAR study was designed in which the tail group (R_2) was modified as well as the 8-position of the tricyclic head group (R_1). Based on the structural differences of R_1 , the designed analogues were classified into three series: $R_1 = H$ (series 1), $R_1 = Br$ (series 2) and $R_1 = OMe$ (series 3).

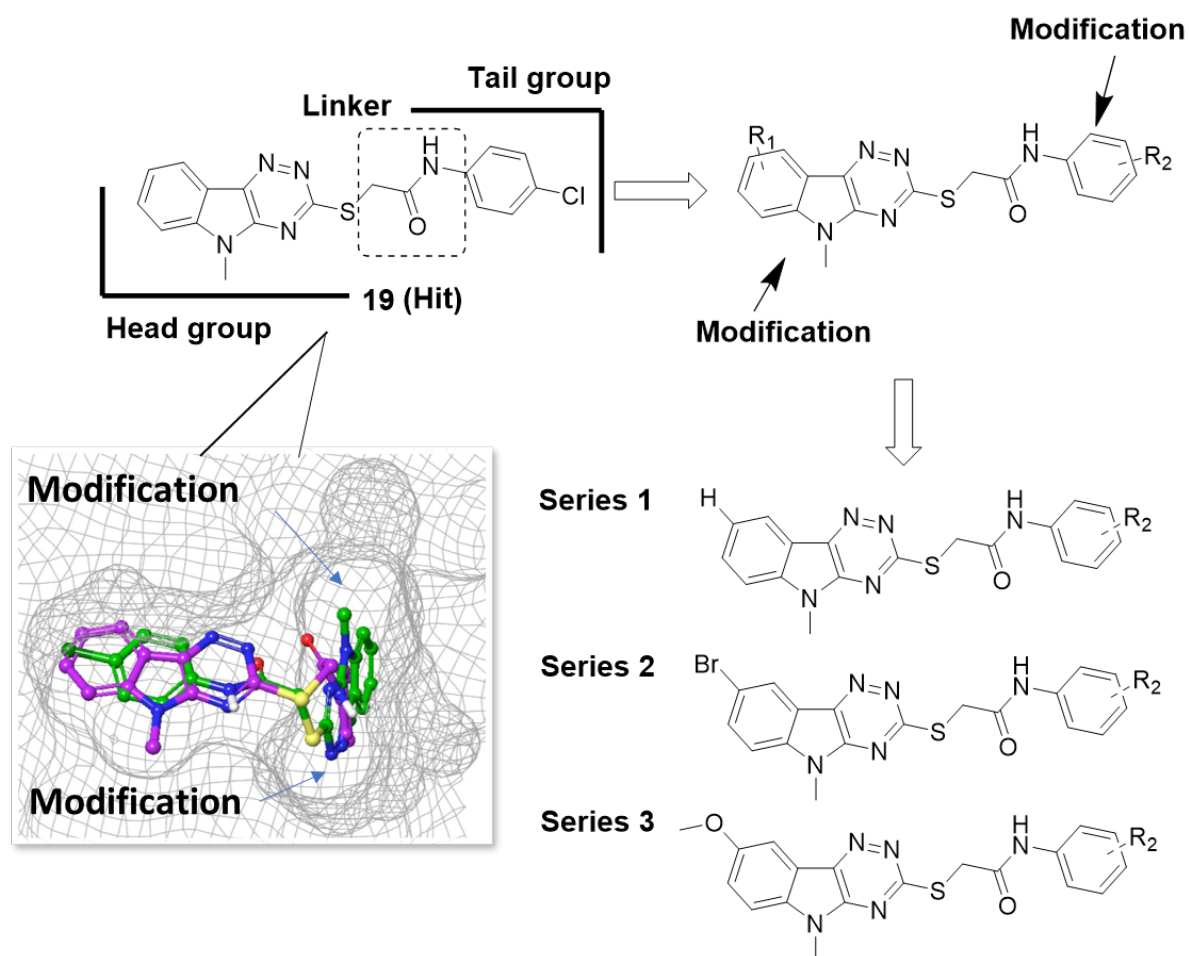


Figure 21. The design of the first SAR study. The docking study shows the possible binding orientations of **19** in the PqsL LBD. The SAR study initially focused on modifying the aryl tail group and the 8-position of the tricyclic head group. In the first series analogues, the head group was initially kept unsubstituted (R₁=H) and a set of diverse tail groups (R₂) were explored. Once finished the design and synthesis of series 1 analogues, different substituents including electron donating (OMe) and withdrawing (Br) groups were introduced to R₁, which allowed to investigate the influence of substituents on the head group.

2.2.1.2 The synthesis of series 1, 2 and 3 compounds in the first SAR study

1,2,4-Triazino[5,6-*b*]indole-3-thiol derivatives have been well documented for their pharmaceutical potential, and have been used in anticonvulsant¹⁶⁰, antiviral¹⁶¹, antimalarial¹⁶² and antileishmanial¹⁶³ inhibitors. In recent publications,¹⁶⁴ 1,2,4-triazino[5,6-*b*]indole-3-thiol analogues have been reported to display antibacteria and antifungal activity against *P. aeruginosa*^{163–165} (**Figure 22**). The functionalization of

1,2,4-triazino[5,6-*b*]indole-3-thiol derivatives has been well studied and in this work the synthetic routes for the preparation of the 1,2,4-triazino[5,6-*b*]indole-3-thiol analogues are shown in **Scheme 1** and **2**^{163,166–168}.

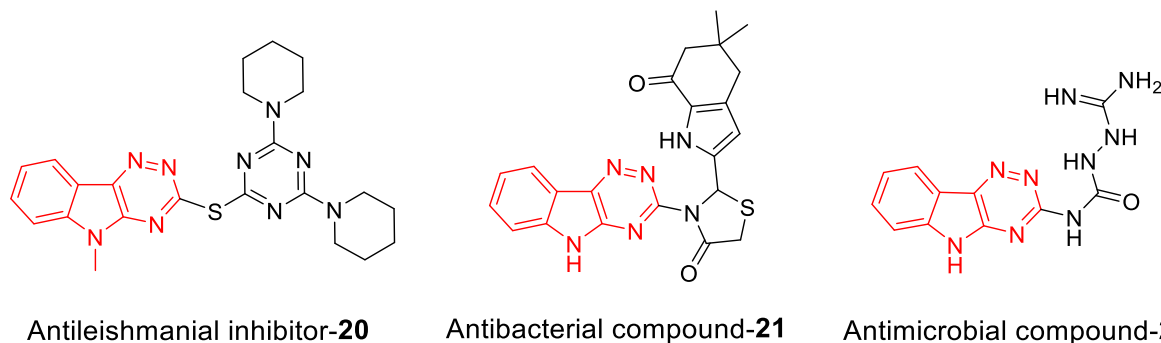
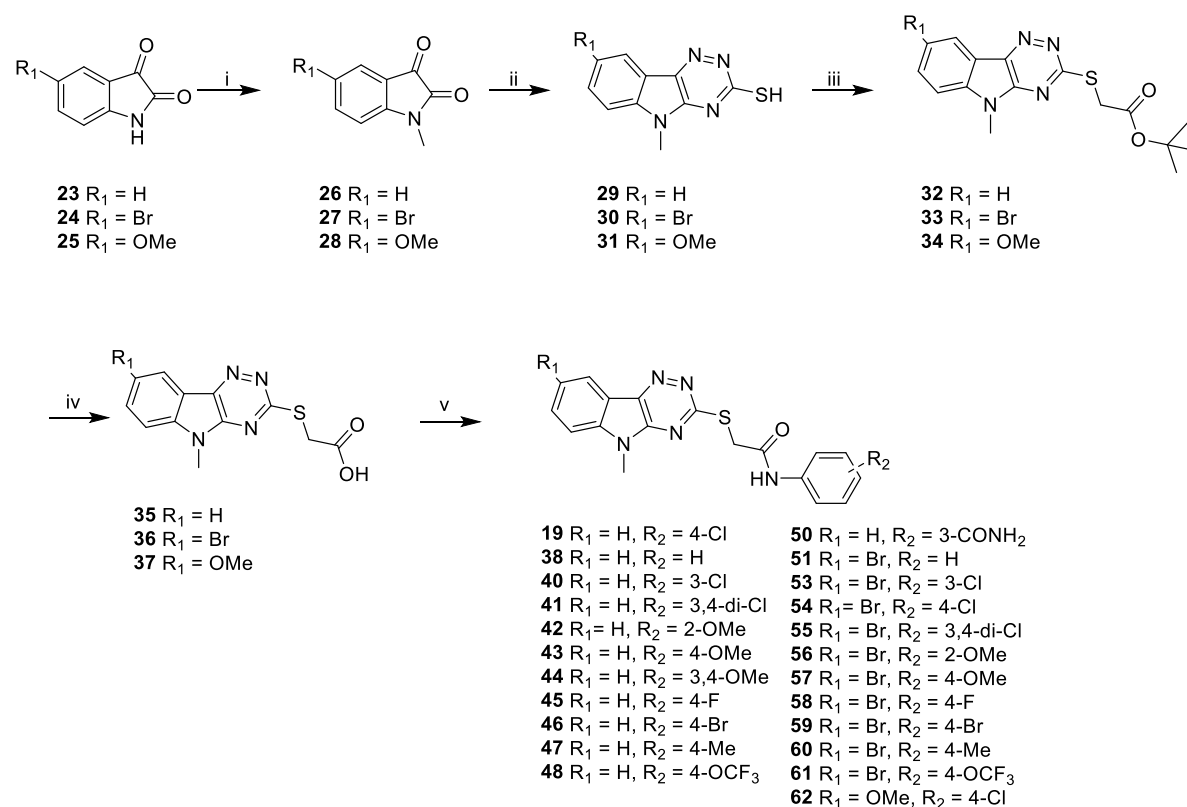


Figure 22. Literature 1,2,4-triazino[5,6-*b*]indole-3-thiol derivatives showed therapeutic potential.^{163–165}

The forward synthetic scheme for the majority of the 1,2,4-triazino[5,6-*b*]indole-3-thiol analogues is depicted in **Scheme 1**. 5-Substituted *N*-methylisatins **26–28** were obtained by methylation of isatin and its analogues **23–25** using CH_3I and NaH in *N,N*-dimethylformamide (DMF) under an inert atmosphere of N_2 . Compounds **26–28** were then cyclised by thiosemicarbazide in the presence of K_2CO_3 base in 1,4-dioxane and H_2O at reflux to afford intermediates **29–31**. The intermediates **35–37** were synthesised through classic nucleophilic aromatic substitution reactions starting from **29–31** using *tert*-butyl-2-bromoacetate and Et_3N as base, followed by deprotection of the *tert*-butyl group using 4M HCl in 1,4-dioxane to achieve free acids **35–37**. The key intermediates **35–37** were then subjected to amide coupling reactions with a wide range of anilines using *N*-Boc-piperazine, 1-[*bis*(dimethylamino)methylene]-1*H*-1,2,3-triazolo[4,5-*b*]pyridinium-3-oxide hexafluorophosphate (HATU) as coupling reagent to give compounds **19**, **38**, and **40–62**.

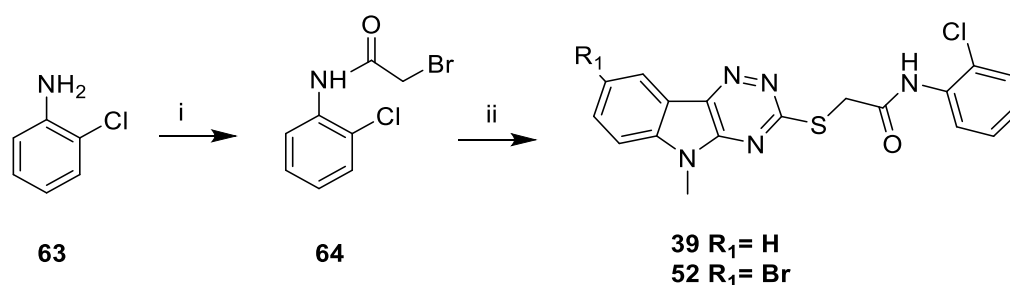
Scheme 1. Preparation of targeted compound 19, 38, 40-51, 53-62



^aReagents and conditions: (i) CH₃I, NaH, DMF, 0°C to rt, N₂, 73%-92%; (ii) thiosemicarbazide, K₂CO₃, Dioxane, H₂O, Reflux, 45%-96%; (iii) *t*-butyl-2-bromoacetate, Triethylamine (Et₃N), toluene, 0 °C to rt, 52%-88%; (iv) 4M HCl in dioxane, rt, >100%; (v) various anilines, HATU, 4-(dimethylamino)pyridine (DMAP), N,N-Diisopropylethylamine (DIPEA), *N*-methylpyrrolidone (NMP), rt, 13%-30%;

Ortho-chloro substituted aniline (**63**) failed in the amide coupling reaction with **35** due to a possible steric hinderance effect with the chlorine atom. Therefore, the preparation of **39** and **52** were using **Scheme 2** starting from alkylation of **63** using bromoacetyl chloride followed by nucleophilic substitution with **29** or **30** to give compound **39** and **52**, respectively.

Scheme 2 Preparation of target compound 39 and 52



^aReagents and conditions: (i) Bromoacetyl chloride, Et₃N, dichloromethane (DCM), 0 °C to rt; (ii) Et₃N, DCM, 0 °C to rt.

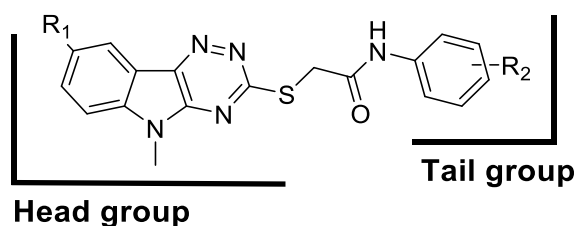
2.2.1.3 The initial structure-activity relationship (SAR) study around the head and tail groups for *pqs* inhibition

The synthesized analogues were then subjected to bioreporter assays for the determination of *pqs* inhibition. The SAR study showed that removal of the chlorine atom at R₂ (**38**), abolished biological activity demonstrating the importance of substitutions on the aryl tail group. Changing the chlorine atom from the *para*- position (hit, **19**) to the *ortho*- or *meta*- positions, **39** and **40** gave no inhibition against PAO1-L and PA14 strains when screened at 10 μM concentration. The 3,4-dichloro substituted analogue (**41**) showed reduced activity against both strains. These results demonstrated that the *para*-substituted chlorine analogue (**19**) was optimal for activity. The influence of introducing substituents at the *para*- position was then investigated.

Replacing the *para*- chlorine (**19**) with fluorine (**45**) caused a loss in activity against both strains. Introducing other electron withdrawing groups (EWGs), such as trifluoromethoxy (**48**) and bromine (**46**), retained activity against PAO1-L. Especially, the bromine substituted analogue (**46**) led to improved PA14 inhibition (IC₅₀ = 1.35 μM). Replacing the chlorine atom with a similarly sized but weakly electron-donating methyl substituent, **47** retained activity against PAO1-L.

Functional groups that can act as either HBD or HBA (amide group) and pure HBA (methoxy group) were also introduced to the aryl group. However, compounds **42-44**, **50** lost activity against both strains.

Table 2. The SAR around the head and tail group



	R ₁	R ₂	Remaining Activity (%) ^{a, b}		IC ₅₀ (μM) ^c	
			PAO1-L	PA14	PAO1-L	PA14
DMSO	/	/	100.00 ± 8.37	100.00 ± 3.87	-	-
Sen19 ^f	/	/	26.20 ± 10.33	24.57 ± 3.87	-	-
7 (M64^f)					0.32 ± 0.14	1.22 ± 0.34
19	H	4-Cl	32.98 ± 10.30	73.41 ± 24.52	0.98 ± 0.15	NA
38	H	H	80.26 ± 23.75	110.15 ± 16.28	-	-
39	H	2-Cl	76.13 ± 8.68	94.78 ± 13.54	-	-
40	H	3-Cl	93.27 ± 11.85	102.86 ± 8.57	-	-
41	H	3,4-di-Cl	71.10 ± 33.97	98.54 ± 9.83	-	-
42	H	2-OMe	62.57 ± 20.40	99.02 ± 6.90	-	-
43	H	4-OMe	79.46 ± 10.56	110.55 ± 19.23	-	-
44	H	3,4-di-OMe	73.90 ± 12.64	-	-	-
45	H	4-F	64.43 ± 9.14	86.31 ± 18.28	-	-
46	H	4-Br	16.83 ± 3.34	22.38 ± 7.58	1.71 ± 0.26	1.35 ± 0.19
47	H	4-Me	-	NA	1.86 ± 0.01	-
48	H	4-OCF ₃	28.71 ± 5.98	95.37 ± 9.13	-	-
50	H	3-CONH ₂	93.86 ± 15.39	-	-	-

	R ₁	R ₂	Remaining Activity (%) ^{a, b}		IC ₅₀ (μM) ^c	
			PAO1-L	PA14	PAO1-L	PA14
51	Br	H	66.21 ± 13.13	98.92 ± 4.46	-	-
52	Br	2-Cl	82.29 ± 15.52	101.68 ± 10.82	-	-
53	Br	3-Cl	42.76 ± 20.18	103.20 ± 9.94	-	-
54	Br	4-Cl	19.71 ± 10.34	17.21 ± 3.90	1.99 ± 0.23	1.60 ± 0.16
55	Br	3,4-di-Cl	17.22 ± 8.07	57.19 ± 18.51	3.1 ± 0.52	7.58 ± 0.82
56	Br	2-OMe	14.23 ± 2.10	24.46 ± 5.72	1.19 ± 0.24	7.36 ± 0.24
57	Br	4-OMe	64.46 ± 10.11	98.09 ± 15.64	-	-
58	Br	4-F	25.95 ± 11.51	73.81 ± 15.12	1.36 ± 0.21	-
59	Br	4-Br	22.65 ± 8.96	78.74 ± 29.54	-	-
60	Br	4-Me	31.82 ± 6.19	NA	-	-
61	Br	4-OCF ₃	22.85 ± 8.98	67.14 ± 21.16	-	-
62	OMe	4-Cl	55.84 ± 6.79	-	-	-

^aData shown are mean values obtained from three independent experiments performed in triplicates. ^b% Remaining Activity (RA%) screening at single concentration (10 μM) in triplicates. ^c The inhibitory effect evaluated using PAO1-LmCTX::PpqsA-lux and PA14mCTX::PpqsA-lux reporter assays. Remaining activity (RA%) values below 50%, compounds were regarded as active. RA% values do not have a linear relationship with IC₅₀. ^dNA : not active. ^e-: not available. ^f positive control. Sen19 is a PqsR antagonist with confirmed IC₅₀ and K_d values. The determination of RA% and IC₅₀ for compounds **7**, **19**, **38-62** was conducted by **Dr. Fadi Soukarieh**.

The effect of substitutions on the 8-position of the tricyclic head group was then investigated and interestingly, when R₁ is either bromine (**51-61**) or methoxy (**62**) compounds displayed a divergent SAR compared with analogues containing an unsubstituted head group (**19**, **38-50**).

Comparing **62** with the original hit **19**, demonstrated that introducing an electron donating methoxy group to R₁, whilst keeping R₂ as *para*-Cl, led to a decrease in *pqs* inhibition activity. Introducing a bromine atom to R₁, **54** retained a moderate *pqs*

inhibitory effect with IC_{50} values of 1.99 μ M and 1.60 μ M against PAO1-L and PA14 strains respectively.

Further SAR study on the 8-bromo-5-methyl-5*H*-[1,2,4]triazino[5,6-*b*]indole analogues showed that removal of the chlorine atom (**51**) reduced activity against both strains emphasizing the importance of substituents on R₂. Changing the chlorine atom from *para*- (**54**) to *ortho*- (**52**) or *meta*- (**53**) positions resulted in a significant decrease in *pqs* inhibition. The 3,4-di-Cl substituted analogue (**55**) was active against both PAO1-L and PA14 strains, which was inactive in the matched-pair analogue **41**. These results showed that the *para*- position on the aryl tail group can be optimal for introducing substituents compared with other positions. The tolerance of substituents at the *para*- position in relation to *pqs* inhibitory activity was then investigated.

Furthermore, replacing the chlorine atom with other EWGs, such as fluorine (**58**), bromine (**59**) or trifluoromethoxy (**61**) retained moderate *pqs* inhibitory effect against PAO1-L but were inactive against PA14. The *para*-methyl (**60**) and *para*-methoxy (**57**) analogues were weakly active against PAO1-L and inactive against PA14. It was also noticed that the *ortho*-methoxy substituted analogue (**56**) restored *pqs* inhibition with IC_{50} values of 1.19 μ M and 7.36 μ M against PAO1-L and PA14 strains respectively, whilst it was inactive in the matched-pair analogue **42**.

In the first SAR study, it was noticed that the 8-bromo-5-methyl-5*H*-[1,2,4]triazino[5,6-*b*]indole and 5-methyl-5*H*-[1,2,4]triazino[5,6-*b*]indole analogues demonstrated divergent SAR results. However, We did not find any compound showing improved activity against PAO1-L compared with **19** but analogues **46**, **54-56** displayed improved *pqs* inhibition against the more clinically relevant PA14 strain.

2.2.2 The second SAR study around the tail group to improve analogues' *pqs* inhibition

2.2.2.1 The design of the second SAR study

Given that analogues bearing an R_2 *para*- substituent displayed the best *pqs* inhibitory activity in the previous SAR studies, it was decided to further investigate SAR through introducing a set of substituents at the *para* position of the aryl tail group.

Assisted by docking studies, it was found that when R_2 was cyanomethyl and R_1 kept as hydrogen, the resulting compound **65** displayed the highest docking score (Glide SP, -8.850) among all compounds (**Figure 23**).

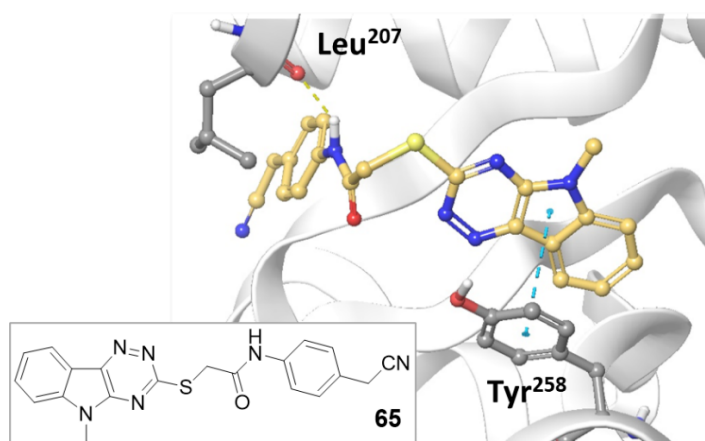


Figure 23. The predicted compound binding mode for **65** in the PqsR LBD. It suggested that the head group of **65** can have a π stacking with Tyr²⁵⁸, whilst the amide linker can act as HBD and hydrogen bond with Leu²⁰⁷. The yellow line indicates hydrogen binding. The blue line indicates a π - π stacking. The scaffold of **65** was represented in yellow.

Inspired by literature compound **7** in which the *para*-phenoxy group of **7** has a π stacking interaction with Tyr²⁵⁸, compound **66**, **67**, and **68** containing a *para*-phenoxy group were designed (**Figure 24**).

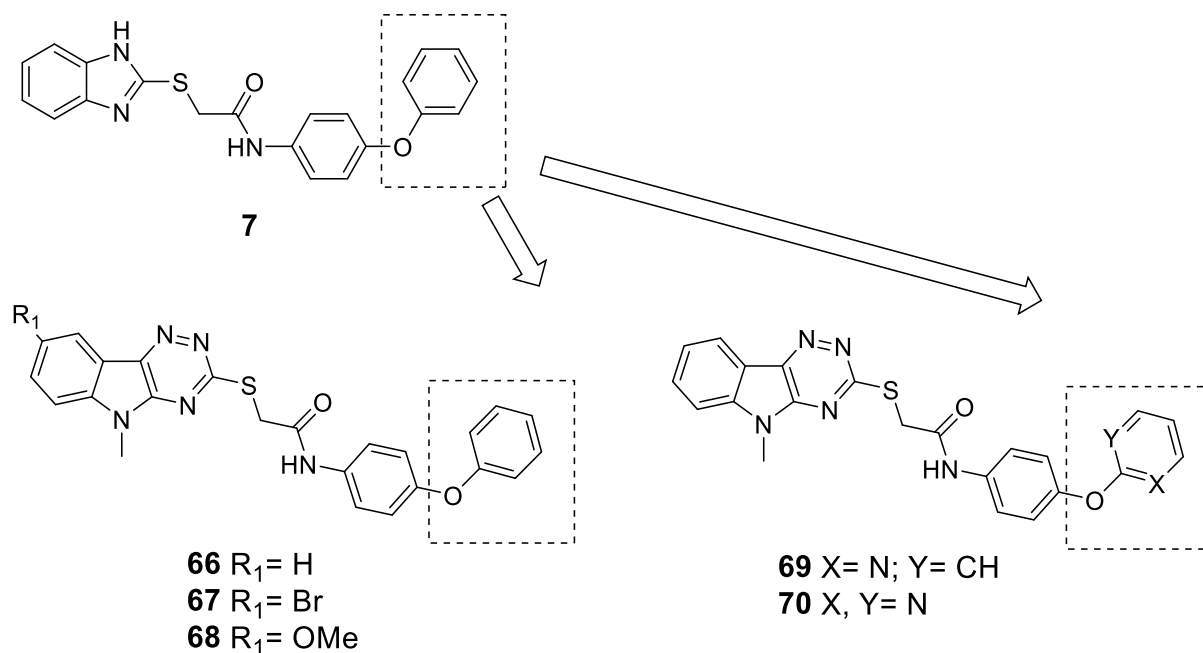


Figure 24. The structure of compound **7** and **66-70**.

Based on the high level of scaffold similarity between **7** and **66** and combined with docking studies, it was hypothesised that **66** may have a similar ligand binding mode to **7** in which the *para*-phenoxy group may also be able to partake in a π -stacking interaction with Tyr²⁵⁸ (**Figure 25**). Based on this hypothesis, compound **69** and **70** were designed to enhance this potential π -stacking by adding inductive electron-withdrawing nitrogen atoms for the design of electron deficient rings.

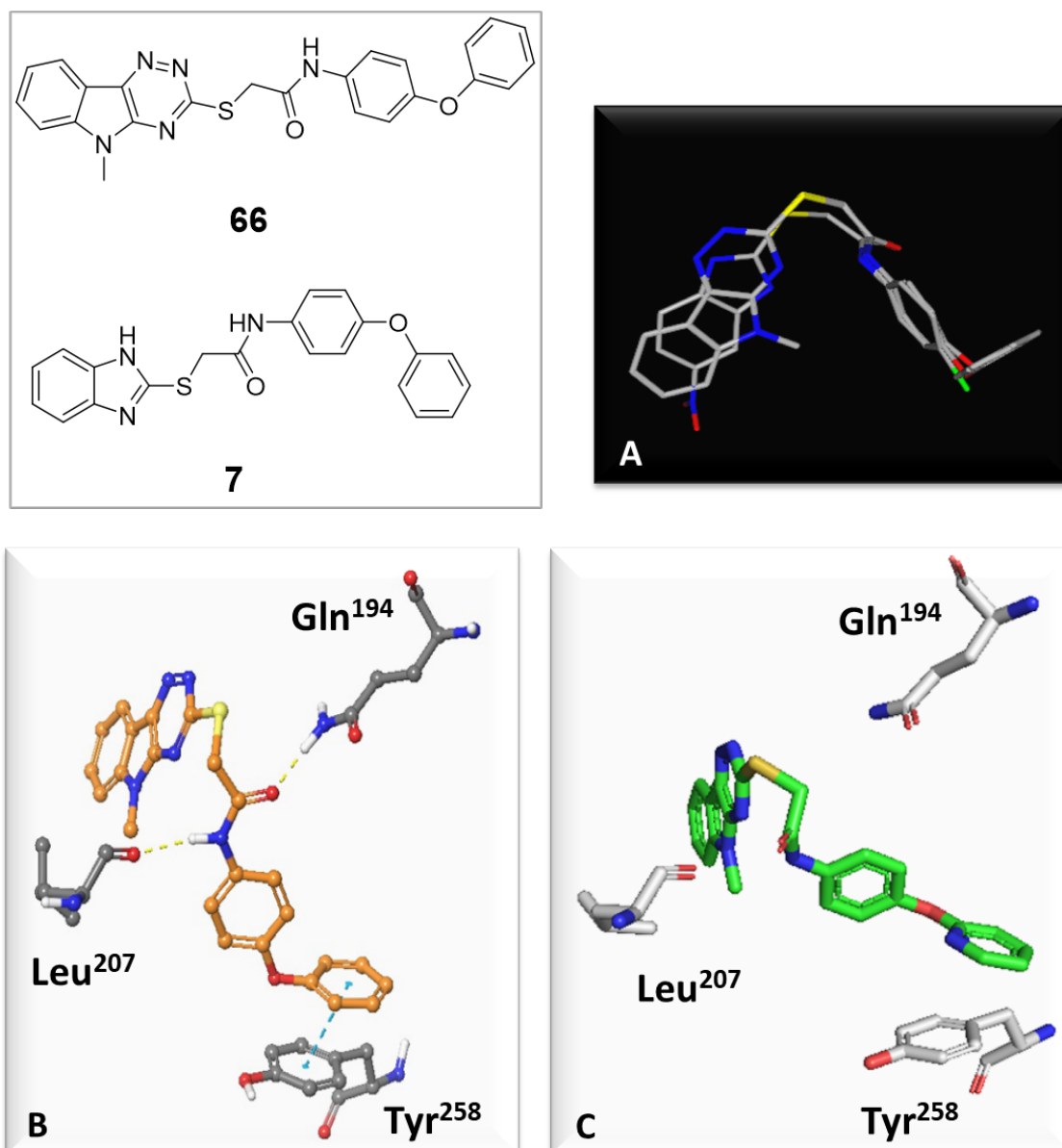


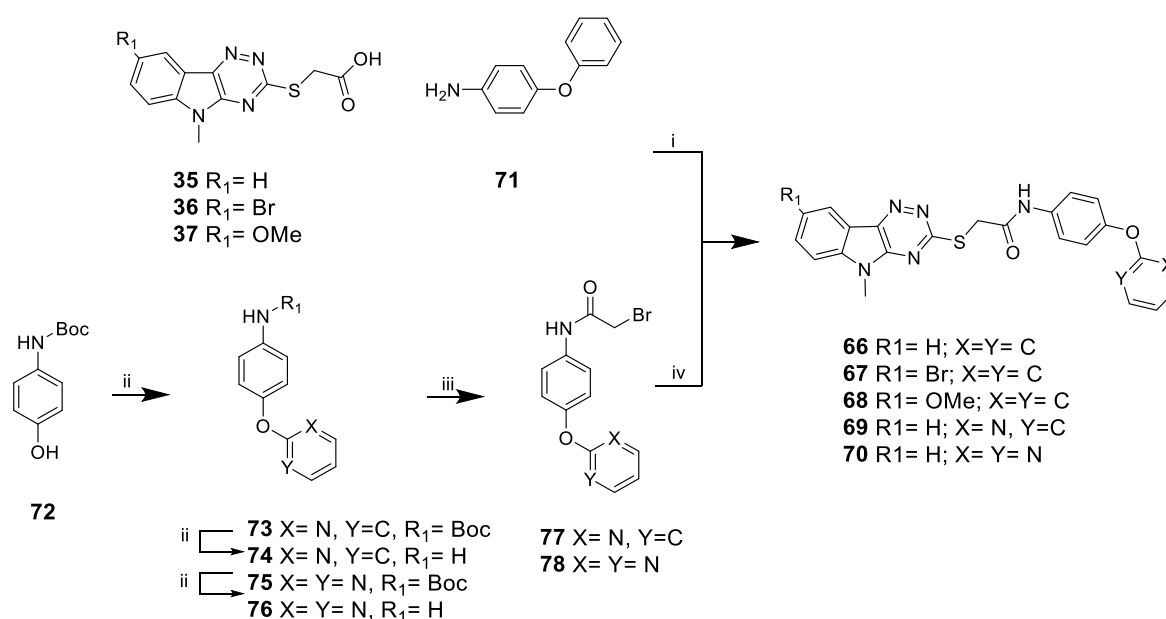
Figure 25. Structural comparison between **7** and **66** and predicted binding mode of **66** and X-ray crystal of **69**-PqsR LBD. (A) 3D- alignment of **7** and **66**. It suggested that compounds **66** and **7** can have a similar ligand binding mode considering the structure similarity; (B) The predicted compound binding mode for **66** in PqsR LBD (PDB: 4JVD). (C) X-ray crystal of **69**-PqsR LBD. Comparing (B) and (C), it was noticed that compound **66** and **69** adapted to PqsR LBD in a similar conformation, which suggested that the docking study can be accurate for the prediction of **66** ligand binding mode. The yellow dash lines indicate hydrogen bond interactions. The blue line indicates a π -stacking. The scaffold of **66** was represented in orange. The scaffold of **69** was represented in green.

2.2.2.2 The synthesis of compound 66-70 for the second SAR study

The synthetic route for **66-70** is summarised in **Scheme 3**. Key intermediates **35-37** were subjected to amide coupling reactions with the aniline **71** using HATU as coupling reagent to give compounds **66-68**.

The *N*-Boc-4-hydroxyaniline **72** was subjected to an Ullmann-type cross coupling reaction with 2-bromopyridine or 2-bromopyrimidine using CuI as catalyst and picolinic acid as the ligand to give *N*-Boc-protected intermediates **73** and **75**. After acidic treatment of **73** and **75**, the resulting anilines **74** and **76** were then subjected to alkylation followed by nucleophilic aromatic substitution reactions with key intermediate **29** to yield analogues **69** and **70**.

Scheme 3 Preparation of target compound 66-70



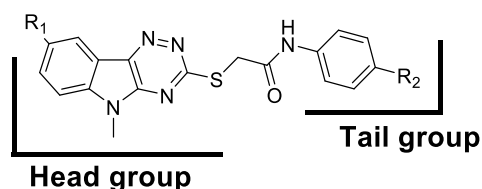
^aReagents and conditions: (i) **71**, HATU, DMAP, NMP, rt (ii) 2-bromopyridine or 2-bromopyrimidine, CuI, picolinic acid, K₃PO₄, DMF, 100°C, 20%; (iii) 4M HCl in 1,4-dioxane, rt, >100%; (iv) **29**, Et₃N, DCM, 0°C to rt, overall 30%.

2.2.2.3 Results for the second SAR study

The synthesized analogues were then evaluated in bioreporter assays for the determination of *pqs* inhibition. These showed that **65** was more active than hit **19** against both PAO1-L and PA14 with IC_{50} values of 0.62 μ M and 2 μ M, respectively **Table 3**. Compounds **66-68** containing a *para*-phenoxy tail group were active against PAO1-L in which **66** was equal potent with **7** and displayed improved *pqs* inhibition than **19** against PAO1-L.

Introducing heteroatoms on the R_2 aromatic substituent, the resulting pyridine-2-yloxy analogue (**69**) was equal potent with **7** against PAO1 strain displaying an IC_{50} value of 0.25 μ M and slightly more potent than **7** against PA14 showing an IC_{50} value of 0.34 μ M.

Table 3. The SAR around the tail group for compound 65-70



	R_1	R_2	Remaining Activity (%) ^{a,b,c,e}		IC_{50} (μ M) ^{c,d,e}	
			PAO1	PA14	PAO1-L	PA14
DMSO			100.00 \pm 8.37	100.00 \pm 3.87	-	-
7^f			-	-	0.32 \pm 0.14	1.22 \pm 0.34
19	H	4-Cl	32.98 \pm 10.30	73.41 \pm 24.52	0.98 \pm 0.15	NA
65	H	cyanomethyl	16 \pm 6.5	19 \pm 5.4	0.62 \pm 0.1	2 \pm 0.17
66	H	phenoxy	11.54 \pm 2.22	15.37 \pm 12.24	0.38 \pm 0.06	0.35 \pm 0.06
67	Br	phenoxy	11.85 \pm 2.32	56.63 \pm 46.23	4.36 \pm 0.42	-
68	OMe	phenoxy	14.49 \pm 2.28	-	4.81 \pm 0.49	3.15 \pm 0.45
69	H	pyridin-2-yloxy	12 \pm 2.7	21 \pm 9.7	0.25 \pm 0.12	0.34 \pm 0.03

	R ₁	R ₂	Remaining Activity (%) ^{a,b,c,e}		IC ₅₀ (μM) ^{c,d,e}	
			PAO1	PA14	PAO1-L	PA14
70	H	pyrimidin-2-yloxy	21 ± 5.5	49 ± 1.0	-	-

^aData shown are mean values obtained from three independent experiments performed in triplicates. ^b% Remaining Activity (RA%) screening at single concentration (10 μM) in triplicates. ^c The inhibitory effect evaluated using PAO1-LmCTX::PpqsA-lux and PA14mCTX::PpqsA-lux reporter assays. Remaining activity (RA%) values below 50%, compounds were regarded as active. RA% values do not have a linear relationship with IC₅₀. ^dNA : not active. ^e-: not available. ^f positive control. The determination of RA% and IC₅₀ for compounds **65-70** was conducted by **Dr. Fadi Soukarieh**.

The X-ray co-crystal structure of **69** in complex with PqsR LBD was determined using soaking method (**Figure 26A**). It revealed that **69** binds to the pqsR LBD hydrophobic pocket where native ligands PQS and HHQ also bind. The tricyclic head group inserts deeply into the hydrophobic pocket, whilst the thioamide linker penetrates through the narrow U-shaped channel. Similar to **7**, the sulfur atom on the linker locked the overall conformation that allowed **66** to bend and accommodate into the hydrophobic pocket. The aromatic tail group points outside the pocket and has a π-stacking interaction with Tyr²⁵⁸ with a distance of 4.55 Å. Interestingly, compound **69** lost the hydrogen bonding with Gln¹⁹⁴ compared with **7** but obtained a new hydrogen bonding interaction with Leu²⁰⁷ with a distance of 3.43 Å. The X-ray structure also showed that the pyridinyl side chain of compound **69** had better overlap with Tyr²⁵⁸ compared to the phenyl side chain of **7** (**Figure 26 B**), which suggested that **69** may have a stronger π stacking interaction with Tyr²⁵⁸.

Compound **69** was found to be more active than **7** PA14 and it may suggest that the π-stacking with Tyr²⁵⁸ could be more important for analogues to retain pqs inhibition than hydrogen bonding interactions. Unfortunately, the co-crystal structures of **66** and **67** in complex with PqsR LBD did not obtain mainly due to poor ligand solubility.

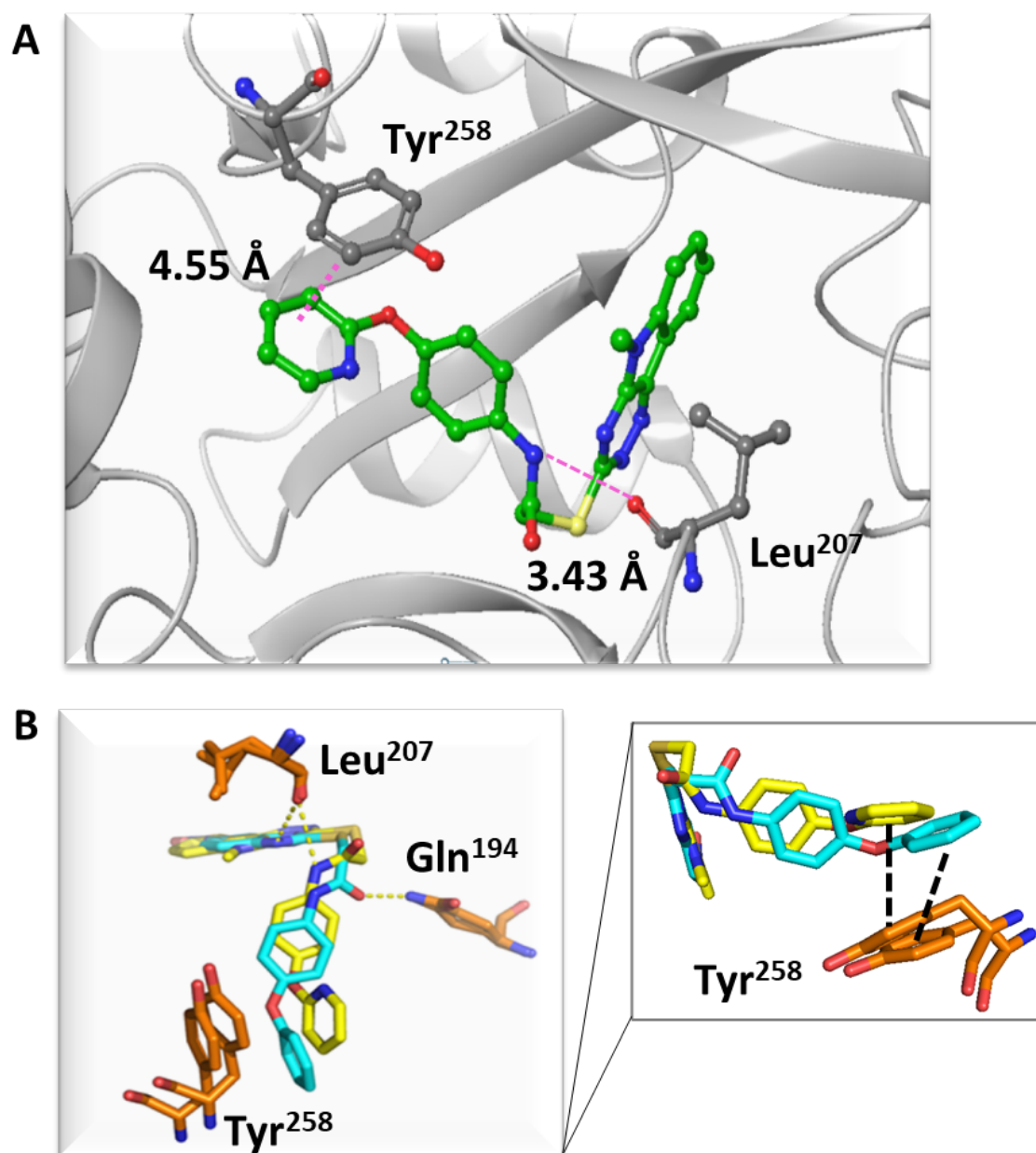


Figure 26. (A) X-ray co-crystal structure of **69** bound to PqsR ligand binding domain with a resolution of 3.2 Å. The scaffold structure of **69** is represented in green. (B) Comparison of ligand binding modes between **69** and **7** in PqsR LBD. The scaffold structure of **69** is represented in blue and **7** is represented in green. The X-ray crystallography experiment was conducted by William Richardson.

2.2.3 The design of compound 79 to improve solubility

The 5-methyl-5*H*-[1,2,4]triazino[5,6-*b*]indole analogues suffer poor solubility mainly due to the planar hydrophobic tricyclic head group. Whilst there are some general formulation approaches to enhance compound solubility such as decrease of particle

size, salt formation and solid suspension formation¹⁶⁹, the improvement of intrinsic compound solubility is more desirable as it can reduce the need to rely up later formulation approaches. In this work, a 4-methylpiperazine group was introduced as an ionizable centre to improve solubility. According to docking study (**Figure 27**), introducing a 4-methylpiperazinyl group at the 3-position of the terminal aryl group, **79** can still bind in the PqsR LBD without unfavourable steric clash.

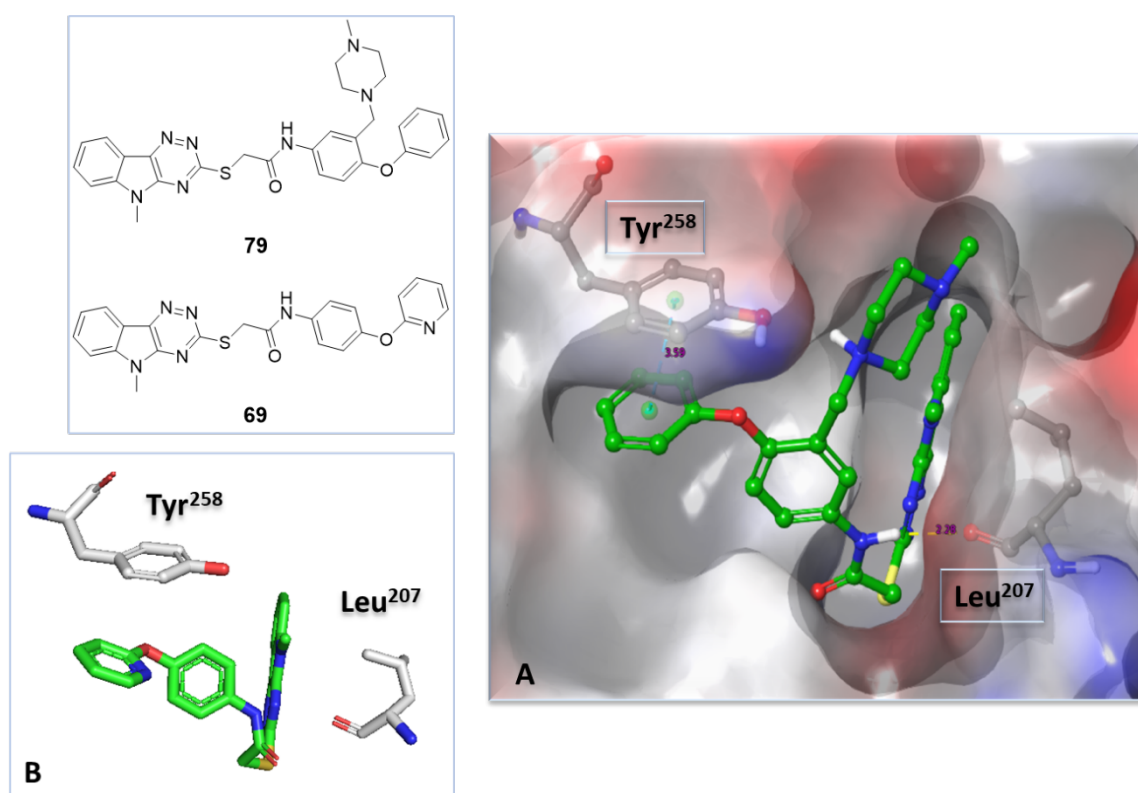


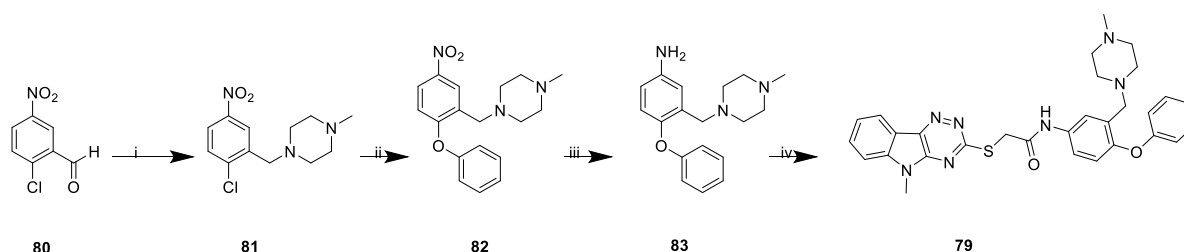
Figure 27. Predicted binding modes of compound **79** with PqsR LBD and **69**-PqsR LBD crystal. (A) Compound **79** is predicted to hydrogen bond with Leu²⁰⁷ and form a π -stacking interaction with Tyr²⁵⁸. Comparing (A) and (B), it was noticed that compounds **69** and **79** adapted in the PqsR LBD in a similar conformation. This suggested that the docking study can be accurate for the prediction of compound **79** ligand binding mode. Hydrogen bonds are shown as yellow dash lines. π stacking is shown as green dash lines. The ligand scaffolds were represented in green.

2.2.3.1 The synthesis of **79**

Compound **79** bearing the *N*-methylpiperazine solubilising moiety was synthesized as outlined in **Scheme 4**. Compound **80** was subjected to reductive amination with 1-

methylpiperazine using $\text{NaBH}(\text{OAc})_3$ as the reducing reagent to give intermediate **81**. Compound **82** was obtained by Ullmann-type cross coupling reaction starting from **81** using CuI as catalyst and picolinic acid as the ligand. Key intermediate **83** was synthesised through nitro reduction from **82** using NH_4Cl and Fe in EtOH and H_2O at $55\text{--}90\text{ }^\circ\text{C}$, followed by amide coupling to give final compound **79**.

Scheme 4. Preparation of **79** from 2-hydroxy-5-nitrobenzaldehyde (**80**)



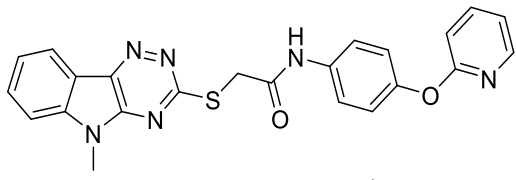
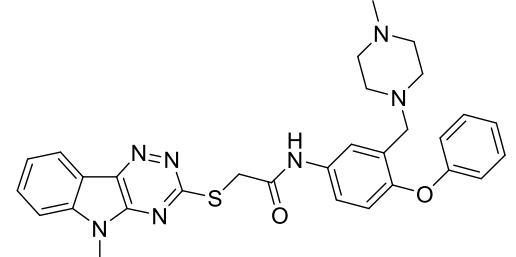
^aReagents and conditions: (i) 1-methylpiperazine, HOAc , sodium triacetoxyborohydride ($\text{NaBH}(\text{OAc})_3$), THF , rt ; (ii) phenol, CuI , picolinic acid, K_3PO_4 , DMF , $100\text{ }^\circ\text{C}$; (iii) NH_4Cl , Fe , EtOH , H_2O , $55\text{--}90\text{ }^\circ\text{C}$; (iv) **35**, HATU, DMAP, DIPEA, NMP, rt .

2.2.3.2 Biophysical and bioreporter assay screening of **79**

Compound **79** was subjected to $\text{mCTX}::\text{P}_{pqsA}\text{-lux}$ -based bioreporter assay based bioreporter assays for the determination of *pqs* inhibition and shown to be inactive *in vitro* assays. This may indicate the poor cell permeability of compound **79** at physiological pH where the majority of compound **79** in solution will be protonated considering the pK_a values of the 4-methylpiperazinyl group (approximate 10.5 and 7.0).

In this thesis, a thermal shift assay (TSA) was introduced as a powerful biophysical method to detect ligand and protein interactions, which detects ligand binding with an affinity range from mM to μM . TSA detects ligand-protein interactions directly and therefore eliminates ligand penetration problems, which is commonly noticed in whole-cell based bioreporter assays.

Table 4. The *in vitro* and physiochemical data for compounds 69 and 79

Compd.	Structure	RA% in PAO1-L ^{a,b,c,d}	ΔT_m ($\pm^\circ\text{C}$)	
			500 (μM) ^{a,e}	250 (μM) ^{a,e}
DMSO	/	100.00 \pm 8.37	0	0
69		12 \pm 2.7	+ 4.4	+ 3.6
79		NA	+ 6.4	+ 6.2

^aData shown are mean values obtained from three independent experiments performed in triplicates. ^b% Remaining Activity (RA%) screening at single concentration (10 μM) in triplicates. ^c The inhibitory effect evaluated using PAO1-LmCTX::PqsA-lux. Remaining activity (RA%) values below 50%, compounds were regarded as active. RA% values do not have a linear relationship with IC_{50} . ^dNA : not active. ^e Thermal shift assay (TSA, $^\circ\text{C}$) at two ligand concentrations (250 and 500 μM) in triplicates. ^f: positive control. The determination of RA% for **69** was conducted by **Dr. Fadi Soukarieh**.

In TSA, PqsR LBD was treated with **79** at 250 μM and 500 μM ligand concentrations in the presence of SYPROTM Orange. As mentioned previously, when the protein unfolds, the environmentally sensitive fluorescent dye, SYPROTM Orange, is able to bind to the protein hydrophobic core, leading to a large increase in fluorescence. Through monitoring the fluorescence change during the protein-unfolding transition process, the melting temperature (T_m), defined as the temperature where 50% of protein sample is unfolded, can be determined. When ligands bind to the protein, this could either stabilize or destabilize the protein reflected as an increase or decrease of T_m . If the ΔT_m is higher than 0.5 $^\circ\text{C}$, it is generally considered that ligand binding has taken place.

Compound **79** stabilized the protein with an increase of ΔT_m value for 6.4 °C and 6.2 °C at 250 μM and 500 μM ligand concentration, respectively **Table 4**, which is higher than the most potent compound **79**. These results suggested that **79** stabilised the PqsR protein and the loss of *pqs* inhibition on the whole cell-based assay may be due to either cell-penetrating or efflux mechanisms.

2.2.4 Investigation of the pharmacophore model based on an SAR exploration around the 5-methyl-5H-[1,2,4]triazino[5,6-b]indole analogues

2.2.4.1 The design of three series of analogues to investigate the pharmacophore for the 5-methyl-5H-[1,2,4]triazino[5,6-b]indole derivatives

The 5-methyl-5H-[1,2,4]triazino[5,6-b]indole analogues are structurally distinct from PqsR native ligands but display common structural features: a tricyclic head group, an aryl tail group and a linear linker. Further SAR was conducted to investigate the influence of these structural features on *pqs* inhibition and the proposed pharmacophore (**Figure 28**).

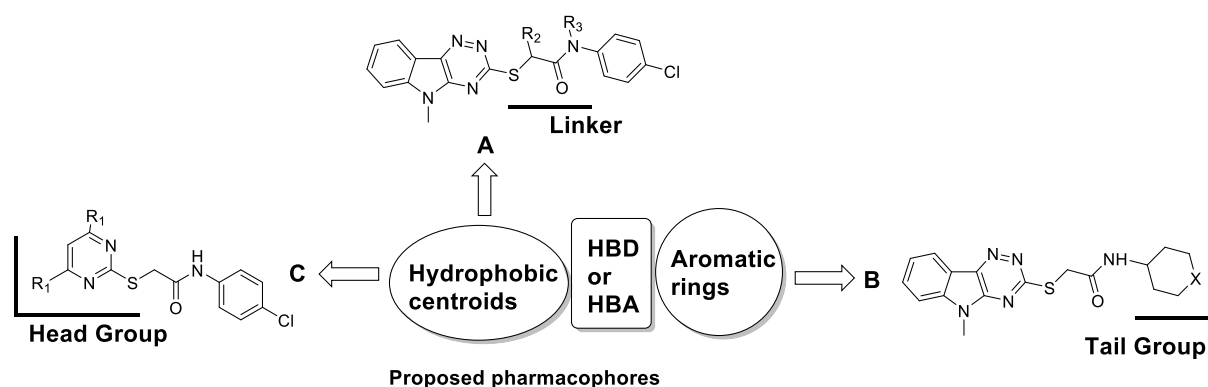


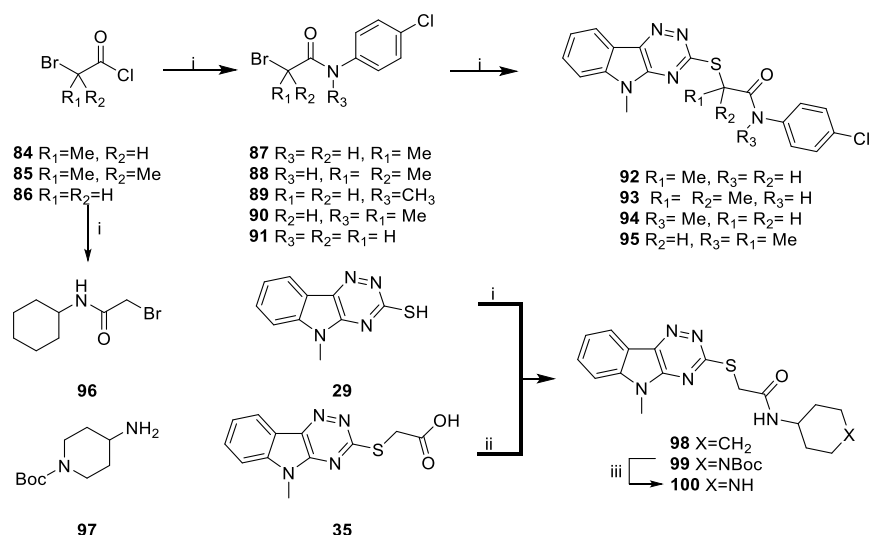
Figure 28. The schematic representation of the design of the SAR study to investigate pharmacophores for the 5-methyl-5H-[1,2,4]triazino[5,6-b]indole derivatives. Methyl groups were introduced to the linker region to investigate the influence of ligand conformation, ligand flexibility and HBD/HBA on *pqs* inhibition (scaffold A). The aryl tail group were replaced to a non-aromatic ring system to investigate the influence of aryl tail group to *pqs* inhibition (scaffold B). In order to investigate the head group ring-

size effects on *pqs* inhibition, the linker and tail group were kept constant as for **19**, whilst the head group were changed to single ring systems (scaffold C).

2.2.4.2 The synthesis of designed analogues

The forward synthetic scheme for the preparation of **92-95**, **98** and **100** was depicted in **Scheme 5**. For analogues with substituted linkers, the *para*-chloro aniline or 4-chloro-*N*-methylaniline was firstly acylated with acyl chlorides **84-86** using Et₃N base to give amide intermediates **87-91**, which were then subjected to nucleophilic substitution to give analogues **92-95**. Intermediate **96** was prepared through acylation of cyclohexanamine with **86**, which was then subjected to nucleophilic substitution with **29** to give **98**. Compound **97** were subjected to amide coupling reactions with **35** using HATU as coupling reagent to give compounds **99** followed by acidic treatment to yield the targeted compound **100**.

Scheme 5. Preparation of 92-95, 98 and 100

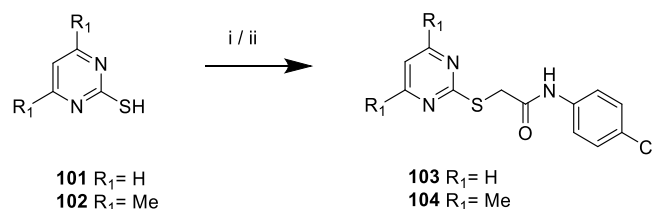


^aReagents and conditions: (i) 4-chloro-*N*-methylaniline or 4-chloro-aniline or **29**, Et₃N, DCM, 0 °C to rt. (ii) **35**, HATU, DMAP, NMP, rt, overall 30%; (iii) 4M HCl in dioxane, rt, >100%;

The preparation for analogues with a single ring system as the head group (**103** and **104**) is represented in **Scheme 6**. 2-Mercaptopyrimidine **101** and its 4,6-dimethyl

analogue **102** were alkylated with intermediate **91** using Et₃N in DCM to give thioethers **101** and **102**.

Scheme 6. Preparation of compounds **101** and **102**

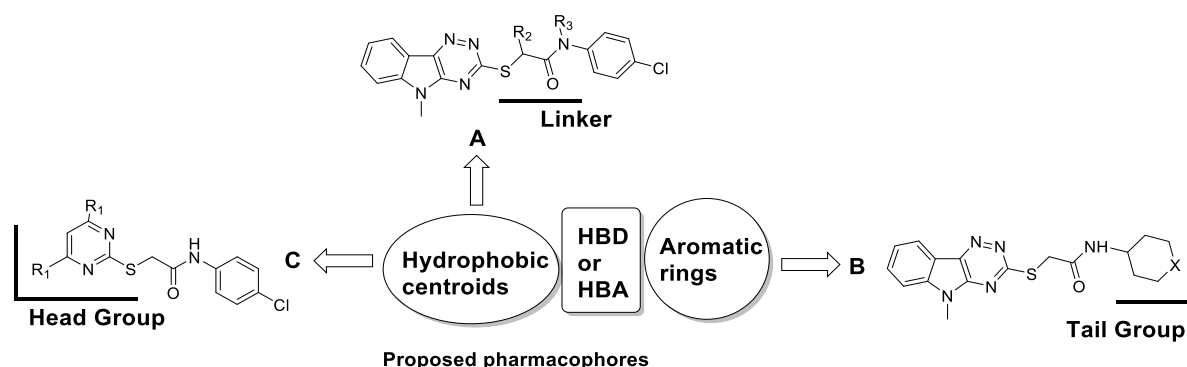


^aReagents and conditions: (i) **101**, **91**, Et₃N, DCM, 0°C to rt, 24%; (ii) **102**, **91**, NaH, DMF, 0°C to rt, 36%.

2.2.4.3 The pharmacophore analysis based on bioreporter assay screening results

The results showed that when introducing methyl groups in R₂ and/or R₃, whilst the head and tail groups were maintained as in **19**, the resulting compounds **92-95** proved inactive against PA01-L and PA14 (Table 5, scaffold A).

Table 5. The *in vitro* data for compounds **92-95**, **98**, **100**, **103**, and **104**



Entry	Scaffold	R ₁ ^d	R ₂	R ₃ ^d	X ^d	Remaining Activity (%) ^{a, b, e}	
						PA01-L	PA14
DMSO		/				100.00 ± 8.37	100.00 ± 3.87
Sen19 ^f		/				26.20 ± 10.33	24.57 ± 3.87

Entry	Scaffold	R ₁ ^d	R ₂	R ₃ ^d	X ^d	Remaining Activity (%) ^{a, b, e}	
						PAO1-L	PA14
92	A	/	CH ₃	H	/	83.60 ± 5.43	/
93	A	/	(CH ₃) ₂	H	/	110.14 ± 8.36	/
94	A	/	H	CH ₃	/	80.24 ± 20.14	97.02 ± 6.36
95	A	/	CH ₃	CH ₃	/	64.64 ± 17.52	96.17 ± 10.74
98	B		/		CH ₂	92.86 ± 12.05	/
100	B		/		NH	100.92 ± 13.33	/
103	C	H		/		NA	/
104	C	CH ₃		/		NA	/

^aData shown are mean values obtained from three independent experiments performed in triplicates. ^b% Remaining Activity (RA%) screening at single concentration (10 μM) in triplicates. ^c The inhibitory effect evaluated using PAO1-LmCTX::PpqsA-lux and PA14mCTX::PpqsA-lux reporter assays. Remaining activity (RA%) values below 50%, compounds were regarded as active. RA% values do not have a linear relationship with IC₅₀. ^dNA : not active. ^e/: not available. ^f positive control. The determination of RA% for compounds **92-95**, **98**, **100** was conducted by **Dr. Fadi Soukarieh**.

The terminal aryl tail group were replaced with a non-aromatic ring system (**Table 5**, **scaffold B**) and the resulting compounds **98** and **100** lost activity. This may result from the loss of π stacking between the aryl tail and Tyr²⁵⁸, which was commonly noticed in previous active analogues. This finding indicates that it is important to retain the terminal group aromaticity for good *pqs* inhibition.

In order to investigate the head group ring-size effects on *pqs* inhibition, the linker and tail group were kept constant as for **19**, whilst the head group were changed to single ring systems (**Table 6**, **scaffold C**). The resulting compounds **103** and **104** lost activity. Both the 5-bromine substituted and unsubstituted 5-methyl-5H-[1,2,4]triazino[5,6-*b*]indole head group can be important *pqs* inhibition in terms of shape complementarity and lipophilicity. With a smaller molecular size, the single ring system analogues can

have a different occupancy for the PqsR LBD compared with the 5-methyl-5H-[1,2,4]triazino[5,6-*b*]indole analogues. Reducing the ring size also significantly changes the lipophilicity reflected by CLogP values decreasing from 3.95 (**19**) to 2.40 (**103**) and 3.40 (**104**). Loss of lipophilicity can affect cell penetration and ultimately influence *pqs* biological activity. Therefore, it appears important to possess a hydrophobic centroid on the compounds scaffold to retain *pqs* inhibition.

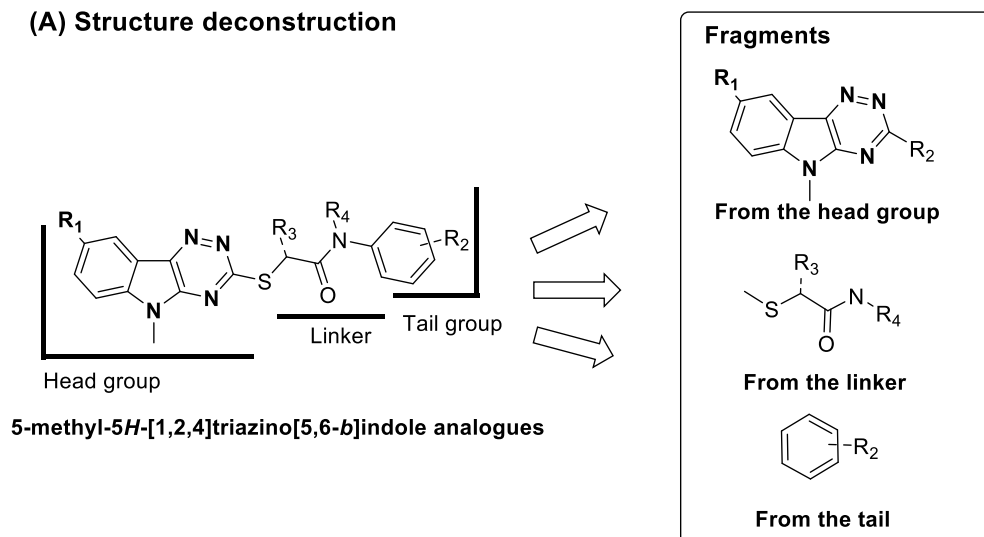
2.2.5 Concept validation investigation for the three essential structure features and their effects on *pqs* inhibition

In the previous pharmacophore investigation, it was shown that structural features including a hydrophobic head group, flexible linker and aryl tail group are essential for the 5-methyl-5H-[1,2,4]triazino[5,6-*b*]indole analogues to retain *pqs* inhibition.

Based on these results, it was decided to use a reversed fragment-based lead discovery method (FBLD) to investigate key structure features and their influences on *pqs* inhibition. In doing so, the drug-sized scaffold of 5-methyl-5H-[1,2,4]triazino[5,6-*b*]indole analogues was deconstructed into fragments, which contain key structure features and bioreporter assay and biophysical methods were used to detect ligand-protein interactions (**Figure 29**).

It was hypothesised that the tricyclic head or aryl tail group fragments should show lower *pqs* inhibition and/or ΔT_m values and along with the growing of these fragments to drug-sized compounds ($350 < \text{Mwt.} < 500$), the compounds *in vitro* and biophysical profiles should improve correspondingly.

(A) Structure deconstruction



(B) Growing key building blocks

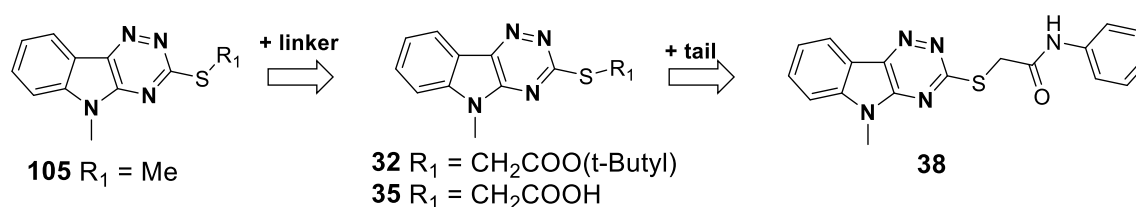
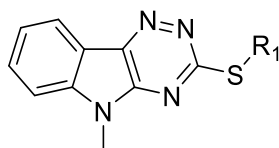


Figure 29. Schematic diagram for the use of FBLD methods in investigation of the essential structure features of 5-methyl-5H-[1,2,4]triazino[5,6-b]indole analogues and their effects on *pqs* inhibition.

The head group fragments **105** was inactive against PAO1-L and PA14 in cell-based bioreporter assays, whilst **105** weakly stabilized PqsR protein observed as an increase of ΔT_m of 0.1 °C at 500 μM (**Table 6**). Incorporating a $\text{CH}_2\text{COO}(t\text{-Butyl})$ linker, the resulting analogue **32** strongly stabilized the PqsR LBD protein observed as a 2.0 °C (500 μM) and 1.36 °C (250 μM) increase of T_m values. Incorporating a CH_2COOH linker, **35** weakly destabilized the protein observed as -0.3 °C ΔT_m value (500 μM). Introducing the aryl tail group, the corresponding *N*-phenyl analogue of **38** was inactive against PAO1-L and PA14 but strongly stabilized the protein observed as 1 °C ΔT_m value (500 μM).

Table 6. The *in vitro* and biophysical data for compound 105, 32, 35, and 38

Entry	R ₁	Remaining Activity (%) ^{a,b,c,d,f}		ΔTm: (± °C) ^{a,e,f}	
		PAO1	PA14	500 (μM)	250 (μM)
DMSO	-	100 ± 8.37	100 ± 3.87	0	0
Sen19	-	26.20 ± 10.33	24.57 ± 3.87	+14.2	+14.2
105	CH ₃	NA	NA	+0.1	0
32	CH ₂ COO(<i>t</i> -Butyl)	NA	NA	+2.0	+1.4
35	CH ₂ COOH	NA	NA	-0.3	-0.1
38	<i>N</i> -CH ₂ CONH-phenyl	80.26 ± 23.75	NA	+1.0	+1.0

^aData shown are mean values obtained from three independent experiments performed in triplicates. ^b% Remaining Activity (RA%) screening at single concentration (10 μM) in triplicates. ^cThe inhibitory effect evaluated using PAO1-LmCTX::PpqsA-*lux* and PA14mCTX::PpqsA-*lux* reporter assays. Remaining activity (RA%) values below 50%, compounds were regarded as active. RA% values do not have a linear relationship with IC₅₀. ^dNA : not active. ^eThermal shift assay (TSA, °C) at two ligand concentrations (250 and 500 μM) in triplicates. ^f-: not available. The determination of analogues RA% was conducted by **Dr. Fadi Soukarieh**. Compound **105** used in this assay were synthesised by project students.

2.3 Conclusion

In this work, a novel series of 1,2,4-triazino[5,6-*b*]indole-3-thiol derivatives were synthesized and shown to be PqsR antagonists in bioreporter assays. X-ray crystallography results on key compounds demonstrated ligand target interactions. A straightforward synthesis of 5-methyl-5*H*-[1,2,4]triazino[5,6-*b*]indole-3-thiol derivatives was reported with overall good yields. 8-Bromo-5-methyl-5*H*-[1,2,4]triazino[5,6-*b*]indole-3-thiol derivatives displayed an overall improved *pqs* inhibition compared to the corresponding *des*-bromo analogues.

Introducing aromatic substituents onto the tail group led to a significant increase in *pqs* inhibition and the corresponding pyridin-2-yloxy analogue **69** was more active than the literature compound **7**. The X-ray crystal structure of **69**-PqsR LBD complex was obtained, which provided insights into the ligand binding mechanism. Further investigations around pharmacophores for the 5-methyl-5*H*-1,2,4-triazino[5,6-*b*]indole-3-thiol analogues suggested that the tricyclic head group, unsubstituted linker and tail group aromaticity are essential for *pqs* inhibitory activity.

In this chapter, fragment-based methods were used for a concept validation experiment where the 5-methyl-5*H*-1,2,4-triazino[5,6-*b*]indole-3-thiol analogues' scaffold were firstly deconstructed into fragments. Assisted by TSA method it was noticed that along with the growing of these fragments to drug-size compounds, the corresponding analogues showed improved biophysical profile. These results suggested the importance of the key structure features for analogues *pqs* inhibition.

Chapter III: Using *in silico*, *in vitro* and biophysical methods for the fragment-based hit identification and optimization for PqsR inhibition

3.1 Introduction and project aim

Fragment-based lead discovery approaches have become an important lead discovery technique for both established and new drug targets in the last 20 years.^{87,124,170,171} However, FBLD methods have not been widely applied in the identification of PqsR antagonists with only three publications at the time of writing this thesis.^{152,172,173}

In the last chapter, a fragment-based lead discovery (FBLD) method was applied in a concept validation experiment where the 5-methyl-5*H*-1,2,4-triazino[5,6-*b*]indole-3-thiol analogue scaffold was deconstructed into fragments. Growing the fragments (MWt < 300) to drug-sized compounds (300 < MWt < 500) afforded a corresponding improvement in *in vitro* pharmacological and biophysical profiles. This finding suggests the fragment-based method can be applied for PqsR antagonist identification. In this chapter, a fragment hit identification and optimization workflow are presented (**Figure 30**).

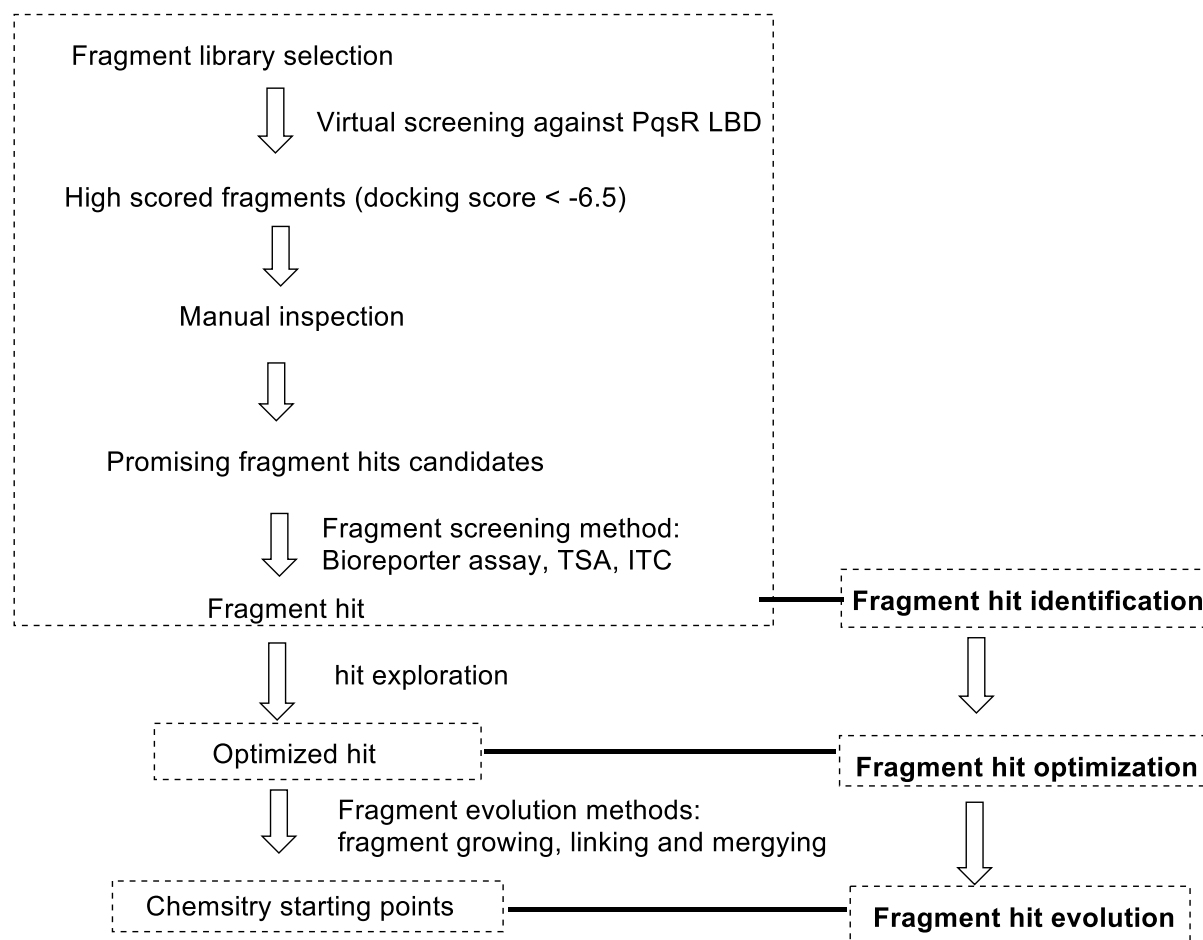


Figure 30. A fragment hit identification, optimization, and evolution workflow. *In silico* methods were used for fragment library screening against PqsR LBD followed by a manual inspection step where fragment hit candidates were then determined. The selected fragments were then subjected to fragment screening using bioreporter assay and biophysical methods, which allowed for the identification of fragment hits. Fragment hits were then advanced to hit exploration to optimise binding interactions before being subjected to the fragment evolution step.

3.2 Using an *in silico* method for fragment screening against PqsR LBD

Biophysical, bioreporter assay and *in silico* methods are commonly used in fragment library screening.^{174,102,175} In this work, an *in silico* method requiring less resource and time investment^{126,176,177,178} was chosen to be the primary virtual screening method.

The previous 5-methyl-5*H*-[1,2,4]triazino[5,6-*b*]indol-3-yl)thiol analogues suffer from poor solubility believed to be due to the hydrophobic aryl head group. It was decided to introduce more sp^3 character to this region to improve both compound solubility and novelty. The selection of fragment libraries for the virtual screening were therefore tailored to sp^3 character rich fragment libraries.

3.2.1 Selection of five fragment libraries for virtual screening

Four fragment libraries from the **Enamine** company were selected for virtual screening, which were: *3D-shape diverse fragment library*, *essential fragment library*, *single pharmacophore library*, and *sp^3 rich fragment library*.

The *essential fragment library* from **Enamine** contains 320 fragments, which stems from literature-reported fragments and molecules with determined protein-ligand crystallography data. All the fragments in this library have been tested for water solubility and chemical stability, and therefore are suitable for secondary biophysical or bioreporter assay screening.

The *Ro3 fragment library* is the world's largest collection of fragments, which contains 2,725,753 fragments. It should be noticed that in this library, toxicophores and chemically reactive motifs were removed to yield better "lead-like" compounds at a later stage.

The *single pharmacophore fragment library* contains 1,500 compounds in which fragments have a single polar group or one motif for ligand-protein interaction. Fragments in this library tend to have lower synthetic complexity compared with the previously mentioned fragment libraries and therefore are more likely to be synthetically accessible in the later follow-up fragment growing stage.

The sp^3 rich fragment library contains 50,272 fragments, in which the F_{sp^3} cut-off score was set at 0.47 and has become the largest and most diverse commercial sp^3 character rich fragment library. It has been shown that a higher F_{sp^3} value can lead to an increased clinical success rate, which may relate to improved solubility and better occupancy of the biological targets of interest.^{107,179}

$$F_{sp^3} = \frac{\text{The number of } sp^3 \text{ carbons}}{\text{The total number of carbons}} \quad (4)$$

3.2.2 Selection of optimal fragment starting points based on the virtual screening results

Docking studies were performed on Maestro using HTVS (High-throughput virtual screening) mode against PqsR LBD crystal structure (PDB code: **4JVD**; force field: OPLS3e).

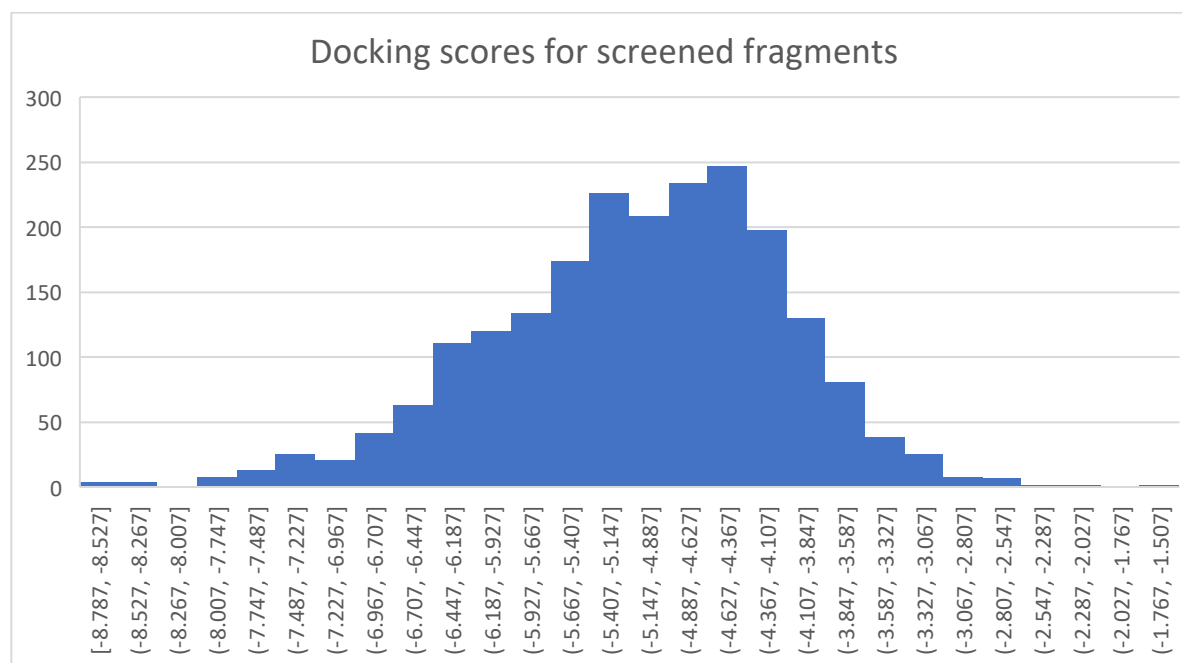


Figure 31. The histogram of docking scores for all molecules screened. Fragments tend to have low affinity to the biological targets reflecting as higher docking scores. Most of the fragments screened for this work displayed docking scores in a range from -5.6 to -4.1.

A manual inspection step of high-scoring fragments was introduced. Fragments with a docking score lower than -6.5 were manually filtered based on their synthetic complexity, the possibility for further chemical modification and their commercial price, which ultimately afforded 7 promising fragment starting points **106-112** (**Figure 32**).

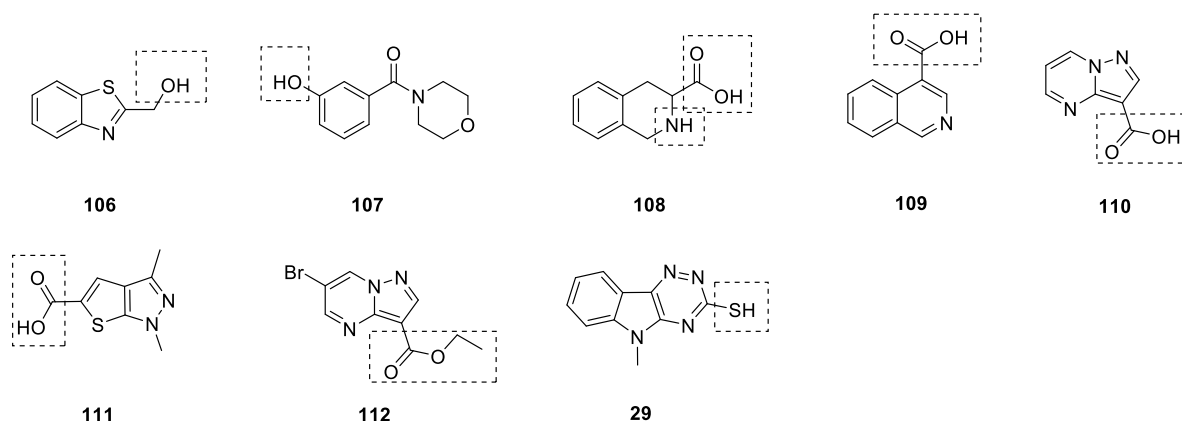


Figure 32. Seven high-scoring fragments from virtual screening **106-112** and the fragment extract from the 5-methyl-5*H*-[1,2,4]triazino[5,6-*b*]indol-3-yl)thiol analogues (**29**). The boxes highlight functionalities from which fragment elaboration can take place.

Fragments **106-112** displayed good fragment-likeness according to the Ro3 and good physicochemical profiles. In particular, the low lipophilic nature of these fragments is beneficial in the later fragment-to-lead modification process (**Table 7**). Fragments **106-112** are all commercially available and have suitable functional groups for further elaboration including carboxylic acid (R-COOH), thiol (R-SH), amine (R-NH₂), and alcohol (R-OH) groups.

Table 7. Fragments physicochemical properties and molecular docking scores

Comp.	Docking score	CLogP ^a	MWt.	HBD/HBA
106	-6.683	1.042	165.21	1/2
107	-7.815	0.645	207.23	1/3
108(S)	-6.760	1.194	177.20	1/2

Comp.	Docking score	CLogP ^a	MWt.	HBD/HBA
108(R)	-7.164	1.194	177.20	1/2
109	-6.890	1.973	173.17	0/3
110	-7.009	0.400	163.14	0/4
111	-7.001	1.746	196.22	0/3
112	-6.571	1.844	270.09	0/3
29	-7.156	2.310	216.26	1/3

^a Calculation of CLogP using software ChemDraw Professional 16.0. Calculation of HBD/A using software MarvinSketch 20.11 at pH 7.4.

Fragments **106-112** showed good docking scores (Maestro, HTVS mode) in a range from -6.571 to -7.815 and all fragments were predicted to fit into the same region in PqsR LBD (**Figure 33a**). Fragment **29** is extracted from the head group of **69** which is a potent PqsR inhibitor from our previous work and was included as a reference fragment in the docking study (**Figure 33j**). Some fragments selected from the virtual screening have better docking scores and CLogP values than **29**, which gave us confidence to continue with these fragments.

The secondary screening using the bioreporter assay, TSA and ITC methods were performed on **106-112** and **29** to confirm fragments binding to PqsR protein.

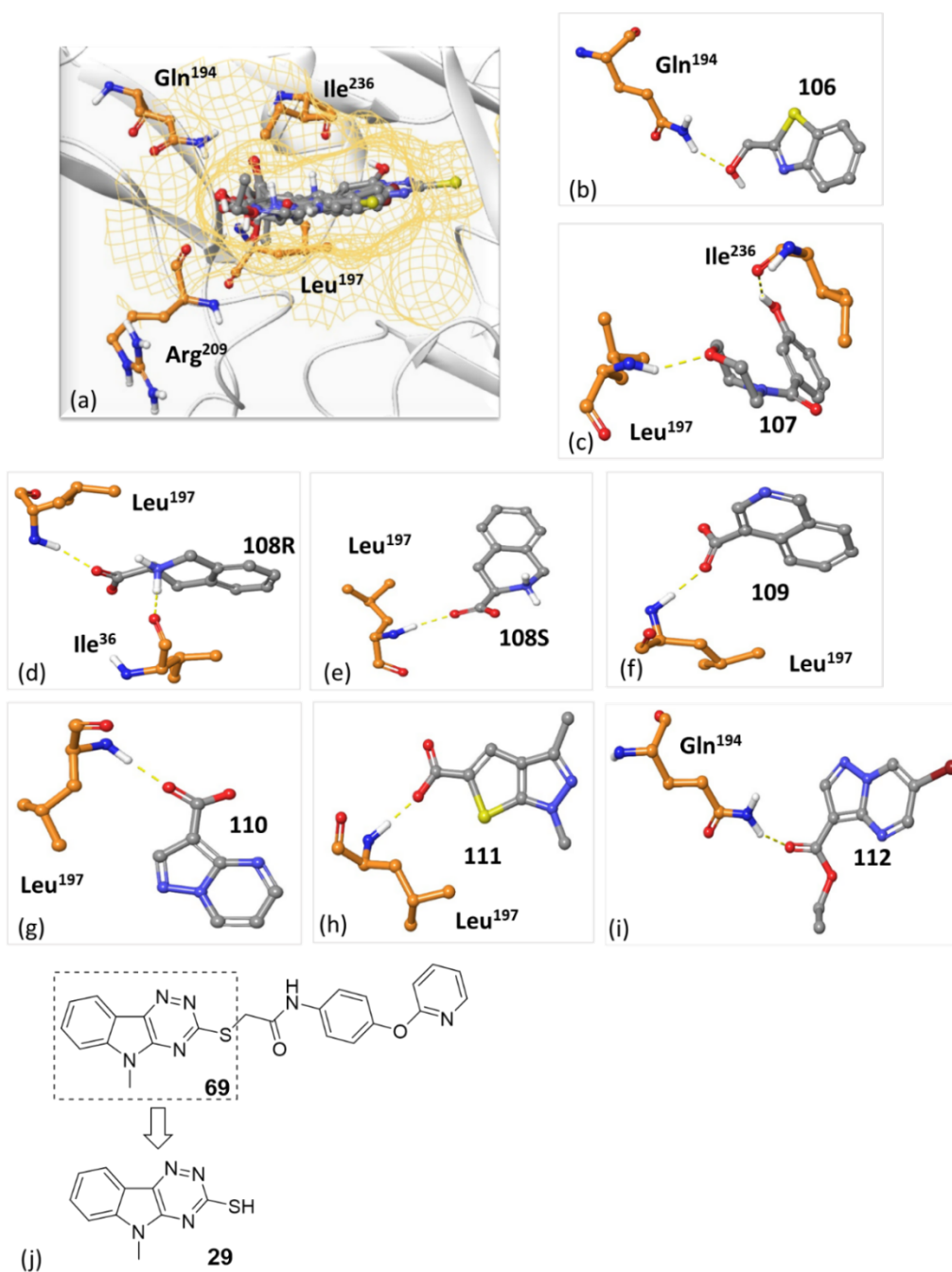


Figure 33. The predicted compound binding mode for **106-112** in the PqsR LBD (**a-i**) (Maestro, PDB: 4jvd). (**a**) Fragments **106-112** were predicted to fit into the same region in PqsR LBD. (**b-i**) Fragments **106-112** were predicted to have hydrogen bonding interactions within local environment. **106** and **112** were predicted to form a hydrogen bond with Gln¹⁹⁴. Fragment **107**, **108**, **109**, **110**, **111** can act as HBAs and have a hydrogen bond interaction with Leu¹⁹⁷. Fragment **108** is a chiral molecule and the R enantiomer was predicted to have hydrogen bond interactions with both Leu¹⁹⁷ and Ile²³⁶, whilst the S enantiomer can only have a hydrogen bonding with Leu¹⁹⁷. Hydrogen bonds are shown as yellow dash lines. The ligand scaffolds were represented in grey. (**j**) The scaffolds for compound **69** and **29**.

3.3 Using bioreporter assay and biophysical methods for the secondary screening on the selected fragments (106-112 and 29)

As introduced in the first chapter, fragments tend to weakly bind to biological targets with affinity values in a range from micromolar (μM) to millimolar (mM), which is a challenge in identifying weak binders. An inappropriate screening method can lead to either false positives or a low hit rate. In this work multiple methods, including bioreporter assay, TSA and ITC methods were used to cross validate fragment candidates in order to yield high quality hits.

3.3.1 Bioreporter assay and TSA screening results on the selected fragments

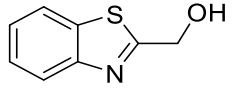
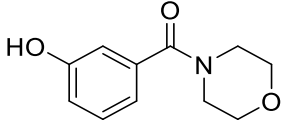
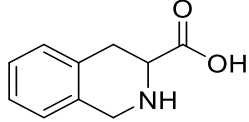
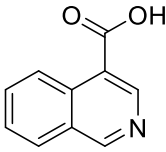
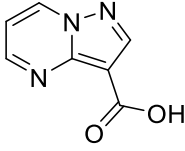
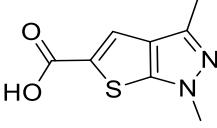
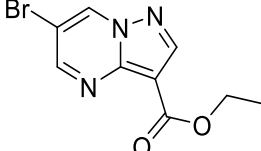
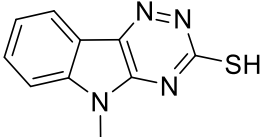
The $\text{mCTX}::P_{pqsA}\text{-lux}$ -based bioreporter was used for the evaluation of the fragments *pqs* inhibition against PAO1-L strain. PAO1-L culture was treated with a 50 μM fragment solution and fragments showing a *pqs* activity reduction greater than 30% (i.e. $\text{RA}\% < 70\%$) were regarded as being weakly active. Results showed that only **106**, **107** and **108** were weakly active against PAO1-L in the initial spot test, however these results could not be repeated in later experiments **Table 8**.

TSA was then introduced to detect fragment and protein interactions. As previously described, SYPRO™ Orange was used as the fluorescent dye to monitor PqsR LBD thermal stability. When ΔT_m is higher than 0.3 °C at 500 μM ligand concentration, it can be inferred that the fragment strongly binds to the protein reflected by a significant thermal stability change.

Fragment **106** strongly stabilized the protein reflected by the observed increase of 0.5 °C ΔT_m value compared with the DMSO reference (**Table 8**). Compound **29** strongly destabilized the protein displayed negative ΔT_m values of -7.7 °C and -

14.4 °C at 250 μM and 500 μM ligand concentrations, respectively. Compounds **107** ($\Delta T_m = -0.3$ °C) and **112** ($\Delta T_m = -0.4$ °C) moderately destabilized the protein, which could attribute to the fragment stabilising the unfolded protein or protein aggregation.¹³¹ Fragments **108-111** did not show a large ΔT_m change at the testing concentrations and were not progressed further.

Table 8. Fragments 106-112 and 29 RA% and TSA screening results

Structure	Comp.	Remaining Activity (%) ^{a,b, c,d,e}		ΔT_m (\pm °C) ^e	
		Initial screening	Repeats	500 (μ M) ^{a,e}	250 (μ M) ^{a,e}
DMSO		100%	100%	0	0
	106	71.2 \pm 6.5	NA	+ 0.5	+ 0.4
	107	67.9 \pm 3.5	NA	- 0.3	-
	108	70.8 \pm 4.2	NA	- 0.2	-
	109	NA	-	+ 0.1	- 0.1
	110	NA	-	+ 0.1	+ 0.3
	111	NA	-	0	+ 0.1
	112	NA	-	- 0.4	- 0.1
	29	NA	-	- 14.4	- 7.7

^aData shown are mean values obtained from three independent experiments performed in triplicates. ^b% Remaining Activity (RA%) screening at single

concentration (50 μM) in triplicates. ^c The inhibitory effect evaluated using PAO1-LmCTX::*PpqsA-lux* reporter assays. Remaining activity (RA%) values below 70%, fragments were regarded as active. RA% values do not have a linear relationship with IC_{50} . ^dNA : not active. ^e“-“: not available. ^fThermal shift assay (TSA, $^{\circ}\text{C}$) at two ligand concentrations (500 and 250 μM) in duplicates or triplicates. The determination of RA% was conducted by **Dr. Fadi Soukarieh** and repeated by me. The determination of TSA (\pm $^{\circ}\text{C}$) was conducted in collaboration with William Richardson.

3.3.2 ITC experiment on 106 and 108

In order to determine the thermodynamic parameters of **106** binding to PqsR protein, ITC experiments were conducted by titrating 5 mM of **106** in the presence of 200 μM PqsR protein solution. The data analysis was conducted in **Origin** software and the resulting binding thermograms for **106** are shown in **Figure 34**.

As the titration progressed, the ligand binding sites became saturated, reflected by the peak of heat changes becoming smaller and at the end of the titrations, a great portion of the binding site was saturated leaving only the heat of dilution. This result confirmed the binding of **106** to PqsR protein with an average dissociation constant (K_d) value of 864.5 μM based on the two titrations. The average change of enthalpy (ΔH) was 6.18 kcal/mol and the stoichiometry (N) was closed to 1. This allowed further calculation of the Gibbs free energy change (ΔG) and entropic contribution to binding ($-\text{T}\Delta S$) according to **equations 5** and **6**, which gave an average ΔG value of 4.18 kcal/mol and $-\text{T}\Delta S$ as 2 kcal/mol.

$$\Delta G = -RT \ln K_d \quad (5)$$

$$\Delta G = \Delta H - \text{T}\Delta S \quad (6)$$

Where R indicates the gas constant, 8.314 $\text{J k}^{-1}\text{mol}^{-1}$ and T indicates temperature in Kelvin.

In general, a favourable enthalpy change can result from hydrogen and van der Waals bonding interactions within the ligand binding site, whilst unfavourable entropy contribution (the positive $-T\Delta S$ value) can be attributed to unfavourable hydrophobic effect and ligand flexibility^{180,181}. The positive $-T\Delta S$ and negative ΔH values of **106** suggest that the binding of **106** to PqsR LBD was mainly enthalpically driven (**Figure 34C**).

The enthalpically favourable and entropy unfavourable binding of **106** to PqsR LBD can be attributed to the flexible alcohol group on **106**. This alcohol group was predicted to have a hydrogen bonding interaction with Gln¹⁹⁴ in the docking study, whilst the rotatable methylene bond can lead to the entropic penalty.

It has been widely accepted that ligands with favourable enthalpic binding signatures are optimal for hit selection as it is easier to increase the entropic contribution but harder to improve enthalpic contribution in later hit-to-lead optimization processes.^{181,182} As such, fragment **106** showing an enthalpically preferred binding towards PqsR protein was selected as hit.

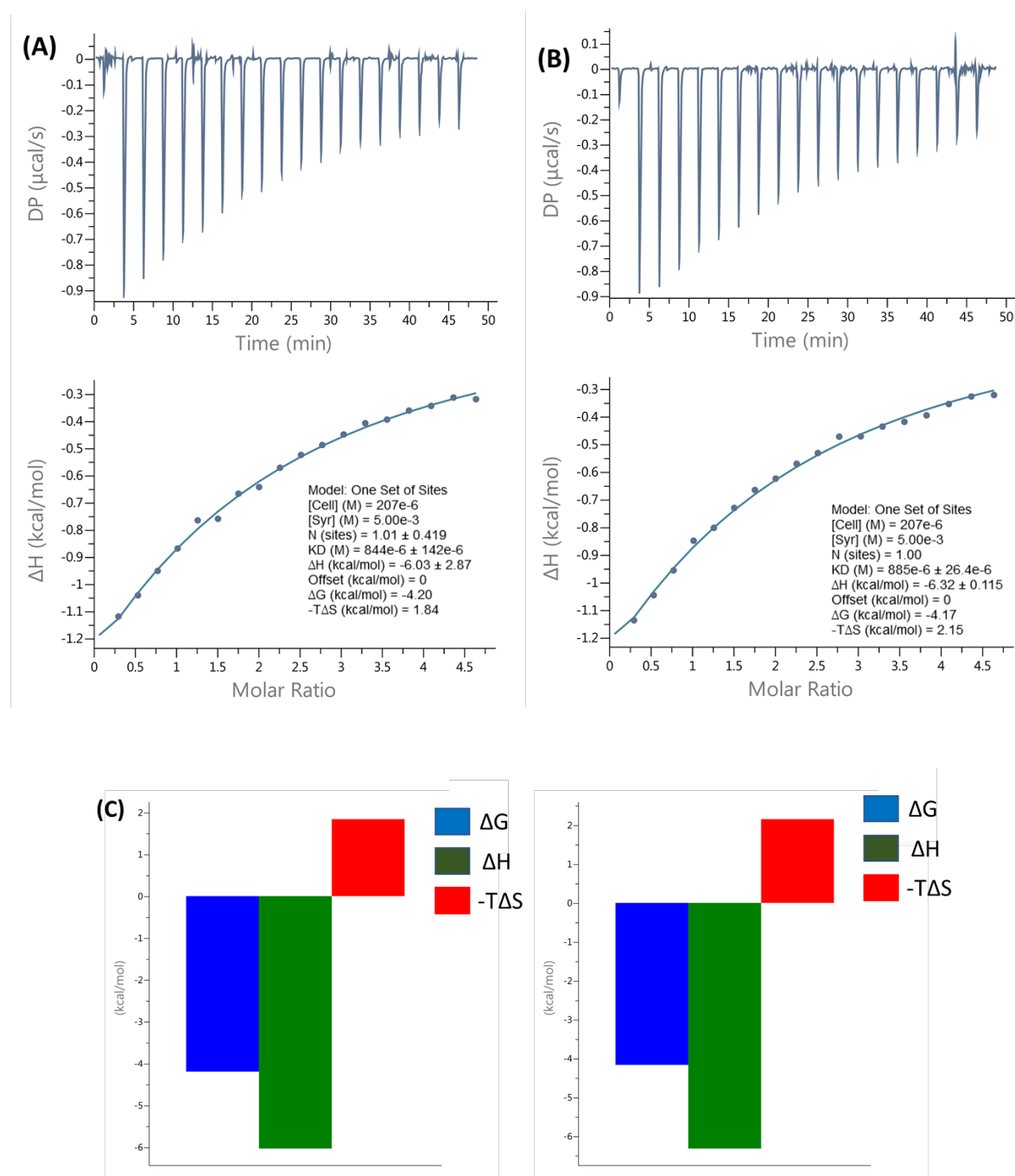


Figure 34. ITC results for **106** in duplicate. (A) and (B) showed the raw data output: the injection peaks (on the top) and the integrated data (on the bottom). The duplicates were using the same experimental setting up by titrating 5 mM **106** in the presence of 200 μ M PqsR protein solution. (C) indicated the thermodynamic parameters for **106**. The determination of **106** binding to PqsR using ITC was conducted by William Richardson.

Binding interaction was not observed when titrating 2 mM of **108** in the presence of 50 μ M PqsR protein, therefore **108** was not progressed further (**Figure 35**).

X-ray crystallography methods were also applied to fragments **106** and **107** in order to obtain detailed fragment binding mode to guide later fragment evolution however no fragment-protein complex was obtained. Ultimately, **106** showing a clear binding to PqsR protein in both TSA and ITC experiments and along with **107** displayed promising TSA results were selected as the hit compounds and progressed to hit modification stage.

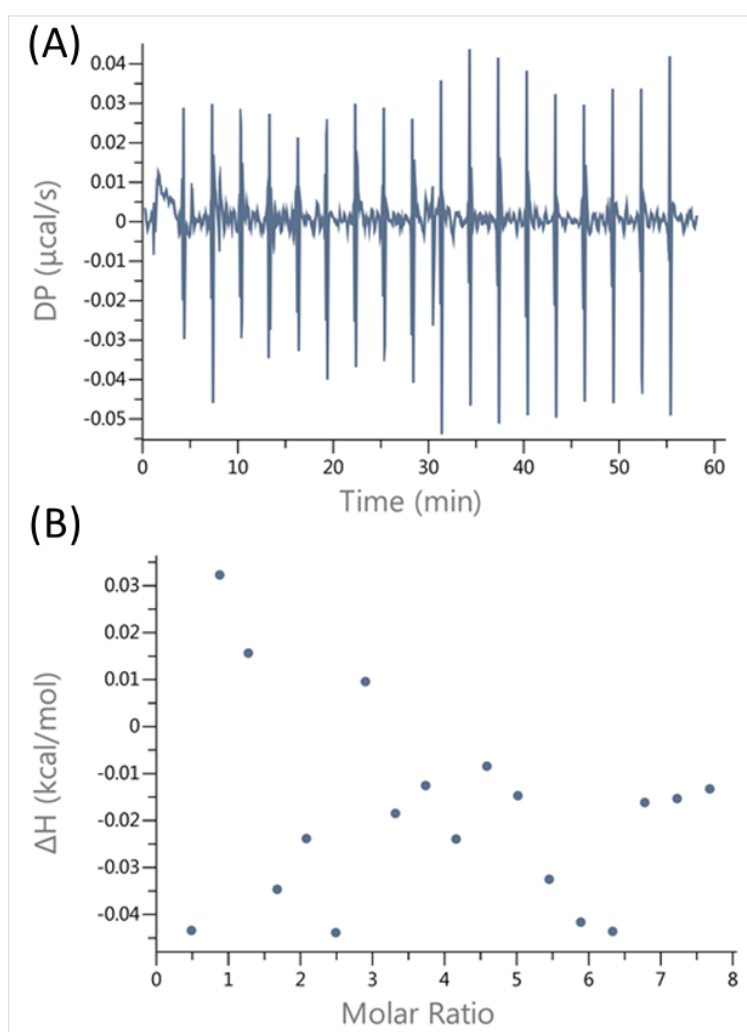


Figure 35. ITC experiment results for **108**. (A) showed the raw data output and (B) showed the integrated data. ITC was conducted by William Richardson.

3.4 Hit optimization I: fragment hit 107 exploration

Hit exploration is essential in terms of sampling chemical space around the initial fragment hits and also enable the optimization of existing molecules or explore new binding interactions within the ligand binding site.

3.4.1 The design of hit exploration study for fragment 107

Fragment **107** contains a 3-hydroxyphenyl ring and a morpholine ring linked through an amide bond in which the 3-hydroxyl group was predicted to hydrogen bond with Gln¹⁹⁴ in docking studies. The hit exploration study initially focused on exploring the electrostatic requirements of ring A by changing the hydroxyl group substitution position or replacing the 3-hydroxyl group with other functional groups (**Scaffold A, 113-117 and 119-126 Figure 36 I**). Through functionalization of the ring B on **107** or replacing it with other six membered ring system, the effect of the ring B was also investigated (**Scaffold A, 118b-d, Figure 36 I**).

Fragment **141** with a different linker was designed to investigate the effect of the amide bond to ligand binding to PqsR protein (**Scaffold B, 141, Figure 36 I**).

A retrosynthetic analysis was applied to 4-benzoylmorpholine analogues (scaffold A and B **Figure 36 II**). This indicated that scaffold A and B can be synthesized from simple building blocks through well documented reactions such as amide bond formation and reductive amination, which provided confidence to build a small fragment library.

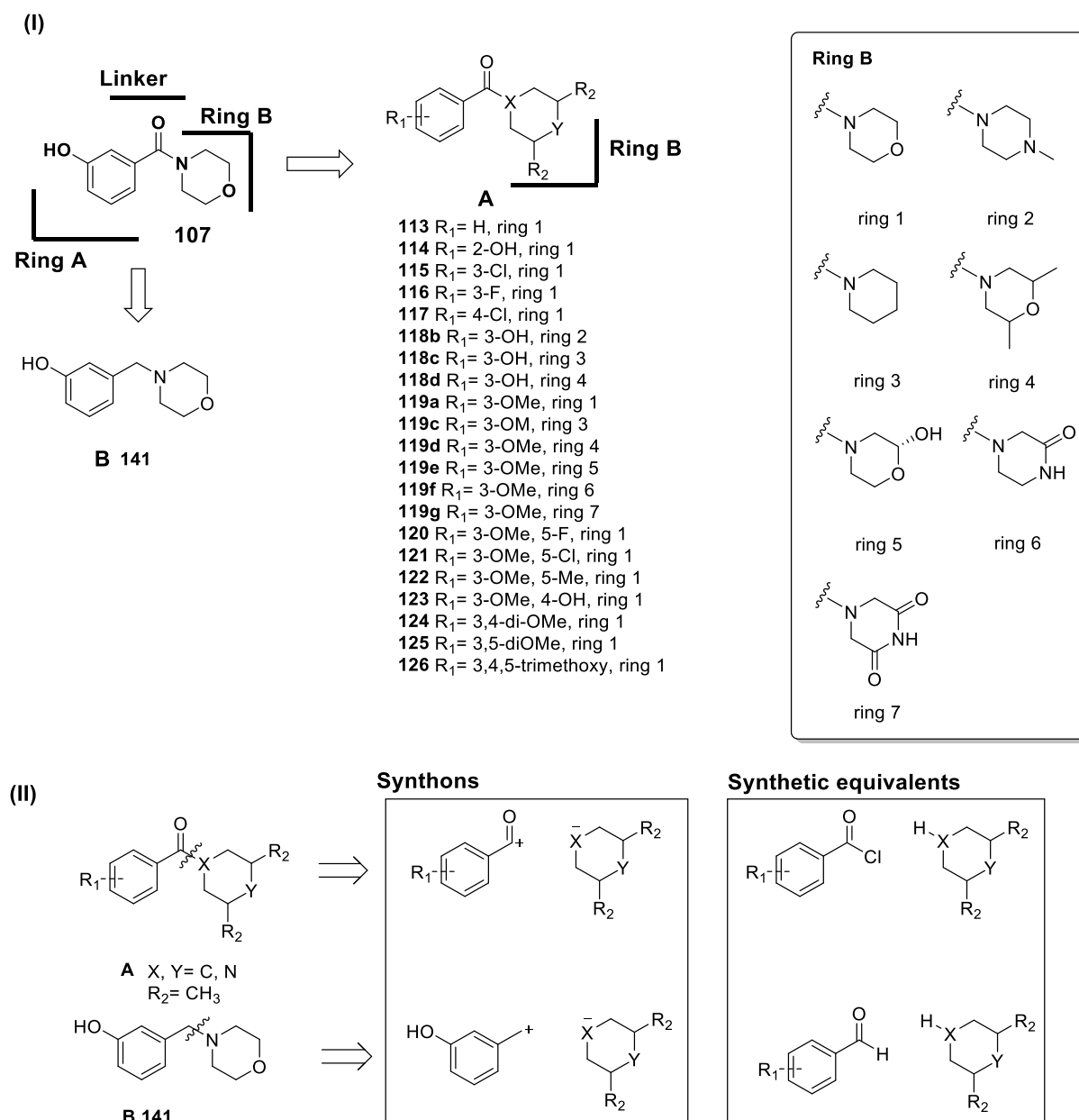


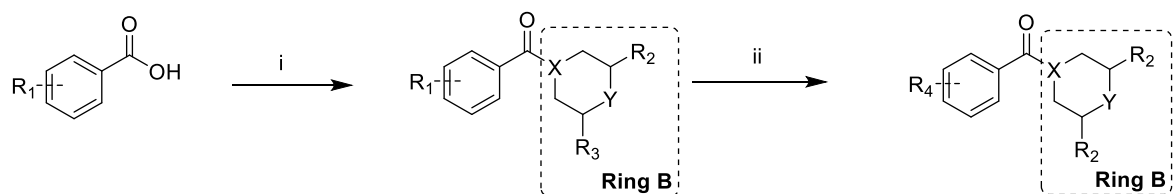
Figure 36. Fragment 107 optimization scheme (I) and retrosynthetic analysis of scaffold A, B and C (II).

3.4.2 The synthesis of designed analogues

The forward synthetic scheme for the majority of designed analogues was depicted in **Scheme 7**. Fragments **113**, **115-117**, **119-127** were achieved by amide coupling reactions where substituted benzoic acids **128-140** were subjected to a wide range of secondary amines, using HATU as coupling reagent to give targeted analogues **113**,

115-117, 119-127. Analogues **119a, 127, 119b-d** were then treated with BBr_3 to demethylate the aryl methyl ethers to give analogues **107, 114, 118b-d**.

Scheme 7. Preparation of targeted compound 107, 113-127.



128 $R_1 = 3\text{-OMe}$

129 $R_1 = 2\text{-OMe}$

130 $R_1 = 3\text{-Cl}$

131 $R_1 = 4\text{-Cl}$

132 $R_1 = 3\text{-F}$

133 $R_1 = 3,4\text{-dimethoxy}$

134 $R_1 = 3,5\text{-dimethoxy}$

135 $R_1 = 3,4,5\text{-trimethoxy}$

136 $R_1 = \text{H}$

137 $R_1 = 3\text{-OMe, 5-F}$

138 $R_1 = 3\text{-OMe, 5-Cl}$

139 $R_1 = 3\text{-OMe, 5-Me}$

140 $R_1 = 3\text{-OMe, 4-OH}$

113 $R_1 = \text{H}$, ring 1

115 $R_1 = 3\text{-Cl}$, ring 1

116 $R_1 = 3\text{-F}$, ring 1

117 $R_1 = 4\text{-Cl}$, ring 1

119a $R_1 = 3\text{-OMe}$, ring 1

119b $R_1 = 3\text{-OMe}$, ring 2

119c $R_1 = 3\text{-OMe}$, ring 3

119d $R_1 = 3\text{-OMe}$, ring 4

119e $R_1 = 3\text{-OMe}$, ring 5

119f $R_1 = 3\text{-OMe}$, ring 6

119g $R_1 = 3\text{-OMe}$, ring 7

120 $R_1 = 3\text{-OMe, 5-F}$, ring 1

121 $R_1 = 3\text{-OMe, 5-Cl}$, ring 1

122 $R_1 = 3\text{-OMe, 5-Me}$, ring 1

123 $R_1 = 3\text{-OMe, 4-OH}$, ring 1

124 $R_1 = 3,4\text{-di-OMe}$, ring 1

125 $R_1 = 3,5\text{-diOMe}$, ring 1

126 $R_1 = 3,4,5\text{-trimethoxy}$, ring 1

127 $R_1 = 2\text{-OMe}$, ring 1

107 $R_1 = 3\text{-OH}$, ring 1

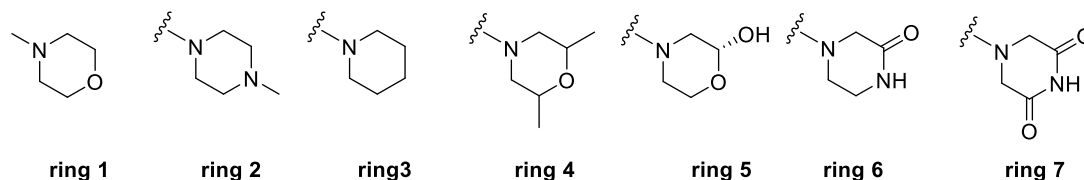
114 $R_1 = 2\text{-OH}$, ring 1

118b $R_1 = 3\text{-OH}$, ring 2

118c $R_1 = 3\text{-OH}$, ring 3

118d $R_1 = 3\text{-OH}$, ring 4

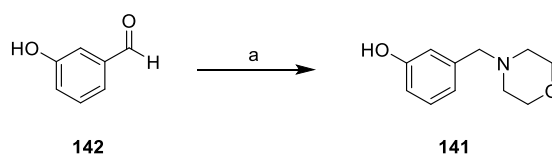
Ring B



^aReagents and conditions: (a) various amines, HATU, DMAP, NMP, DIPEA, rt; (b) BBr_3 , DCM, rt.

The preparation of **141** is represented in **Scheme 8**. 3-Hydroxybenzaldehyde (**142**) and morpholine were subjected to reductive amination using $\text{NaBH}(\text{OAc})_3$ as reducing reagent in THF to give **141**.

Scheme 8. Preparation of targeted compound 141.



^aReagents and conditions: (a) **142**, morpholine, $\text{NaBH}(\text{OAc})_3$, HOAc, THF, rt.

3.4.2 The results for the hit exploration study around 107

The mCTX::P_{pqsA}-lux-based bioreporter assay and TSA methods were applied for the evaluation of fragment *pqs* inhibition and ligand binding to PqsR protein in this hit exploration study. For the PAO1-LmCTX::P_{pqsA}-lux reporter assays, PAO1-L strain was treated with a 50 μM fragment solution in DMSO/PPS buffer and fragments showing a *pqs* activity reduction greater than 70% (i.e. RA% < 70%) were regarded as being active. In TSA, the PqsR protein was treated with a fragment solution at 500 μM ligand concentration in the presence of the environmental sensitive fluorescent dye, SYPRO™ Orange.

The hit exploration study initially focused on modifying ring A, whilst the linker and ring B were kept consistent as a morpholine ring as in **107** (Table 9, compounds **113-117**, **119a**, **120-126**). Removal of the hydroxyl group (**113**) or changing the hydroxyl group from the *meta*-(**107**) to the *ortho*- (**114**) position, caused compound to exhibit no inhibition against PAO1-L at 50 μM screening concentration. When replacing the *meta*-hydroxyl group with a *meta*-methoxy group, **119a** weakly stabilized the protein, observed as a 0.1°C increase for ΔT_m. The 3,4-dimethoxy substituted analogue **124** weakly stabilized the protein (ΔT_m = + 0.1°C), whilst the 4-hydroxy-3-methoxy substituted analogue **123** weakly destabilized the PqsR protein (ΔT_m = - 0.1°C. The 3, 5-di-substituted analogues **120-122** and **125** were inactive in the bioreporter assay, whilst **125** (R₁= 3,5-diOMe) and **122** (R₁= 3-OMe-5-Me) weakly destabilized PqsR protein observed as a 0.1°C decrease of ΔT_m. The 3,4,5-trimethoxy substituted analogue **126** weakly stabilized PqsR protein observed by an increase of ΔT_m value for 0.2 °C. Replacing the 3-hydroxyl group with halogen atoms, including chlorine (**115**,

117) and fluorine (**116**) caused the resulting analogues to show no inhibition against PAO1-L at 50 μM screening concentration.

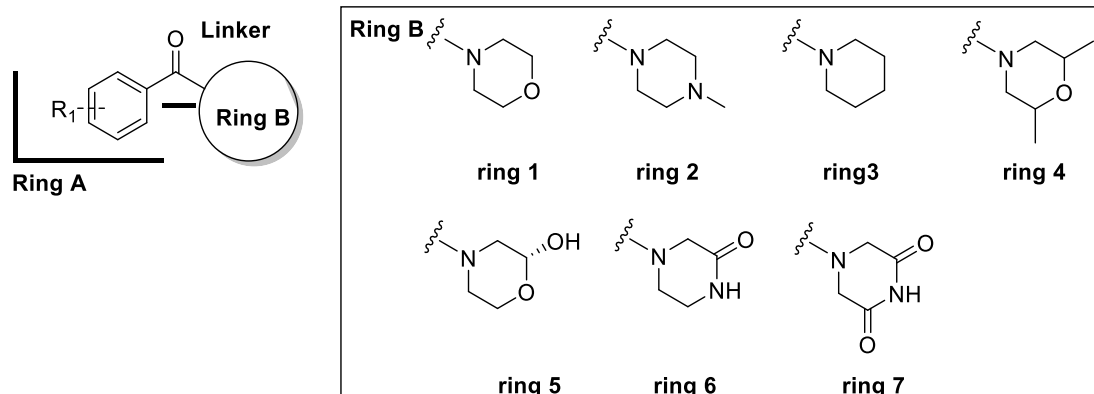
The hit exploration study then focused on modifying ring B and the linker, whilst ring A was kept consistent as a 3-hydroxyphenyl ring (**Table 10**, compounds **118b-d**). Replacing the morpholine ring (**107**) with 4-methylpiperazine (**118b**) or piperidine (**118c**), caused no *pqs* inhibition at screening concentrations. Introducing methyl groups to R₂ proved unsuccessful as **118d** was inactive in the bioreporter assay. Replacing the amide linker with a methylene linker as in **141** caused a loss of binding to the PqsR protein ($\Delta T_m = 0^\circ\text{C}$)

Further hit exploration study was focused on modifying ring B, whilst kept ring A consistent as 3-methoxyphenyl group (compounds **119b-g**). Fragments where ring B was a 4-methylpiperazinyl (**119b**) or piperidinyl (**119c**) showed no *pqs* inhibitory activity. Introducing HBA (an alcohol group) on ring B, **119e** weakly destabilized PqsR, which was observed as a 0.2°C decrease of ΔT_m . Fragment **119g** containing a piperazine-2,6-dione ring B weakly destabilized PqsR observed as a 0.3°C decrease of ΔT_m . Introducing a piperazin-2-one ring as ring B, **119f** weakly stabilized PqsR protein observed as an increase in ΔT_m value for 0.3°C .

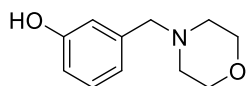
Through the hit exploration study around **107**, no fragment was found to display improved *in vitro* and biophysical profiles, except analogues **119g** and **119f** that were both weakly influenced thermal stability of PqsR

Table 9. The hit exploration study around fragment 107

Scaffold A



Scaffold B



ID	Scaffold	R ₁	Ring B	Remaining activity (RA) % PAO1-L ^{a,b,c,d,e}	ΔT (\pm °C) ^{e,f}
DMSO				100.0%	0
107	A	3-OH	11	NA	- 0.3
113	A	H	Ring 1	NA	/
114	A	2-OH	Ring 1	NA	/
115	A	3-Cl	Ring 1	NA	/
116	A	3-F	Ring 1	NA	/
117	A	4-Cl	Ring 1	NA	/
118b	A	3-OH	Ring 2	NA	/
118c	A	3-OH	Ring 3	NA	/
118d	A	3-OH	Ring 4	NA	/
119a	A	3-OMe	Ring 1	NA	+ 0.1
119b	A	3-OMe	Ring 2	NA	/
119c	A	3-OMe	Ring 3	NA	/
119d	A	3-OMe	Ring 4	NA	/
119e	A	3-OMe	Ring 5	NA	- 0.2
119g	A	3-OMe	Ring 7	NA	- 0.3
119f	A	3-OMe	Ring 6	NA	+ 0.3

ID	Scaffold	R ₁	Ring B	Remaining activity (RA) % PAO1-L ^{a,b,c,d,e}	ΔT (\pm °C) ^{e,f}
120	A	3-OMe-5-F	Ring 1	NA	/
121	A	3-OMe-5-Cl	Ring 1	NA	/
122	A	3-OMe-5-Me	Ring 1	/	- 0.1
123	A	3-OMe-4-OH	Ring 1	NA	- 0.1
124	A	3,4-di-OMe	Ring 1	NA	+ 0.1
125	A	3,5-di-OMe	Ring 1	NA	- 0.1
126	A	3,4,5-trimethoxy	Ring 1	NA	+ 0.2
141	B	/	/	NA	0

^aData shown are mean values obtained from three independent experiments performed in triplicates. ^b% Remaining Activity (RA%) screening at single concentration (50 μ M) in triplicates. ^cThe inhibitory effect evaluated using PAO1-LmCTX::PpqsA-lux reporter assays. Remaining activity (RA%) values below 70%, fragments were regarded as active. RA% values do not have a linear relationship with IC₅₀. ^dNA : not active. ^e"/": Not available. ^fThermal shift assay (TSA, °C) at 500 μ M ligand concentrations in duplicates or triplicates. The determination of TSA (\pm °C) was conducted in collaboration with William Richardson.

3.5 Hit optimization II: hit exploration around fragment 106

The influence of the key structural features of fragment binding to PqsR protein was investigated by introducing a methyl group onto the existing linker (**Figure 37**, compound **143**) or replacing the alcohol group with a primary amine group (**Figure 37**, **144**). Some close analogues of **106** with low synthetic complexity were also investigated (**Figure 37**, **145a-c** and **146b**) in order to find fragments with improved binding affinity compared to **106**.

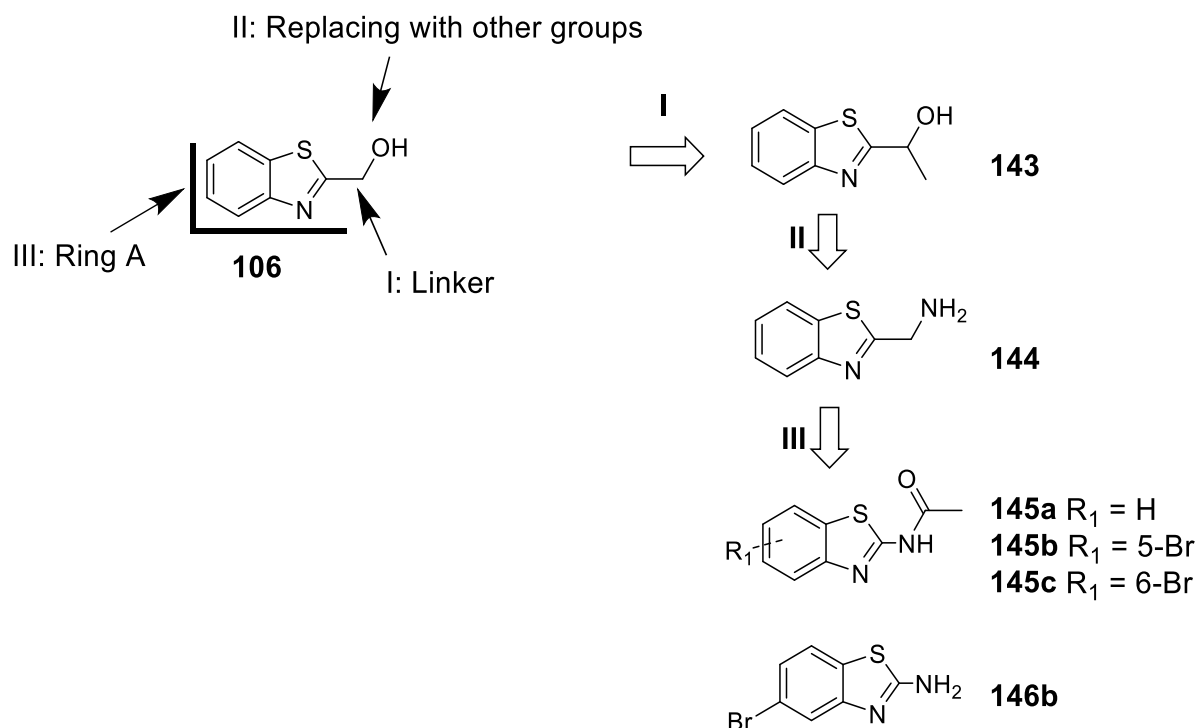
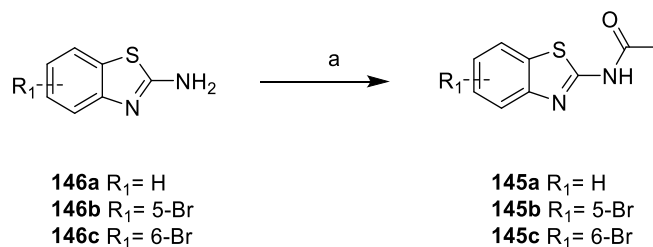


Figure 37. The design of the hit exploration around **106**.

3.5.1 The synthesis of designed analogues

Analogues with the benzothiazole core group (**145a-c**) were synthesized as outlined in **Scheme 9**. Substituted 2-aminobenzothiazoles (**146a-c**) were subjected to acetylation using acetic anhydride in the presence of DIPEA to give target analogues **145a-c**.

Scheme 9 Preparation of targeted compound **145a-c**



^aReagents and conditions: acetic anhydride, DIPEA, DMF, 60°C, ~80%-90%.

3.5.2 The results for the hit exploration study around 106

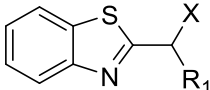
In the hit exploration study around **106**, TSA and ITC methods were applied for the evaluation of the fragments binding to PqsR protein.

By introducing a methyl group on to the linker, fragment **143** may have lost the ability to form key binding interaction towards PqsR as there was no observable change of the ΔT_m value.

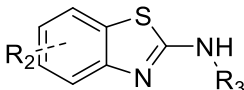
Replacing the alcohol group with a tertiary amine group, **144** destabilized the PqsR protein observed as a decrease of ΔT_m value of 0.2 °C at 500 μM screening concentration.

The benzothiazole analogue **145a** strongly stabilized the protein observed as an increase of ΔT_m value for 1.1 °C at 500 μM ligand concentration. Further introducing bromine atoms at the 5 (**145b**) or 6 (**145c**) positions of the benzothiazole ring, stabilized the protein observed as increase of ΔT_m values for 1.9 and 1.1 °C at 500 μM ligand concentration, respectively.

Table 10. The hit exploration study around fragment 106



A



B

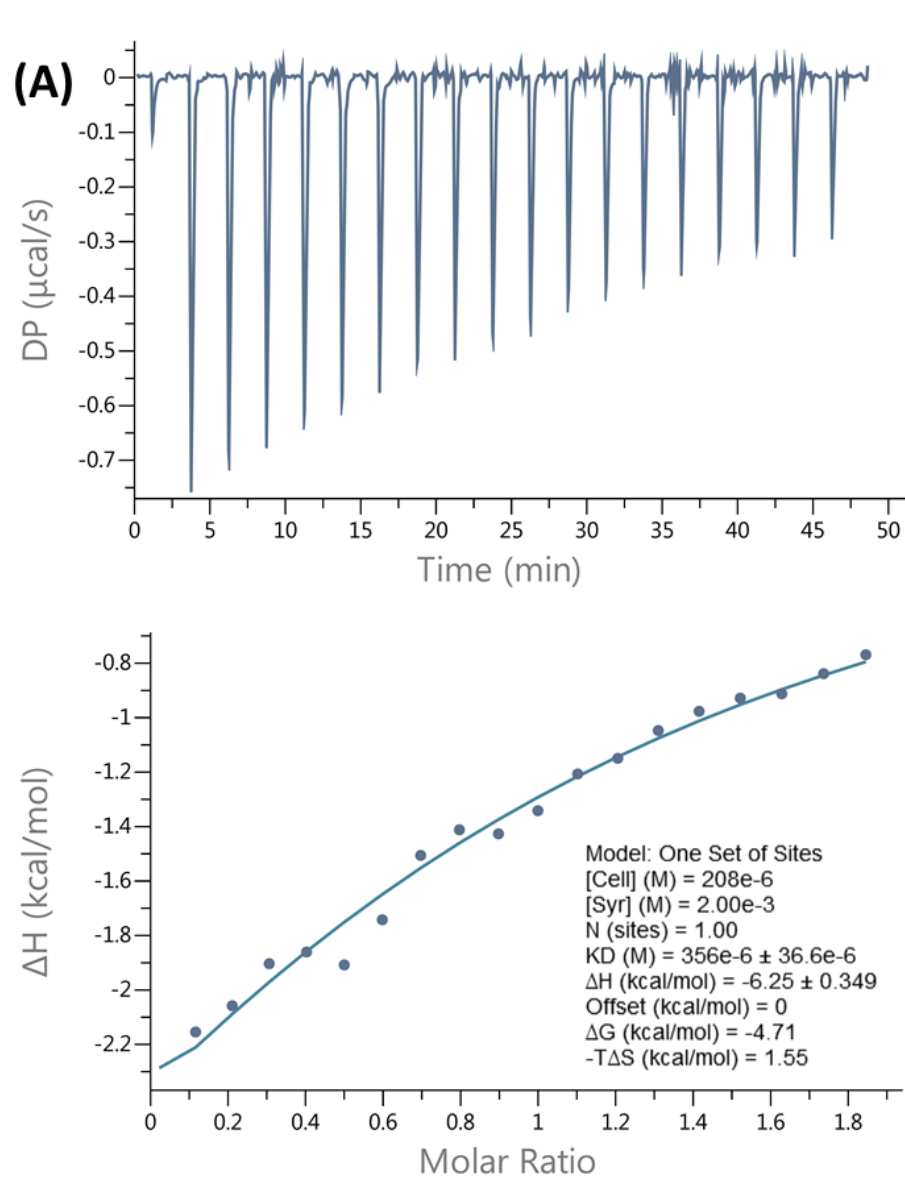
ID	Scaffold	R ₁	X	R ₂	R ₃	ΔT (\pm °C) ^{a,b}		K _d (μM)	
						500 μM	250 μM	No.1	No.2
DMSO						0	0		
106	A	H	OH	/	/	+ 0.5	+ 0.4	844	885
143	A	CH ₃	OH	/	/	0	0	/	/

ID	Scaffold	R ₁	X	R ₂	R ₃	$\Delta T (\pm ^\circ\text{C})^{a,b}$		$K_d (\mu\text{M})$	
						500 μM	250 μM	No.1	No.2
144	A	H	NH ₂	/	/	-0.2	0	/	/
145a	B	/	/	H	COCH ₃	+ 1.1	+ 0.5	356	409
145b	B	/	/	5-Br	COCH ₃	+ 1.9	/	/	/
145c	B	/	/	6-Br	COCH ₃	+ 1.1	/	39.5	/
146b	B	/	/	5-Br	H	/	/	142	75

^aThermal shift assay (TSA, °C) at 500 μM and 250 μM ligand concentrations in duplicates. ^b"/": not available. The determination of TSA (\pm °C) was conducted in collaboration with William Richardson. K_d values was obtained from ITC experiment.

ITC experiment was conducted to further confirm the binding interactions and determine thermodynamic parameters of **145a**, **145c** and **146b** to PqsR protein.

When titrating 5 mM **145a** in the presence of 200 μM PqsR protein solution, it confirmed the binding of **145a** to PqsR with an average K_d value of 382.5 μM based on two titrations. The average change of enthalpy (ΔH) was 6.6 kcal/mol and the average values of Gibbs free energy change (ΔG) was 4.6 kcal/mol, whilst the average $-\Delta S$ value was calculated as 1.9 kcal/mol (**Figure 38**).^{180,181}



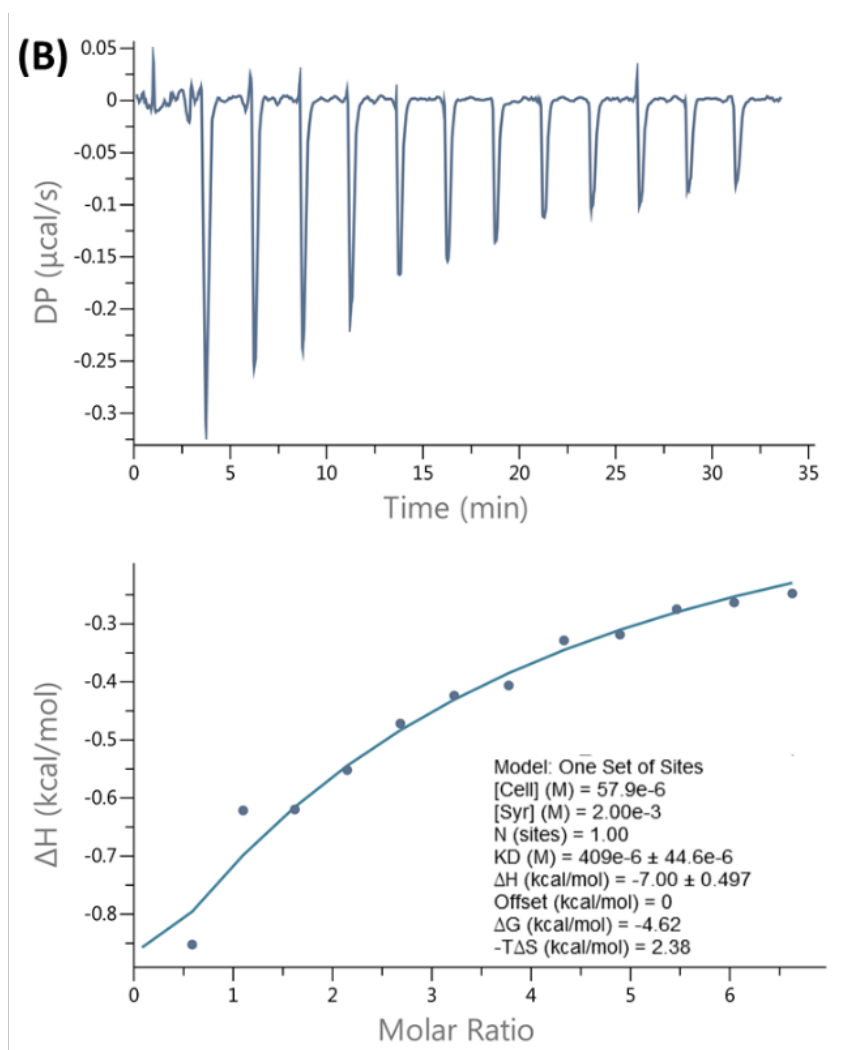


Figure 38. ITC results for **145a** in duplicates (A) and (B) including the injection peaks (on the top), the integrated data (at the bottom). The ITC experiment was designed and conducted by William Richardson.

Titrating 5 mM **145c** in the presence of 250 μM PqsR protein solution confirmed the binding of **145c** to PqsR protein with a K_d value as 39.5 μM and ΔH value was 2.20 kcal/mol. It was noticed that the N value was 3.5. In general, the high N value can result from multiple binding sites on the protein, ligand solubility issue and the selection of an inappropriate binding model. As there is only one ligand binding site on the PqsR protein, the high N value may attribute to the poor solubility of **145c** in the testing buffer or multiple binding interactions occurred in the same pocket (**Figure 39**).

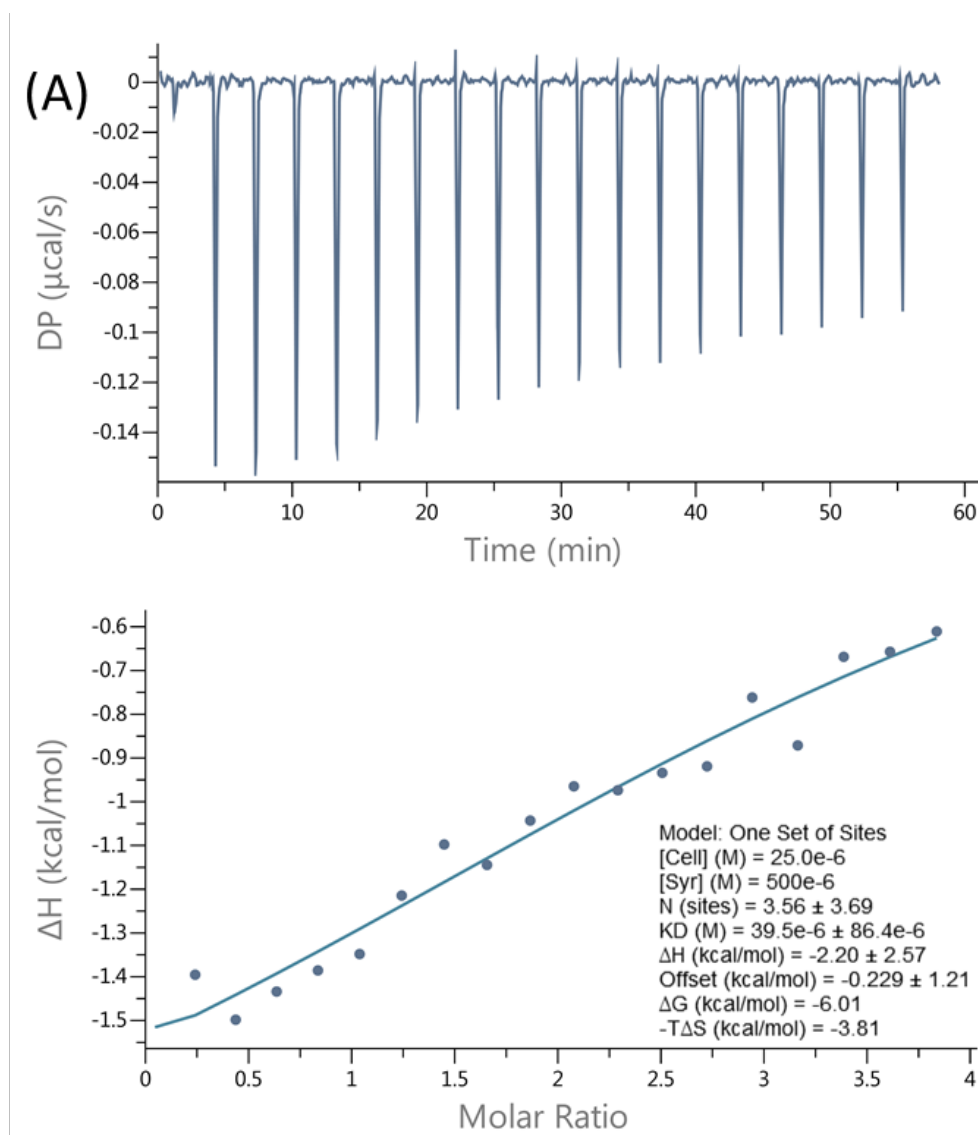
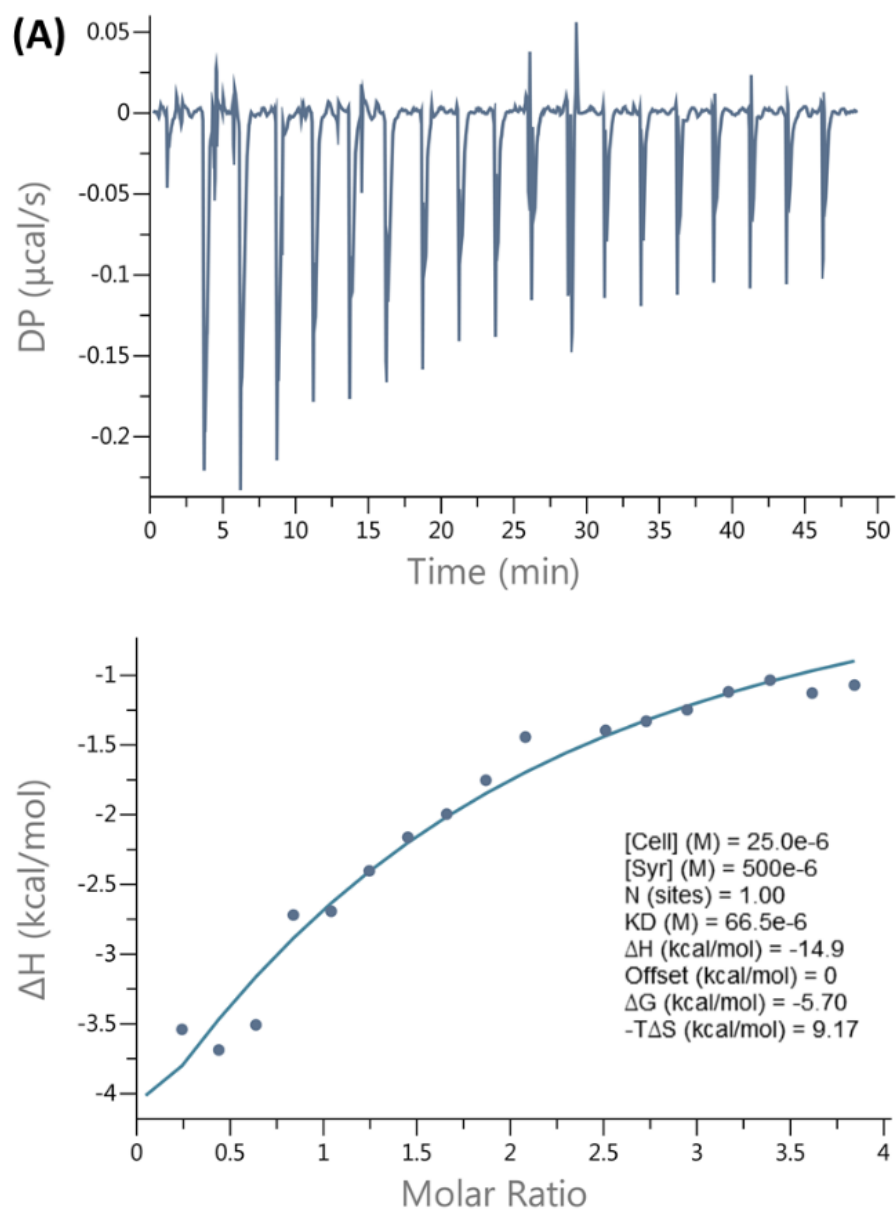


Figure 39. ITC results for **145c**: (A) the injection peaks (on the top), the integrated data (at the bottom). The ITC experiment was designed and conducted by William Richardson.

In order to improve the aqueous solubility of the bromo-substituted benzothiazole analogues, the free amine analogue (**146b**) was used in the ITC experiment instead of the corresponding acetamide (**145b**). Titrating 5 mM of **146b** in the presence of 250 μM PqsR protein solution confirmed the binding of **146b** to PqsR protein with an average K_d value of 108 μM based on two titrations. The ΔH was 20.5 kcal/mol and N was 1. Further calculation gave an average ΔG value as 5.43 kcal/mol and $-T\Delta S$ as 15.1 kcal/mol (**Figure 40**).



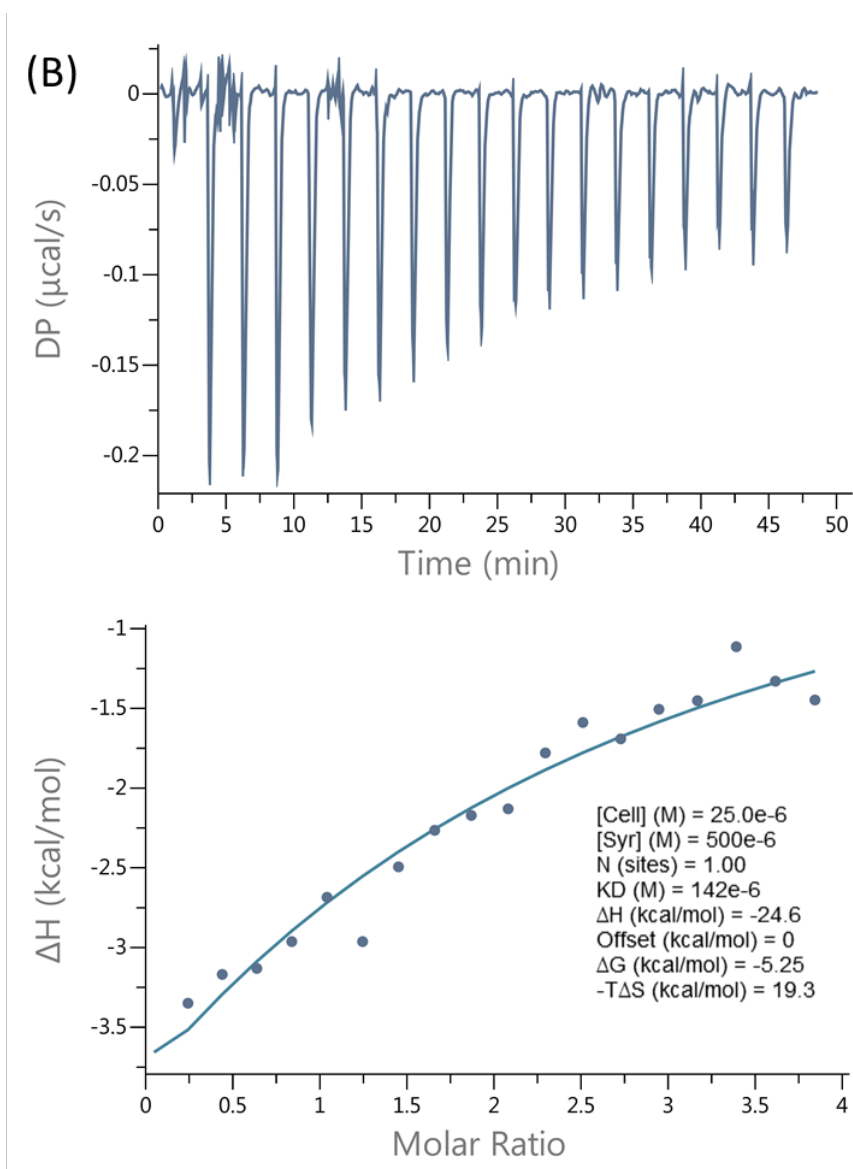


Figure 40. ITC results for **146b**: the injection peaks (A), the integrated data (B) and the thermodynamic parameters (C). The ITC experiment was designed and conducted in collaboration with William Richardson.

3.6 Conclusion

In this work, a novel workflow combining *in silico*, bioreporter assay and biophysical methods in fragment library screening and hit validation and optimisation was carried out.

Virtual screening was selected as the primary screening method followed by a manual inspection step on the high docking scoring fragments where fragments were assessed based on synthetic complexity.

The selected fragments **106-112** were subjected to bioreporter assay, TSA, and/or ITC methods for the validation of fragment binding to PqsR protein.¹⁸³

Compounds **106** and **107** with confirmed binding interactions were regarded as initial hits and advanced to hit exploration study and led to fragments **145a**, **145c** and **146b** with improved binding affinity.

All the synthesised fragments were collected to build a small fragment library which can be used to sample other biological targets of interest.

Chapter IV: Using fragment-based method for the discovery of novel PqsR antagonists for the treatment of *P. aeruginosa* infections

4.1 Introduction and aim

In the last chapter, through a virtual screening of fragment libraries against PqsR LBD followed by TSA and ITC screening, fragments **106**, **144**, **145a** and **146b** were identified following confirmation of ligand binding interaction with PqsR protein and desirable hit-likeness (**Figure 41**).

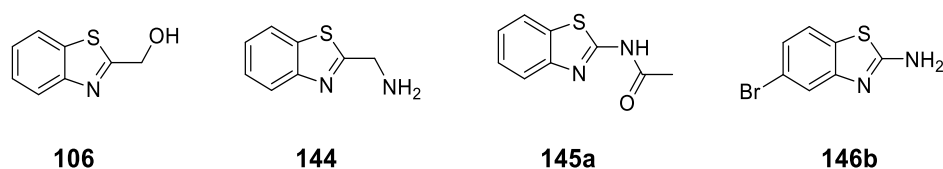
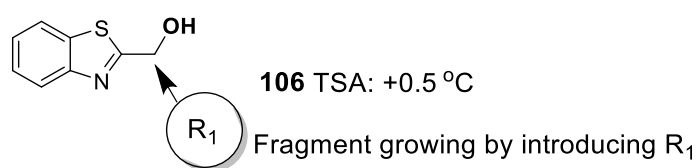


Figure 41. Structure of fragment hits **106**, **144**, **145a** and **146b** and all compounds follows Ro3.

In this chapter, fragment evolution methods including fragment growing, linking, and merging methods were applied to fragments **106**, **144**, **145a** and **146b** for the identification of lead-like PqsR inhibitors (**Figure 42**).

Scheme I



Scheme II

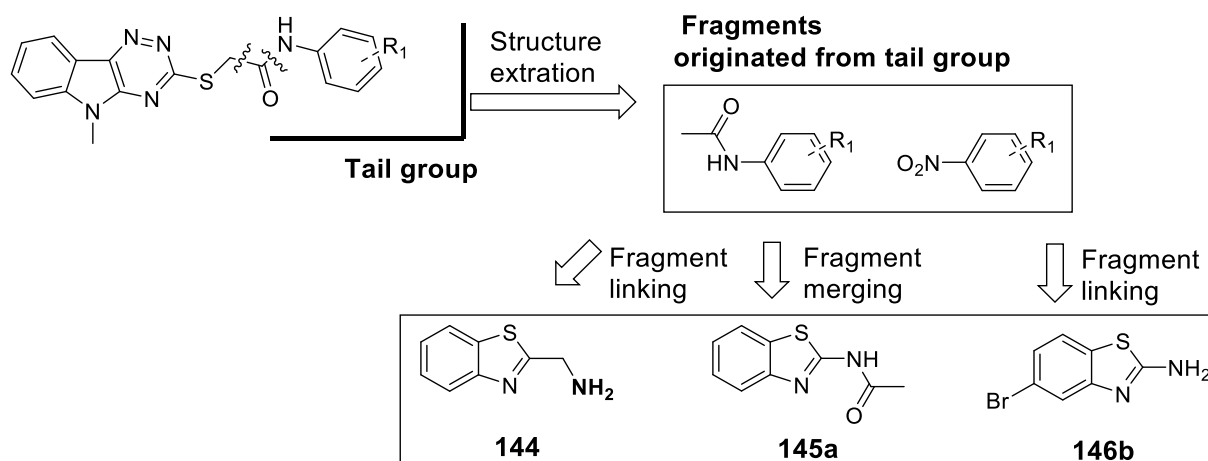


Figure 42. Schematic representation of fragment hit evolution methods. **Scheme I** illustrated fragment evolution strategy for **106**: fragment **106** was advanced through a fragment growing method by intruding a range of alkyl chains at R₁. **Scheme II** illustrated fragment evolution strategies for fragment **144**, **145a**, and **146b**: structure extraction of the tail groups of the 5-methyl-5*H*-[1,2,4]triazino[5,6-*b*]indol-3-yl)thiol analogues to give fragments followed by fragment linking or merging with fragments **144**, **145a** and **146b**.

The crystal structure of PqsR LBD with two bound 2-methyl-2, 4-pentanediol (MPD) molecules in two sub-pockets (pocket 1 and 2) has been reported (**Figure 43**). This finding suggested that PqsR LBD can be occupied by two small ligands at the same time and inspired us to explore fragments bind to these two adjacent pockets at the same time.

It was hypothesized that low affinity fragments bind to a sub-pocket of PqsR LBD may not be able to be detected by TSA or bioreporter assays, whilst these weak binding interactions may cause a subtle conformational change of the ligand binding pocket. This subtle conformational change of PqsR LBD may enhance the binding of a second fragment to another sub-pocket. In doing so, these two fragments can functionalize as

synergistic combinations observed as the fragment cocktails displaying a greater effect in bioreporter assay and biophysical experiments than the single fragments.

In this work, a synergistic experiment assisted by TSA and mCTX::*PpqsA-lux* based bioreporter assay was designed for the identification of synergistic fragment pairs.

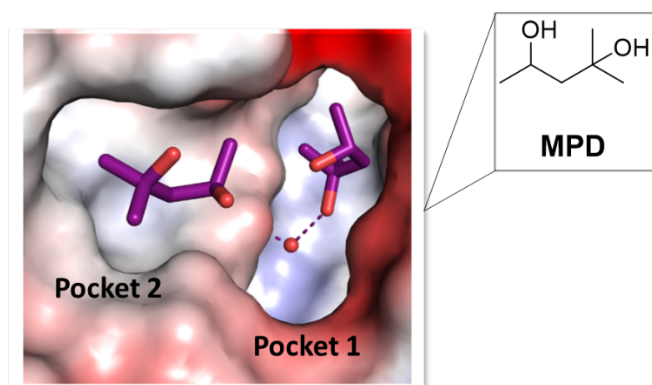


Figure 43. Crystal structure of PqsR LBD with two bound MPD molecules in PqsR LBD (pocket 1 and 2).¹¹ The scaffold of MPD was represented in purple (PDB code :4jvc).

4.2 Advancing **106** through a fragment growing method

Fragment **106** weakly stabilized the PqsR protein observed as a 0.5 °C decrease of ΔT_m at 500 μM screening concentration in TSA. However, growing fragment **106** by introducing a methyl group at R_1 , affording fragment **143** led to no observable ΔT_m change in TSA (**Figure 44**).

Natural hydroxyquinoline-based agonist PQS and the benzothiazole analogues such as **106** both contain a bicyclic core and alcohol groups (**Figure 44**) and the biological activity of the hydroxyquinoline analogues is alkyl chain length dependent. Shortening the heptyl side chain of PQS decreases agonist potency in the PAO1 strain, whilst, lengthening the heptyl side chain to either an octyl or nonyl chain maintains potent

agonism. It was also demonstrated that replacing the linear heptyl chain in PQS with aromatic substituents (**147a** and **147b**) abolished agonist activity.^{156,184–186}

Based on the scaffold similarity between the benzothiazole analogues and PQS, it was hypothesized that the *pqs* inhibition of the benzothiazole analogues can also be alkyl chain length dependent. A fragment growing method was applied to **106** by lengthening the alkyl chain at R₁, which led to the design of compounds **148a-d** (Figure 44).

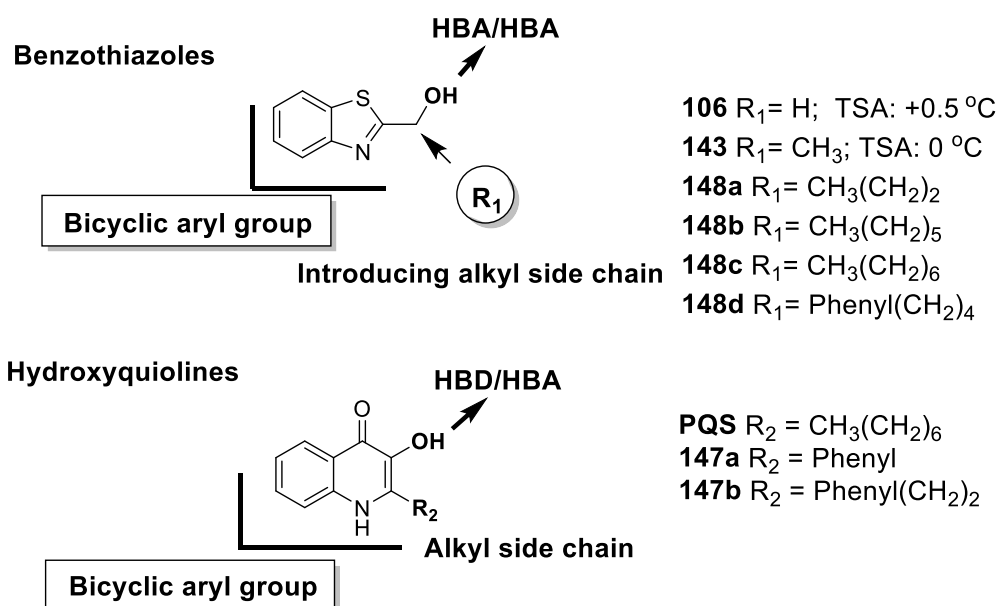
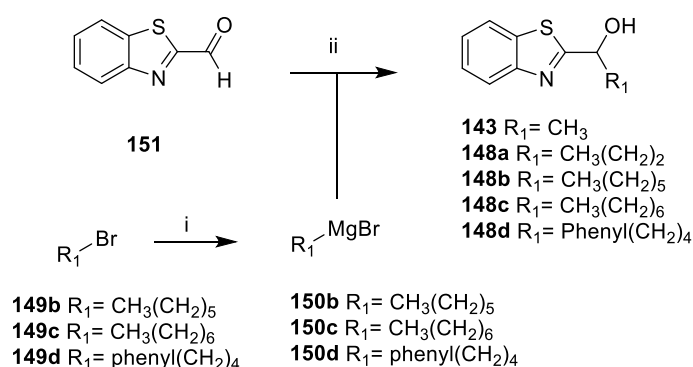


Figure 44. Structure comparison between the hydroxyquinoline and benzothiazole analogues.

4.2.1 The synthesis of designed analogues **143**, **148a-d**

The forward synthetic scheme for the benzo[*d*]thiazol-2-yl-1-ol analogues **143** and **148a-d** is shown in **Scheme 10**. Benzothiazole-2-carboxaldehyde **151** was subjected to Grignard reactions to give the secondary alcohols **143**, and **148a-d** in which the Grignard reagents **150b-d** were prepared from bromides **149b-d** reacting with Mg under an inert atmosphere of N₂.

Scheme 10 Preparation of compounds 143 and 148a-d

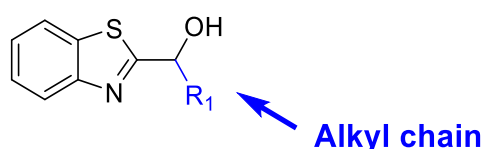


^a Reagents and conditions: (i) Mg, I₂, THF, N₂, reflux; (ii) CH₃MgBr or CH₃(CH₂)₂MgBr or **150a-d**, THF, N₂, rt.

4.2.2 Bioreporter assay and TSA screening results for designed analogues 143 and 148a-d

Lengthening the alkyl chain from a methyl group (**143**) to a propyl chain (**148a**) destabilized the PqsR protein as evidenced by a negative ΔT_m value of -0.4 °C at 500 μ M ligand concentration (**Table 11**). Introducing a hexyl (**148b**) or heptyl (**148c**) chain at R₁, strongly stabilized the protein observed as an increase of ΔT_m value of 0.9 °C for both compounds. Compounds **148b** and **148c** also showed *pqs* inhibition in the PAO1-LmCTX::*PpqsA-lux* reporter assay observed as RA% values of 60% and 63% at 50 μ M screening concentration, respectively.

Table 11. Analogues 56, 84, 108, 109 110 and 111 physicochemical properties, RA% and TSA screening results



ID	R ₁	MWt.	CLogP	RA% ^{a,b,c}	ΔT_m (\pm °C) ^d
106	H	165.21	1.042	105.18 \pm 2.29	+0.5

ID	R ₁	MWt.	CLogP	RA% ^{a,b,c}	ΔTm (±°C) ^d
143	CH ₃	179.04	1.35	94.66 ± 7.17	0
148a	CH ₃ (CH ₂) ₂	207.29	2.41	93.52 ± 8.42	-0.4
148b	CH ₃ (CH ₂) ₅	249.37	4.00	59.98 ± 6.08	+0.9
148c	CH ₃ (CH ₂) ₆	263.40	4.53	63.44 ± 8.89	+0.9
148d	Phenyl(CH ₂) ₄	297.42	4.36	64.37 ± 6.46	-0.3

^aData shown are mean values obtained from three independent experiments performed in triplicates. The data are shown as mean ± standard deviation (SD) ^b% Remaining Activity (RA%) were obtained through PAO1-LmCTX::*PpqsA-lux* reporter assay screening at single concentration (50 μM) in triplicates. ^c Remaining activity (RA%) values below 70%, fragments were regarded as active. RA% values do not have a linear relationship with IC₅₀. ^dThermal shift assay (TSA, °C) at 500 μM ligand concentrations in duplicates. The determination of TSA (± °C) was conducted in collaboration with William Richardson.

The high CLogP values of **148b-c** might well contribute to the improved *pqs* inhibition in the bioreporter assay. Higher lipophilicity can improve ligand binding affinity to biological targets and ligand penetration ratio through biological membranes,^{187–189} lengthening the alkyl chain leads to an increase in ligand lipophilicity which might ultimately affect *pqs* inhibition.

Truncation of the linear alkyl side chain in combination with the addition of a terminal aryl group led the discovery of **148d**, which retained *pqs* inhibition with a RA% of 64% at 50 μM screening concentration in the bioreporter assay against PAO1-L. Compound **148d** also weakly destabilized the PqsR protein reflected as a 0.3 °C (500 μM) decrease of ΔTm in TSA. Compared with the hydroxyquinoline analogues (PQS, **147a-b**) which have limited tolerance for introducing aromatic tail groups, the benzothiazole analogues may have better tolerance for R₁ variation in terms of *pqs* inhibition.

4.3 Extract fragments from the 5-methyl-5H-[1,2,4]triazino[5,6-b]indol-3-yl)thiol analogues

In the SAR study around the 5-methyl-5H-[1,2,4]triazino[5,6-b]indol-3-yl)thiol analogues, it was noticed that variations of the terminal aryl tail groups led to *pqs* inhibitory activity difference (Figure 45).

It was surmised that the aryl tail groups of **38**, **19**, **65**, **69** and **79** contribute to the observed differences in *pqs* inhibition. These compounds were then subjected to structure deconstruction (Figure 45), which led to the design of fragments **152a-d**, **81** and **82**.

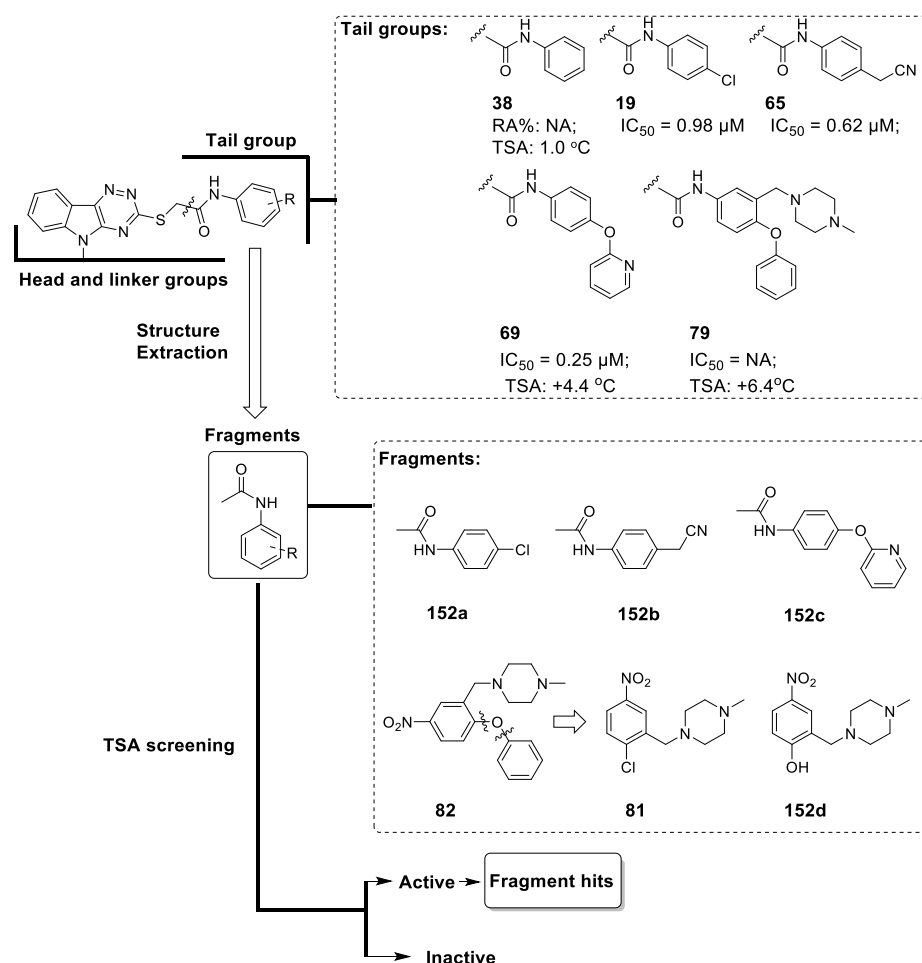


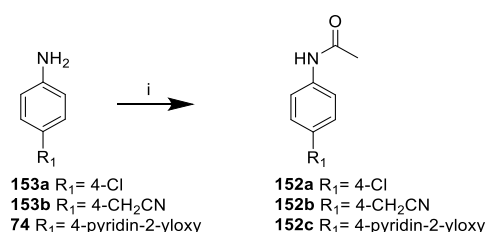
Figure 45. A FBLD scheme starting from structure extraction of the tail groups of the 5-methyl-5H-[1,2,4]triazino[5,6-b]indol-3-yl)thiol analogues to give fragments **81**, **82**, and **152a-d**. Compounds **38**, **19**, **65**, **69** and **79** were drug-sized PqsR antagonists,

which share identical head and linker groups but displayed different *in vitro* profiles. It was hypothesised that fragments extracted from the tail group of the 5-methyl-5H-[1,2,4]triazino[5,6-*b*]indol-3-yl)thiol analogues may also bind to the PqsR LBD and possess a similar binding mode as the tail groups of the original drug-sized molecules.

4.3.1 The synthesis of designed fragments 152a-c

The synthetic route for **152a-c** are summarized in **scheme 11**. The 4-substituted anilines **153a-b** and **74** were subjected to acetylation using acetic anhydride to give **152a-c**. Fragment **81** and **82** were synthetic intermediates from previous series.

Scheme 11 Preparation of designed fragments 152a-c

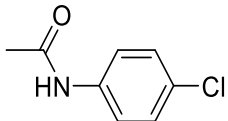
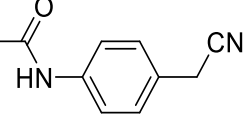
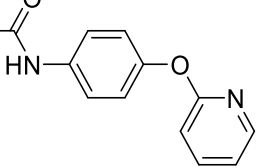
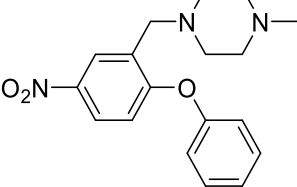
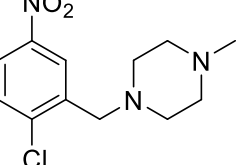
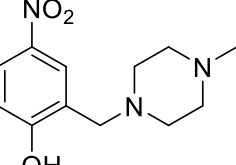
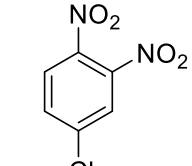
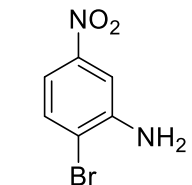


^aReagents and conditions: (i) acetic anhydride, DCM, 40°C.

4.3.2 The screening of fragments 152a-d, 81 and 82 using TSA

As compounds **19** and **65** were equally potent in the bioreporter assay, it was hypothesised that **152a** and **152b** originating from the tail groups of **19** and **65** should display similar biophysical and bioreporter assay screening profiles. Surprisingly, the two fragments displayed divergent TSA results. Fragment **152a** strongly stabilized the PqsR protein reflected by an observed increase of ΔT_m value for 1.1 °C, whilst **152b** had a minimal influence on the protein thermal stability **Table 12**.

Table 12. Fragments 81, 82, 152a-d TSA screening results

ID	Structure	CLogP	$\Delta T_m (\pm ^\circ\text{C})^{a,b}$	
			500 μM	250 μM
DMSO			0	0
152a		2.13	+1.1	+1.1
152b		0.58	+0.2	+0.2
152c		1.76	-0.7	-0.3
82		4.29	-0.8	-0.5
81		2.91	-0.3	-0.2
152d		2.11	+0.2	+0.1
152e		2.34	+5.3	+3.5
152f		2.27	+1.3	+0.9

^aThermal shift assay (TSA, $^\circ\text{C}$) at 500 μM and 250 μM ligand concentrations in duplicates. ^bThe determination of TSA ($\pm ^\circ\text{C}$) was conducted in collaboration with William Richardson.

Fragment **152c** originating from compound **69**, strongly destabilized the PqsR protein reflected by an observed decrease of ΔT_m value for 0.7 °C. Fragmentation of **79** led to the identification of **82** which strongly destabilized PqsR protein observed as a decrease of ΔT_m value for 0.8 °C at 500 μM ligand concentration. Further deconstruction of **82** led to the identification of fragments **81** and **152d**, where **81** weakly destabilized the protein and **152d** weakly stabilized the protein at 500 μM ligand concentration in TSA.

These results suggested that electron deficient aromatic ring systems, such as fragment **152a** can be preferable in terms of increasing PqsR protein thermal stability. In order to prove this assumption, fragments **152e** and **152f** with strong electron withdrawing groups (nitro groups and halogen atoms) were screened using TSA method and both fragments strongly stabilized the PqsR protein. With similar CLogP values, fragments **152e** displayed higher ΔT_m value than **152f**, which may attribute to more electron deficient nature of **152e**.

Fragment **152a** strongly stabilized the PqsR protein and was progressed for ITC experiment to determine the thermodynamic parameters.

4.3.3 Determination of the thermodynamic parameters of **152a** using ITC

Titrating 1 mM **152a** in the presence of 250 μM PqsR protein solution confirmed the binding of **152a** to PqsR protein with a binding affinity (K_d) value as 30.0 μM . The ΔH was observed as - 4.97 kcal/mol and N was 1 (**Figure 46**). This allowed further calculation for the average values of ΔG as 6.08 kcal/mol and $-T\Delta S$ as 1.2 kcal/mol. The negative ΔH and $-T\Delta S$ values indicates favourable entropic and enthalpic binding signatures of **152a**. Considering the favourable entropic and enthalpic binding

signatures and the strong binding interaction to PqsR protein, **152a** was selected as a promising fragment candidate for fragment linking and merging methods.

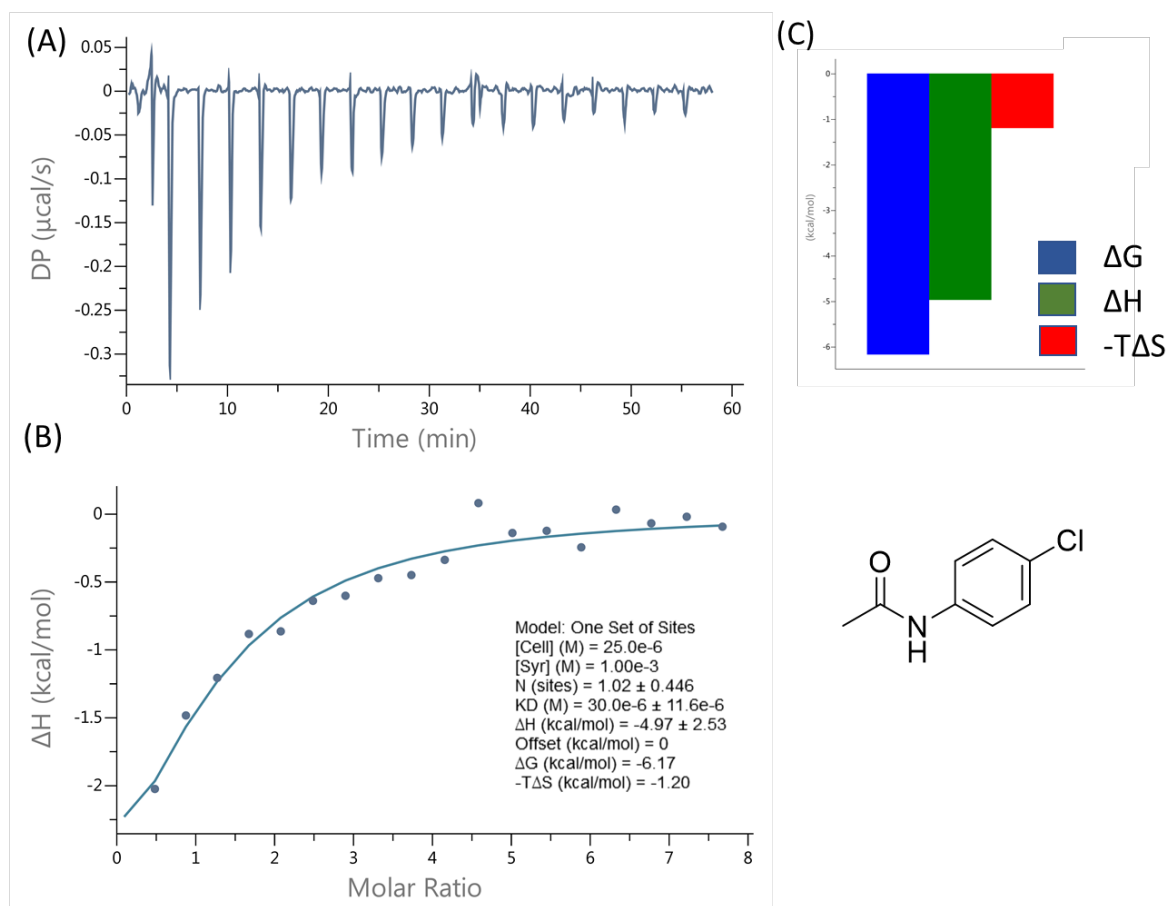


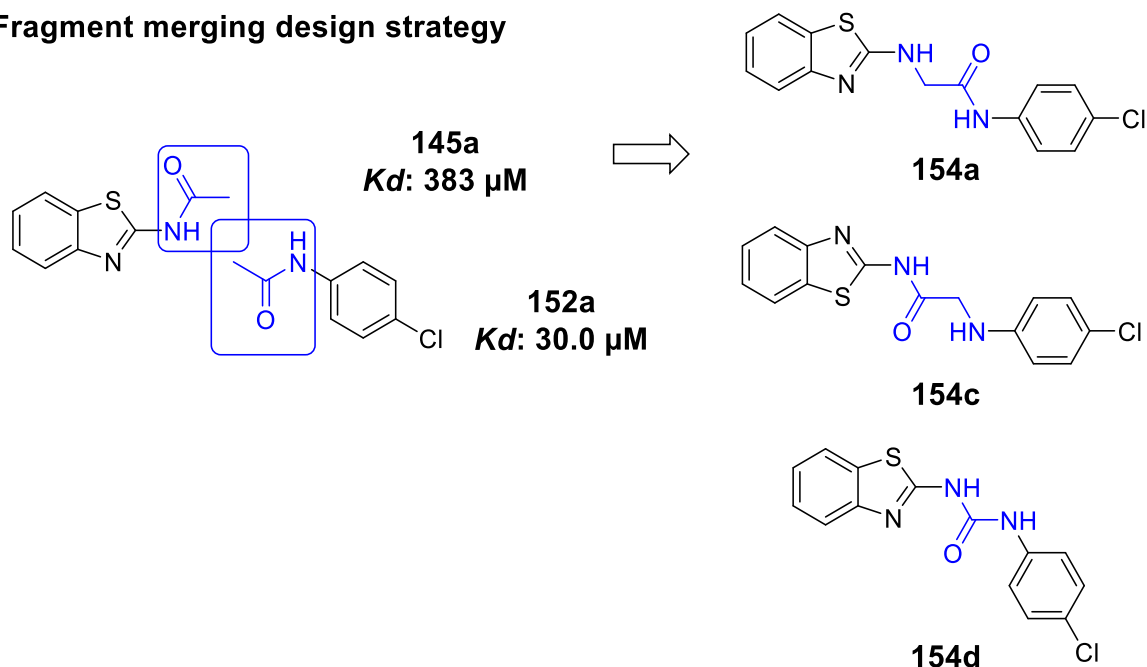
Figure 46. ITC results for **152a**: (A) the injection peaks (B) the integrated data (C) the thermodynamic parameters. The ITC experiment was designed and conducted by William Richardson.

4.4 Applying fragment linking and merging methods between strong PqsR fragment binders benzothiazole analogues (**145a** and **146b**) and **152a**

The binding thermodynamic parameters of the amino benzothiazole analogues (**145a**, **146b**) and **152a** to PqsR protein was previously confirmed through ITC experiments. However, X-ray co-crystal structures for these fragments bound to PqsR LBD are still not determined. Fragment linking, and merging methods were applied to fragments

pairs **145a** with **152a** and **146b** with **152a** and led to the design of compounds **154a,c,d** and **154b** respectively (**Figure 47**). Due to time limitation, only **154a** and **154b** were synthesized.

Fragment merging design strategy



Fragment Linking design strategy

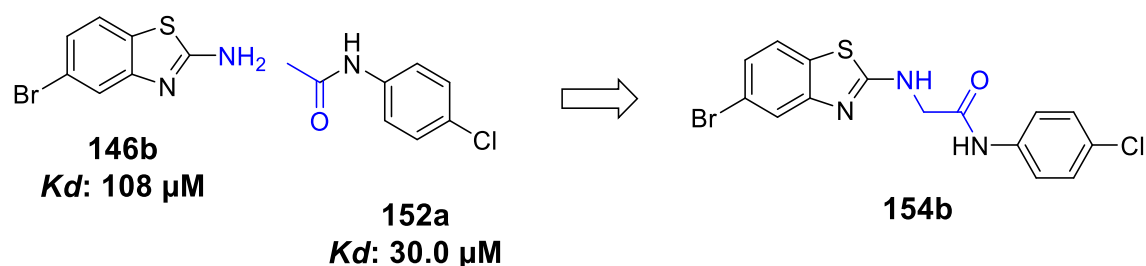


Figure 47. Schematic representation of the fragment linking and merging strategy between **145a** with **152a** and **146b** with **152a**. *Kd* values were obtained from ITC experiments. There are multiple merging strategies can be applied between fragments **145a** and **152a** and examples were displayed as **154a**, **154c** and **154d**, however due to time limitation only compound **154a** was synthesized.

Compound **154a** was predicted to bind to the PqsR LBD where the 2-aminobenzothiazole group is predicted to act as a HBD through hydrogen bonding with Leu²⁰⁷. Compound **154b** could bind to the same PqsR ligand binding site where

the amino group could hydrogen bond with Leu²⁰⁷ and the 4-chlorophenyl group is predicted to partake in a face to edge π -stacking interaction with Tyr²⁵⁸ (**Figure 48**).

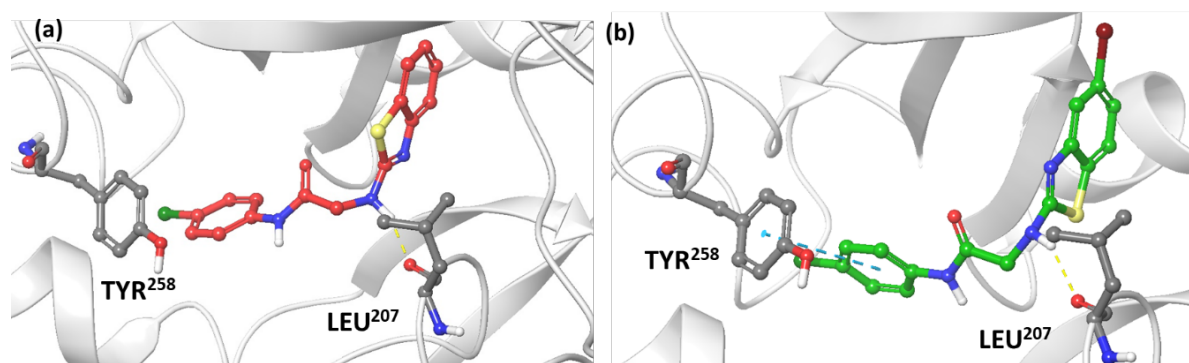
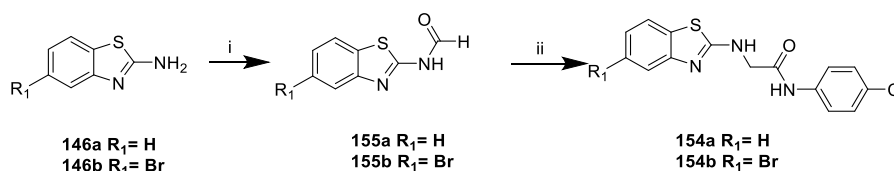


Figure 48. Predicted binding modes of compound **154a** (a) and **154b** (b) in PqsR LBD. Hydrogen bonds are shown as yellow dash lines. π -stacking interaction is shown as blue dash lines. The ligand scaffolds were represented in red (**154a**) and green (**154b**).

4.4.1 The synthesis of designed compounds **154a** and **154b**

The preparation of the 2-aminobenzothiazole analogues **154a** and **154b** is represented in **Scheme 12**. Intermediate *N*-formamides **146a-b** were firstly deprotonated by NaH under an inert atmosphere of N₂ and then reacted with the electrophile 2-bromo-*N*-(4-chlorophenyl)acetamide (**91**) through nucleophilic substitution to give compounds **154a-b**.

Scheme 12 Preparation of **154a** and **154b**

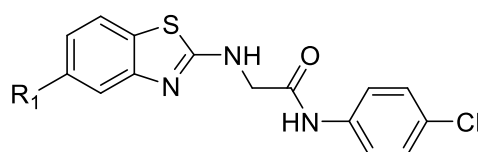


^aReagents and conditions: (i) acetic anhydride, formic acid, 40°C, N₂. (ii) **91**, NaH, DMF, 0°C to rt.

4.4.2 The biophysical and *in vitro* profiles of compounds 154a-b

Merging fragments **145a** and **152a** led to the design and synthesis of compound **154a** which was inactive in the bioreporter assay against PAO1-L. Applying a fragment linking method between two strong PqsR binders **146b** and **152a** led to the discovery of **154b**. Compound **154b** showed a RA% value of 34% at 10 μ M screening concentration against PAO1-L in the mCTX::*PpqsA-lux* based bioreporter assay, which also strongly stabilized PqsR protein observed as an increase of ΔT_m value for 1.9 $^{\circ}$ C at 500 μ M ligand concentration in TSA.

Table 13. The biophysical and bioreporter assay screening profiles for compound 174 and 175



Compd.	R ₁	RA% ^{a,b}	ΔT (\pm° C) ^{c,d}
154a	H	86.40 \pm 6.03	/
154b	Br	33.92 \pm 2.92	+ 1.9

^aThe inhibitory effect evaluated using PAO1-LmCTX::*PpqsA-lux* reporter assay at single concentration (10 μ M) in triplicates. ^bThe data are shown as mean \pm standard deviation (SD). ^cThermal shift assay (TSA, $^{\circ}$ C) at 500 μ M ligand concentrations in duplicates. ^d"/" indicates Not available. The determination of TSA (\pm° C) was conducted in collaboration with William Richardson.

4.5 Fragment linking strategy between a weak binder 144 and a strong binder 152a

Fragment **144** weakly destabilized the PqsR protein observed as a decrease of ΔT_m value for 0.2 $^{\circ}$ C at 500 μ M ligand concentration in TSA. A fragment linking strategy was

applied to between fragments **144** and **152a**, which led to the design of compounds **156a-c** with different linkers (**Figure 49**).

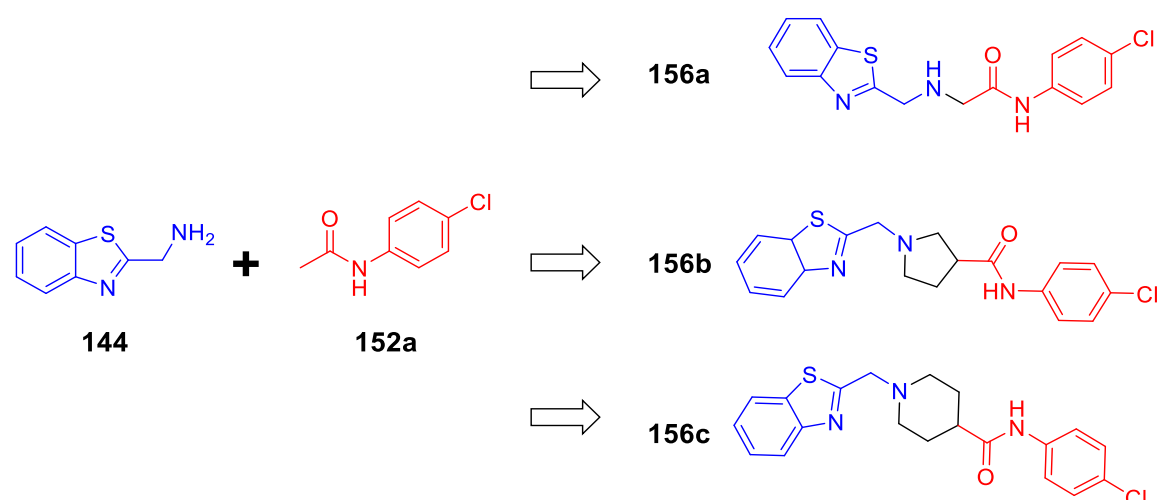


Figure 49. Schematic representation of the fragment linking strategy between **144** and **152a** through different linkers.

Compounds **156a-c** share a high scaffold similarity and were predicted to bind to the same region in the PqsR LBD. The 4-chlorophenyl groups of compounds **156a-b** can insert deeply in the pocket, whilst **156c** may flip in the pocket with the 4-chlorophenyl group pointing outside (**Figure 50**).

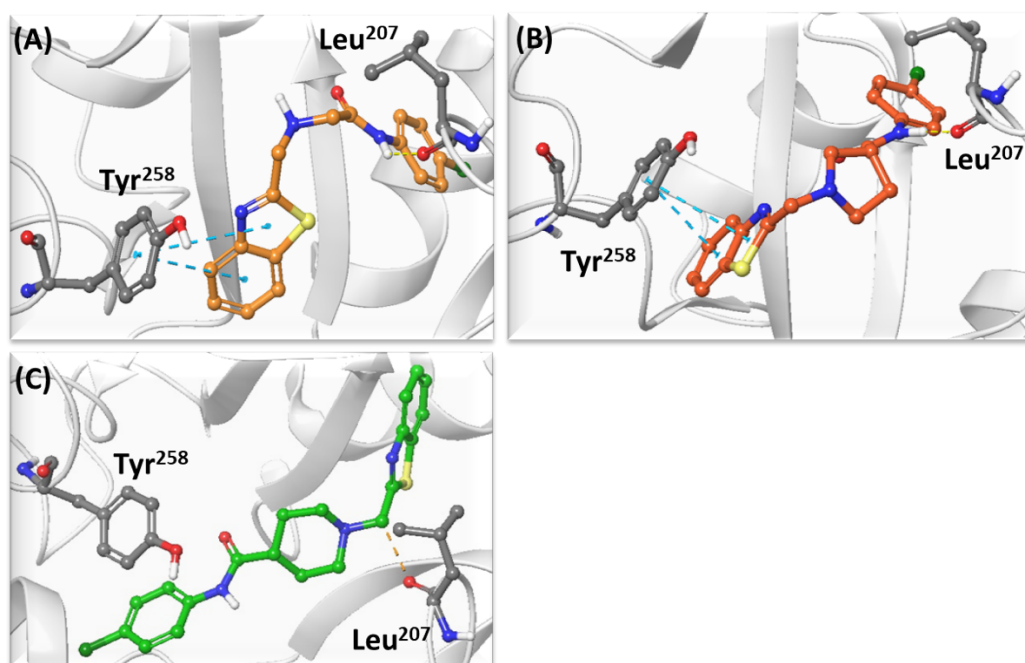


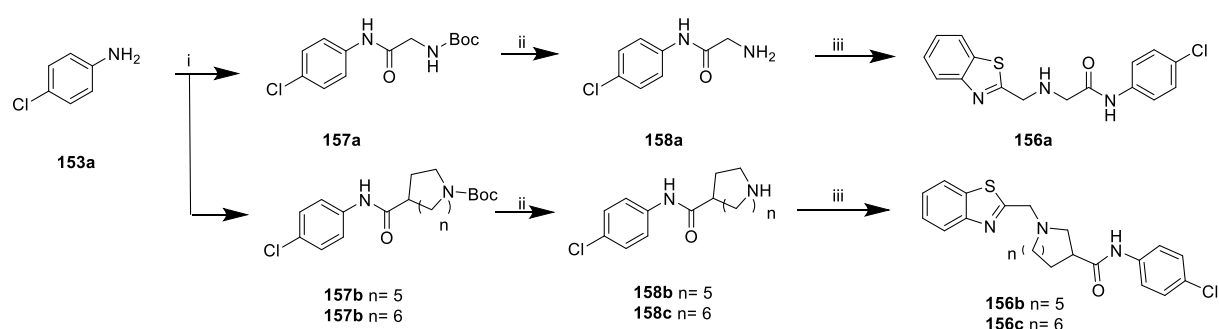
Figure 50. Predicted binding modes of compound **156a** (A), **156b** (B) and **156c** (C) in PqsR LBD. Hydrogen bonds are shown as yellow dash lines. π -tacking interaction

is shown as blue dash lines. The unfavourable clash is shown as orange dash line. The ligand scaffolds were represented in orange (**156a**), red (**156b**) and green (**156c**).

4.5.1 The synthesis of designed compound 156a-c

The preparation for **156a-c** is outlined in **Scheme 13**. Compound **153a** was subjected to amide coupling to react with Boc-glycine, Boc-proline and *N*-Boc-piperidine-4-carboxylic acid using HATU as coupling reagent to give compounds **157a-c**. After the acidic treatment of **157a-c** using 4M HCl in dioxane, the resulting analogues **158a-c** were then subjected to reductive amination with benzo[*d*]thiazole-2-carbaldehyde using NaBH(OAc)₃ as reducing reagent to give analogues **156a-c**.

Scheme 13 Preparation of 156a-c



^aReagents and conditions: (i) HATU, DIPEA, DMAP, NMP, rt. (ii) 4M HCl in 1,4-dioxane, rt, >100%; (iii) benzo[*d*]thiazole-2-carbaldehyde, NaBH(OAc)₃, HOAc, THF, rt, N₂.

4.5.2 The bioreporter assay screening results for compound 156a-c

Fragments **144** and **152a** were linked through a range of linkers, including linear alkyl linker and ring systems and the resulting analogues **156a-c** were subjected to the PAO1-LmCTX::Ppq*sA-lux* reporter assay for the assessment of *pqs* inhibition. Whilst compounds **156a-c** were predicted to bind to PqsR LBD in docking studies, these compounds unfortunately proved inactive in the later bioreporter assay (**Figure 51**).

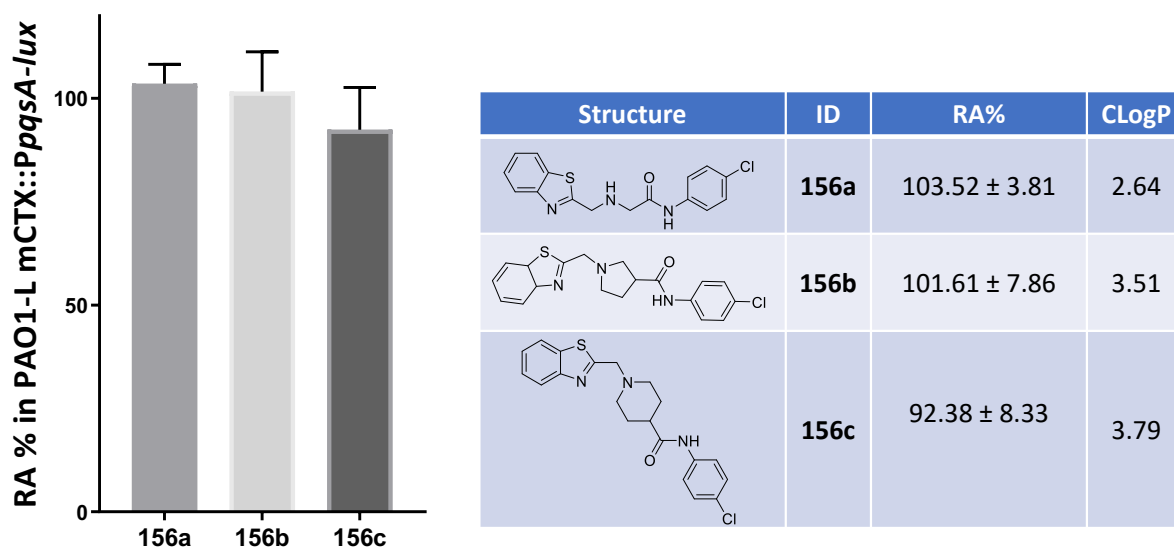


Figure 51. Inhibitory effect of **156a-c** through the PAO1-LmCTX::PpqsA-lux reporter assay. Remaining activity (RA%) values below 50%, compounds were regarded as active. Compounds **156a-c** were screened at single concentration (10 μ M) in triplicates. The data is shown as mean \pm standard deviation (SD)

4.6 Exploration of synergistic combinations assisted by the mCTX::PpqsA-lux-based bioreporter assay and TSA

As mentioned previously, it was hypothesized that PqsR LBD can be occupied by two small ligands at the same time and these two fragments can functionalize as synergistic combinations observed as the fragment cocktails displaying a greater effect in bioreporter assay and biophysical experiments than the single fragments. In order to explore fragment synergistic combinations, experiments were designed using the mCTX::PpqsA-lux-based bioreporter assay and TSA method.

The mCTX::PpqsA-lux-based bioreporter assay was incorporated for the assessment of single fragments and fragment combinations *pqs* inhibition. Statistical analysis was introduced to compare the *pqs* inhibition differences between single fragment solutions and fragment cocktails solutions. Statistical analysis between three or more data sets was performed by Ordinary one-way ANOVA followed by Tukey's multiple

comparisons test with a single pooled variance. A p -value lower than 0.05 is considered to represent a significant difference. Statistical analysis was performed using GraphPad Prism version 8.1.2 (GraphPad Software, Inc., La Jolla, CA, USA).

Fragments **81**, **105**, **107**, **108** and **125** were selected from the in-house fragment library for the exploration of fragment synergistic combinations (**Figure 52**). All fragments showed no pqs inhibition observed as pqs activity reduction less than 10% (i.e. RA% > 90%) in the mCTX::*PpqsA-lux*-based bioreporter assay at 50 μ M screening concentration (**Table 14**).

For the determination of fragment pairs pqs inhibition, PAO1-L was treated with 50 μ M final concentration of the cocktail fragment solutions, which was prepared from two evenly mixed fragment solutions. In this work, fragment pairs: **81** and **108**, **81** and **107**, **81** and **105**, **81** and **125** were screened accordingly.

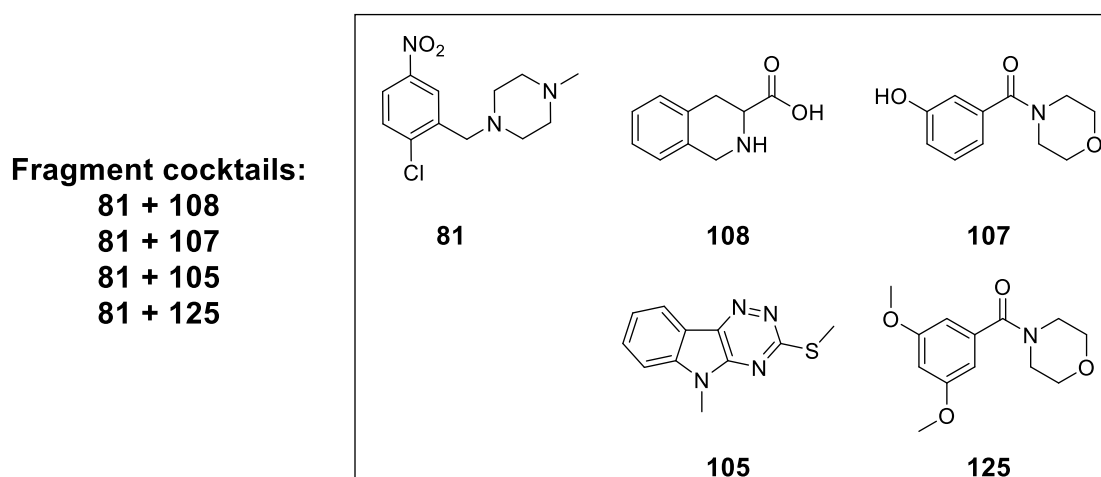


Figure 52. Fragments selected for synergistic exploration.

It was surprisingly to notice that the fragment cocktail containing **81** and **108** showed pqs inhibition with a RA% value of 62% **Table 14**, which was more potent than single fragment solutions (**Figure 53**).

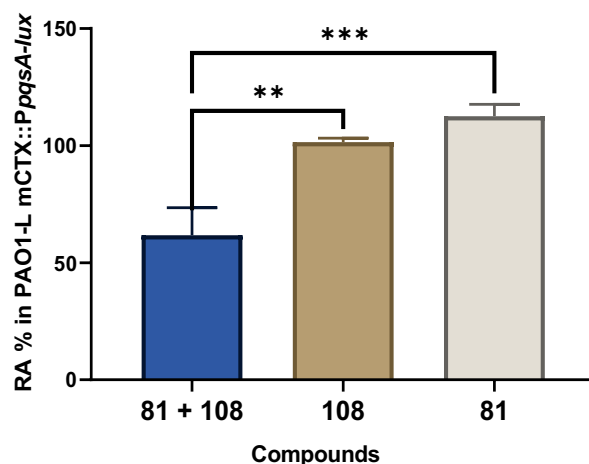
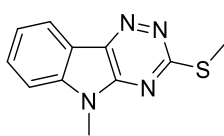
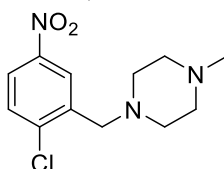
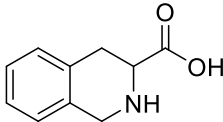
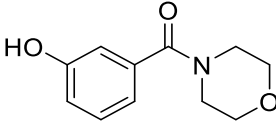
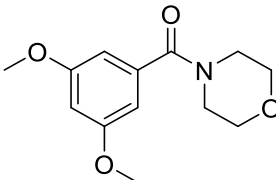
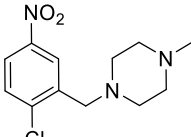
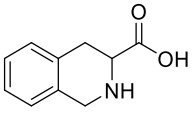
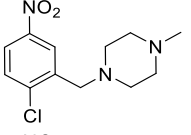
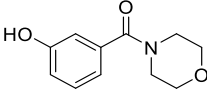
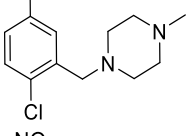
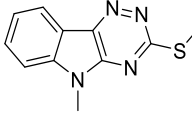
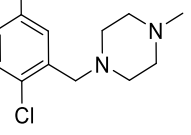
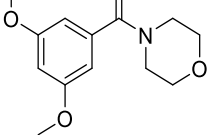


Figure 53. The inhibitory effect of single fragments **81** and **108** and the fragment cocktail containing both **81** and **108** through the PAO1-LmCTX::PpqsA-lux reporter assay at single concentration (50 μ M) in triplicates. Ordinary one-way ANOVA was used for statistical analysis, ** $P < 0.01$; *** $P < 0.001$. The data are shown as mean \pm standard deviation (SD).

The same group of the fragment pairs were screened again using TSA for the assessment of fragments thermal stability to PqsR protein **Table 14**. Surprisingly, the fragment combination of **81** and **108** with the strongest *pqs* inhibition did not influence the thermal stability of PqsR protein observed as 0 $^{\circ}$ C ΔT_m value. The divergent screening results for fragment pairs **81** and **108** in biophysical and bioreporter assays suggested that the two fragments may bind to different biological targets. The combination of **81** and **105** strongly destabilized the protein reflected by the observed decrease of ΔT_m value of 1.7 $^{\circ}$ C.

Table 14. TSA and *in vitro* screening results for fragment combinations

No.	Structure	RA% ^{a,b,c}	ΔT (\pm° C) ^d
DMSO		100.00%	0
105		101.60 \pm 2.49	+0.1
81		112.54 \pm 4.08	-0.3

No.	Structure	RA% ^{a,b,c}	ΔT (\pm °C) ^d
108		101.41 \pm 1.37	-0.2
107		110.32 \pm 1.82	-0.3
125		104.34 \pm 1.38	-0.1
81 + 108	 	61.66 \pm 9.66	0.0
81 + 107	 	71.56 \pm 9.88	-0.4
81 + 105	 	73.41 \pm 13.43	-1.7
81 + 125	 	83.10 \pm 7.21	0.0

^aData shown are mean values obtained from three independent experiments performed in triplicates. ^bThe data are shown as mean \pm standard deviation (SD) ^b% Remaining Activity (RA%) screening at single concentration (50 μ M) in triplicates. ^cRA% values below 70%, compounds were regarded as active ^dThermal shift assay (TSA, °C) at 500 μ M ligand concentrations in duplicates. The determination of TSA (\pm °C) was conducted in collaboration with William Richardson

4.7 Conclusion

Fragment **106** was advanced through a fragment growing method, with the resulting compounds **148b-d** showing improved *pqs* inhibition in the PAO1-LmCTX::*PpqsA-lux* reporter assay. Application of a fragment linking strategy between **146b** and **152a** led to the design of compound **154b**, which showed *pqs* inhibition in the mCTX::*PpqsA-*

lux based bioreporter assay observed as 34% RA% at 10 μ M screening concentration against PAO1-L.

Synergistic fragment combinations were explored and fragment pairs **81** and **108**, **81** and **105** showed improved *in vitro* or biophysical profiles in combination than in single fragments. Unfortunately, due to COVID time restrictions further planned work could not be completed in this area and will be present in the next chapter.

Chapter V: Conclusions and future work

5.1 Conclusions

P. aeruginosa, a nosocomial pathogen, has become a serious public health threat due to its high mortality and morbidity rates.^{1,2,3,4} Current treatment for *P. aeruginosa* infections remains as antibiotics, despite the wide spread of multi-drug-resistant *P. aeruginosa* demonstrating resistance to nearly all antibiotics.^{190 191,192} The *pqs* system is not vital for bacteria survival and the inhibition of *pqs* system is able to attenuate pathogenicity of *P. aeruginosa*.^{5,6,10} The *pqs* system transcriptional regulator PqsR, also known as MvfR¹⁰ is key in regulating virulence factors. PqsR mutants display significantly attenuated pathogenicity in multiple animal models.¹¹ Therefore, PqsR antagonists are regarded as a promising alternative to antibiotics.¹² In this work, different hit-to-lead optimisation methods were applied for the identification of novel PqsR antagonists to overcome *P. aeruginosa* infections.

5.1.1 A classic hit-to-lead optimization process to find PqsR antagonists

In chapter II, a hit-to-lead optimization process was presented starting from hit compound **19** obtained from a virtual screening. This was developed into lead compound **69**, which displays enhanced *pqs* inhibition in both PAO1-L and PA-14 strains (**Figure 54**).

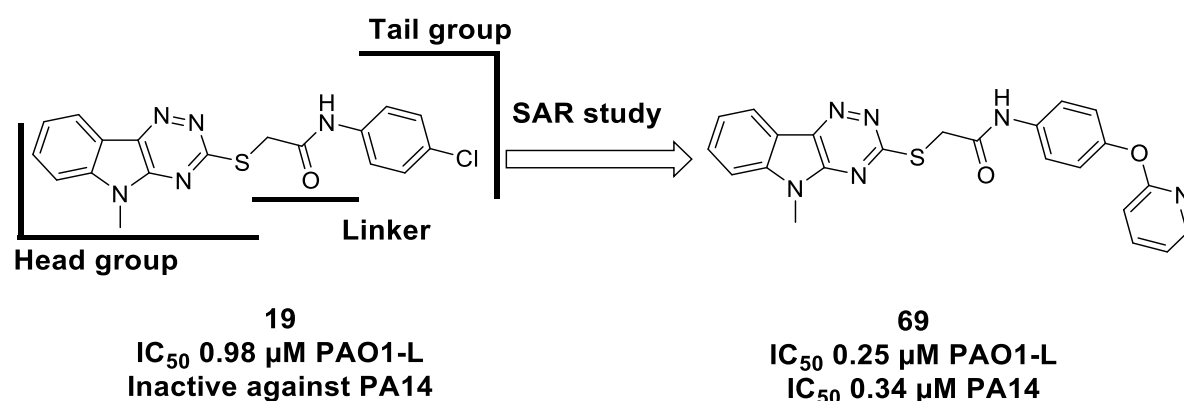


Figure 54. The schematic representation of the hit-to-lead optimization process starting from **19** to the potent lead compound **69**. The *pqs* inhibitory effect evaluated using PAO1-LmCTX::*PpqsA-lux* and PA14mCTX::*PpqsA-lux* reporter assays.

The X-ray co-crystal structure of **69** in complex with PqsR LBD was determined (**Figure 55A**) and revealed that the sulfur atom presented in the linker region locked the overall conformation allowing **69** to bend and accommodate into the hydrophobic pocket. The amide linker present in **69** hydrogen bonds with Leu²⁰⁷, whilst the 4-(pyridin-2-yloxy)phenyl tail group points outside the pocket and has a π -stacking interaction with Tyr²⁵⁸ with a 4.55 Å distance. Interestingly, the pyridinyl side chain of compound **69** had a better overlap with Tyr²⁵⁸ compared with the phenyl side chain of **7** (**Figure 55B**). Compound **7** is the only reported PqsR antagonist displaying *in vivo* activity in a mouse lung infection model.¹⁹³ The better overlapping with Tyr²⁵⁸ may indicate a stronger π stacking interaction with **69** compared to **7**, which may result in greater *pqs* inhibition of **69**.

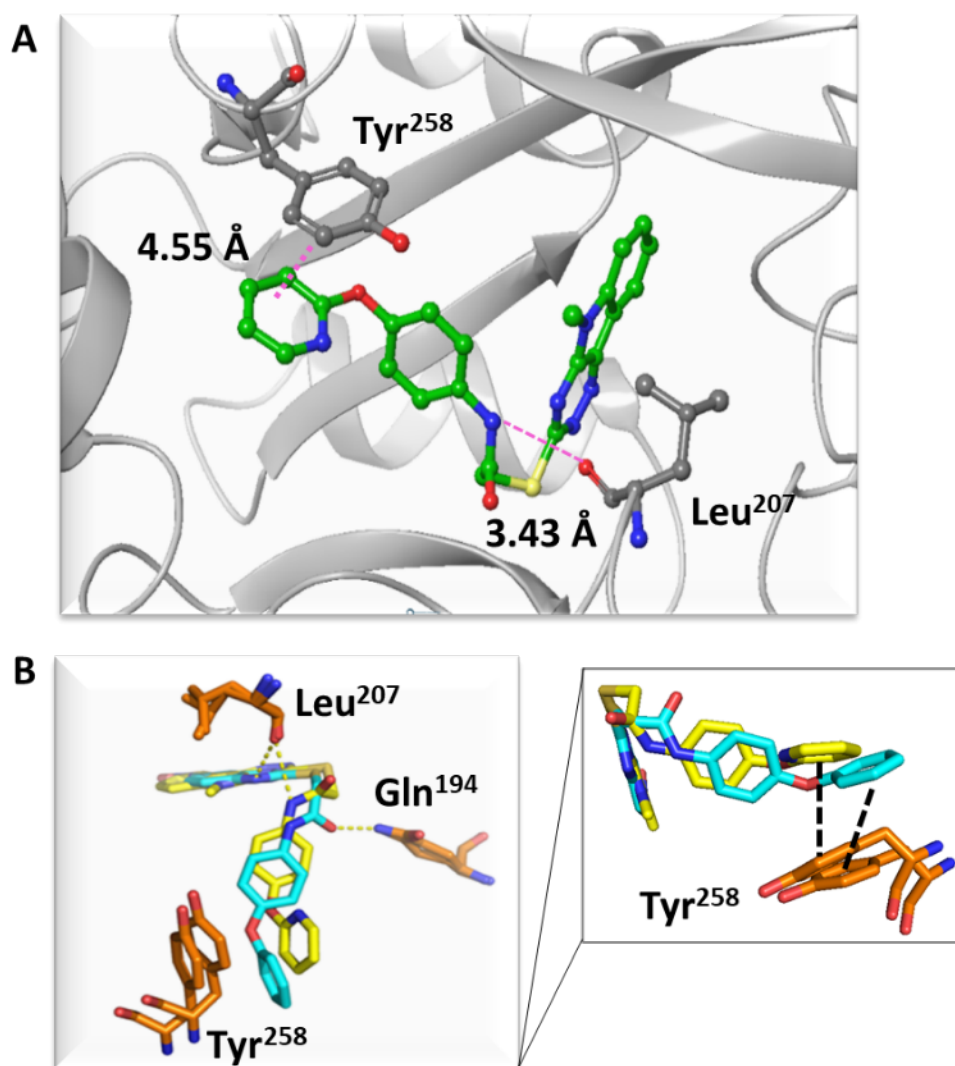


Figure 55. (A) X-ray co-crystal structure of **69** bound to PqsR ligand binding domain with a resolution of 3.2 Å. The scaffold structure of **69** shown in green while nitrogen, oxygen, and sulfur atoms presented in blue, red, and yellow. The protein structure shown in grey and residues Tyr²⁵⁸ and Leu²⁰⁷ labelled in black. (B) The comparison of **69** and **7** in complex with PqsR LBD. The ligands scaffolds are presented in blue (**7**) and yellow (**69**). The π stacking of **7** is slightly off the edge compared with **69**.

The pharmacophore for the 5-methyl-5*H*-[1,2,4]triazino[5,6-*b*]indol-3-yl)thiol analogues were also investigated through SAR studies which suggested that the tricyclic head group, flexible linker, and aromatic tail group were key in retaining analogous *pqs* inhibition (Figure 56).

The scaffold for
5-methyl-5H-[1,2,4]triazino[5,6-*b*]indol-3-yl)thio analogues

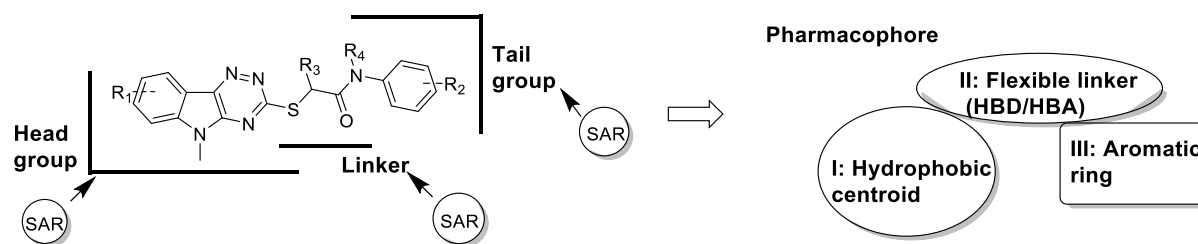


Figure 56. The schematic representation for the pharmacophores of the 5-methyl-5H-[1,2,4]triazino[5,6-*b*]indol-3-yl)thiol analogues

Assisted by TSA analysis, a concept validation experiment was conducted and it showed that gradually introducing key building blocks i.e. linker groups and tail groups, to the head group, the resulting compounds showed improved biophysical profiles in TSA (**Figure 57**).

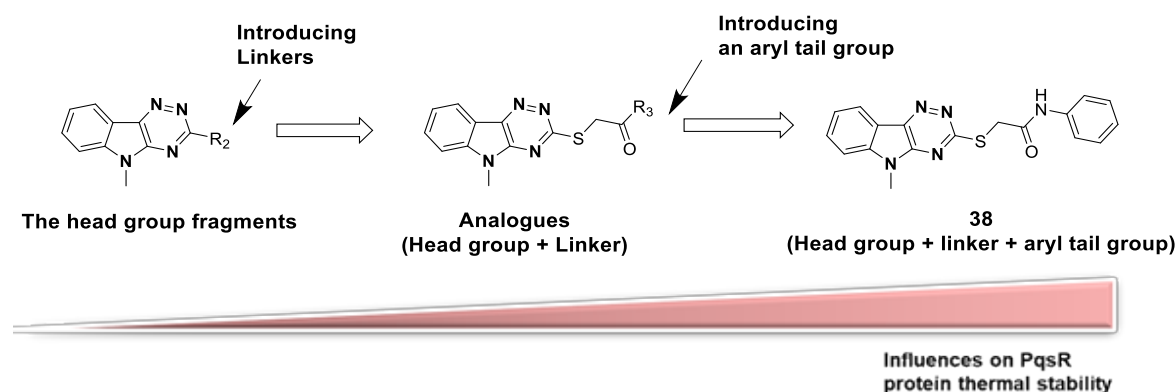


Figure 57. Schematic representation of the concept validation experiment. Growing of fragments to the drug-sized molecule **38**, analogues biophysical profile improved correspondingly.

5.1.2 PqsR antagonist fragment hit identification and optimisation

Fragment-based lead discovery approaches have become an important lead discovery technique for both well-characterized or new drug targets in the last 20 years.

^{87,124,170,171} However, FBLD methods have not been widely applied in identification of PqsR antagonists with only three publications so far (at the time of writing). ^{152,172,173}

In chapter III, fragment-based methods were used for the discovery of new PqsR antagonists including fragment hit identification, optimisation, and evolution (**Figure 58**).

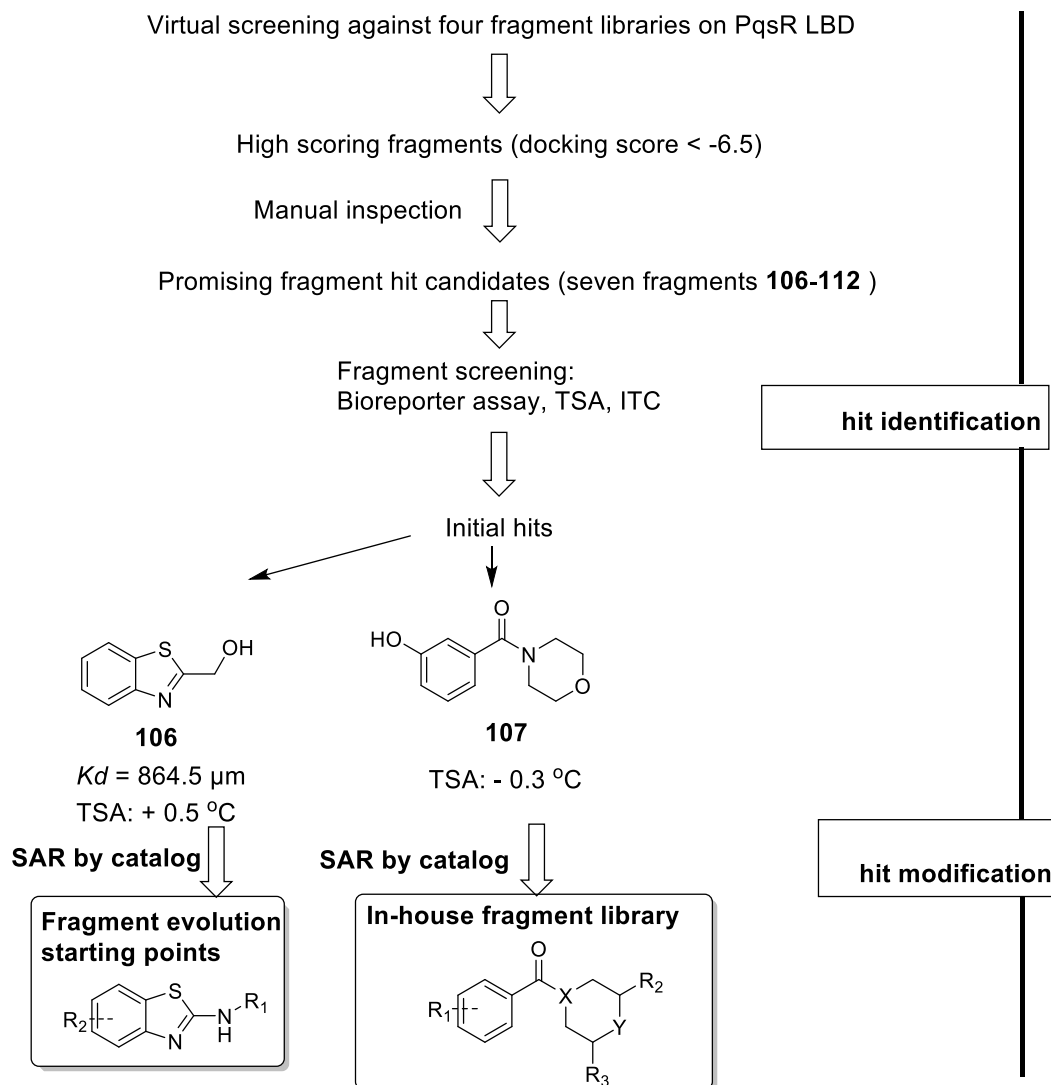


Figure 58. The workflow of fragment-based method in fragment hit identification and optimisation. ITC experiment was used for the determination of K_d for **106**. Thermal shift assay (TSA, $^\circ\text{C}$) was incorporated to determine fragments biophysical profiles where fragments were screened at 250 μM , 500 μM ligand concentrations in duplicates or triplicates.

In this work, a virtual screening on the PqsR ligand binding domain (LBD) against four fragment libraries was firstly conducted through a high-throughput virtual screening mode (PDB code: **4JVD**; Maestro, force field: OPLS3e). After a manual inspection step on high scoring fragments (docking score <math>< -6.5</math>), seven promising fragments

106-112 were selected for further *in vitro* and biophysical screening (**Figure 59**). Fragment **106** showing a clear binding to PqsR protein in both TSA and ITC experiments and was selected along with **107** also displaying promising results in TSA, progressed to hit modification stage.

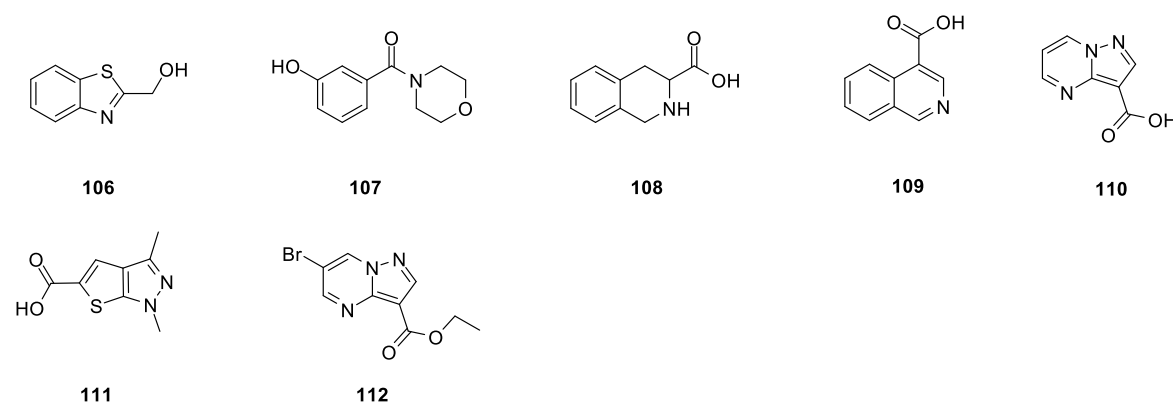


Figure 59. The structure of initial seven fragment hit candidates.

Fragment **106** and **107** were progressed to hit exploration studies leading to the discovery of **149**, **151** and **152** displaying improved ligand binding interactions against PqsR protein in TSA and ITC experiment (**Figure 60**). Fragments **106**, **149**, **151** and **152** with confirmed binding affinities were progressed to hit-to-lead optimization. In addition, a small in-house library by collecting all the fragments the group and synthesized so far were built, which will be used to screen against other biological targets.

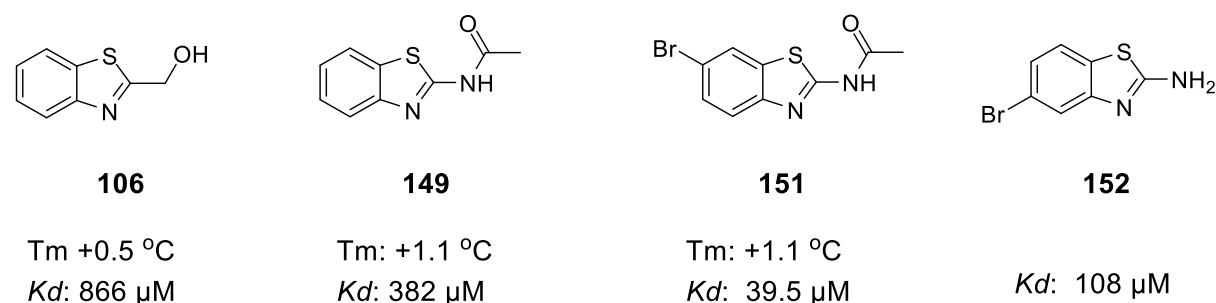


Figure 60. TSA and ITC results for fragment **106**, **149**, **151** and **152**. Fragments were screened at 500 μM ligand concentration to obtain ΔT_m values. K_d values were obtained from ITC experiments.

5.1.3 Using fragment growing, linking, and merging methods advancing PqsR antagonist fragment hits.

Fragment hits **106**, **144**, **145a** and **146b** were evolved to drug-sized molecules (350 < MWt. < 500) through fragment growing, linking, and merging methods (**Figure 61**).

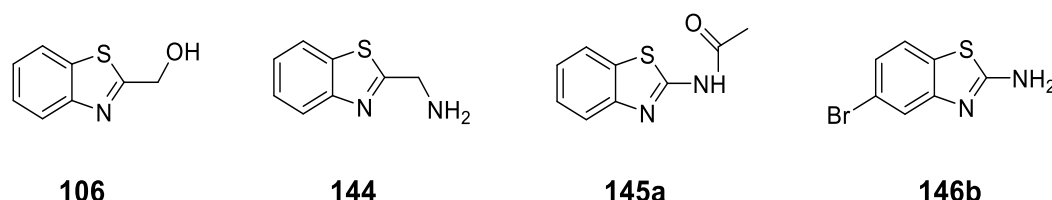


Figure 61. Structure of fragment hits **106**, **144**, **145a** and **146b**. A fragment growing method was applied on **106** and through lengthening the alkyl chain at R₁ (**Figure 62**) compounds **148b-d** were discovered, showing improved biophysical profiles and *pqs* inhibition in the PAO1-LmCTX::*PpqsA-lux* reporter assay.

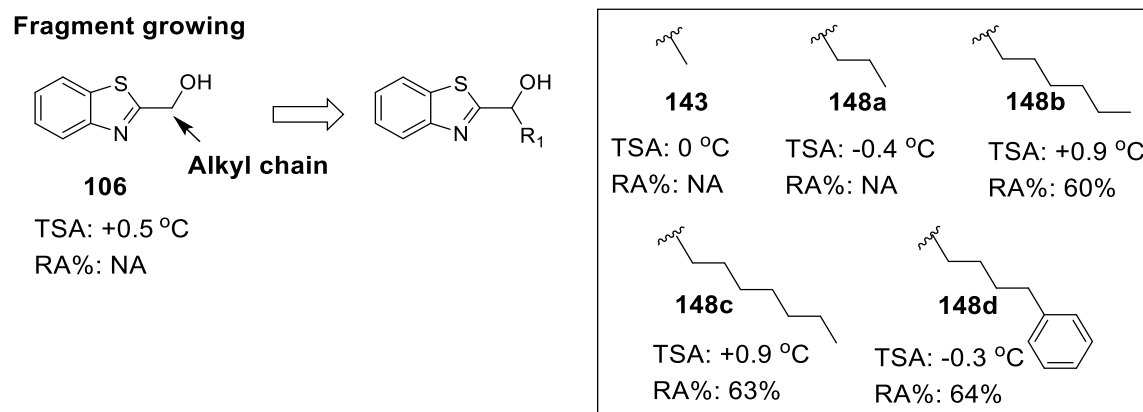


Figure 62. Schematic representation of fragment growing strategy on **106**. PAO1-LmCTX::*PpqsA-lux* reporter assay was used for the evaluation of compounds *pqs* inhibition screened at 50 μM ligand concentration. Thermal shift assay (TSA, °C) was conducted for the determination of analogues biophysical profiles and compounds were screened at 500 μM ligand concentrations in duplicates. “NA” indicates not active.

Fragment linking and merging methods were applied on 2-benzothiazolamine analogues (**145a-b** and **144**) with **152a** leading to the design and synthesis of **154a-b**, and **156a-c** (**Figure 63**).

Fragment linking between **145b** and **152a** led to the design and synthesis of compound **154b**, which showed *pqs* inhibition in the bioreporter assay against PAO1-L observed as a RA% value of 34% at 10 μ M screening concentration. Compound **154b** also strongly stabilized PqsR protein observed as an increase of ΔT_m value for 1.9 $^{\circ}$ C at 500 μ M ligand concentration in TSA.

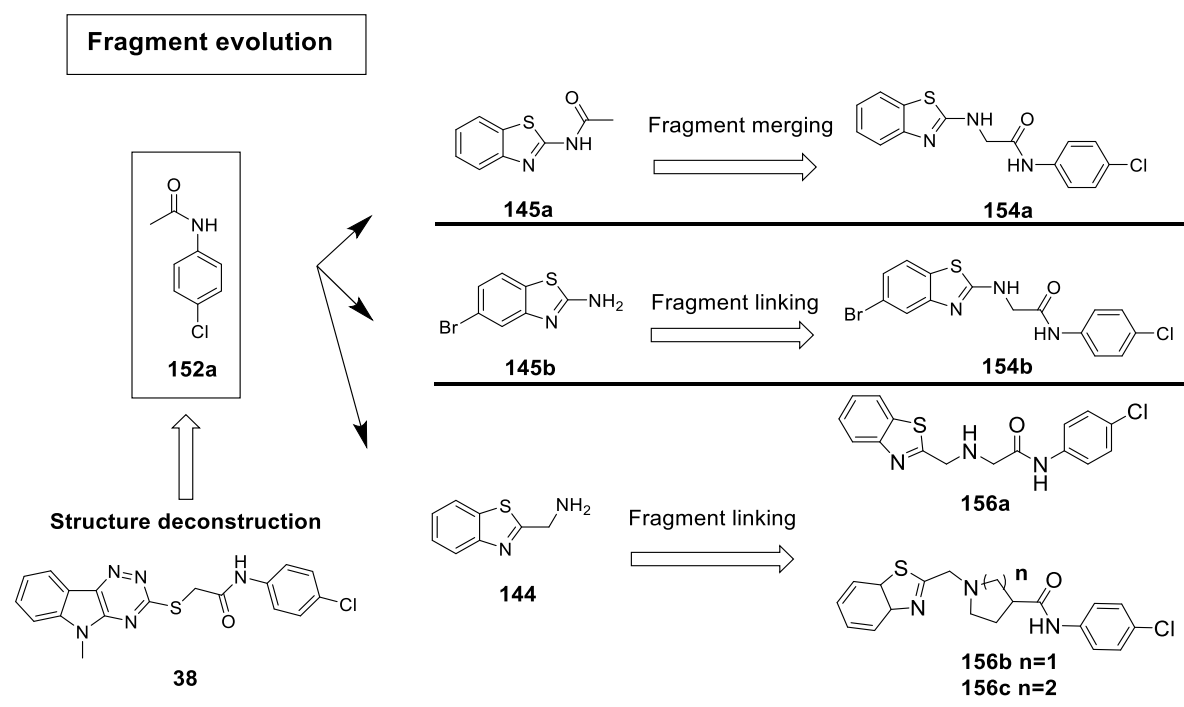


Figure 63. The schematic illustration of structure deconstruction of **38** to **152a** functionalized as a promising fragment growing vector followed by fragment linking and merging strategies with fragments **145a-b** and **144**.

Fragment synergistic combinations were also explored and two pairs of fragment pairs (**107** and **108**, **171** and **105**) demonstrated better *in vitro* and/or biophysical profiles in combinations than the single fragments (**Figure 64**).

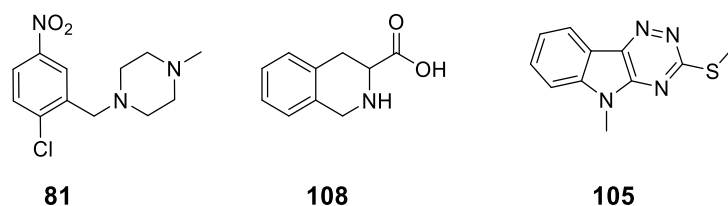


Figure 64. The structure of fragments **81**, **108**, and **105**.

5.2 Future work

In previous work, fragment-based methods were used for the identification of PqsR antagonist fragments and some fragment hits were advanced to lead-like molecules ($350 < \text{Mwt} < 500$) displaying *pqs* inhibition in PAO1-LmCTX::*PpqsA-lux* reporter assay. Unfortunately, due to COVID time restrictions some planned work could not be completed and will therefore be proposed here.

5.2.1 Further modification on compound 154b

Through a fragment linking strategy between **146b** and **152a**, compound **154b** was identified showing moderate *pqs* inhibition in the PAO1-LmCTX::*PpqsA-lux* reporter assay observed as 34% RA% at 10 μM screening concentration.

In continuation of this work, the IC_{50} value of **154b** in PAO1-LmCTX::*PpqsA-lux* reporter assay should be determined followed by SAR studies around **154b** to further optimise *pqs* inhibition (**Figure 65**). The X-ray crystallography and biophysical assays should also conduct on selected analogues. For the lead compound the metabolic stability test and in vivo assays should also be considered.

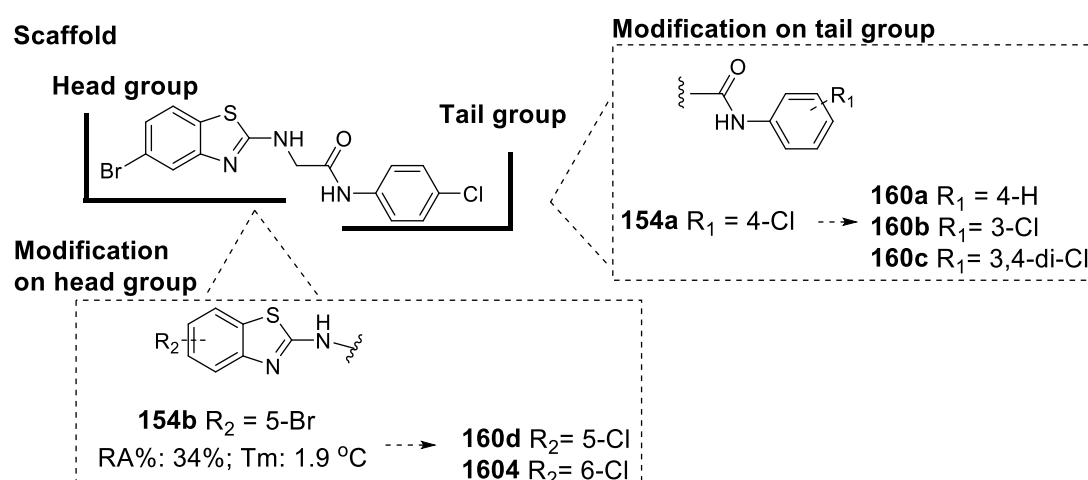


Figure 65. Schematic representation of the proposed SAR study on **154b**. Compound **154b** showed *pqs* in the bioreporter assay observed as a RA% value of 34% at 10 μM

screening concentration against PAO1-L. Compound **154b** stabilized PqsR protein observed as an increase of ΔT_m value for 1.9 °C at 500 μM ligand concentration in TSA. The SAR study around the tail group of **154b** could start from removal of the chlorine atom (**160a**). The following design for this SAR study could be guided by Topliss tree, which is a non-mathematical strategy widely used for the exploration of substituents on a benzene ring or substituted phenyl ring.^{194–196} The SAR study of the head group could start from changing the substituted position of the bromine atom or replacing the bromine to other halogen atoms (**160d-e**).

5.2.2 Further modification on 148d

Through a fragment growing method on **106**, compound **148d** was identified displaying moderate *pqs* inhibition against PAO1-L with a RA% value of 64%. Also, compound **148d** weakly destabilized the PqsR protein reflected as a 0.3 °C (500 μM) decrease of ΔT_m in TSA. In the recent experiment, it showed confirmed *pqs* inhibition with an IC_{50} value of 150.9 μM , which provided some confidence in continuation of this work. In order to further improve *pqs* inhibition, compound **148d** can be subjected to an SAR study, which is proposed in **Figure 66**. If resulting analogues showed significant increasing *pqs* inhibition, the X-ray crystallography and biophysical assays should also conduct on selected analogues. For the lead compound the metabolic stability test and in vivo assays should also be considered.

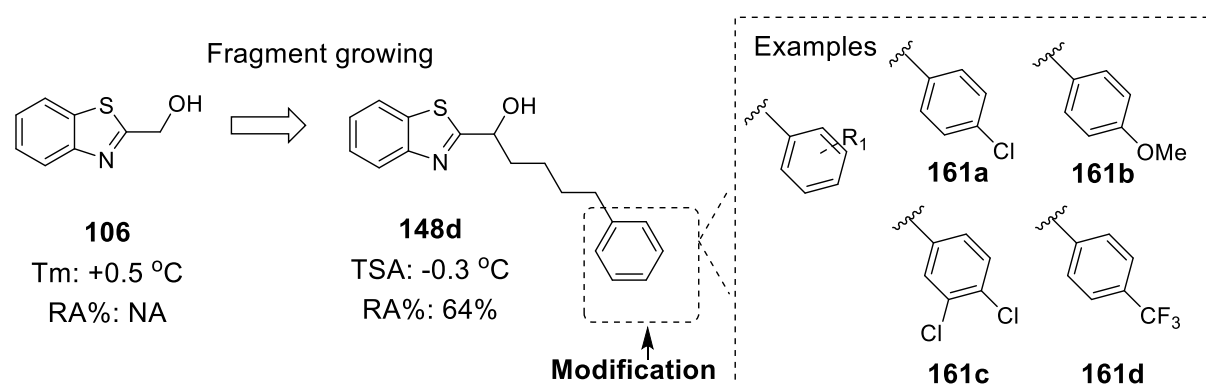


Figure 66. Schematic representation of the proposed SAR study on **167**. The design for this SAR study would be guided by Topliss tree and the examples for the SAR study around the tail group of **148d** were presented as **161a-d**. The experiment for the determination of **148d** IC_{50} value was recently conducted by William Richardson and compound **148d** showed an IC_{50} value of 150.9 μM in PAO1-LmCTX::PpqsA-lux reporter assay.

5.2.3 Advancing synergistic pairs

In the previous work, fragment pairs **81** and **108**, **81** and **105** were identified demonstrating better *in vitro* and/or biophysical profiles in combinations than the single fragments. It would be interesting to explore the fragment binding modes through X-ray crystallography experiment. These fragment pairs can also act good starting points for fragment linking methods to be advanced to drug-sized molecules. In continuation of this work, the fragment linking method can be applied to these two pairs of fragments.

Both **81** and **108** have multiple HBDs and HBAs including amines and carboxylic acid groups, which can be pharmacophores and key for bioactivity. These functional groups can also act as chemical elaboration points offering straightforward routes to linkage. In order to investigate the influence of these structural features on *pqs* inhibition, fragments **81** and **108** were linked through different linkers (**Figure 67**, **scheme I**, **162a-c**).

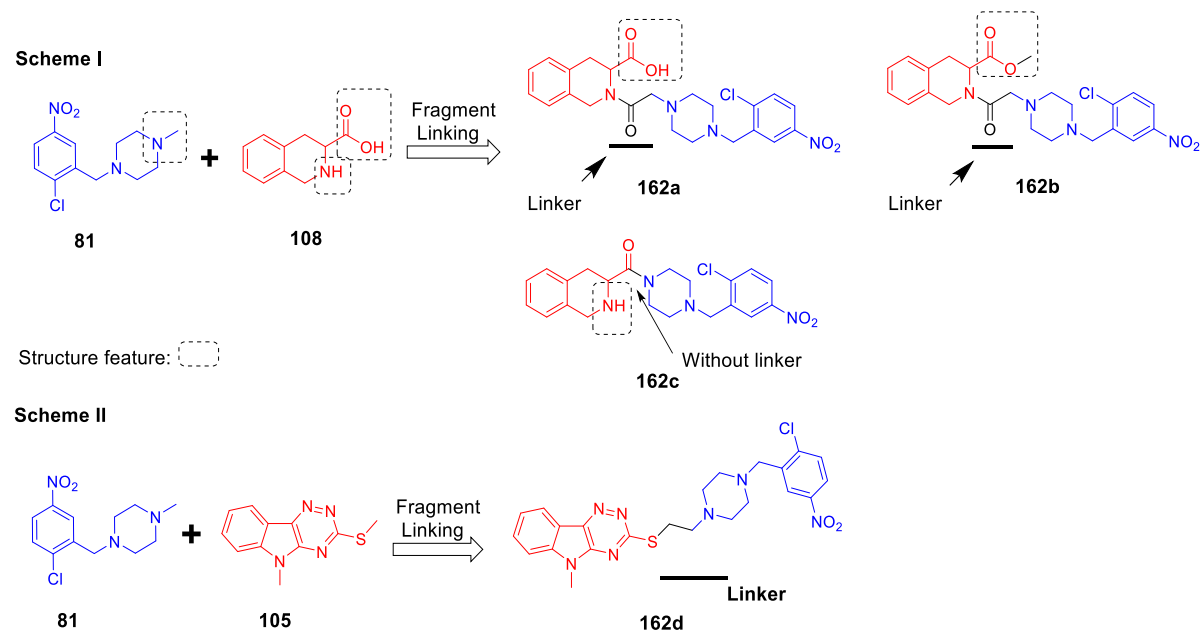


Figure 67. Schematic representation of the proposed fragment linking methods: fragment pair **81** and **108** **Scheme I**, fragment pair **81** and **105** **Scheme II**. A direct

linking between the tertiary amine of **81** and the carboxylate acid of **108** led to analogue **162c**. Adding a simple linker between the secondary amine on the 1,2,3,4-tetrahydroisoquinoline core of **108** and tertiary amine of **81**, the resulting analogue **162a** keeps the 3-carboxylic acid group. Replacing the carboxylic acid group with a methyl carboxylate group led to the design of analogue **162b**. The proposed fragment linking strategy on fragment pair **81** and **105** led to the design of compound **162d**.

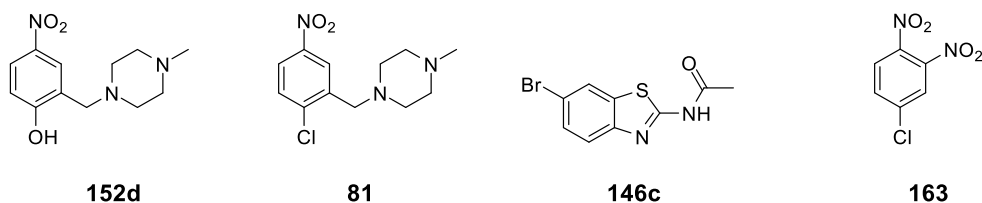
Although fragment pair **81** and **105** destabilized the PqsR protein, it would be interesting to link this fragment pair and analysis the biophysical profile of the resulting compound **162d**.

5.2.4 Finding dual PqsA/R or PqsA inhibitors through fragment-based methods

The quorum sensing (QS) system in *P. aeruginosa* is highly interconnected and complicated. Inhibition of multiple signalling cascades in the QS system is more efficient in terms of attenuating *P. aeruginosa* pathogenicity.^{185,197–199} PqsA is the key enzyme for the biosynthesis of the signalling molecules HHQ and PQS in the QS system and the inhibition of PqsA can significantly attenuate the generation and secretion of *P. aeruginosa* virulence factors.^{7,200–202} The crystal structure of PqsA has been recently published, which provides some confidence to investigate dual PqsA/R or PqsA inhibitors.

In order to find fragments targeting PqsA and/or PqsR proteins, screening of an in-house fragment library against PqsA and PqsR proteins through TSA was conducted. Fragment **152d**, **81**, **146c** and **163** were shown to change the thermal stability for both PqsA and PqsR proteins (**Figure 68**). Through using TSA, some fragments **119a**, **119f**, **119d**, **105**, **123** and **164** were identified to strongly destabilize the PqsA protein and had a minimal influence on the thermal stability of PqsR protein (**Figure 69**). When fragments bind to the protein unfolded form or cause protein aggregation, it causes protein destabilization reflecting as negative ΔT_m values. Advancing these fragments

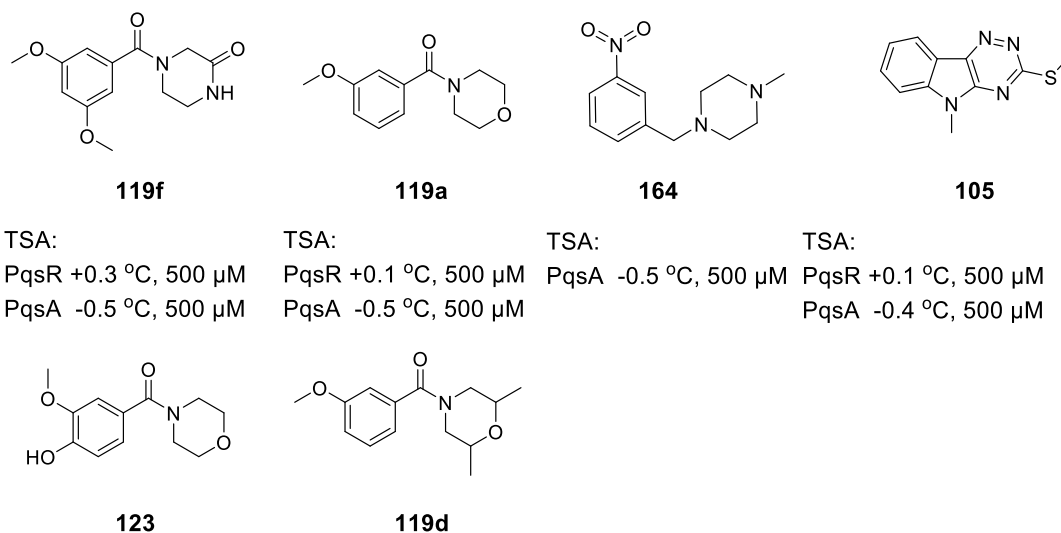
can be challenging and orthogonal screening is required to cross validate these fragments.



TSA: PqsR +0.2 °C, 500 μM PqsA -0.7 °C, 500 μM	TSA: PqsR -0.3 °C, 500 μM PqsA -0.6 °C, 1 mM	TSA: PqsR +1.1 °C, 500 μM PqsA -1.1 °C, 500 μM	TSA: PqsR -5.3 °C, 500 μM PqsA -14.3 °C, 500 μM
--	--	--	---

Figure 68. Fragments influenced thermal stability for both PqsA and PqsR. Fragments were screened at 500 μM or 1 mM ligand concentrations in triplicates for the determination of ΔT_m values in TSA. This TSA was conducted by William Richardson.

In the TSA for the screening of fragments against PqsA protein, it was noticed that PqsA protein have low tolerance to DMSO and the native ligand of PqsA protein anthranilate acid stabilised the protein with an increase of ΔT_m value of 1.0 °C. These results suggested that TSA may not be suitable for the PqsA screening and orthogonal screening is required to cross validate all the fragment hits mentioned.



TSA: PqsR +0.3 °C, 500 μM PqsA -0.5 °C, 500 μM	TSA: PqsR +0.1 °C, 500 μM PqsA -0.5 °C, 500 μM	TSA: PqsA -0.5 °C, 500 μM	TSA: PqsR +0.1 °C, 500 μM PqsA -0.4 °C, 500 μM
--	--	------------------------------	--

TSA: PqsR -0.1 °C, 500 μM PqsA -0.3 °C, 500 μM	TSA: PqsA -0.5 °C, 500 μM
--	------------------------------

Figure 69. Fragments influence thermal stability for PqsA protein. Fragments were screened at 500 μM or 1 mM ligand concentrations in triplicates for the determination of ΔT_m values in TSA. This TSA was conducted by William Richardson.

Experimental

6.1 Microbiological Experiments

6.1.1 PqsR bioreporter assay

6.1.1.1 Bacterial strains

The *P. aeruginosa* strains used in the thesis are listed in **Supplementary table 1**.

Supplementary table 1. Bacterial strains used in the thesis

Strain	Description	Reference/origin
PAO1-L	Wild type <i>P. aeruginosa</i> from Université de Lausanne, Switzerland	B. Holloway via D.Haas
PAO1-L miniCTX:: <i>PpqsA-lux</i>	PAO1-L with the reporter construction <i>PpqsA-luxCDABE</i> inserted in the specific <i>attB</i> site of the Chromosome. ²⁰³ Tc ^R (plasmid with tetracycline resistance gene)	[²⁰³] Soukarieh et al.
PA14	Wild type UCBPP-PA14	Rahme et al., 1995
PA14 miniCTX:: <i>PpqsA-lux</i>	PA14 with chromosomal mini-CTX:: <i>PpqsA-luxCDABE</i> ; Tc ^R	Soukarieh et al.

6.1.1.2 Preparing bacterial cultures for single concentration PqsR bioreporter assays

Overnight culture of strains PAO1-L miniCTX::*PpqsA-lux* and PA14 miniCTX::*PpqsA-lux* in separate universal containers were created. Each universal container contains a single colony of strains, 5 mL LB medium and Gentamicin at 20 µg/mL. Cultural overnight at 37 °C with shaking at 200 r.p.m. The optical density at 600 nm (OD₆₀₀) for

the overnight culture was determined on the next day. Strains were prior to use when OD_{600} was approximately 2.5. Strains PAO1-L and PA14 stocks solution (20 mL) were prepared by diluting the overnight culture with fresh LB medium in universal containers to OD_{600} of 0.02.

6.1.1.3 Bioluminescence reporter gene assay for 50 μ M single concentration spot test

50 mM tested compound stock solution in DMSO was diluted to 100 μ M by adding 1 μ L of stock solution to 500 μ L LB medium in an Eppendorf. Adding 100 μ L of the diluted compound solution to three wells of a Grenier 96 well flat black plate to obtain results in triplicates. To each of wells containing 100 μ L tested compound was added 100 μ L PAO1-L or PA14 stock culture to give final 50 μ M concentration. The plate was run by a luminometer-spectrometer (Tecan GENios Pro) at 37°C for 24 h to 30 h monitoring a kinetic cycle (OD_{600}) and luminescence every 30 min.

The readouts of the OD_{600} and luminescence were taken from the peak of the luminescence and normally observed between 8 to 9 h. The results were normalized against the native control containing 0.1% DMSO to give remaining active data.

A similar methodology was applied for the 50 μ M single concentration spot test for synergistic combinations. Fragments were diluted to 200 μ M by adding 2 μ L of stock solution to 500 μ L LB medium in an Eppendorf. Two 50 μ L of 200 μ M fragment solutions were added to the same well of a Grenier 96 well to give a final 100 μ M mixed solution and this step was repeated three times to give results in triplicates. To each of wells containing 100 μ L mixed solution was added 100 μ L PAO1-L or PA14

stock culture to give final 50 μM concentration and the plate was run by a luminometer-spectrometer (Tecan GENios Pro) using the same script as mentioned before.

In order to remove cytotoxicity compounds, the bacteria growth curve should be monitored and compared with DMSO control. Compounds inhibition to LuxABCDE protein should also be determined in order to eliminate false positives.

6.2 Biophysical experiments

6.2.1 Thermal shift assay (TSA)

The melting temperature (T_m) of PqsR⁹⁴⁻³⁰⁹ in the presence and absence of inhibitors was determined using 96-well fluorescence-based thermal shift assay. The 10 mM DMSO fragments stocks were diluted to 5 mM and 2.5 mM using DMSO. The Mastermix contains 500 μL of 1.5 mg/mL PqsR⁹⁴⁻³⁰⁹ and 500 μL 40 \times SYPRO™ Orange Protein Gel Stain (5,000X Concentrate in DMSO, ThermoFisher). 10 μL of the Mastermix was dispensed into each well of a MicroAmp 96-well qPCR plate and followed by pipetting of 35 μL of buffer and 5 μL of diluted fragments stocks to give a final compound concentration of 500 μL and 250 μL at 10% (v/v) DMSO. For DMSO positive control, 5 μL of DMSO was dispensed into the mixture of 10 μL Mastermix and 35 μL buffer. For the negative control, 5 μL Sypro orange was mixed with 40 μL buffer and 5 μL DMSO to ensure compounds did not interference with the dye. Each compound and control groups were assessed in duplicate or triplicate. The plate was sealed with MicroAmp optical adhesive film and centrifuged at 300 r.m.p for 3 minutes. The plate was incubated for 5 minutes at 30°C in the Real-time PCR instrument (Applied Biosystems 7500 instrument) with a step size of 1°C/min. Data was analysed using NAMI software package to determine T_m values. The ΔT_m values were

calculated as $\Delta T_m = T_m (\text{compound}) - T_m (\text{DMSO control})$. Buffer solution was prepared by William Richard containing 50 mM Tricine, 500 mM sodium chloride, and 10% Glycerol (pH = 8.5) and screened compounds stocks were prepared as 10 mM in DMSO.

6.2.2 Isothermal titration calorimetry (ITC)

ITC titrations were performed to detect direct binding between PqsR⁹⁴⁻³⁰⁹ and fragments using MicroCal PEAQ-ITC (Malvern). Fragment DMSO stock solutions were diluted with the experimental buffer resulting a final DMSO concentration of 10% (v/v). The buffer used for dilution and protein purification was provided by William Richard (Buffer: 20 mM Tricine-NaOH (pH = 8), 250 mM NaCl and 2.5% Glycerol).

Using Malvern's software, the cell and syringe were washed before each titration. ITC measurements were routinely performed the using pre-defined 19 injections method with a single 0.4 μL injection, followed by 18, 2 μL injections.

The sample cell was load with 25 μM PqsR⁹⁴⁻³⁰⁹ with a final DMSO concentration of 10% (v/v) in buffer where the protein sample and buffer were provided by William Richard. The syringe was loaded with 500 μM compound solution in buffer with a final DMSO concentration of 10% (v/v). To correct for heats of dilution, the buffer solution was titrated into protein solution to correct the base line of the final titrating base line.

6.3 Molecular Docking

6.3.1 Protein structure preparation

The X-ray crystal structure of PqsR LBD in complex with native agonist NHQ (PDB code: 4JVD) was used as protein template and prepared with Protein Preparation

Wizard in Maestro (Schrödinger, LLC, 2017, New York, NY) using default setting in which waters were deleted, hydrogens were added, and bond orders were assigned.

6.3.2 Grid generation

Prepared protein structure was used to general Glide scoring grid for later docking study using Receptor Grid Generation. The scoring grid box was generated based on the centroid of workspace ligand in a default size.

6.3.3 Ligand preparation

Fragment libraries and compounds were prepared using LipPrep with Epik (Schrödinger, LLC, 2017, New York, NY) to generate lowest energy conformations for each compound in desalt and tautomeric state. The targeted pH was set as 7.5 ± 0.2 to generate protonation state.

6.3.4 Molecular Docking

Two scoring protocols were used for the docking: Glide HTVS (high throughput virtual screening) and Glide SP (standard precision) in default parameters using the force field is OPLS3. The screening of fragment libraries was used Glide HTVS and the drug-sized molecules was used Glide SP. The number of poses for each ligand was set to 5 and the top three poses was saved based on Glide docking scores and reported.

6.4 Chemistry experimental section

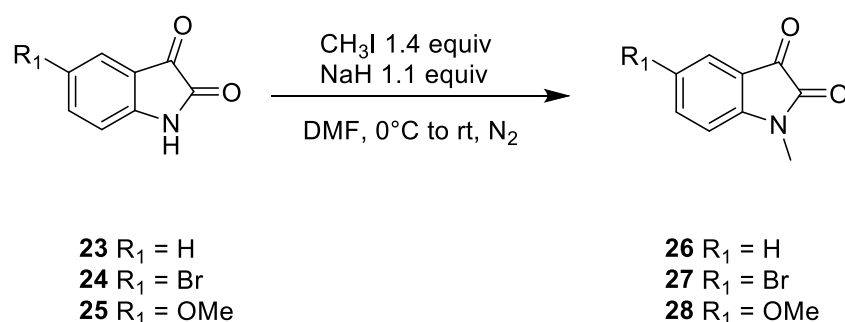
6.4.1 General chemistry

Reagents and anhydrous solvents were purchased from Sigma Aldrich, Alfa Aesar and Fisher Scientific and were used without further purification. Nuclear magnetic resonance: $^1\text{H-NMR}$ and $^{13}\text{C-NMR}$, were obtained at room temperature using a Bruker AV400, spectrometer operating at 400 MHz. The samples were prepared in deuterated solvent: $\text{DMSO-}d_6$ and chloroform- d . Chemical shifts (δ) were recorded in ppm and coupling constants (J) were recorded in Hz. The spectra were analyzed using MestReNova12.0.1 software. Mass spectrometry: Analytical HPLC were performed on a Shimadzu UFLCXR system coupled to an Applied Biosystems API2000. Two columns thermostated at 40°C were used. **Column one:** Phenomenex Gemini-NX $3\mu\text{m-110A C18}$, $50\times 2\text{mm}$ **Column two:** Phenomenex Luna $3\mu\text{m (PFP2) 110A}$, $50\times 2\text{mm}$. **Column three:** Waters X terra MS C8 $2.5\mu\text{m}$, $4.6\times 30\text{mm}$. Flow rate $0.5\text{mL}/\text{min}$. UV detection at 220 (channel2) and 254nm (channel1). SHORT Gradient: Pre-equilibration run for one min at 5% B; then method run: 5 to 98% solvent B in 2min, 98% B for 2min, 98 to 5% B in 0.5min then 5% for one min. LONG Gradient: Pre-equilibration run for one min at 5% B; then method run: 5% B for 0.5min, 10 to 98% solvent B in 8min, 98% B for 2min, 98 to 5% B in 0.5min then 5% B for one min. Solvent A: 0.1% Formic Acid in water; solvent B: 0.1% Formic Acid in MeCN. Chromatography: Thin-layer chromatography (TLC) was performed, UV light and standard TLC stains were used to visualise the Merck Silica gel 60 Å F254 plates. Retention factors (R_f) in a given solvent system are reported to two decimal places. Compounds were purified via column chromatography using either a Thompson pump or normal phase Interchim Puriflash pre-packed cartridges consisting of $50\mu\text{M}$ silica,

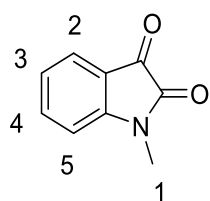
or a glass column using Merck Geduran silica gel 60 Å (230-240 μm) Column size selected was generally 40-60 times the loading amount.

6.4.2 Synthesis

General Procedure 1: Preparation of 1-methyl-2,3-indolinediones **26-28**



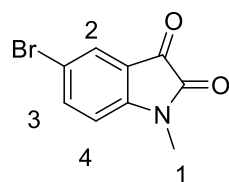
To a solution of 2,3-indolinediones **23-25** in anhydrous DMF (10 mL/mmol) at 0°C under N₂ protection, NaH 60% dispersion in mineral oil (1.1 equiv) was added in one portion. The mixture was stirred for 45 minutes followed by addition of iodomethane (1.4 equiv). The mixture was then slowly warmed up to room temperature and stirred for further 6 hours. The mixture was poured into Sat. NH₄Cl (100 mL) and stirred vigorously for 10 minutes. The resulting suspension was extracted with ethyl acetate (50 mL × 3). The combined organic layers were washed with brine, dried over Na₂SO₄, and concentrated. The crude compound was purified by column chromatography (eluent PET/EtOAc 5:1) to give the desired compound.



Reaction code: liu180-007

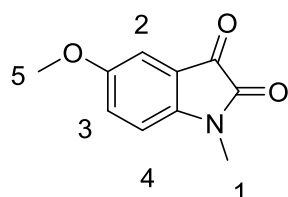
1-Methylindoline-2,3-dione (26) was prepared according to general procedure 1 starting from 2,3-indolinedione (**23**) (3.00 g, 20.40 mmol). The crude product was purified by column chromatography (eluent PET/EtOAc 5:1) to give an orange solid (3.03 g, 92%): ¹H NMR (400 MHz, DMSO-*d*₆) δ 7.67 (td, *J* = 7.8, 1.4 Hz, 1H, H-2), 7.53 (dd, *J* = 7.5, 1.5 Hz, 1H, H-4), 7.20 – 7.06 (m, 2H, H-3 and H-5), 3.14 (s, 3H, H-1). ¹³C NMR (101 MHz, DMSO-*d*₆) δ 183.9, 158.6, 151.82, 138.64, 124.69, 123.65, 117.82,

111.02, 26.47. LCMS m/z calc. for $C_9H_7NO_2$ $[M]^+$: 161.1, found 161.1 with t_R 2.48 min, purity 95%.



Reaction code: liu180-005

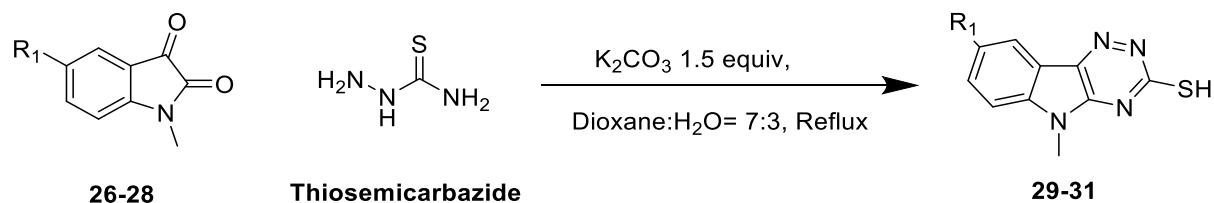
5-Bromo-1-methylindoline-2,3-dione (27) was prepared according to general procedure 1 starting from 5-bromo-2,3-indolinedione (**24**) (5.00 g, 22.12 mmol). The crude product was purified by column chromatography (eluent PET/EtOAc 5:1) to give an orange solid (3.91 g, 73 %): 1H NMR (400 MHz, $DMSO-d_6$) δ 7.86 (dd, $J = 8.4, 2.1$ Hz, 1H, H-3), 7.70 (d, $J = 2.1$ Hz, 1H, H-2), 7.13 (d, $J = 8.4$ Hz, 1H, H-4), 3.14 (s, 3H, H-1). ^{13}C NMR (101 MHz, $DMSO-d_6$) δ 182.69, 158.31, 150.75, 140.25, 126.95, 119.65, 115.33, 113.19, 26.60. LCMS m/z calc. for $C_9H_6BrNO_2$ $[M]^+$: 241.2, found 240.2 with t_R 2.52 min, purity 95%.



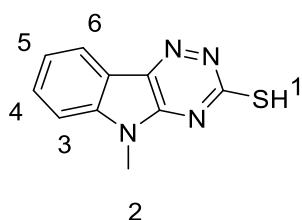
Reaction code: liu180-137

5-Methoxy-1-methylindoline-2,3-dione (28) was prepared according to general procedure 1 starting from 5-methoxyindoline-2,3-dione (**25**) (2.00g, 11.29 mmol). The crude product was purified by column chromatography (eluent PET/EtOAc 5:1) to give an orange solid (1.89 g, 88 %): 1H NMR (400 MHz, $DMSO-d_6$) δ 7.26 (dt, $J = 8.6, 2.7$ Hz, H-4), 7.13 (q, $J = 2.4$ Hz, 1H, H-2), 7.11 – 7.04 (m, 1H, H-3), 3.78 (s, 3H, H-5), 3.12 (s, 3H, H-1). ^{13}C NMR (101 MHz, $DMSO-d_6$) δ 184.20, 158.65, 156.22, 145.67, 124.31, 118.30, 112.06, 109.59, 56.36, 26.50. LCMS m/z calc. for $C_{10}H_9NO_3$ $[M]^+$: 191.1, found 191.1 with t_R 2.28 min, purity 95%.

General procedure 2 Preparation of 5-methyl-5H-[1,2,4]triazino[5,6-b]indole-3-thiols 29-31

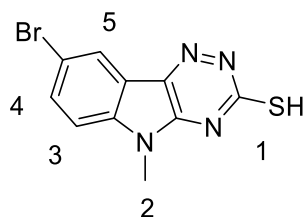


A mixture of 1-methyl-2, 3-indolinediones **26-28**, thiosemicarbazide (1.1 equiv) and K₂CO₃ (1.5 equiv) in the mixture of 70% dioxane and 30% water 10 mL/mmol was refluxed for 16 hours. On cooling, the mixture was filtered and concentrated. The mixture was diluted with water (10 mL) and recrystallized in acetic acid. The crude compounds were used directly for next steps without further purification.



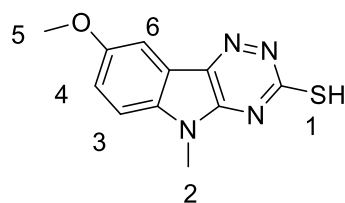
Reaction code: liu180-49

5-Methyl-5H-[1,2,4]triazino[5,6-*b*]indole-3-thiol (29) was prepared according to general procedure 2 starting from 1-methylindoline-2,3-dione (**26**) (1.63 g, 10.055 mmol). The product was obtained as an orange solid (0.99 g, 45%): ¹H NMR (400 MHz, DMSO-*d*₆) δ 14.56 (s, 1H, H-1), 8.05 (d, *J* = 7.6 Hz, 1H, H-6), 7.76 – 7.61 (m, 2H, H-3 and H-4), 7.41 (td, *J* = 7.5, 1.1 Hz, 1H, H-5), 3.67 (s, 3H, H-2). ¹³C NMR (101 MHz, Chloroform-*d*) δ 177.36, 132.43, 124.32, 122.77, 110.81, 20.78. LCMS *m/z* calc. for C₁₀H₈N₄S [M]⁺: 216.3, found 216.2 with *t*_R 2.22 min, purity 95 %.



Reaction code: liu180-17

8-Bromo-5-methyl-5H-[1,2,4]triazino[5,6-*b*]indole-3-thiol (30) was prepared according to general procedure 2 starting from 5-bromo-1-methylindoline-2,3-dione (**27**) (1.00 g, 4.16 mmol). The product was obtained as an orange solid (1.23 g, 86%): ¹H NMR (400 MHz, DMSO-*d*₆) δ 14.68 (s, 1H, H-1), 8.22 (d, *J* = 2.0 Hz, 1H, H-5), 7.88 (dd, *J* = 8.6, 2.0 Hz, 1H, H-4), 7.64 (d, *J* = 8.7 Hz, 1H, H-3), 3.65 (s, 3H, H-2). ¹³C NMR (101 MHz, DMSO-*d*₆) δ 179.98, 148.73, 143.62, 134.82, 134.34, 124.39, 119.89, 115.89, 113.99, 21.54. LCMS *m/z* calc. for C₁₀H₇BrN₄S[M]⁺: 295.2, found 295.1 with *t*_R 2.47 min, purity 95%.

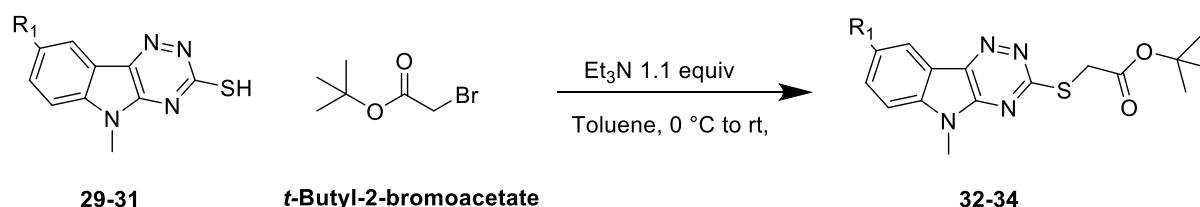


Reaction code: liu180-189

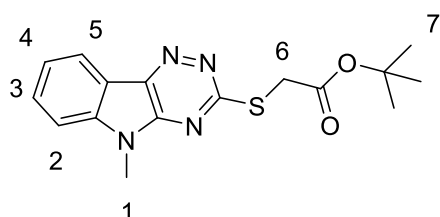
8-Methoxy-5-methyl-5H-[1,2,4]triazino[5,6-*b*]indole-3-thiol (31) was prepared according to general procedure 2 starting from 5-methoxy-1-methylindoline-2,3-dione (**28**) (1.519 g, 7.9449 mmol). The product was obtained as an orange solid (1.89 g, 96.7%): ^1H NMR (400 MHz, $\text{DMSO-}d_6$) δ 13.49 (s, 1H, H-1), 7.55 (app.d, $J = 8.9$ Hz, 2H, H-6 and H-3), 7.27 (d, $J = 8.8$ Hz, 1H, H-4), 3.85 (s, 3H, H-5), 3.62 (s, 3H, H-2). ^{13}C NMR (101 MHz, $\text{DMSO-}d_6$) δ 179.77, 172.55, 156.48, 148.34, 138.44, 135.63, 119.34, 118.64, 112.76, 56.34, 21.68. LCMS m/z calc. for $\text{C}_{11}\text{H}_{10}\text{N}_4\text{OS}$ $[\text{M}]^+$: 246.3, found 246.3 with t_{R} 2.31 min, purity 85%.

*Apparent multiples indicants coupling constants accidentally coincide (abbreviate as app.)

General Procedure 3 Preparation of tert-butyl 2-((5-methyl-5H-[1,2,4]triazino[5,6-*b*]indol-3-yl)thio)acetates 32-34

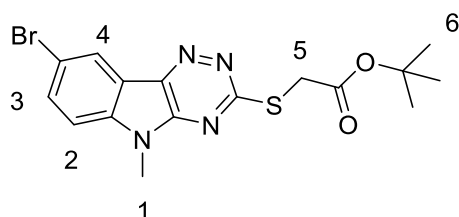


Under the protection of N_2 , tert-Butyl bromoacetate (1.0 equiv.) was added dropwise to a suspension of 5-methyl-5H-[1,2,4]triazino[5,6-*b*]indole-3-thiols (**29-31**) (1 equiv) and triethylamine (1.1 equiv) in anhydrous toluene (5 mL/mmol) at 0°C . Reaction mixture was allowed slowly warm up to room temperature and stirred for 3 hours. Reaction mixture was quenched by water and stirred at room temperature for further 5 minutes. The mixture was then dilute with water and then extracted by EtOAc (50 mL \times 3). The organic layers were combined and washed with brine and dried over Na_2SO_4 . The crude compound was purified by column chromatography.

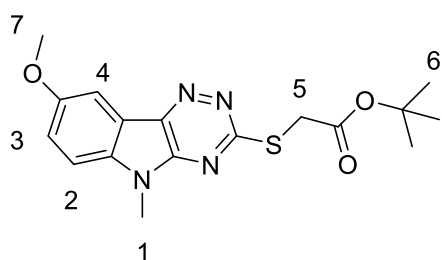


Reaction code: liu180-55

tert-Butyl 2-((5-methyl-5H-[1,2,4]triazino[5,6-b]indol-3-yl)thio)acetate (32) was prepared according to general procedure 3 starting from 5-methyl-5H-[1,2,4]triazino[5,6-b]indole-3-thiol (**29**) (0.40 g, 1.83 mmol). The crude product was purified by column chromatography (eluent PET/EtOAc 4:1) to give a white solid (0.37 g, 62%): ¹H NMR (400 MHz, DMSO-*d*₆) δ 8.36 (d, *J* = 7.6 Hz, 1H, H-5), 7.79 (app.d, *J* = 4.1 Hz, 2H, H-3 and H-2), 7.51 (m, 1H, H-4), 4.10 (s, 2H, H-6), 3.83 (s, 3H, H-1), 1.42 (s, 9H, H-7). ¹³C NMR (101 MHz, Chloroform-*d*) δ 168.04, 166.84, 146.43, 141.42, 141.14, 130.74, 122.90, 122.12, 118.01, 109.84, 82.07, 34.54, 28.03, 27.22. LCMS *m/z* calc. for C₁₆H₁₈N₄O₂S [M]⁺: 330.2, found 330.4 with *t*_R 2.91 min, purity 95%.

**Reaction code: liu180-21**

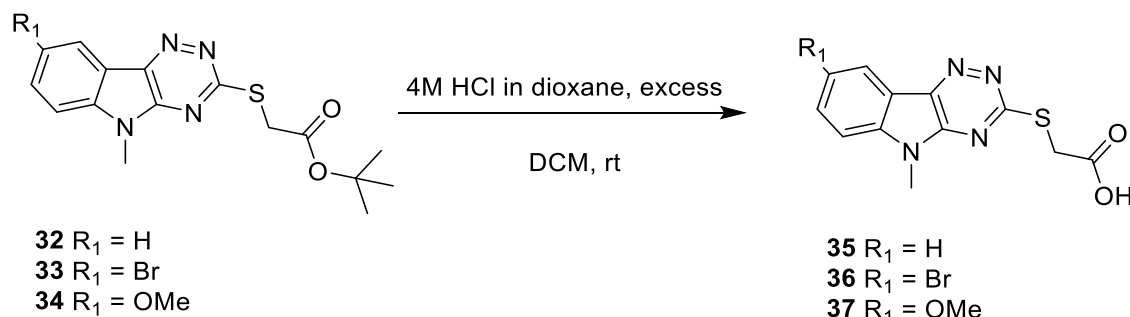
tert-Butyl 2-((8-bromo-5-methyl-5H-[1,2,4]triazino[5,6-b]indol-3-yl)thio)acetate (33) was prepared according to general procedure 3 starting from 8-bromo-5-methyl-5H-[1,2,4]triazino[5,6-b]indole-3-thiol (**30**) (0.15 g, 0.53 mmol). The crude product was purified by column chromatography (eluent PET/EtOAc 4:1) to give a yellow solid (0.19 g, 88%): ¹H NMR (400 MHz, DMSO-*d*₆) δ 8.52 (d, *J* = 2.0 Hz, 1H, H-4), 7.94 (dd, *J* = 8.7, 2.0 Hz, 1H, H-3), 7.78 (d, *J* = 8.7 Hz, 1H, H-2), 4.11 (s, 2H, H-5), 3.81 (s, 3H, H-1), 1.42 (s, 9H, H-6). ¹³C NMR (101 MHz, Chloroform-*d*) δ 167.92, 167.77, 146.62, 140.30, 140.13, 133.43, 125.09, 119.92, 116.10, 111.39, 82.22, 34.61, 28.02, 27.41. LCMS *m/z* calc. for C₁₆H₁₇BrN₄O₂S [M]⁺: 408.0, found 408.3 with *t*_R 3.05 min, purity 95%.

**Reaction code: liu180-207**

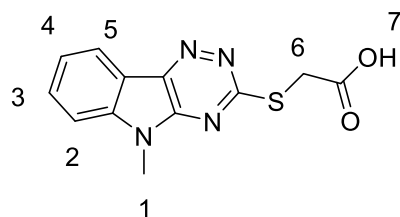
tert-Butyl 2-((8-methoxy-5-methyl-5H-[1,2,4]triazino[5,6-b]indol-3-yl)thio)acetate (34) was prepared according to general procedure 3 starting from 8-methoxy-5-methyl-5H-[1,2,4]triazino[5,6-b]indole-3-thiol (**31**) (0.80 g, 3.25 mmol). The crude product was purified by column chromatography (eluent PET/EtOAc 4:1) to give a

yellow solid (0.6481g, 55.39%): ^1H NMR (400 MHz, $\text{DMSO-}d_6$) δ 7.86 (d, J = 2.5 Hz, 1H, H-4), 7.71 (d, J = 8.9 Hz, 1H, H-2), 7.39 (dd, J = 8.9, 2.6 Hz, 1H, H-3), 4.09 (s, 2H, H-5), 3.91 (s, 3H, H-7), 3.79 (s, 3H, H-1), 1.42 (s, 9H, H-7). ^{13}C NMR (101 MHz, $\text{DMSO-}d_6$) δ 168.22, 166.59, 156.29, 146.38, 141.35, 136.43, 119.93, 118.35, 112.68, 104.66, 81.63, 56.34, 34.25, 28.15, 27.83. LCMS m/z calc. for $\text{C}_{17}\text{H}_{20}\text{N}_4\text{O}_3\text{S}$ $[\text{M}]^+$: 360.2, found 360.4 with t_{R} 2.91 min, purity 95%.

General Procedure 4 Preparation of 2-((5-methyl-5H-[1,2,4]triazino[5,6-b]indol-3-yl)thio)acetic acids 35-37

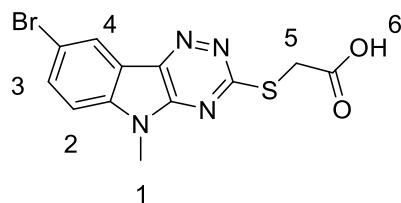


tert-butyl 2-((5-methyl-5H-[1,2,4]triazino[5,6-*b*]indol-3-yl)thio)acetates (**32-34**) (1 equiv) were dissolved in small amount of DCM (2 mL/mmol), 4M HCl in dioxane (excess) was added to the suspension. The mixture was then allowed to stir at room temperature overnight. Solvent was removed under vacuum to yield light yellow solid. The crude product was washed with diethyl ether and DCM and was used directly for next steps without further purification.



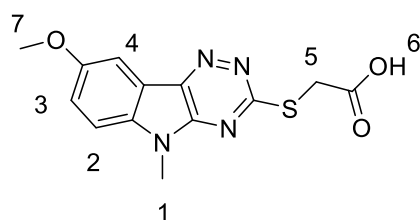
Reaction code: 180-61

2-((5-Methyl-5H-[1,2,4]triazino[5,6-*b*]indol-3-yl)thio)acetic acid (35) was prepared according to general procedure 4 starting from *tert*-butyl 2-((5-methyl-5H-[1,2,4]triazino[5,6-*b*]indol-3-yl)thio)acetate (**32**) (0.40 g, 1.21 mmol). The product was obtained as a yellow solid (280 mg, 84.34%): ^1H NMR (400 MHz, $\text{DMSO-}d_6$) δ 8.34 (d, J = 7.7 Hz, 1H, H-5), 7.79 (app. d, J = 4.0 Hz, 2H, H-2 and H-3), 7.51 (m, 1H, H-4), 4.10 (s, 2H, H-6), 3.83 (s, 3H, H-1). ^{13}C NMR (101 MHz, $\text{DMSO-}d_6$) δ 170.50, 166.81, 146.54, 142.14, 131.47, 123.40, 121.92, 117.75, 111.70, 79.46, 33.58, 27.81. LCMS m/z calc. for $\text{C}_{12}\text{H}_{10}\text{N}_4\text{O}_2\text{S}$ $[\text{M}]^+$: 274.3, found 274.3 with t_{R} 2.40 min, purity 95%.



Reaction code: liu180-35

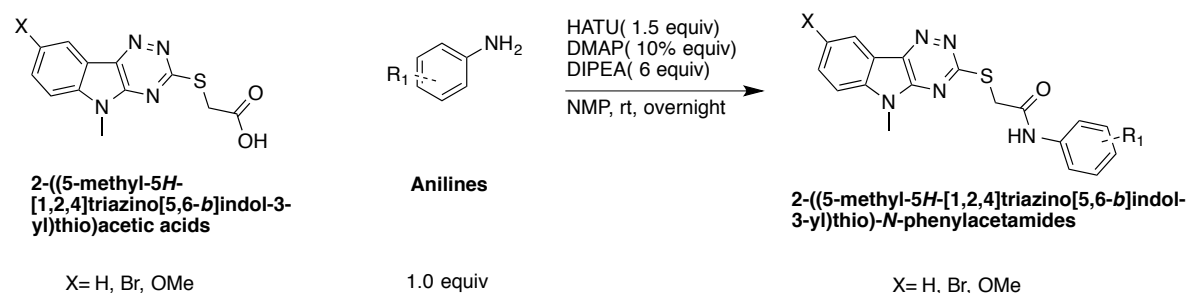
2-((8-bromo-5-methyl-5H-[1,2,4]triazino[5,6-b]indol-3-yl)thio)acetic acid (36) was prepared according to general procedure 4 starting from *tert*-butyl 2-((8-bromo-5-methyl-5H-[1,2,4]triazino[5,6-b]indol-3-yl)thio)acetate (**33**) (0.54 g, 1.32 mmol). The product was obtained as a yellow solid (0.38 g, 81.7%): ^1H NMR (400 MHz, $\text{DMSO-}d_6$) δ 8.50 (d, $J = 2.0$ Hz, 1H, H-4), 7.94 (dd, $J = 8.7, 2.0$ Hz, 1H, H-3), 7.78 (d, $J = 8.7$ Hz, 1H, H-2), 4.14 (s, 2H, H-5), 3.81 (s, 3H, H-1). ^{13}C NMR (101 MHz, $\text{DMSO-}d_6$) δ 168.10, 146.66, 140.93, 133.76, 124.20, 119.65, 115.51, 115.49, 113.88, 81.73, 34.30, 28.15. LCMS m/z calc. for $\text{C}_{12}\text{H}_9\text{BrN}_4\text{O}_2\text{S}$ $[\text{M}]^+$: 354.2, found 353.19 with t_R 2.63 min, purity 95%.



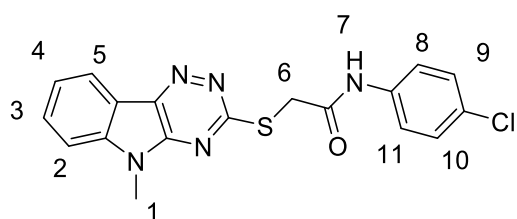
Reaction code: liu180-209

2-((8-Methoxy-5-methyl-5H-[1,2,4]triazino[5,6-b]indol-3-yl)thio)acetic acid (37) was prepared according to general procedure 4 starting from *tert*-butyl 2-((8-methoxy-5-methyl-5H-[1,2,4]triazino[5,6-b]indol-3-yl)thio)acetate **34** (0.54 g, 1.32 mmol). The product was obtained as a yellow solid (0.38 g, >100%): ^1H NMR (400 MHz, $\text{DMSO-}d_6$) δ 7.76 (d, $J = 2.5$ Hz, 1H, H-4), 7.65 (d, $J = 8.9$ Hz, 1H, H-1), 7.35 (dd, $J = 8.8, 2.5$ Hz, 1H, H-3), 4.14 (s, 2H, H-5), 3.88 (s, 3H, H-7), 3.75 (s, 3H, H-1). ^{13}C NMR (101 MHz, $\text{DMSO-}d_6$) δ 170.39, 166.31, 156.34, 146.32, 141.06, 136.56, 120.00, 118.20, 112.72, 104.77, 56.32, 33.57, 27.88. LCMS m/z calc. for $\text{C}_{13}\text{H}_{12}\text{N}_4\text{O}_3\text{S}$ $[\text{M}]^+$: 43, found 304.3 with t_R 2.46 min, purity 85%.

General Procedure 5 Preparation of 2-((5-methyl-5H-[1,2,4]triazino[5,6-b]indol-3-yl)thio)-N-phenylacetamides

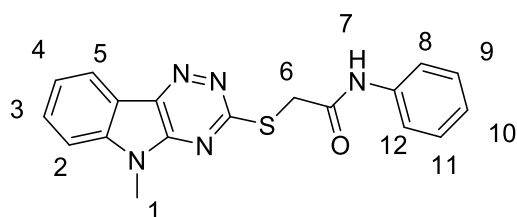


2-((5-Methyl-5H-[1,2,4]triazino[5,6-b]indol-3-yl)thio)acetic acids (1 equiv), HATU (3 equiv), DMAP (0.1 equiv) and amines (1 equiv) was dissolved in 1mL/mmol anhydrous NMP and stirred at room temperature for 5 minutes before addition of DIPEA (6 equiv). The mixture was allowed to stir at room temperature for overnight. The reaction was monitored by TLC and quenched by addition of water. The reaction mixture was stirred for 5 minutes and the diluted with water and was extracted by EtOAc three times and the combined organic layers were combined and washed with Sat. NaHCO₃ and brine and dried over Na₂SO₄. The crude product was purified by column chromatography.



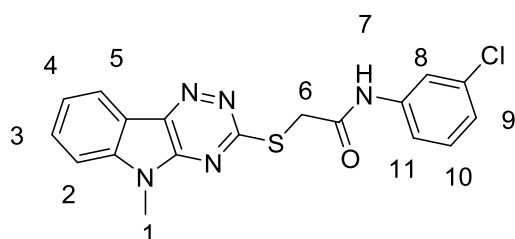
Reaction code: liu180-71

N-(4-chlorophenyl)-2-((5-methyl-5H-[1,2,4]triazino[5,6-b]indol-3-yl)thio)acetamide (19) was prepared according to general procedure 5 starting from using **35** (0.050 g, 0.18 mmol) and 4-Chloroaniline (0.023 g, 0.18 mmol). The crude product was purified by column chromatography (eluent PET/EtOAc 2:1) to give a white solid (0.022 g, 31%): ¹H NMR (400 MHz, DMSO-*d*₆) δ 10.56 (s, 1H, H-7), 8.32 (d, *J* = 7.9 Hz, 1H, H-5), 7.81 – 7.72 (m, 2H, H-2 and H-3), 7.71 – 7.63 (m, 2H, H-8 and H-11), 7.48 (td, *J* = 6.9, 5.9, 2.2 Hz, 1H, H-4), 7.42 – 7.33 (m, 2H, H-9 and H-10), 4.28 (s, 2H, H-6), 3.77 (s, 3H, H-1). ¹³C NMR (101 MHz, DMSO-*d*₆) δ 167.07, 166.92, 146.51, 142.05, 141.40, 138.50, 131.38, 129.19, 127.37, 123.32, 121.86, 121.11, 117.71, 111.62, 35.99, 27.72. LCMS *m/z* calc. for C₁₈H₁₄ClN₅OS [M]⁺: 383.3, found 383.85 with *t*_R 2.84 min, purity 95%.



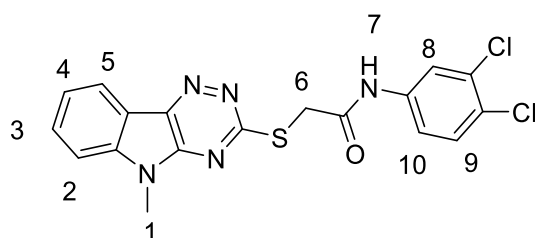
Reaction code: liu180-89

2-((5-Methyl-5H-[1,2,4]triazino[5,6-*b*]indol-3-yl)thio)-*N*-phenylacetamide (38) was prepared according to general procedure **5** starting from using **35** (0.050 g, 0.18 mmol) and aniline (0.017 g, 0.18 mmol). The crude product was purified by column chromatography (eluent PET/EtOAc 2:1) to give a white solid (0.013g, 20%): ^1H NMR (400 MHz, $\text{DMSO-}d_6$) δ 10.42 (s, 1H, H-7), 8.33 (d, $J = 7.8$ Hz, 1H, H-5), 7.81 – 7.72 (m, 2H, H-8 and H-12), 7.66 – 7.58 (m, 2H, H-9 and H-11), 7.49 (ddd, $J = 8.1, 5.2, 3.0$ Hz, 1H, H-3), 7.32 (app. t, $J = 7.9$ Hz, 2H, H-2 and H-4), 7.11 – 7.02 (m, 1H, H-10), 4.28 (s, 2H, H-6), 3.79 (s, 3H, H-1). ^{13}C NMR (101 MHz, $\text{DMSO-}d_6$) δ 167.17, 166.70, 146.54, 142.07, 141.40, 139.56, 131.39, 129.27, 123.83, 123.34, 121.88, 119.57, 117.74, 111.65, 36.01, 27.75. LCMS m/z calc. for $\text{C}_{18}\text{H}_{15}\text{N}_5\text{OS}$ $[\text{M}]^+$: 349.3, found 349.4 with t_{R} 2.72 min, purity 95%.



Reaction code: liu180-93

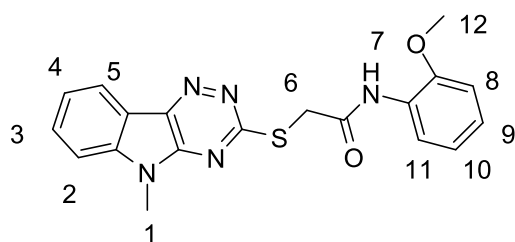
***N*-(3-chlorophenyl)-2-((5-methyl-5H-[1,2,4]triazino[5,6-*b*]indol-3-yl)thio)acetamide (40)** was prepared according to general procedure **5** starting from **35** (0.040 g, 0.15 mmol) and 3-Chloroaniline (0.019 g, 0.15 mmol). The crude product was purified by column chromatography (eluent PET/EtOAc 2:1) to give white solid (0.013 g, 23%): ^1H NMR (400 MHz, $\text{DMSO-}d_6$) δ 10.62 (s, 1H, H-7), 8.34 (d, $J = 7.8$ Hz, 1H, H-5), 7.84 (t, $J = 2.0$ Hz, 1H, H-8), 7.78 (app. d, $J = 3.9$ Hz, 2H, H-3 and H-11), 7.54 – 7.43 (m, 2H, H-2 and H-10), 7.36 (t, $J = 8.1$ Hz, 1H, H-4), 7.18 – 7.05 (m, 1H, H-9), 4.29 (s, 2H, H-6), 3.78 (s, 3H, H-1). ^{13}C NMR (101 MHz, $\text{DMSO-}d_6$) δ 167.19, 167.01, 146.55, 142.11, 141.46, 140.98, 133.60, 131.42, 131.02, 123.56, 123.35, 121.91, 119.00, 117.94, 117.74, 111.67, 36.01, 27.74. LCMS m/z calc. for $\text{C}_{18}\text{H}_{16}\text{ClN}_5\text{OS}$ $[\text{M}]^+$: 383.4, found 383.85 with t_{R} 2.87 min, purity 95%.



Reaction code: liu180-99

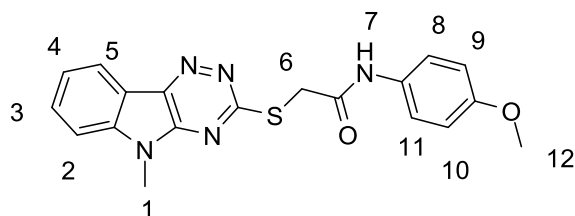
***N*-(3,4-Dichlorophenyl)-2-((5-methyl-5H-[1,2,4]triazino[5,6-*b*]indol-3-yl)thio)acetamide (41)** was prepared according to general procedure **5** using **35** (0.070 g, 0.25 mmol) and 3,4-Dichloroaniline (0.041 g, 0.25 mmol). The crude product

was purified by column chromatography (eluent PET/EtOAc 2:1) to give a white solid (0.005 g, 5%): ^1H NMR (400 MHz, $\text{DMSO-}d_6$) δ 10.73 (s, 1H, H-7), 8.33 (d, $J = 7.8$ Hz, 1H, H-5), 8.02 (d, $J = 2.4$ Hz, 1H, H-8), 7.84 – 7.74 (m, 2H, H-3 and H-10), 7.60 (d, $J = 8.8$ Hz, 1H, H-9), 7.56 – 7.43 (m, 2H, H-2 and H-4), 4.29 (s, 2H, H-6), 3.78 (s, 3H, H-1). ^{13}C NMR (101 MHz, $\text{DMSO-}d_6$) δ 167.37, 166.94, 146.55, 142.12, 141.48, 139.62, 131.53, 131.44, 131.28, 125.26, 123.37, 121.91, 120.72, 119.61, 117.74, 111.69, 36.00, 27.75. LCMS m/z calc. for $\text{C}_{18}\text{H}_{14}\text{Cl}_2\text{N}_5\text{OS}$ $[\text{M}+\text{H}]^+$: 418.3, found 418.2 with t_{R} 2.95 min, purity 95%.



Reaction code: liu180-141

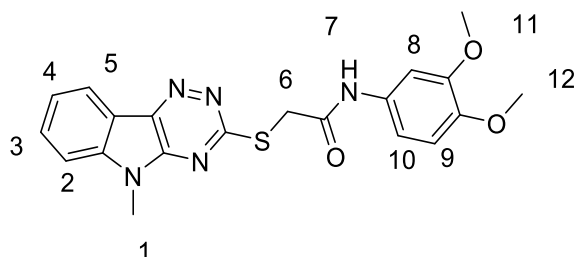
***N*-(2-Methoxyphenyl)-2-((5-methyl-5*H*-[1,2,4]triazino[5,6-*b*]indol-3-yl)thio)acetamide (42)** was prepared according to general procedure 5 using 35 (0.070 g, 0.26 mmol) and 2-methoxyaniline (0.031 g, 0.26 mmol). The crude product was purified by column chromatography (eluent PET/EtOAc 2:1) to give a yellow solid (0.0245 g, 51%): ^1H NMR (400 MHz, $\text{DMSO-}d_6$) δ 9.70 (s, 1H, H-7), 8.35 (d, $J = 7.7$ Hz, 1H, H-5), 8.10 – 8.00 (m, 1H, H-11), 7.78 (app. q, $J = 5.2, 3.8$ Hz, 2H, H-2 and H-3), 7.50 (ddd, $J = 8.1, 5.2, 3.1$ Hz, 1H, H-4), 7.10 – 6.98 (m, 2H, H-9 and H-10), 6.96 – 6.82 (m, 1H, H-8), 4.31 (s, 2H, H-6), 3.81 (s, 3H, H-12), 3.78 (s, 3H, H-1). ^{13}C NMR (101 MHz, $\text{DMSO-}d_6$) δ 167.14, 166.92, 149.42, 146.54, 142.19, 141.55, 131.53, 127.77, 124.70, 123.44, 121.92, 121.30, 120.78, 117.74, 111.70, 111.49, 35.64, 28.56, 27.78. LCMS m/z calc. for $\text{C}_{20}\text{H}_{18}\text{N}_5\text{O}_3\text{S}$ $[\text{M}]^+$: 370.3, found 379.44 with t_{R} 2.80 min, purity 95%.



Reaction code: 180-143

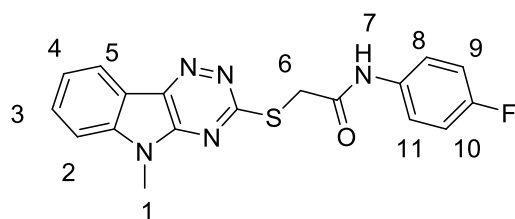
***N*-(4-Methoxyphenyl)-2-((5-methyl-5*H*-[1,2,4]triazino[5,6-*b*]indol-3-yl)thio)acetamide (43)** was prepared according to general procedure 5 using 36 (0.070 g, 0.26 mmol) and 4-methoxyaniline (0.031 g, 0.26 mmol). The product was obtained as a yellow solid (0.095 g, 98 %): ^1H NMR (400 MHz, $\text{DMSO-}d_6$) δ 10.27 (s,

1H, H-7), 8.32 (d, $J = 7.7$ Hz, 1H, H-5), 7.88 – 7.70 (m, 2H, H-2 and H-3), 7.56 – 7.51 (m, 2H, H-8 and H-11), 7.48 (ddd, $J = 2.6, 5.6, 8.1$ Hz, 1H, H-4), 6.96 – 6.71 (m, 2H, H-9 and H-10), 4.25 (s, 2H, H-6), 3.79 (s, 3H, H-12), 3.72 (s, 3H, H-11). ^{13}C NMR (101 MHz, DMSO- d_6) δ 167.20, 166.15, 155.75, 146.45, 142.06, 141.37, 132.70, 131.38, 123.33, 121.86, 121.13, 117.75, 114.37, 111.64, 38.71, 35.88, 27.74. LCMS m/z calc. for $\text{C}_{19}\text{H}_{17}\text{N}_5\text{O}_2\text{S}$ $[\text{M}]^+$: 379.2, found 379.44 with t_{R} 2.70 min, purity 95%.



Reaction code: liu195-43/ 180-147

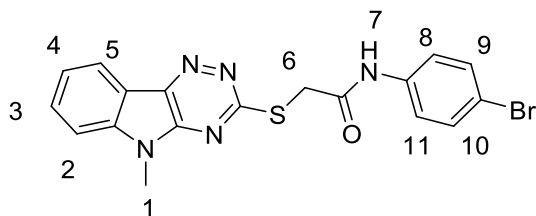
***N*-(3,4-Dimethoxyphenyl)-2-((5-methyl-5H-[1,2,4]triazino[5,6-*b*]indol-3-yl)thio)acetamide (44)** was prepared according to general procedure 5 using **35** (0.070 g, 0.26 mmol) and 4-methoxyaniline (0.039 g, 0.26 mmol). The crude product was purified by column chromatography (eluent PET/EtOAc 2:1) to give white solid (0.003 g, 3 %): ^1H NMR (400 MHz, DMSO- d_6) δ 10.28 (s, 1H, H-7), 8.30 (d, $J = 7.7$ Hz, 1H, H-5), 7.81 – 7.68 (m, 2H, H-2 and H-8), 7.47 (ddd, $J = 2.4, 5.8, 8.0$ Hz, 1H, H-3), 7.35 (d, $J = 2.4$ Hz, 1H, H-10), 7.12 (dd, $J = 2.4, 8.6$ Hz, 1H, H-4), 6.90 (d, $J = 8.7$ Hz, 1H, H-9), 4.25 (s, 2H, H-6), 3.78 (s, 3H, H-1), 3.72 (d, $J = 0.9$ Hz, 6H, H-11 and H-12). ^{13}C NMR (101 MHz, DMSO- d_6) δ 167.19, 166.20, 149.03, 146.52, 145.36, 142.04, 141.36, 133.18, 131.36, 123.32, 121.84, 117.72, 112.56, 111.62, 111.47, 104.72, 56.18, 55.81, 35.96, 27.74. LCMS m/z calc. for $\text{C}_{20}\text{H}_{20}\text{N}_5\text{O}_3\text{S}$ $[\text{M}+\text{H}]^+$: 410.5, found 410.2 with t_{R} 2.62 min, purity 95%.



Reaction code: liu180-115

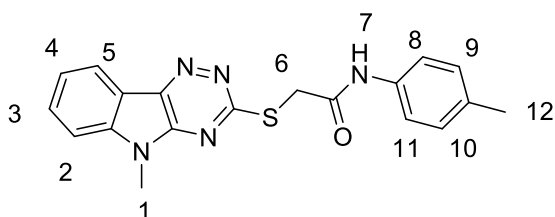
***N*-(4-fluorophenyl)-2-((5-methyl-5H-[1,2,4]triazino[5,6-*b*]indol-3-yl)thio)acetamide (45)** was prepared according to general procedure 5 using **35** (0.070 g, 0.26 mmol) and 4-Fluoroaniline (0.028 g, 0.26 mmol). The crude product was purified by column chromatography (eluent PET/EtOAc 2:1) to give a white solid (0.030 g, 32%): ^1H NMR (400 MHz, DMSO- d_6) δ 10.48 (s, 1H, H-7), 8.33 (d, $J = 7.8$ Hz, 1H, H-5), 7.86 – 7.71 (m, 2H, H-8 and H-11), 7.69 – 7.59 (m, 2H, H-2 and H-3), 7.49 (ddd, $J = 8.0, 5.3, 2.9$ Hz, 1H, H-4), 7.16 (app. t, $J = 8.9$ Hz, 2H, H-9 and H-10),

4.27 (s, 2H, H-6), 3.78 (s, 3H, H-1). ^{13}C NMR (101 MHz, $\text{DMSO-}d_6$) δ 167.12, 166.64, 158.50 (d, $J = 240.3$ Hz, $^1J_{\text{CF}}$), 146.54, 142.08, 141.41, 135.96, 131.40, 123.34, 121.88, 121.34 (d, $J = 8.0$ Hz, $^3J_{\text{CF}}$), 117.74, 115.85 (d, $J = 22.3$ Hz), 111.65, 27.74. LCMS m/z calc. for $\text{C}_{18}\text{H}_{14}\text{FN}_5\text{OS}$ $[\text{M}+\text{H}]^+$: 367.1, found 367.40 with t_{R} 2.75 min, purity 95%.



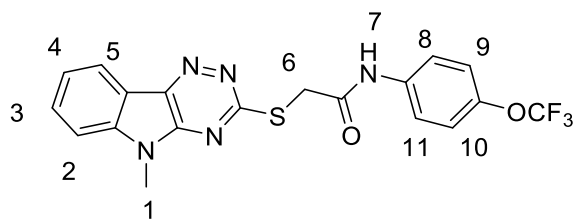
Reaction code: liu180-127

***N*-(4-Bromophenyl)-2-((5-methyl-5*H*-[1,2,4]triazino[5,6-*b*]indol-3-yl)thio)acetamide (46)** was prepared according to general procedure 5 using **35** (0.070 g, 0.26 mmol) and 4-bromoaniline (0.044 g, 0.26 mmol). The crude product was purified by column chromatography (eluent PET/EtOAc 2:1) to give a white solid (0.030 g, 27%): ^1H NMR (400 MHz, $\text{DMSO-}d_6$) δ 10.56 (s, 1H, H-7), 8.33 (d, $J = 7.7$ Hz, 1H, H-5), 7.89 – 7.72 (m, 2H, H-2 and H-3), 7.69 – 7.57 (m, 2H, H-8 and H-9), 7.55 – 7.43 (m, 3H, H-4 and H-9 and H-10), 4.28 (s, 2H, H-6), 3.77 (s, 3H, H-1). ^{13}C NMR (101 MHz, $\text{DMSO-}d_6$) δ 167.08, 166.94, 146.55, 142.10, 141.43, 138.92, 132.11, 131.42, 123.36, 121.90, 121.50, 117.75, 115.40, 111.68, 36.01, 27.75. LCMS m/z calc. for $\text{C}_{18}\text{H}_{14}\text{BrN}_5\text{OS}$ $[\text{M}]^+$: 429.0, found 428.31 with t_{R} 2.87 min, purity 95%.

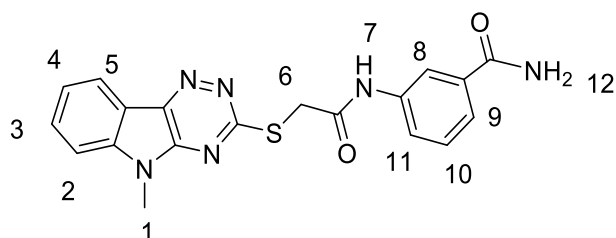


Reaction code: 180-149

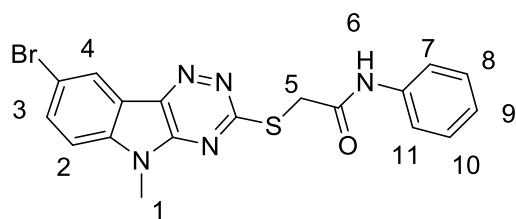
2-((5-Methyl-5*H*-[1,2,4]triazino[5,6-*b*]indol-3-yl)thio)-*N*-(*p*-tolyl)acetamide (47) was prepared according to general procedure 5 using **35** (0.070 g, 0.26 mmol) and 4-methoxyaniline (0.027 g, 0.26 mmol). The crude product was purified by column chromatography (eluent PET/EtOAc 2:1) to give a white solid (0.032 g, 35 %): ^1H NMR (400 MHz, $\text{DMSO-}d_6$) δ 10.33 (s, 1H, H-7), 8.29 (d, $J = 7.8$ Hz, 1H, H-5), 7.74 (app. d, $J = 6.8$ Hz, 2H, H-4 and H-3), 7.49 (app. dd, $J = 17.2, 7.7$ Hz, 3H, H-2 and H-8 and H11), 7.12 (app. d, $J = 8.0$ Hz, 2H, H-9 and H-10), 4.26 (s, 2H, H-6), 3.76 (s, 3H, H-1), 2.25 (s, 3H, H-12). ^{13}C NMR (101 MHz, $\text{DMSO-}d_6$) δ 167.19, 166.43, 146.48, 142.00, 141.33, 137.06, 132.74, 131.33, 129.63, 123.29, 121.82, 119.58, 117.70, 111.57, 35.98, 27.72, 20.91. LCMS m/z calc. for $\text{C}_{19}\text{H}_{18}\text{N}_5\text{OS}$ $[\text{M}]^+$: 363.1, found 363.44 with t_{R} 2.78 min, purity 95%.

**Reaction code: liu180-77**

2-((5-Methyl-5H-[1,2,4]triazino[5,6-*b*]indol-3-yl)thio)-*N*-(4-(trifluoromethoxy)phenyl)acetamide (48) was prepared according general procedure 5 starting from **35** (0.050 g, 0.18 mmol) and 4-(trifluoromethoxy)aniline (0.032 g, 0.18 mmol). The crude product was purified by column chromatography (eluent PET/EtOAc 2:1) to give a white solid (0.005 g, 6%): ^1H NMR (400 MHz, DMSO- d_6) δ 10.63 (s, 1H, H-7), 8.33 (d, $J = 7.9$ Hz, 1H, H-5), 7.84 – 7.62 (m, 4H, H-2, -3, -8 and -11), 7.49 (ddd, $J = 8.1, 5.3, 2.8$ Hz, 1H, H-4), 7.34 (app. d, $J = 8.6$ Hz, 2H, H-9 and H-10), 4.29 (s, 2H, H-6), 3.78 (d, $J = 1.7$ Hz, 3H, H-1). ^{13}C NMR (101 MHz, DMSO- d_6) δ 178.30, 167.05, 167.00, 146.55, 142.10, 141.44, 144.06, 138.74, 131.41, 123.35, 122.18, 121.90, 120.92, 117.74, 111.66, 35.95, 27.75. LCMS m/z calc. for $\text{C}_{19}\text{H}_{14}\text{F}_3\text{N}_5\text{O}_2\text{S}$ $[\text{M}]^+$: 433.4, found 433.41 with t_{R} 2.91 min, purity 95%.

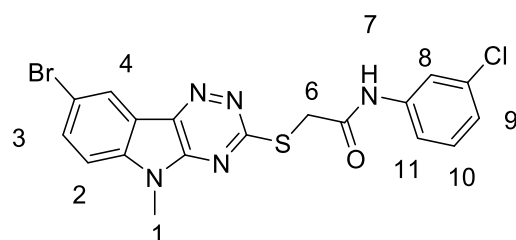
**Reaction code: liu180-185**

3-(2-((5-Methyl-5H-[1,2,4]triazino[5,6-*b*]indol-3-yl)thio)acetamido)benzamide (50) was prepared according to general procedure 5 using **35** (0.10 g, 0.36 mmol) and 3-aminobenzamide (0.050 g, 0.36 mmol). The crude product was purified by column chromatography (eluent DCM/0.7 M MeOH 20:1) to give a grey solid (0.055 g, 34%): ^1H NMR (400 MHz, DMSO- d_6) δ 10.55 (s, 1H, H-7), 8.29 (d, $J = 7.7$ Hz, 1H, H-5), 8.10 (t, $J = 1.9$ Hz, 1H, H-8), 7.94 (s, 1H, H-9), 7.84 – 7.75 (m, 1H, H-3), 7.76 – 7.68 (m, 2H, H-12), 7.56 (dt, $J = 7.7, 1.3$ Hz, 1H, H-2), 7.46 (ddd, $J = 8.0, 6.0, 2.2$ Hz, 1H, H-4), 7.38 (app. dd, $J = 17.4, 9.5$ Hz, 2H, H-10 and H-11), 4.29 (s, 2H, H-6), 3.76 (s, 3H and H-1). ^{13}C NMR (101 MHz, DMSO- d_6) δ 168.27, 167.10, 166.90, 146.50, 142.02, 141.37, 139.56, 135.63, 131.36, 129.11, 123.30, 122.58, 122.29, 121.84, 119.21, 117.70, 111.59, 35.97, 27.72. LCMS m/z calc. for $\text{C}_{19}\text{H}_{16}\text{N}_6\text{O}_2\text{S}$ $[\text{M}+\text{H}]^+$: 393.3, found 393.44 with t_{R} 2.44 min, purity 95%.



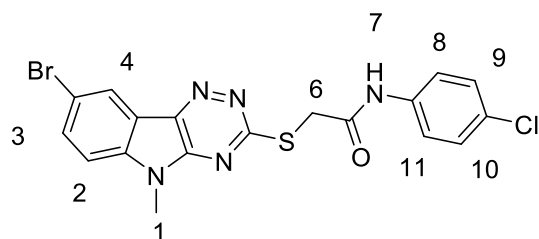
Reaction code: liu180-83

2-((8-Bromo-5-methyl-5H-[1,2,4]triazino[5,6-b]indol-3-yl)thio)-N-phenylacetamide (51) was prepared according to general procedure 5 starting from using **36** (0.050 g, 0.14 mmol) and aniline (0.013 g, 0.14 mmol). The crude product was purified by column chromatography (eluent PET/EtOAc 2:1) to give a white solid (0.015 g, 25%): ^1H NMR (400 MHz, $\text{DMSO-}d_6$) δ 10.42 (s, 1H, H-6), 8.49 (d, $J = 1.9$ Hz, 1H, H-4), 7.93 (app. dd, $J = 8.7, 2.0$ Hz, 1H, H-3), 7.76 (d, $J = 8.7$ Hz, 1H, H-2), 7.62 (app. d, $J = 7.9$ Hz, 2H, H-7 and H-11), 7.32 (t, $J = 7.9$ Hz, 2H, H-8 and H-10), 7.06 (t, $J = 7.4$ Hz, 1H, H-9), 4.29 (s, 2H, H-5), 3.78 (s, 3H, H-1). ^{13}C NMR (101 MHz, $\text{DMSO-}d_6$) δ 167.96, 166.60, 146.71, 140.94, 140.52, 139.54, 133.69, 132.07, 129.27, 129.14, 124.16, 123.84, 119.71, 119.57, 115.44, 113.85, 36.03, 27.91. LCMS m/z calc. for $\text{C}_{18}\text{H}_{14}\text{BrN}_5\text{OS}$ $[\text{M}]^+$: 429.2, found 428.3 with t_{R} 2.87 min, purity 95%.



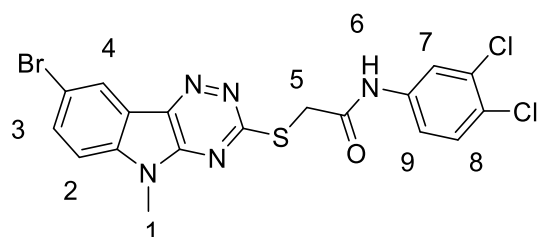
Reaction code: liu180-91 and 195-45

2-((8-Bromo-5-methyl-5H-[1,2,4]triazino[5,6-b]indol-3-yl)thio)-N-(3-chlorophenyl)acetamide (53) was prepared according to general procedure 5 starting from using **36** (0.050 g, 0.14 mmol) and 3-Chloroaniline (0.018 g, 0.14 mmol). The crude product was purified by column chromatography (eluent PET/EtOAc 2:1) to give a white solid (0.010g, 15.4%): ^1H NMR (400 MHz, $\text{DMSO-}d_6$) δ 10.63 (s, 1H, H-7), 8.50 (d, $J = 1.9$ Hz, 1H, H-4), 7.93 (dd, $J = 8.7, 2.0$ Hz, 1H, H-3), 7.84 (t, $J = 2.1$ Hz, 1H, H-8), 7.76 (d, $J = 8.6$ Hz, 1H, H-2), 7.52 – 7.45 (m, 1H, H-11), 7.35 (d, $J = 8.1$ Hz, 1H, H-9), 7.16 – 7.07 (m, 1H, H-10), 4.29 (s, 2H, H-6), 3.77 (s, 3H, H-1). LCMS m/z calc. for $\text{C}_{18}\text{H}_{13}\text{BrClN}_5\text{OS}$ $[\text{M}]^+$: 464.2, found 472.7 with t_{R} 2.98 min, purity 95%.



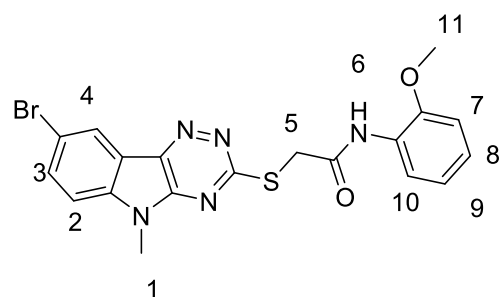
Reaction code: liu180-31/45

2-((8-Bromo-5-methyl-5H-[1,2,4]triazino[5,6-b]indol-3-yl)thio)-N-(4-chlorophenyl)acetamide (54) was prepared according to general procedure 5 starting from using **36** (0.050 g, 0.1415 mmol) and 4-Chloroaniline (0.020 g, 0.1562 mmol). The crude product was purified by column chromatography (eluent PET/EtOAc 2:1) to give a white solid (0.010 g, 15%): ^1H NMR (400 MHz, $\text{DMSO-}d_6$) δ 10.57 (s, 1H, H-7), 8.50 (d, J = 2.0 Hz, 1H, H-4), 7.93 (dd, J = 8.7, 2.0 Hz, 1H, H-3), 7.76 (d, J = 8.7 Hz, 1H, H-2), 7.72 – 7.60 (m, 2H, H-8 and H-11), 7.42 – 7.34 (m, 2H, H-9 and H-10), 4.28 (s, 2H, H-6), 3.77 (s, 3H, H-1). ^{13}C NMR (101 MHz, $\text{DMSO-}d_6$) δ 167.86, 166.82, 146.71, 140.96, 140.55, 138.49, 133.71, 129.20, 127.38, 124.18, 121.11, 119.71, 115.45, 113.86, 36.01, 27.90. LCMS m/z calc. for $\text{C}_{18}\text{H}_{13}\text{BrClN}_5\text{OS}$ $[\text{M}+\text{H}]^+$: 462.3, found 462.75 with t_R 2.91 min, purity 95%.

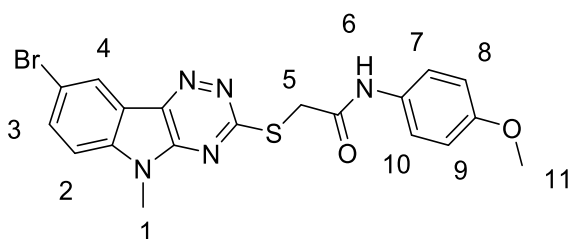


Reaction code: liu180-97

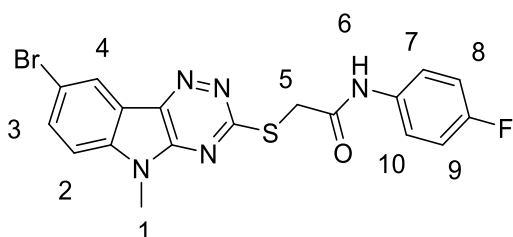
2-((8-Bromo-5-methyl-5H-[1,2,4]triazino[5,6-b]indol-3-yl)thio)-N-(3,4-dichlorophenyl)acetamide (55) was prepared according to general procedure 5 using **36** (0.070 g, 0.20 mmol) and 3,4-dichloroaniline (0.035 g, 0.21 mmol). The crude product was purified by column chromatography (eluent PET/EtOAc 2:1) to give white solid (0.005 g, 5%): ^1H NMR (400 MHz, $\text{DMSO-}d_6$) δ 10.73 (d, J = 7.6 Hz, 1H, H-6), 8.50 (d, J = 1.9 Hz, 1H, H-4), 8.02 (d, J = 2.3 Hz, 1H, H-7), 7.94 (dd, J = 8.7, 1.9 Hz, 1H, H-9), 7.76 (d, J = 8.7 Hz, 1H, H-3), 7.60 (d, J = 8.8 Hz, 1H, H-2), 7.53 (dd, J = 8.9, 2.4 Hz, 1H, H-8), 4.29 (s, 2H, H-5), 3.76 (s, 3H, H-1). ^{13}C NMR (101 MHz, $\text{DMSO-}d_6$) δ 167.37, 166.94, 146.55, 142.12, 141.48, 139.62, 131.53, 131.44, 131.28, 125.26, 123.37, 121.91, 120.72, 119.61, 117.74, 111.69, 36.00, 27.75. LCMS m/z calc. for $\text{C}_{18}\text{H}_{12}\text{BrCl}_2\text{N}_5\text{OS}$ $[\text{M}]^+$: 497.1, found 497.19 with t_R 3.06 min, purity 95%.

**Reaction code: liu180-139**

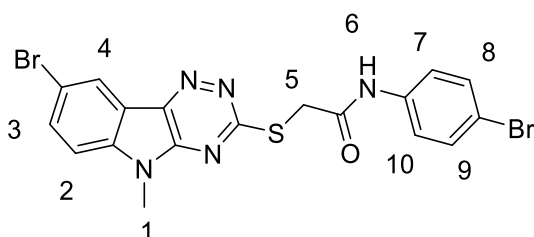
2-((8-Bromo-5-methyl-5H-[1,2,4]triazino[5,6-b]indol-3-yl)thio)-N-(2-methoxyphenyl)acetamide (56) was prepared according to general procedure 5 using **36** (0.070 g, 0.20 mmol) and 2-methoxyaniline (0.023 g, 0.20 mmol). The crude product was purified by column chromatography (eluent PET/EtOAc 2:1) to give a yellow solid (0.026 g, 28%): ^1H NMR (400 MHz, $\text{DMSO-}d_6$) δ 9.69 (s, 1H, H-6), 8.51 (d, $J = 2.0$ Hz, 1H, H-4), 8.03 (dd, $J = 1.5, 8.0$ Hz, 1H, H-10), 7.94 (dd, $J = 2.0, 8.7$ Hz, 1H, H-3), 7.77 (d, $J = 8.7$ Hz, 1H, H-2), 7.11 – 6.96 (m, 2H, H-7 and H-8), 6.89 (ddd, $J = 1.9, 6.9, 8.5$ Hz, 1H, H-9), 4.32 (s, 2H, H-5), 3.80 (app. d, $J = 2.5$ Hz, 6H, H-1 and H-11). ^{13}C NMR (101 MHz, $\text{DMSO-}d_6$) δ 167.72, 167.01, 149.48, 141.05, 140.66, 133.81, 127.75, 124.74, 124.19, 121.40, 120.77, 119.70, 115.53, 113.89, 111.50, 56.10, 35.69, 27.93. LCMS m/z calc. for $\text{C}_{19}\text{H}_{16}\text{BrN}_5\text{O}_2\text{S}$ $[\text{M}]^+$: 459.3, purity 95%.

**Reaction code: liu180-133**

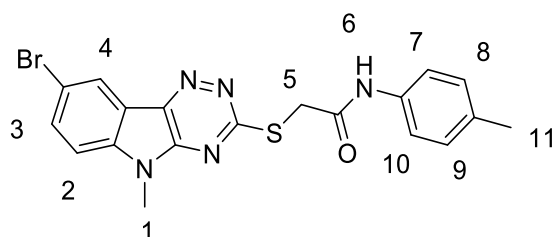
2-((8-Bromo-5-methyl-5H-[1,2,4]triazino[5,6-b]indol-3-yl)thio)-N-(4-methoxyphenyl)acetamide (57) was prepared according to general procedure 5 using **36** (0.070 g, 0.20 mmol) and 4-methoxyaniline (0.023 g, 0.20 mmol). The crude product was purified by column chromatography (eluent PET/EtOAc 2:1) to give a light yellow solid (0.017 g, 18%): ^1H NMR (400 MHz, $\text{DMSO-}d_6$) δ 10.28 (s, 1H, H-6), 8.49 (d, $J = 2.0$ Hz, 1H, H-4), 7.93 (dd, $J = 8.7, 2.0$ Hz, 1H, H-3), 7.76 (d, $J = 8.7$ Hz, 1H, H-2), 7.56 – 7.49 (m, 2H, H-7 and H-10), 6.93 – 6.85 (m, 2H, H-8 and H-9), 4.25 (s, 2H, H-5), 3.78 (s, 3H, H-11), 3.72 (s, 3H, H-1). ^{13}C NMR (101 MHz, $\text{DMSO-}d_6$) δ 168.03, 166.05, 155.76, 146.72, 140.94, 140.50, 133.68, 132.69, 124.15, 121.13, 119.72, 115.44, 114.38, 113.85, 38.72, 35.90, 27.92. LCMS m/z calc. for $\text{C}_{19}\text{H}_{16}\text{BrN}_5\text{O}_2\text{S}$ $[\text{M}]^+$: 458.3, found 458.33 with t_R 2.87 min, purity 95%.

**Reaction code: liu180-113**

2-((8-Bromo-5-methyl-5H-[1,2,4]triazino[5,6-b]indol-3-yl)thio)-N-(4-fluorophenyl)acetamide (58) was prepared according to general procedure 5 using **36** (0.070 g, 0.20 mmol) and 4-Fluoroaniline (0.022g, 0.20 mmol). The crude product was purified by column chromatography (eluent PET/EtOAc 2:1) to give a white solid (0.027g, 30%): ^1H NMR (400 MHz, $\text{DMSO-}d_6$) δ 10.48 (s, 1H, H-6), 8.49 (d, J = 2.0 Hz, 1H, H-4), 7.92 (dd, J = 8.7, 2.0 Hz, 1H, H-3), 7.75 (d, J = 8.7 Hz, 1H, H-2), 7.68 – 7.57 (m, 2H, H-7 and H-10), 7.16 (app. t, J = 8.9 Hz, 2H, H-8 and H-9), 4.27 (s, 2H, H-5), 3.77 (s, 3H, H-1). ^{13}C NMR (101 MHz, $\text{DMSO-}d_6$) δ 167.91, 166.55, 146.71, 140.95, 140.54, 135.92, 133.70, 124.17, 121.38, 121.30, 119.70, δ 115.85 (d, J = 22.4 Hz, $^2J_{\text{CF}}$), 115.45, 113.85, 35.93, 27.90. LCMS m/z calc. for $\text{C}_{18}\text{H}_{13}\text{BrFN}_5\text{OS}$ $[\text{M}]^+$: 446.3, found 446.30 with t_{R} 2.88 min, purity 95%.

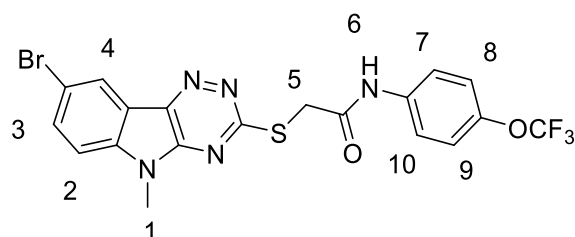
**Reaction code: liu180-131**

2-((8-Bromo-5-methyl-5H-[1,2,4]triazino[5,6-b]indol-3-yl)thio)-N-(4-bromophenyl)acetamide (59) was prepared according to general procedure 5 using **36** (0.070 g, 0.20 mmol) and 4-bromoaniline (0.034 g, 0.20 mmol). The crude product was purified by column chromatography (eluent PET/EtOAc 2:1) to give a yellow solid (0.007g, 7%): ^1H NMR (400 MHz, $\text{DMSO-}d_6$) δ 10.57 (s, 1H, H-6), 8.49 (d, J = 2.0 Hz, 1H, H-4), 7.93 (dd, J = 8.7, 2.1 Hz, 1H, H-3), 7.76 (d, J = 8.7 Hz, 1H, H-2), 7.64 – 7.56 (m, 2H, H-7 and H-10), 7.55 – 7.44 (m, 2H, H-8 and H-9), 4.28 (s, 2H, H-5), 3.76 (s, 3H, H-1). ^{13}C NMR (101 MHz, $\text{DMSO-}d_6$) δ 167.08, 166.95, 146.55, 142.10, 141.44, 138.92, 132.11, 131.42, 123.36, 121.91, 121.50, 117.75, 115.39, 111.68, 36.01, 27.75. LCMS m/z calc. for $\text{C}_{18}\text{H}_{13}\text{Br}_2\text{N}_5\text{OS}$ $[\text{M}]^+$: 507.2, found 507.20 with t_{R} 2.87 min, purity 95%.



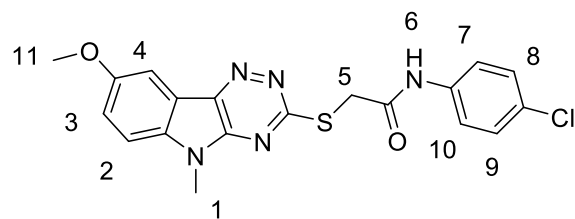
Reaction code: liu180-151

2-((8-Bromo-5-methyl-5H-[1,2,4]triazino[5,6-b]indol-3-yl)thio)-N-(p-tolyl)acetamide (60) was prepared according to general procedure 5 using **36** (0.070 g, 0.20 mmol) and 2-methoxyaniline (0.030 g, 0.20 mmol). The crude product was purified by column chromatography (eluent PET/EtOAc 2:1) to give a white solid (0.015 g, 12 %): ^1H NMR (400 MHz, $\text{DMSO-}d_6$) δ 10.34 (s, 1H, H-6), 8.47 (d, $J = 2.0$ Hz, 1H, H-2), 7.91 (dd, $J = 8.7, 2.0$ Hz, 1H, H-3), 7.74 (d, $J = 8.7$ Hz, 1H, H-4), 7.51 (app. d, $J = 8.4$ Hz, 2H, H-7 and H-10), 7.12 (app. d, $J = 8.1$ Hz, 2H, H-8 and H-9), 4.27 (s, 2H, H-5), 3.77 (s, 3H, H-1), 2.25 (s, 3H, H-11). ^{13}C NMR (101 MHz, $\text{DMSO-}d_6$) δ 168.00, 166.33, 146.69, 140.91, 140.49, 137.05, 133.67, 132.74, 129.63, 124.14, 119.70, 119.58, 115.44, 113.84, 36.00, 27.91, 20.92. LCMS m/z calc. for $\text{C}_{19}\text{H}_{17}\text{BrN}_5\text{OS}$ $[\text{M}+\text{H}]^+$: 442.1, found 442.1 with t_R 2.95 min, purity 95%.

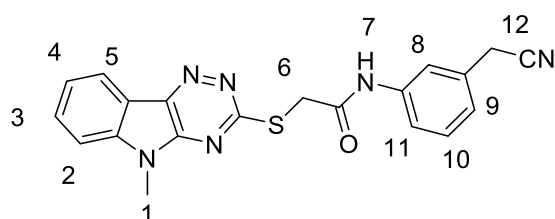


Reaction code: liu180-51

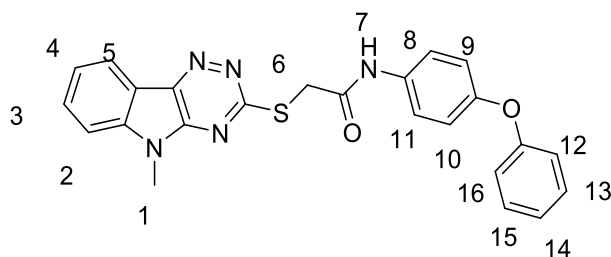
2-((8-Bromo-5-methyl-5H-[1,2,4]triazino[5,6-b]indol-3-yl)thio)-N-(4-(trifluoromethoxy)phenyl)acetamide (61) was prepared according to general procedure 5 starting from using **36** (0.050 g, 0.14 mmol) and 4-(trifluoromethoxy)aniline (0.021 mL, 0.16 mmol). The crude product was purified by column chromatography (eluent PET/EtOAc 2:1) to give a white solid (0.007 g, 9%): ^1H NMR (400 MHz, $\text{DMSO-}d_6$) δ 10.63 (s, 1H, H-6), 8.48 (d, $J = 2.0$ Hz, 1H, H-4), 7.92 (dd, $J = 8.7, 2.0$ Hz, 1H, H-2), 7.83 – 7.64 (m, 3H, H-3, -7 and -10), 7.34 (app. d, $J = 8.6$ Hz, 2H, H-8 and H-9), 4.29 (s, 2H, H-5), 3.77 (d, $J = 5.3$ Hz, 3H, H-1). ^{13}C NMR (101 MHz, $\text{DMSO-}d_6$) δ 167.83, 167.00, 166.91, 146.70, 142.09, 140.95, 140.56, 138.73, 133.70, 124.16, 122.18, 120.93, 119.69, 119.33, 115.45, 113.85, 111.66, 35.97, 27.74. LCMS m/z calc. for $\text{C}_{19}\text{H}_{13}\text{BrF}_3\text{N}_5\text{O}_2\text{S}$ $[\text{M}+\text{H}]^+$: 512.1, found 512.31 with t_R 3.05 min, purity 95%.

**Reaction code: liu180-267**

N-(4-chlorophenyl)-2-((8-methoxy-5-methyl-5H-[1,2,4]triazino[5,6-b]indol-3-yl)thio)acetamide (62) was obtained according to general procedure 5 using 37 (0.10 g, 0.33 mmol) and 4-chloroaniline (0.046 g, 0.36 mmol). The crude product was purified by column chromatography (eluent PET/EtOAc 2:1) to give a white solid (0.020 g, 15%): ^1H NMR (400 MHz, $\text{DMSO-}d_6$) δ 10.56 (s, 1H, H-6), 7.84 (d, $J = 2.8$ Hz, 1H, H-4), 7.67 (app. dd, $J = 11.3, 8.7$ Hz, 3H, H-2, -7 and -10), 7.44 – 7.31 (m, 3H, H-3, -8, and -9), 4.26 (s, 2H, H-5), 3.90 (s, 3H, H-1), 3.74 (s, 3H, H-11). ^{13}C NMR (101 MHz, $\text{DMSO-}d_6$) δ 166.96, 166.92, 156.25, 146.43, 141.38, 138.51, 136.45, 129.20, 127.36, 121.10, 119.87, 118.37, 112.67, 104.68, 56.32, 35.96, 27.76. LCMS m/z calc. for $\text{C}_{19}\text{H}_{17}\text{ClN}_5\text{O}_2\text{S}$ $[\text{M}]^+$: 413.3, found 413.88 with t_R 2.86 min, purity 95%.

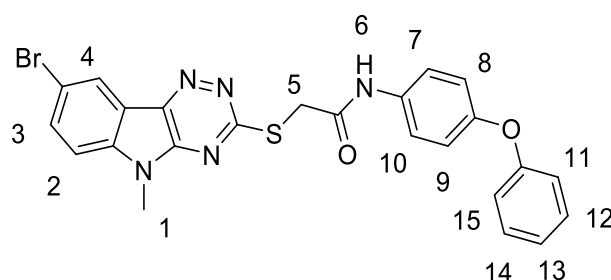
**Reaction code: 195-105**

N-(4-(cyanomethyl)phenyl)-2-((5-methyl-5H-[1,2,4]triazino[5,6-b]indol-3-yl)thio)acetamide (65) was obtained according to general procedure 5 using 35 (0.080 g, 0.029 mmol) and 2-(4-aminophenyl)acetonitrile (0.043 g, 0.32 mmol). The crude product was purified by column chromatography (eluent PET/EtOAc 2:1) to give a white solid (58.9 mg, 52%): ^1H NMR (400 MHz, $\text{DMSO-}d_6$) δ 10.52 (d, $J = 10.1$ Hz, 1H, H-7), 8.29 (d, $J = 7.7$ Hz, 1H, H-5), 7.95 (s, 1H, H-8), 7.78 – 7.68 (m, 2H, H-3 and H-11), 7.67 – 7.60 (m, H, H-2), 7.46 (ddd, $J = 1.8, 6.5, 8.0$ Hz, 1H, H-4), 7.30 (app. d, $J = 8.3$ Hz, 2H, H-9 and H-10), 4.27 (s, 2H, H-12), 3.97 (s, 2H, H-6), 3.76 (s, 3H, H-1). ^{13}C NMR (101 MHz, $\text{DMSO-}d_6$) δ 167.12, 166.85, 146.49, 142.01, 141.34, 138.94, 131.39, 129.04, 126.39, 123.33, 121.84, 120.00, 119.81, 117.67, 111.58, 35.96, 27.70, 22.30. LCMS m/z calc. for $\text{C}_{20}\text{H}_{17}\text{N}_6\text{OS}$ $[\text{M}+\text{H}]^+$: 389.4, found 389.3 with t_R 2.66 min, purity > 95%.



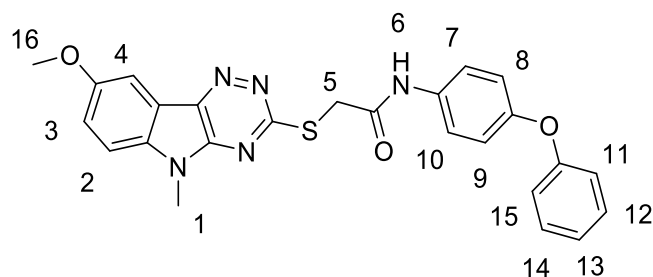
Reaction code: liu180-195

2-((5-Methyl-5H-[1,2,4]triazino[5,6-b]indol-3-yl)thio)-N-(4-phenoxyphenyl)acetamide (66) was prepared according to general procedure 5 using **35** (0.10 g, 0.36 mmol) and 4-phenoxyaniline (0.067 g, 0.36 mmol). The crude product was purified by column chromatography (eluent PET/EtOAc 2:1) to give a white solid (0.094 g, 58%): ^1H NMR (400 MHz, DMSO- d_6) δ 10.45 (s, 1H, H-7), 8.35 – 8.27 (m, 1H, H-5), 7.82 – 7.71 (m, 2H, H-2 and H-3), 7.70 – 7.60 (m, 2H, H-8 and H-11), 7.48 (ddd, J = 8.1, 5.6, 2.6 Hz, 1H, H-4), 7.40 – 7.31 (m, 2H, H-13 and H-15), 7.13 – 7.05 (m, 1H, H-14), 7.04 – 6.92 (m, 4H, H-9, -10, -13 and -15), 4.28 (s, 2H, H-6), 3.79 (s, 3H, H-1). ^{13}C NMR (101 MHz, DMSO- d_6) δ 174.23, 166.53, 142.06, 141.39, 135.47, 131.38, 130.43, 123.46, 123.32, 121.86, 121.29, 119.98, 118.34, 117.74, 111.63, 35.93, 27.75. LCMS m/z calc. for $\text{C}_{24}\text{H}_{19}\text{N}_5\text{O}_2\text{S}$ $[\text{M}]^+$: 442.3, found 441.51 with t_{R} 2.95 min, purity 95%.



Reaction code: liu180-197

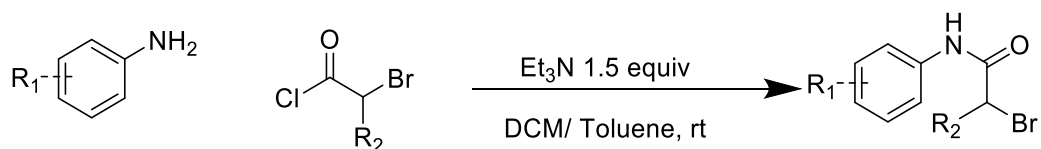
2-((8-Bromo-5-methyl-5H-[1,2,4]triazino[5,6-b]indol-3-yl)thio)-N-(4-phenoxyphenyl)acetamide (67) was obtained according to general procedure 5 using **36** (0.10 g, 0.28 mmol) and 4-phenoxyaniline (0.052 g, 0.28 mmol). The crude product was purified by column chromatography (eluent PET/EtOAc 2:1) to give a white solid (0.027 g, 18%): ^1H NMR (400 MHz, DMSO- d_6) δ 10.46 (s, 1H, H-6), 8.47 (d, J = 2.0 Hz, 1H, H-4), 7.91 (dd, J = 8.7, 2.0 Hz, 1H, H-3), 7.74 (d, J = 8.7 Hz, 1H, H-2), 7.68 – 7.58 (m, 2H, H-7 and H-10), 7.42 – 7.29 (m, 2H, H-12 and H-14), 7.13 – 7.07 (m, 1H, H-13), 7.05 – 6.90 (m, 4H, H-8, -9, -11, -15), 4.28 (s, 2H, H-5), 3.78 (s, 3H, H-1). ^{13}C NMR (101 MHz, DMSO- d_6) δ 166.43, 157.78, 152.30, 146.68, 140.92, 140.51, 135.45, 133.67, 130.43, 124.13, 123.47, 121.29, 119.97, 119.68, 118.35, 115.44, 113.83, 35.96, 27.92. LCMS m/z calc. for $\text{C}_{24}\text{H}_{18}\text{BrN}_5\text{O}_2\text{S}$ $[\text{M}]^+$: 521.2, found 520.41 with t_{R} 3.06 min, purity 95%.



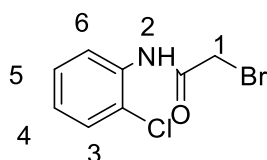
Reaction code: liu180-269

2-((8-Methoxy-5-methyl-5H-[1,2,4]triazino[5,6-*b*]indol-3-yl)thio)-*N*-(4-phenoxyphenyl)acetamide (68) was obtained according to general procedure 5 using **36** (0.10 g, 0.33 mmol) and 4-phenoxyaniline (0.067 g, 0.36 mmol). The crude product was purified by column chromatography (eluent PET/EtOAc 2:1) to give a white solid (0.063 g, 41%): $^1\text{H NMR}$ (400 MHz, $\text{DMSO-}d_6$) δ 10.45 (s, 1H, H-6), 7.84 (d, $J = 2.5$ Hz, 1H, H-4), 7.76 – 7.58 (m, 3H, H-2, -12 and -14), 7.37 (app. td, $J = 8.3, 7.8, 2.5$ Hz, 3H, H-13, -7 and -10), 7.10 (t, $J = 7.4$ Hz, 1H, H-3), 7.05 – 6.89 (m, 4H, H-11, -15, -8, -9), 4.26 (s, 2H, H-5), 3.90 (s, 3H, H-1), 3.77 (s, 3H, H-16). $^{13}\text{C NMR}$ (101 MHz, $\text{DMSO-}d_6$) δ 166.99, 166.56, 157.79, 156.25, 152.28, 146.44, 141.36, 136.45, 135.47, 130.43, 123.46, 121.28, 119.98, 119.85, 118.38, 118.35, 112.66, 104.67, 56.32, 35.91, 27.78. LCMS m/z calc. for $\text{C}_{25}\text{H}_{21}\text{N}_5\text{O}_3\text{S}$ $[\text{M}]^+$: 471.4, found 471.54 with t_R 2.96 min, purity 95%.

General procedure 6 Preparation of 2-bromo-*N*-phenylacetamides



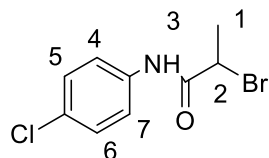
Anilines (1 equiv) was dissolved in DCM (5 mL/mmol) followed by addition of Et_3N (1.5 equiv) and bromoacetyl chlorides (1 equiv) at 0°C under N_2 protection. Reaction mixture was allowed slowly warm up to room temperature. Reactions were monitored by TLC. Once the reaction finished, solvent was removed under vacuum and crude product was used directly without further purification.



Reaction code: liu180-177

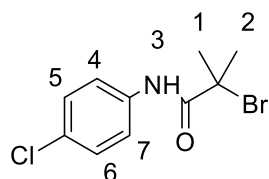
2-Bromo-*N*-(2-chlorophenyl)acetamide (64) was prepared according to general procedure 6 using 2-chloroaniline (**63**) (0.30 g, 2.35 mmol) and 2-bromoacetyl chloride

(0.37 g, 2.35 mmol). The crude product was obtained as a white crystal (0.19 g, 33% crude yield)



Reaction code: liu180-227

2-Bromo-N-(4-chlorophenyl)propanamide (87) was prepared according to general procedure **6** using 4-chloroaniline (0.50 g, 3.94 mmol) and 2-bromoacetyl chloride (0.67 g, 3.94 mmol). The crude product was purified by column chromatography (eluent PET/EtOAc 5:1) to give a white solid (0.24 g, 24%): ^1H NMR (400 MHz, DMSO- d_6) δ 10.46 (s, 1H, H-3), 7.72 – 7.55 (m, 2H, H-4 and H-7), 7.54 – 7.22 (m, 2H, H-5 and H-6), 4.69 (q, J = 6.7 Hz, 1H, H-2), 1.75 (d, J = 6.6 Hz, 3H, H-1). ^{13}C NMR (101 MHz, DMSO- d_6) δ 168.08, 138.00, 129.26, 127.86, 121.32, 44.73, 21.76. LCMS m/z calc. for $\text{C}_9\text{H}_9\text{BrClNO}$ $[\text{M}]^+$: 263.0, found 262.53 with t_R 2.74 min, purity 95%.



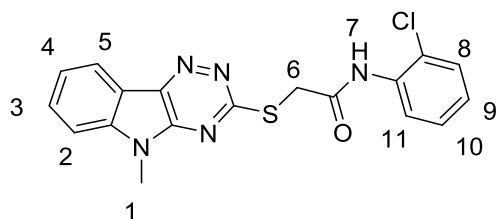
Reaction code: liu180-245

2-Bromo-N-(4-chlorophenyl)-2-methylpropanamide (88) was prepared according to general procedure **6** using 4-chloroaniline (0.20 g, 1.57 mmol) and 2-bromo-2-methylpropanoyl bromide (0.36 g, 1.57 mmol). The crude product was purified by column chromatography (eluent PET/EtOAc 5:1) to give a white solid (0.53 g, >100%): ^1H NMR (400 MHz, DMSO- d_6) δ 9.93 (s, 1H, H-3), 7.72 (app. dd, J = 8.6, 1.9 Hz, 2H, H-4 and H-7), 7.38 (app. dt, J = 8.7, 1.8 Hz, 2H, H-5 and H-6), 2.00 (s, 6H, H-1 and H-2). ^{13}C NMR (101 MHz, DMSO- d_6) δ 169.93, 138.07, 128.92, 128.07, 122.48, 60.93, 31.16, 30.94. 6. LCMS m/z calc. for $\text{C}_{10}\text{H}_{11}\text{BrClNO}$ $[\text{M}]^+$: 277.1, found 276.56 with t_R 2.88 min, purity 95%.

general procedure 7 Preparation of 2-((5-methyl-5H-[1,2,4]triazino[5,6-b]indol-3-yl)thio)-N-(4-phenoxyphenyl)acetamides

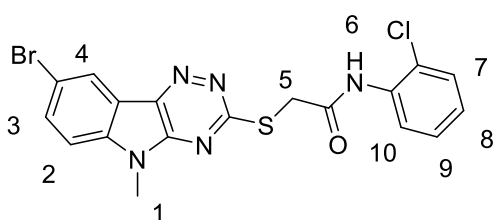


5-Methyl-5*H*-[1,2,4]triazino[5,6-*b*]indoles-3-thiols (1 equiv) was dissolved in 5 mL/mmol of DCM and Et₃N (1.5 equiv) was added to the suspension followed by addition of 2-bromo-*N*-phenylacetamides (1 equiv) at 0°C under N₂. Reaction mixture was allowed slowly warm up to room temperature and stir for 4 hours. The reaction was monitored by TLC. Once the reaction finished, solvent was removed under vacuum. The crude product was purified by column chromatography.



Reaction code: liu180-181

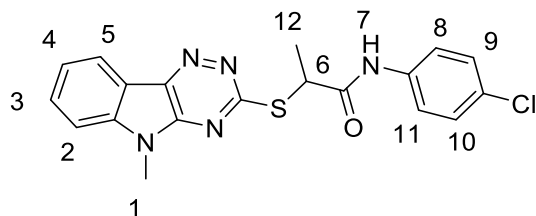
***N*-(2-chlorophenyl)-2-((5-methyl-5*H*-[1,2,4]triazino[5,6-*b*]indol-3-yl)thio)acetamide (39)** was prepared according to general procedure 7 using 2-bromo-*N*-(2-chlorophenyl)acetamide (**64**) (0.10 g, 0.41 mmol) and 5-methyl-5*H*-[1,2,4]triazino[5,6-*b*]indole-3-thiol (**29**) (0.088 g, 0.41 mmol). The crude product was purified by column chromatography (eluent PET/EtOAc 2:1) to give a white solid (0.029 g, 18%): ¹H NMR (400 MHz, DMSO-*d*₆) δ 9.93 (s, 1H, H-7), 8.34 (d, *J* = 7.7 Hz, 1H, H-5), 7.87 – 7.73 (m, 3H, H-2, -3, -11), 7.50 (app. ddd, *J* = 7.7, 5.1, 2.4 Hz, 2H, H-8 and H-10), 7.40 – 7.25 (m, 1H, H-9), 7.18 (td, *J* = 7.7, 1.6 Hz, 1H, H-4), 4.35 (s, 2H, H-6), 3.81 (s, 3H, H-1). ¹³C NMR (101 MHz, DMSO-*d*₆) δ 167.33, 166.90, 146.55, 142.14, 141.50, 135.29, 131.47, 129.94, 127.99, 126.66, 125.83, 123.39, 121.93, 117.74, 111.68, 35.43, 27.85. LCMS *m/z* calc. for C₁₈H₁₄ClN₅OS [M]⁺: 383.2, found 383.85 with *t*_R 2.82 min, purity 95%.



Reaction code: liu180-191

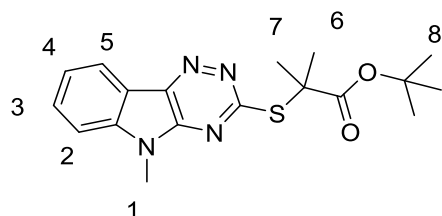
2-((8-Bromo-5-methyl-5*H*-[1,2,4]triazino[5,6-*b*]indol-3-yl)thio)-*N*-(2-chlorophenyl)acetamide (52) was prepared according to general procedure 7 using bromo-*N*-(2-chlorophenyl)acetamide (**64**) (0.100 g, 0.3387 mmol) and **30** (0.083 g, 0.3387 mmol). The crude product was purified by column chromatography (eluent PET/EtOAc 2:1) to give a white solid (0.053 g, 35%): ¹H NMR (400 MHz, DMSO-*d*₆) δ 9.94 (s, 1H, H-6), 8.50 (t, *J* = 2.8 Hz, 1H, H-4), 7.93 (dt, *J* = 9.3, 2.7 Hz, 1H, H-3), 7.88 – 7.64 (m, 2H, H-2 and H-10), 7.50 (dd, *J* = 7.9, 1.6 Hz, 1H, H-9), 7.43 – 7.25 (m, 1H, H-7), 7.23 – 7.08 (m, 1H, H-8), 4.36 (app. d, *J* = 3.3 Hz, 2H, H-5), 3.80 (s, 3H, H-1).

^{13}C NMR (101 MHz, DMSO- d_6) δ 167.71, 167.22, 146.72, 140.99, 140.61, 135.28, 133.76, 129.96, 127.98, 126.70, 126.29, 125.94, 124.20, 119.69, 115.50, 113.88, 35.45, 28.00. LCMS m/z calc. for $\text{C}_{18}\text{H}_{13}\text{BrClN}_5\text{OS}$ $[\text{M}]^+$: 463.0, found 462.75 with t_R 3.01 min, purity 95%.



Reaction code: liu180-235

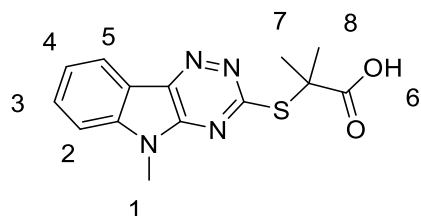
***N*-(4-chlorophenyl)-2-((5-methyl-5*H*-[1,2,4]triazino[5,6-*b*]indol-3-yl)thio)propanamide (92)** was prepared according to general procedure 7 using **87** (0.20 g, 0.93 mmol) and **29** (0.24 g, 0.93 mmol). The crude product was purified by column chromatography (eluent PET/EtOAc 2:1) to give a white solid (0.083 g, 22%): ^1H NMR (400 MHz, DMSO- d_6) δ 10.61 (s, 1H, H-7), 8.30 (d, $J = 7.7$ Hz, 1H, H-5), 7.75 (app. d, $J = 5.9$ Hz, 2H, H-2 and H-3), 7.68 (app. d, $J = 8.6$ Hz, 2H, H-8 and H-11), 7.47 (ddd, $J = 8.0, 6.0, 2.3$ Hz, 1H, H-4), 7.38 (app. d, $J = 8.8$ Hz, 2H, H-9 and H-10), 4.85 (q, $J = 7.0$ Hz, 1H, H-6), 3.77 (s, 3H, H-1), 1.68 (d, $J = 7.1$ Hz, 3H, H-12). ^{13}C NMR (101 MHz, DMSO- d_6) δ 170.55, 166.85, 146.49, 142.08, 141.47, 138.40, 131.42, 129.19, 127.53, 123.33, 121.88, 121.25, 117.71, 111.61, 45.12, 27.76, 18.65. LCMS m/z calc. for $\text{C}_{19}\text{H}_{16}\text{ClN}_5\text{OS}$ $[\text{M}]^+$: 397.2, found 397.8 with t_R 3.03 min, purity 95%.



Reaction code: liu180-225

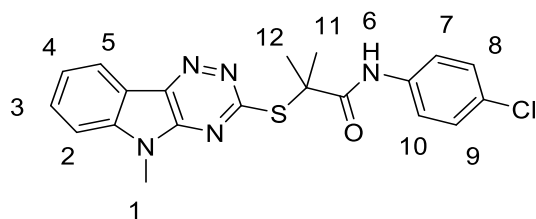
***tert*-Butyl 2-methyl-2-((5-methyl-5*H*-[1,2,4]triazino[5,6-*b*]indol-3-yl)thio)propanoate:** To a solution of *tert*-butyl 2-((5-methyl-5*H*-[1,2,4]triazino[5,6-*b*]indol-3-yl)thio)acetate (**29**) (0.30 g, 0.91 mmol) in anhydrous DMF (10 mL) at 0°C under N_2 protection, NaH 60% dispersion in mineral oil (0.11 g, 2.72 mmol) was added in one portion. The mixture was stirring for 45 minutes followed by addition of iodomethane (0.64 g, 4.54 mmol) dropwise. The mixture was then slowly warmed up to room temperature and stirred for overnight. The mixture was poured into Sat. NH_4Cl (60 mL) and stirred vigorously for 10 minutes. The resulting suspension was extracted with EtOAc (30 mL \times 3). The combined organic layers were washed with brine, dried over Na_2SO_4 , and concentrated. The crude compound was purified by column chromatography to give a white solid (0.17 g, 52 % yield): ^1H NMR (400 MHz, DMSO-

d_6) δ 8.35 (dt, $J = 7.7, 1.0$ Hz, 1H, H-5), 7.86 – 7.73 (m, 2H, H-2 and H-3), 7.50 (ddd, $J = 8.0, 5.6, 2.6$ Hz, 1H, H-4), 3.80 (s, 3H, H-1), 1.71 (app. s, 6H, H-6 and H-7), 1.31 (s, 9H, H-8). ^{13}C NMR (101 MHz, DMSO- d_6) δ 172.64, 167.06, 146.27, 141.99, 141.11, 131.39, 123.36, 121.90, 117.84, 111.64, 80.83, 51.95, 27.88, 27.83, 26.52. LCMS m/z calc. for $\text{C}_{18}\text{H}_{22}\text{N}_4\text{O}_2\text{S}$ $[\text{M}]^+$: 358.2, found 358.46 with t_{R} 3.03 min, purity 95%.



Reaction code: liu180-229

2-Methyl-2-((5-methyl-5H-[1,2,4]triazino[5,6-b]indol-3-yl)thio)propanoic acid: tert-butyl 2-methyl-2-((5-methyl-5H-[1,2,4]triazino[5,6-b]indol-3-yl)thio)propanoate (0.064 g, 0.18 mmol) were dissolved in DCM (3 mL), and 4 mL 4M HCl in dioxane (excessive) was added to the suspension. The mixture was then allowed to stir at room temperature for 24 hours. Solvent removed under vacuum to give light yellow solid. The crude compound was washed with diethyl ether and DCM and was used directly for the next step without further purification (0.038 g, 70%): ^1H NMR (400 MHz, DMSO- d_6) δ 8.32 (d, $J = 7.7$ Hz, 1H, H-5), 7.84 – 7.71 (m, 2H, H-2 and H-3), 7.49 (ddd, $J = 8.0, 5.7, 2.4$ Hz, 1H, H-4), 3.80 (s, 3H, H-1), 1.73 (app. s, 6H, H-7 and H-8). ^{13}C NMR (101 MHz, DMSO- d_6) δ 175.34, 167.06, 146.30, 142.07, 141.02, 131.47, 123.40, 121.91, 117.79, 111.66, 51.64, 27.83, 26.60. LCMS m/z calc. for $\text{C}_{14}\text{H}_{14}\text{N}_4\text{O}_2\text{S}$ $[\text{M}]^+$: 302.1, found 302.35 with t_{R} 2.55 min, purity 90%.



Reaction code: liu180-265

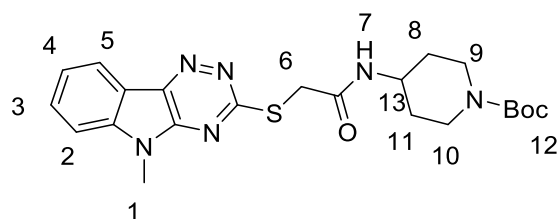
6.4.2.4 Preparation of N-(4-chlorophenyl)-2-methyl-2-((5-methyl-5H-[1,2,4]triazino[5,6-b]indol-3-yl)thio)propanamide (93)

Method 1: N-(4-chlorophenyl)-2-methyl-2-((5-methyl-5H-[1,2,4]triazino[5,6-b]indol-3-yl)thio)propanamide was prepared according to general procedure 5 using 2-methyl-2-((5-methyl-5H-[1,2,4]triazino[5,6-b]indol-3-yl)thio)propanoic acid.

Method 2: To a solution of 5-methyl-5H-[1,2,4]triazino[5,6-b]indole-3-thiol (**29**) (0.100 g, 0.46 mmol) in anhydrous DMF (10 mL) at 0 °C under N_2 protection, NaH 60%

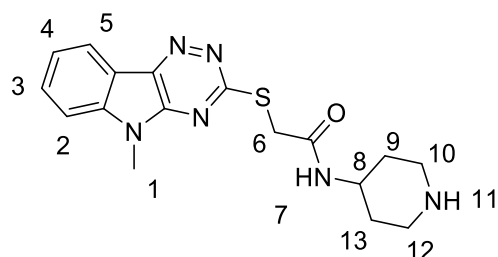
dispersion in mineral oil (0.020g, 0.51 mmol) was added in one portion. The mixture was stirred for 45 minutes followed by addition of 2-bromo-*N*-(4-chlorophenyl)-2-methylpropanamide (**88**) (0.128 g, 0.46 mmol). The mixture was then slowly warmed up to room temperature and stirred for overnight. The mixture was poured into Sat. NH₄Cl (60 mL) and stirred vigorously for 10 minutes. The resulting suspension was extracted with EtOAc (30 mL × 3). The combined organic layers were washed with brine, dried over Na₂SO₄, and concentrated. The crude product was purified by column chromatography (eluent PET/EtOAc 3:1) to give a yellow solid (0.140 g, 74%): ¹H NMR (400 MHz, DMSO-*d*₆) δ 9.98 (s, 1H, H-6), 8.29 (dt, *J* = 7.8, 1.0 Hz, 1H, H-5), 7.85 – 7.62 (m, 4H, H-2, -3, -7 and -10), 7.45 (ddd, *J* = 8.0, 6.7, 1.5 Hz, 1H, H-4), 7.38 – 7.17 (m, 2H, H-8 and H-9), 3.73 (s, 3H, H-1), 1.81 (app. s, 6H, H-11 and H-12). ¹³C NMR (101 MHz, DMSO-*d*₆) δ 172.39, 166.56, 146.24, 141.98, 141.26, 138.68, 131.44, 128.76, 127.36, 123.33, 122.25, 121.90, 117.71, 111.60, 52.77, 27.78, 26.61. LCMS *m/z* calc. for C₂₀H₁₈ClN₅OS [M]⁺: 411.2, found 411.91 with *t*_R 2.99 min, purity 95%.

Preparation of *tert*-butyl 4-(2-((5-methyl-5*H*-[1,2,4]triazino[5,6-*b*]indol-3-yl)thio)acetamido)piperidine-1-carboxylate



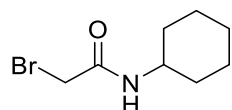
Reaction code: liu195-003/ liu180-281

***tert*-Butyl 4-(2-((5-methyl-5*H*-[1,2,4]triazino[5,6-*b*]indol-3-yl)thio)acetamido)piperidine-1-carboxylate (**99**)** was prepared according to general procedure **5** using **35** (0.100 g, 0.36 mmol) and *tert*-butyl 4-aminopiperidine-1-carboxylate (0.073 g, 0.36 mmol). The crude compound was purified by column chromatography (eluent PET/EtOAc 3:1) to give a yellow solid (0.150 g, 90 %): ¹H NMR (400 MHz, DMSO-*d*₆) δ 8.34 (d, *J* = 7.7 Hz, 1H, H-7), 8.26 (d, *J* = 7.7 Hz, 1H, H-5), 7.84 – 7.70 (m, 2H, H-2 and H-3), 7.50 (ddd, *J* = 3.5, 4.8, 8.0 Hz, 1H, H-4), 4.04 (s, 2H, H-6), 3.88- 3.71 (m, 6H, H-1 and H-13, H-9, H-10), 2.86 (app. d, *J* = 10.1 Hz, 2H, H-9 and H-10), 1.73 (app. dd, *J* = 3.8, 13.0 Hz, 2H, H-8 and H-11), 1.40 (s, 9H, H-12), 1.35 – 1.20 (m, 2H, H-8 and H-11). ¹³C NMR (101 MHz, DMSO-*d*₆) δ 167.28, 166.83, 154.38, 142.05, 131.37, 123.34, 121.87, 117.77, 111.65, 79.12, 48.95, 46.69, 34.95, 30.58, 28.54, 27.82. LCMS *m/z* calc. for C₂₂H₂₈N₆O₃S [M+H]⁺: 457.5, found 457.1 with *t*_R 2.76 min.

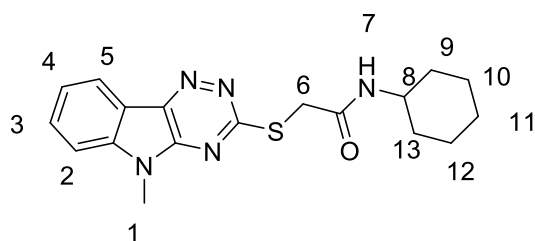


Reaction code: liu195-009

Preparation of 2-((5-methyl-5H-[1,2,4]triazino[5,6-b]indol-3-yl)thio)-N-(piperidin-4-yl)acetamide (100). **99** (0.352 g, 0.77 mmol) was dissolved in DCM (5 mL), 3 mL 4M HCl in dioxane (excessive) was added, and the reaction mixture was allowed to stir at room temperature for 6 hours. The reaction was monitored by TLC. Once the reaction finished, solvent was removed under vacuum, 7 N NH₃ in Methanol (10 mL) was added, the solvent was allowed to stir at room temperature for 3 hours. Solvent was removed under vacuum. The crude product was purified by column chromatography (eluent DCM: 0.7 N NH₃ in MeOH (10:1)). A grey solid (0.14 g, 51%). ¹H NMR (400 MHz, Chloroform-*d*) δ 8.48 – 8.40 (m, 1H, H-7), 7.75 (td, *J* = 1.2, 7.7 Hz, 1H, H-5), 7.59 – 7.47 (m, 3H, H-2, -3 and -4), 3.99 (s, 2H, H-6), 3.97 – 3.91 (m, 1H, H-8), 3.87 (s, 3H, H-1), 3.15 (app. d, *J* = 12.9 Hz, 2H, H-10 and H-12), 2.85 – 2.73 (m, 2H, H-10 and H-12), 1.98 (app. d, *J* = 13.6 Hz, 2H, H-9 and H-13), 1.60 – 1.39 (m, 2H, H-9 and H-13). ¹³C NMR (101 MHz, Chloroform-*d*) δ 168.51, 166.77, 146.52, 142.00, 131.37, 123.37, 122.66, 117.96, 110.06, 45.66, 43.78, 34.74, 30.55, 27.47. LCMS *m/z* calc. for C₁₇H₂₀N₆OS [M+H]⁺: 357.4, found 357.2 with *t_R* 1.95 min.

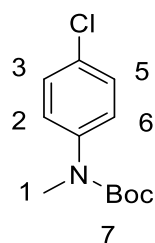


Preparation of 2-bromo-N-cyclohexylacetamide 96 Cyclohexanamine (0.200g, 2.02 mmol) was dissolved in 10 mL DCM, Et₃N (0.224 g, 2.22 mmol) was added at 0 °C under N₂, followed by addition of 2-bromoacetyl chloride (0.32 g, 2.02 mmol). Reaction mixture was allowed to warm up to room temperature and stirred for 4 hours and monitored by TLC. Once the reaction finished, solvent was removed under vacuum and crude product was used directly for the next step without purification.



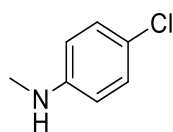
Reaction code: liu180-291

Preparation of *N*-cyclohexyl-2-((5-methyl-5*H*-[1,2,4]triazino[5,6-*b*]indol-3-yl)thio)acetamide (98). **29** (0.100 g, 0.46 mmol) was dissolved in 5 mL DCM at 0 °C, Et₃N (0.051 g, 0.51 mmol) was added followed by addition of **96** (0.102 g, 0.46 mmol). Reaction was allowed warm up to room temperature and stirred for 4 hours and monitored by TLC. Solvent was removed under vacuum and the crude product was purified by column chromatography (eluent PET/EtOAc 3:1) to give a white solid (0.153 g, 94%). ¹H NMR (400 MHz, DMSO-*d*₆) δ 8.33 (dd, *J* = 7.7, 0.9 Hz, 1H, H-7), 8.14 (d, *J* = 7.9 Hz, 1H, H-5), 7.89 – 7.66 (m, 2H, H-2 and H-3), 7.49 (ddd, *J* = 8.0, 4.8, 3.5 Hz, 1H, H-4), 4.03 (s, 2H, H-6), 3.83 (s, 3H, H-1), 3.55 (td, *J* = 9.6, 8.5, 3.7 Hz, 1H, H-8), 1.81 – 1.71 (m, 2H, H-6), 1.67 (app. dt, *J* = 12.0, 3.4 Hz, 2H, H-9 and 13), 1.55 (app. d, *J* = 12.4 Hz, 2H, H-9 and 13), 1.33 – 1.05 (m, 6H, H-10, 11, and 12). ¹³C NMR (101 MHz, DMSO-*d*₆) δ 167.39, 166.48, 146.53, 142.04, 141.28, 131.34, 123.33, 121.86, 117.78, 111.65, 48.50, 35.02, 32.82, 27.82, 25.65, 24.97. LCMS *m/z* calc. for C₁₈H₂₁N₅OS⁺[M]⁺: 355.2, found 355.4 with *t*_R 2.75 min, purity 95%.



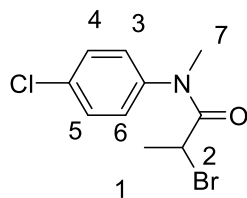
Reaction code: liu195-019

Preparation of *tert*-butyl (4-chlorophenyl)(methyl)carbamate. To a solution of *tert*-butyl (4-chlorophenyl) carbamate (1.00 g, 4.39 mmol) in anhydrous DMF (12 mL) at 0°C under N₂ protection, NaH 60% dispersion in mineral oil (0.210 g, 5.27 mmol) was added in one portion. The mixture was stirring for 45 minutes followed by addition of iodomethane (0.935 g, 6.59 mmol) dropwise. The mixture was then slowly warmed up to room temperature and stirred for overnight. The mixture was poured into Sat. NH₄Cl (60 mL) and stirred vigorously for 10 minutes. The resulting suspension was extracted with EtOAc (50 mL × 3). The combined organic layers were washed with brine, dried over Na₂SO₄, and concentrated. The crude compound was purified by column chromatography (eluent PET/EtOAc 5:1) to give a clear oil (1.00 g, 94%). ¹H NMR (400 MHz, DMSO-*d*₆) δ 7.43 – 7.36 (m, 2H, H-2 and H-6), 7.34 – 7.26 (m, 2H, H-3 and H-5), 3.17 (s, 3H, H-1), 1.40 (s, 9H, H-7). ¹³C NMR (101 MHz, DMSO-*d*₆) δ 153.96, 142.84, 129.70, 128.84, 127.50, 80.34, 37.29, 28.35. Purity >95%.



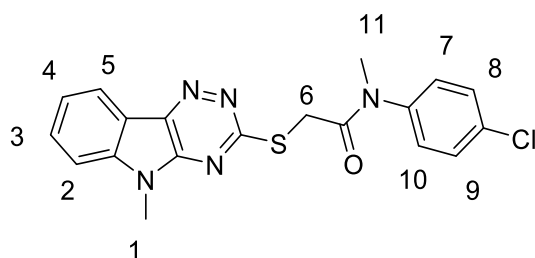
Preparation of 4-chloro-*N*-methylaniline: *tert*-butyl (4-chlorophenyl)(methyl)carbamate (1.00 g, 4.15 mmol) were dissolved in DCM (5 mL), 3 mL 4M HCl in dioxane (excessive) was added. The mixture was then allowed to stir

at room temperature for 24 hours. Solvent removed under vacuum to give a white solid as HCl salt. The 4-chloro-N-methylaniline·HCl then dissolved in DCM and added excessive Et₃N to neutralize the HCl salt. Solvent removed under vacuum and the crude product (brown oil) was used directly for the next step without further purification.



Reaction code: liu195-27

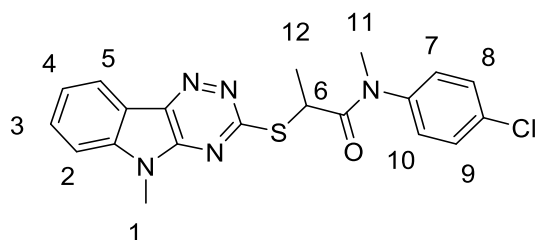
Preparation of 2-bromo-N-(4-chlorophenyl)-N-methylacetamide (90). The preparation for **90** was based on general procedure **6**. **4-chloro-N-methylaniline** (**6**, 0.10 g, 0.71 mmol) were dissolved in DCM (5 mL) at room temperature. Et₃N (0.079 g, 0.78 mmol) was added followed by addition of 2-bromopropanoyl chloride (0.12 g, 0.71 mmol). Reaction was stirred for 4 hours and monitored by TLC. Solvent was removed under vacuum and the crude product was purified by column chromatography. (eluent PET/EtOAc 6:1) to give a grey solid (149 mg, 76%). ¹H NMR (400 MHz, Chloroform-*d*) δ 7.44 (app. d, *J* = 8.3 Hz, 2H, H-3 and H-6), 7.26 (app. d, *J* = 8.2 Hz, 2H, H-4 and H-5), 4.24 (q, *J* = 6.6 Hz, 1H, H-2), 3.28 (s, 3H, H-7), 1.74 (d, *J* = 6.7 Hz, 3H, H-1). ¹³C NMR (101 MHz, Chloroform-*d*) δ 169.47, 141.35, 134.42, 130.22, 128.64, 38.78, 38.13, 21.74. LCMS *m/z* calc. for C₁₀H₁₁BrClNO [M+H]⁺: 277, found 278.1 with *t*_R 2.80 min, purity > 95%.



Reaction code: liu195-23

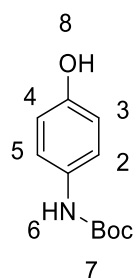
N-(4-chlorophenyl)-N-methyl-2-((5-methyl-5H-[1,2,4]triazino[5,6-*b*]indol-3-yl)thio)acetamide (94) was prepared according to general procedure **7** using 2-bromo-N-(4-chlorophenyl)-N-methylacetamide **89** (0.050 g, 0.19 mmol) and **29** (0.041 g, 0.19 mmol). The crude product was purified by column chromatography (eluent PET/EtOAc 1:1) to give a white solid (32.5 mg, 43%): ¹H NMR (400 MHz, DMSO-*d*₆) δ 8.32 (d, *J* = 7.8 Hz, 1H, H-5), 7.78 (app. d, *J* = 4.1 Hz, 2H, H-2 and H-3), 7.65 – 7.35 (m, 5H, H-4, -7, -8, -9, -10), 4.05 (app. d, *J* = 22.3 Hz, 2H, H-6), 3.76 (s, 3H, H-1), 3.23 (s, 3H, H-11). ¹³C NMR (101 MHz, DMSO-*d*₆) δ 170.55, 166.85, 146.49, 142.08, 141.47, 138.40, 131.42, 129.19, 127.53, 123.33, 121.88, 121.25, 117.71, 111.61,

45.12, 27.76, 18.65. LCMS m/z calc. for $C_{19}H_{16}ClN_5OS$ $[M]^+$: 397.2, found 397.8 with t_R 3.03 min, purity 95%.



Reaction code: liu195-31

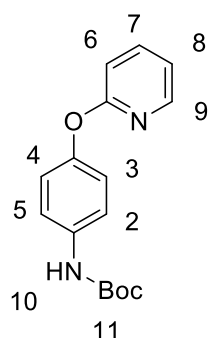
***N*-(4-chlorophenyl)-*N*-methyl-2-((5-methyl-5*H*-[1,2,4]triazino[5,6-*b*]indol-3-yl)thio)propanamide (95)** was prepared according to general procedure 7 using **29** (0.050 g, 0.23 mmol) and **90** (0.064 g, 0.23 mmol). Reaction was allowed warm up to room temperature and stirred for overnight and monitored by TLC. Solvent was removed under vacuum and the crude product was purified by column chromatography (eluent PET/EtOAc 1:1) to give a grey solid (59 mg, 76%). 1H NMR (400 MHz, $DMSO-d_6$) δ 8.33 (d, $J = 7.7$ Hz, 1H, H-5), 7.79 (app. d, $J = 3.8$ Hz, 2H, H-2 and H-3), 7.69 – 7.40 (m, 3H, H-4, -7, -10), 7.36 (app. d, $J = 8.0$ Hz, 2H, H-8 and H-9), 4.80 (q, $J = 6.9$ Hz, 1H, H-6), 3.70 (s, 3H, H-1), 3.20 (s, 3H, H-11), 1.51 (d, $J = 6.9$ Hz, 3H, H-12). ^{13}C NMR (101 MHz, $DMSO-d_6$) δ 171.18, 170.94, 166.01, 146.30, 142.40, 142.15, 141.44, 132.85, 131.49, 130.07, 129.96, 123.38, 121.91, 117.69, 111.61, 55.39, 44.54, 37.69, 27.62, 24.57, 22.19, 19.31. LCMS m/z calc. for $C_{20}H_{19}ClN_5OS$ $[M+H]^+$: 412.2, found 412.2 with t_R 2.90 min, purity > 95%.



Reaction code: liu195-75

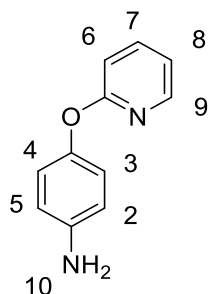
Preparation of *tert*-butyl (4-hydroxyphenyl)carbamate (72). 4-aminophenol (0.50 g, 4.58 mmol) were dissolved in DCM (10 mL) at room temperature. $(Boc)_2O$ (1.20 g, 5.50 mmol) was added followed by addition of Et_3N (0.69 g, 6.87 mmol). Reaction was stirred for overnight and monitored by TLC. Solvent was removed under vacuum and diluted with water (50 mL). The resulting suspension was extracted with EtOAc (30 mL \times 3). The combined organic layers were washed with brine, dried over Na_2SO_4 , and concentrated. The crude compound was purified by column chromatography (eluent PET/EtOAc 4:1) to give a white solid (493.8 mg, 52%). 1H NMR (400 MHz, $Chloroform-d$) δ 7.36 (app. d, $J = 8.8$ Hz, 2H, H-2 and H-5), 7.14 – 7.02 (m, 2H, H-4

and H-3), 6.52 (s, 1H, H-6), 1.57 (s, 9H, H-7). ^{13}C NMR (101 MHz, Chloroform-*d*) δ 152.72, 152.03, 146.47, 135.95, 121.68, 119.36, 83.44, 28.34. LCMS m/z calc. for $\text{C}_{11}\text{H}_{15}\text{NO}_3$ $[\text{M}+\text{H}]^+$: 210.2, found 210.2 with t_{R} 2.52 min, purity > 95%.



Reaction code: liu 195-83

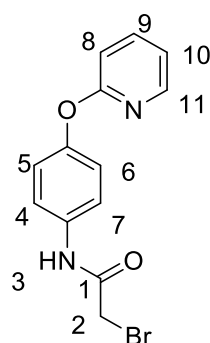
Preparation of *tert*-butyl (4-(pyridin-2-yloxy)phenyl)carbamate (73). *tert*-butyl (4-hydroxyphenyl)carbamate (**72**) (0.1 g, 0.48 mmol), 2-bromopyridine (0.091 g, 0.58 mmol), the ligand (0.012 g, 0.096 mmol), CuI (0.010 g, 0.048 mmol) and K_3PO_4 (0.20 g, 0.96 mmol) were dissolved in DMSO (10 mL) under the protection of N_2 , the reaction was then heated under 90 °C for overnight and monitored by TLC. Once the reaction was finished, then it was allowed to cool to room temperature. The reaction mixture was diluted with water (50 mL). The resulting suspension was extracted with EtOAc (30 mL \times 3). The combined organic layers were washed with brine, dried over Na_2SO_4 , and concentrated. The crude compound was purified by column chromatography (eluent PET/EtOAc 5:1) to give a colorless oil (27.5 mg, 20%). ^1H NMR (400 MHz, Chloroform-*d*) δ 8.21 (ddd, J = 0.8, 2.0, 5.0 Hz, 1H, H-9), 7.69 (ddd, J = 2.1, 7.2, 8.3 Hz, 1H, H-7), 7.40 (app. d, J = 8.4 Hz, 2H, H-4 and H-3), 7.17 – 7.06 (m, 2H, H-2 and H-5), 7.00 (ddd, J = 1.0, 5.0, 7.2 Hz, 1H, H-8), 6.89 (dt, J = 0.9, 8.3 Hz, 1H, H-6), 6.56 (s, 1H, H-10), 1.54 (s, 9H, H-11). ^{13}C NMR (101 MHz, Chloroform-*d*) δ 163.95, 152.87, 149.37, 147.59, 139.52, 135.18, 121.84, 118.30, 111.18, 82.88, 28.35. LCMS m/z calc. for $\text{C}_{16}\text{H}_{17}\text{N}_2\text{O}_3$ $[\text{M}+\text{H}]^+$: 287.1, found 287.2 with t_{R} 2.85 min, purity > 95%.



Reaction code: liu195-89

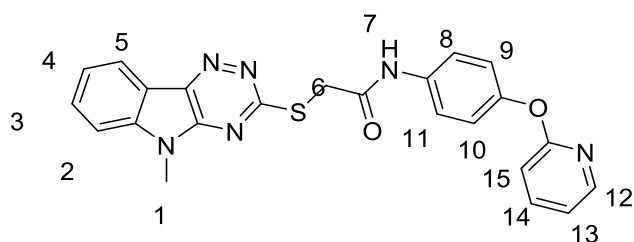
Preparation of 4-(pyridin-2-yloxy)aniline (74). *tert*-butyl (4-(pyridin-2-yloxy)phenyl)carbamate (**73**) (0.182 g, 0.63 mmol) were dissolved in DCM (8 mL), 3

mL 4M HCl in dioxane (excessive) was added. The mixture was then allowed to stir at room temperature for overnight. Solvent removed under vacuum to give a white solid as HCl salt. The Preparation of 4-(pyridin-2-yloxy)aniline·HCl then dissolved in DCM and added excessive Et₃N to neutralize the HCl salt. Solvent removed under vacuum and the crude product (brown oil) was used directly for the next step without further purification. The crude yield was >100%. ¹H NMR (400 MHz, Chloroform-*d*) δ 12.07 (s, 2H, H-10), 8.19 (dd, *J* = 2.0, 4.9 Hz, 1H, H-9), 7.64 (ddd, *J* = 2.0, 7.2, 8.3 Hz, 1H, H-7), 7.02 – 6.90 (m, 3H, H-6, -8, -3), 6.84 (dd, *J* = 1.0, 8.3 Hz, 1H, H-4), 6.76 – 6.67 (m, 2H, H-5 and H-2). ¹³C NMR (101 MHz, Chloroform-*d*) δ 164.54, 147.74, 146.04, 143.50, 139.19, 122.29, 117.87, 116.14, 110.78.



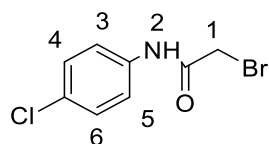
Reaction code: liu195-91

Preparation of 2-bromo-N-(4-(pyridin-2-yloxy)phenyl)acetamide (77). 4-(pyridin-2-yloxy)aniline **74** (0.163 g, 0.64 mmol) was dissolved in 8 mL DCM at 0 °C, Et₃N (0.097 g, 0.95 mmol) was added followed by addition of 2-bromoacetyl chloride (0.12 g, 0.64 mmol). Reaction was allowed warm up to room temperature and stirred for overnight and monitored by TLC. Solvent was removed under vacuum and the crude product was purified by column chromatography (eluent PET/EtOAc 5:1) to give a solid (71 mg, 47%). ¹H NMR (400 MHz, Chloroform-*d*) δ 8.19 (dd, *J* = 2.0, 5.1 Hz, 1H, H-11), 7.64 (ddd, *J* = 2.0, 7.1, 8.2 Hz, 1H, H-9), 6.99 – 6.90 (m, 3H, H-4, -7 and -10), 6.83 (dd, *J* = 1.0, 8.3 Hz, 1H, H-8), 6.76 – 6.67 (m, 2H, H-5 and H-6), 3.65 (s, 2H, H-2). ¹³C NMR (101 MHz, Chloroform-*d*) δ 164.54, 147.74, 146.04, 143.50, 139.19, 122.29, 117.88, 116.14, 110.78, 45.81. LCMS *m/z* calc. for C₁₃H₁₁BrN₂O₂ [M]⁺: 307.1, found 307.0 with t_R 2.59 min, purity > 95%.



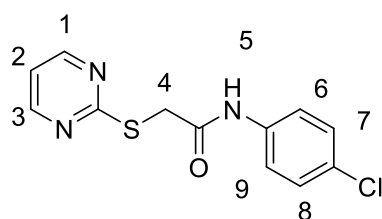
Reaction code: liu195-93

Preparation of 2-((5-methyl-5H-[1,2,4]triazino[5,6-*b*]indol-3-yl)thio)-*N*-(4-(pyridin-2-yloxy)phenyl)acetamide (69). **29** (0.030 g, 0.14 mmol) was dissolved in 8 mL DCM at 0 °C, Et₃N (0.021 g, 0.21 mmol) was added to the suspension followed by addition of **77** (0.051 g, 0.17 mmol). Reaction was allowed warm up to room temperature and stirred for overnight and monitored by TLC. Solvent was removed under vacuum and the crude product was purified by column chromatography (eluent PET/EtOAc 1:1) to give a white solid (39 mg, 64%). ¹H NMR (400 MHz, DMSO-*d*₆) δ 10.48 (s, 1H, H-7), 8.40 – 8.20 (m, 1H, H-5), 8.19 – 8.03 (m, 1H, H-12), 7.83 (ddd, *J* = 2.0, 7.2, 8.2 Hz, 1H, H-14), 7.76 (d, *J* = 1.0 Hz, 1H, H-2), 7.67 – 7.60 (m, 2H, H-2 and H-3), 7.49 (ddd, *J* = 2.6, 5.6, 8.0 Hz, 1H, H-4), 7.14 – 7.05 (m, 3H, H-8, -11, -15), 6.99 (dd, *J* = 1.0, 8.3 Hz, 1H, H-13), 4.28 (s, 2H, H-6), 3.80 (s, 3H, H-1). ¹³C NMR (101 MHz, Chloroform-*d*) δ 167.21, 167.08, 150.16, 147.70, 146.55, 142.15, 139.35, 134.91, 131.51, 123.44, 122.66, 121.76, 121.07, 118.33, 117.96, 111.22, 110.16, 35.75, 27.53. LCMS *m/z* calc. for C₂₃H₁₈N₆O₂S [M+H]⁺: 443.5, found 443.2 with *t*_R 2.78 min, purity > 95%.



Reaction code: liu195-77

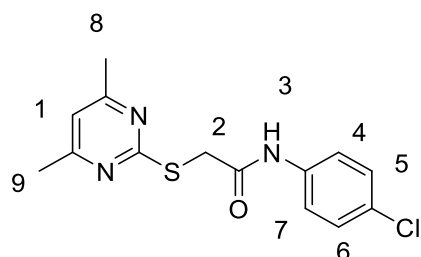
Preparation of 2-bromo-*N*-(4-chlorophenyl)acetamide (91). 4-chloroaniline (0.30 g, 2.36 mmol) was dissolved in 10 mL DCM at 0 °C, Et₃N (0.36 g, 3.54 mmol) was added to the suspension followed by addition of 2-bromoacetyl chloride (0.37 g, 2.36 mmol). Reaction was allowed warm up to room temperature and stirred for 4 hours and monitored by TLC. Solvent was removed under vacuum and the crude product was used directly for the next step. LCMS *m/z* calc. for C₈H₇BrClNO [M+H]⁺: 250.5, found 250.0 with *t*_R 2.63 min.



Reaction code: liu195-113

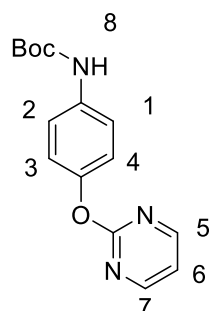
Preparation of *N*-(4-chlorophenyl)-2-(pyrimidin-2-ylthio)acetamide (103). To a solution of pyrimidine-2-thiol **101** (0.05 g, 0.45 mmol) in anhydrous DMF (6 mL) at 0°C under N₂ protection, NaH 60% dispersion in mineral oil (0.20 g, 0.49 mmol) was added in one portion. The mixture was stirring for 45 minutes followed by addition of 2-bromo-*N*-(4-chlorophenyl)acetamide (0.133 g, 0.54 mmol) dropwise. The mixture was then slowly warmed up to room temperature and stirred for overnight. The mixture was poured into Sat. NH₄Cl (30 mL) and stirred vigorously for 3 minutes. The resulting

suspension was extracted with EtOAc (10 mL × 3). The combined organic layers were washed with brine, dried over Na₂SO₄, and concentrated. The crude compound was purified by column chromatography (eluent PET/EtOAc 2:1) to give a white solid (30 mg, 24%). ¹H NMR (400 MHz, Chloroform-*d*) δ 9.21 (s, 1H, H-5), 8.65 (app. d, *J* = 4.9 Hz, 2H, H-1 and H-3), 7.51 – 7.35 (m, 2H, H-6 and H-9), 7.29 (app. d, *J* = 5.4 Hz, 2H, H-7 and H-8), 7.15 (t, *J* = 4.9 Hz, 1H, H-2), 3.93 (s, 2H, H-4). ¹³C NMR (101 MHz, Chloroform-*d*) δ 171.15, 167.10, 157.63, 136.45, 129.27, 129.01, 120.88, 117.57, 35.54. LCMS *m/z* calc. for C₁₂H₁₀ClN₃OS [M]⁺: 279.7, found 279.3 with *t_R* 2.67 min, purity > 95%.



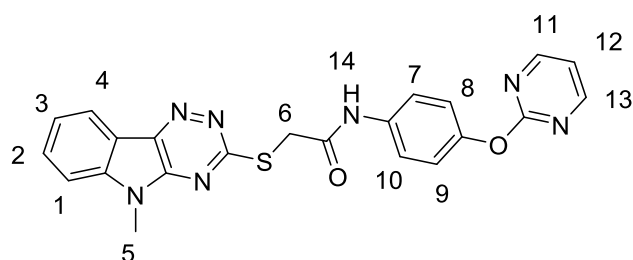
Reaction code: liu195-119

Preparation of *N*-(4-chlorophenyl)-2-((4,6-dimethylpyrimidin-2-yl)thio)acetamide **104.** 4,6-dimethylpyrimidine-2-thiol **102** (0.080 g, 0.57 mmol) was dissolved in 8 mL DCM at 0 °C, Et₃N (0.087 g, 0.86 mmol) was added followed by addition of 2-bromo-*N*-(4-chlorophenyl)acetamide (0.170 g, 0.68 mmol). Reaction was allowed warm up to room temperature and stirred for overnight and monitored by TLC. Solvent was removed under vacuum and the crude product was purified by column chromatography (eluent PET/EtOAc 2:1) to give a white solid (63 mg, 36%). ¹H NMR (400 MHz, Chloroform-*d*) δ 9.56 (s, 1H, H-3), 7.46 – 7.38 (m, 2H, H-4 and H-7), 7.27 (app. d, *J* = 6.7 Hz, 2H, H-5 and H-6), 6.86 (s, 1H, H-1), 3.90 (s, 2H, H-2), 2.51 (app. s, 6H, H-8 and H-9). ¹³C NMR (101 MHz, Chloroform-*d*) δ 167.65, 136.67, 129.02, 120.86, 116.75, 35.49, 23.96. LCMS *m/z* calc. for C₁₄H₁₄ClN₃OS [M+H]⁺: 308.8, found 308.1 with *t_R* 2.83 min, purity > 95%.

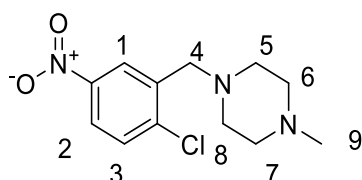


The preparation of *tert*-butyl (4-(pyrimidin-2-yloxy)phenyl)carbamate (75**).** 2-chloropyrimidine (0.45 g, 3.93 mmol), **72** (0.55 g, 2.62 mmol) and K₂CO₃ (0.36 g, 2.62 mmol) was dissolved in NMP (10 mL) and heated at 100 °C under N₂ overnight monitored by TLC. Once the reaction was finished, it was allowed to cool to room

temperature and dilute with water (100 mL). The resulting suspension was then extracted with EtOAc (30 mL \times 3). The combined organic layers were washed with brine (30 mL), dried over Na₂SO₄, and concentrated. The crude compound was purified by column chromatography (eluent PET/EtOAc 2:1) to give a yellow solid (250 mg, 33%). ¹H NMR (400 MHz, DMSO-*d*₆) δ 9.38 (s, 1H, H-8), 8.62 (app. d, *J* = 4.8 Hz, 2H, H-5 and 7), 7.48 (app. d, *J* = 8.4 Hz, 2H, H-1 and 2), 7.24 (t, *J* = 4.7 Hz, 1H, H-6), 7.08 (app. d, *J* = 8.8 Hz, 2H, H-3 and 4), 1.49 (s, 9H, Boc). ¹³C NMR (101 MHz, DMSO-*d*₆) δ 174.24, 160.43, 153.34, 147.86, 137.11, 122.26, 119.71, 117.19, 79.51, 28.60. LCMS *m/z* calc. for C₁₅H₁₇N₃O₃ [M]⁺: 287.3, found 287.7 with *t*_R 2.71 min, purity >95%.



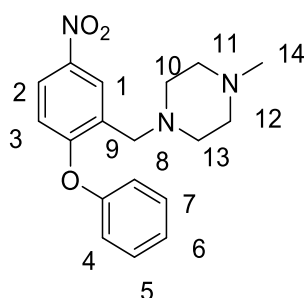
The preparation of target compound 2-((5-Methyl-5H-[1,2,4]triazino[5,6-*b*]indol-3-yl)thio)-*N*-(4-(pyrimidin-2-yloxy)phenyl)acetamide (70). The intermediate **76** was prepared using the similar manner as **74** and used directly for the next step. LCMS *m/z* calc. for C₁₀H₉N₃O [M]⁺: 187.2, found 187.7 with *t*_R 0.33 min. **78** (0.065 g, 0.238 mmol), **35** (0.064 g, 0.238 mmol), HATU (0.135 g, 0.357 mmol), DIPEA (0.165 mL, 0.952 mmol) and DMAP (0.030 g, 0.0238 mmol) were dissolved in NMP (2 mL). Reaction mixture was allowed to stir at room temperature for overnight monitored by TLC. The crude product was purified by column chromatography (eluent PET/EtOAc 1:1) to give a white solid (31 mg, 29%). ¹H NMR (400 MHz, DMSO-*d*₆) δ 10.50 (s, 1H, H-14), 8.63 (app. d, *J* = 4.8 Hz, 2H, H-11 and 13), 8.31 (d, *J* = 7.8 Hz, 1H, H-4), 7.75 (app. d, *J* = 5.2 Hz, 2H, H-1 and 2), 7.67 (app. d, *J* = 8.5 Hz, 2H, H-7 and 10), 7.47 (ddd, *J* = 2.6, 5.8, 8.2 Hz, 1H, H-3), 7.25 (t, *J* = 4.8 Hz, 1H, H-12), 7.16 (app. d, *J* = 8.4 Hz, 2H, H-8 and 9), 4.30 (s, 2H, H-6), 3.79 (s, 3H, H-5). ¹³C NMR (101 MHz, DMSO-*d*₆) δ 167.13, 166.67, 165.37, 160.47, 148.77, 146.53, 142.06, 141.40, 136.67, 131.38, 123.32, 122.46, 121.88, 120.83, 117.73, 117.30, 111.61, 35.96, 27.76. LCMS *m/z* calc. for C₂₂H₁₇N₇O₂S [M+H]⁺: 444.5, found 444.3 with *t*_R 2.62 min, purity >95%.



Reaction code 211-25

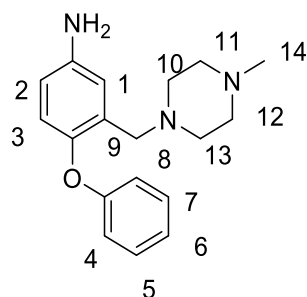
The preparation of 1-(2-chloro-5-nitrobenzyl)-4-methylpiperazine (81). **47b** (1.00 g, 5.40 mmol) and 1-methylpiperazine (0.539 g, 5.40 mmol), HOAc (1 drop) were

dissolved in THF at rt under N₂ and reaction mixture was allowed to stir for overnight, NaHB(OAc)₃ was added then and further stirred for 7 h and monitored by TLC. Once finished, the mixture was poured into Sat. NH₄Cl (50 mL) and stirred vigorously for 3 minutes. The resulting suspension was extracted with EtOAc (10 mL × 3). The combined organic layers were washed with brine, dried over Na₂SO₄, and concentrated. The crude compound was purified by column chromatography (eluent MeOH/EtOAc 1:10) to give a yellow solid (0.732 g, 50.6%). ¹H NMR (400 MHz, Chloroform-*d*) δ 8.38 (d, *J* = 2.8 Hz, 1H, H-1), 8.02 (dd, *J* = 2.8, 8.7 Hz, 1H, H-2), 7.49 (d, *J* = 8.7 Hz, 1H, H-3), 3.65 (s, 2H, H-4), 2.49 (app. s, 8H, H-5~8), 2.33 (s, 3H, H-9). ¹³C NMR (101 MHz, Chloroform-*d*) δ 146.75, 140.74, 138.39, 130.25, 125.05, 122.84, 58.58, 54.95, 52.92, 45.81. LCMS *m/z* calc. for C₁₂H₁₆ClN₃O₂ [M]⁺:269.7, found 269.8 with *t*_R 0.95 min, purity > 95%.



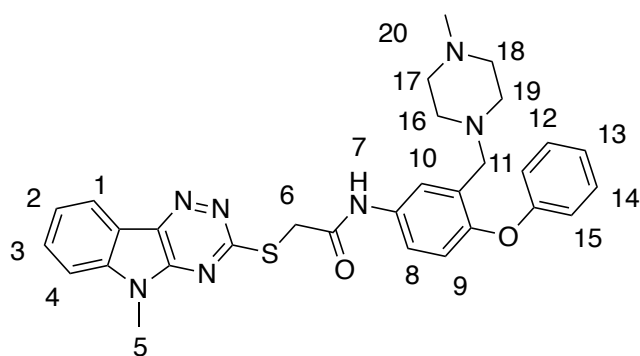
Reaction code Liu211-125

The preparation of 1-methyl-4-(5-nitro-2-phenoxybenzyl)piperazine (82). **81** (0.100 g, 0.37 mmol) and phenol (52 mg, 0.55 mmol) were dissolved in DMF heated to 90 °C under N₂ overnight. The reaction was monitored by TLC. Once finished, the mixture was poured into Sat. NH₄Cl (50 mL) and stirred vigorously for 3 minutes. The resulting suspension was extracted with EtOAc (10 mL × 3). The combined organic layers were washed with brine, dried over Na₂SO₄, and concentrated. The crude compound was purified by column chromatography (eluent EtOAc/MeOH 3:1) to give a yellow oil (23 mg, 10%). ¹H NMR (400 MHz, Chloroform-*d*) δ 8.43 (d, *J* = 2.8 Hz, 1H, H-1), 8.05 (dd, *J* = 9.0, 2.8 Hz, 1H, H-2), 7.43 (app. dd, *J* = 8.5, 7.0 Hz, 2H, H-5 and 7), 7.24 (td, *J* = 7.4, 1.1 Hz, 1H, H-3), 7.09 – 7.00 (m, 2H, H-4 and 8), 6.82 (d, *J* = 9.0 Hz, 1H, H-6), 3.73 (s, 2H, H-9), 2.81- 2.37(m, 8H, H-10~13), 2.34 (s, 3H, H-14). ¹³C NMR (101 MHz, Chloroform-*d*) δ 161.08, 155.33, 142.97, 130.24, 129.81, 126.20, 124.95, 123.95, 119.90, 116.41, 55.43, 55.10, 52.92, 45.93. LCMS *m/z* calc. for C₁₈H₂₁N₃O₃ [M]⁺: 327.4, found 327.8 with *t*_R 2.18 min, purity > 95%.



Reaction code Liu211-145

The preparation of 3-((4-methylpiperazin-1-yl)methyl)-4-phenoxyaniline (83). 82 (0.183 mg, 0.55 mmol) was dissolved in 8 mL EtOH at 55 °C under N₂, NH₄Cl (75 mg, 1.39 mmol) dissolved in 0.11 mL water and Fe (0.16 g, 2.79 mmol) were added and heated to 90 °C overnight.. The reaction was monitored by TLC. Once finished, solvent was removed under vacuum and diluted with water (30 mL). The resulting suspension was extracted with EtOAc (15 mL × 3). The combined organic layers were washed with brine, dried over Na₂SO₄, and concentrated. The crude compound was purified by column chromatography (eluent EtOAc/MeOH 1:1) to give pink solid (158 mg, 93 %). ¹H NMR (400 MHz, Chloroform-*d*) δ 7.30 – 7.23 (m, 2H, H-5 and 7), 7.02 – 6.96 (m, 1H, H-6), 6.87 (app. dd, *J* = 4.1, 2.1 Hz, 2H, H- 4 and 8), 6.84 (dd, *J* = 2.1, 1.0 Hz, 1H, H-1), 6.82 (d, *J* = 8.4 Hz, 1H, H-3), 6.60 (dd, *J* = 8.5, 2.9 Hz, 1H, H-2), 3.59 (app. d, *J* = 18.8 Hz, 2H, NH₂), 3.42 (s, 2H, H-9), 2.45 (app. d, *J* = 31.0 Hz, 8H, H-10~13), 2.27 (s, 3H, H-14). ¹³C NMR (101 MHz, Chloroform-*d*) δ 159.27, 146.20, 143.12, 131.53, 129.44, 122.19, 121.55, 117.08, 116.17, 114.96, 56.19, 55.15, 53.05, 46.06. LCMS *m/z* calc. for C₁₈H₂₃N₃O [M+H]⁺:298.4, found 298.1 with t_R 0.70 min, purity > 95%.



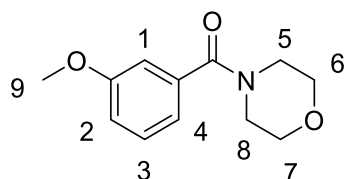
Reaction code Liu211-161

2-((5-Methyl-5H-[1,2,4]triazino[5,6-b]indol-3-yl)thio)-N-(3-((4-methylpiperazin-1-yl)methyl)-4-phenoxyphenyl)acetamide (79). The target compound **79** was prepared from **35** (13 mg, 0.045 mmol) and **83** (13 mg, 0.045 mmol) according to the general procedures. The crude product was purified by column chromatography (eluent MeOH/EtOAc 1:3) to give a yellow solid (13 mg, 54%). ¹H NMR (400 MHz, Chloroform-*d*) δ 9.79 (s, 1H, H-7), 8.48 – 8.40 (m, 1H, H-1), 8.13 – 8.03 (m, 1H, H-8),

7.78 – 7.72 (m, 1H, H-3), 7.61 (d, $J = 2.7$ Hz, 1H, H-10), 7.55 – 7.44 (m, 3H, H-4, 12 and 14), 7.01 (t, $J = 7.4$ Hz, 1H, H-2), 6.88 (d, $J = 8.7$ Hz, 1H, H-9), 6.86 – 6.80 (m, 2H, H-11 and 15), 6.78 – 6.71 (m, 1H, H-13), 3.86 (s, 2H, H-6), 3.24 (s, 3H, H-5), 2.87 – 2.50 (m, 8H, H-16~19), 2.04 (s, 3H, H-20). ^{13}C NMR (101 MHz, DMSO- d_6) δ 167.13, 166.57, 158.46, 149.83, 142.10, 141.44, 136.01, 131.44, 130.34, 123.37, 122.88, 121.89, 121.21, 120.10, 117.74, 117.16, 111.68, 55.50, 54.06, 51.21, 44.20, 35.95, 27.77. LCMS m/z calc. for $\text{C}_{30}\text{H}_{31}\text{N}_7\text{O}_2\text{S}$ $[\text{M}+\text{H}]^+$: 554.7, found 554.2 with t_{R} 2.28 min, purity 95%.

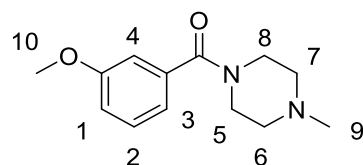
General procedure 8 preparation of phenyl(morpholino)methanones

Benzoic acids (1 equiv), HATU (1.5 equiv), DMAP (0.1 equiv) and amines (1 equiv) was dissolved in 1mL/mmol anhydrous NMP and stirred at room temperature for 5 minutes before addition of DIPEA (6 equiv). The mixture was allowed to stir at room temperature for overnight. The reaction was monitored by TLC and quenched by addition of water. The reaction mixture was stirred for 5 minutes and the diluted with water and was extracted by EtOAc three times and the combined organic layers were combined and washed with Sat. NaHCO_3 and brine and dried over Na_2SO_4 . The crude product was purified by column chromatography.



Reaction code: Liu211-137

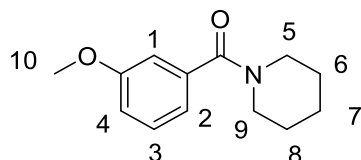
(3-Methoxyphenyl)(morpholino)methanone (119a) was prepared according to general procedure 8 using 3-methoxybenzoic acid **128** (0.10 g, 0.66 mmol) and morpholine (0.066 g, 0.79 mmol). The crude product was purified by column chromatography (eluent PET/EtOAc 4:1) to give a clear colorless oil (0.16 g, 55%). ^1H NMR (400 MHz, Chloroform- d) δ 7.35 – 7.28 (m, 1H, H-1), 7.04 – 6.90 (m, 3H, H-2, 3 and 4), 3.82 (s, 3H, H-9), 3.81 – 3.26 (m, 8H, H-5~8). ^{13}C NMR (101 MHz, Chloroform- d) δ 170.19, 159.73, 136.64, 129.69, 119.08, 115.66, 112.53, 66.92, 55.38, 38.62. LCMS m/z calc. for $\text{C}_{12}\text{H}_{15}\text{N}_3\text{O}$ $[\text{M}]^+$: 222.3, found 221.8 with t_{R} 2.29 min, purity > 95%.



Reaction code: Liu211-139

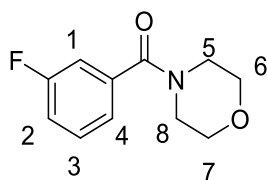
(3-Methoxyphenyl)(4-methylpiperazin-1-yl)methanone (119b) was prepared according to general procedure 8 using 3-methoxybenzoic acid (**128**) (0.10 g, 0.66

mmol) and 1-methylpiperazine (0.79 g, 0.79 mmol). The crude product was purified by column chromatography (eluent PET/EtOAc 4:1) to give a brown oil (0.079 g, 52%). ^1H NMR (400 MHz, Chloroform-*d*) δ 7.37 – 7.27 (m, 1H, H-1), 7.01 – 6.93 (m, 3H, H-2, 3, 4), 3.84 (s, 3H, H-10), 3.85-3.76 (m, 2H, H-8 and 5), 3.45 (m, 2H, H-8 and 5), 2.56-2.43 (m, 2H, H-6 and 7), 2.43-2.34 (m, 2H, H-6 and 7), 2.34 (s, 3H, H-9). ^{13}C NMR (101 MHz, Chloroform-*d*) δ 170.06, 159.65, 137.13, 129.59, 119.08, 115.51, 112.41, 55.37, 46.05. LCMS *m/z* calc. for $\text{C}_{13}\text{H}_{18}\text{N}_2\text{O}_2$ $[\text{M}+\text{H}]^+$: 235.3, found 235.0 with t_{R} 0.32 min, purity > 95%.



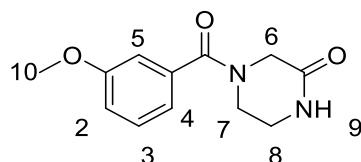
Reaction code: Liu211-147

(3-Methoxyphenyl)(piperidin-1-yl)methanone (119c) was prepared according to general procedure **8** using 3-methoxybenzoic acid (**128**) (0.10 g, 0.66 mmol) and piperidine (0.79 g, 0.79 mmol). The crude product was purified by column chromatography (eluent PET/EtOAc 3:1) to give a colorless oil (0.10 g, 69%). ^1H NMR (400 MHz, Chloroform-*d*) δ 7.41 – 7.23 (m, 1H, H-1), 7.06 – 6.86 (m, 3H, H-2, 4, 3), 3.83 (s, 3H, H-10), 3.71 (app. s, 2H, H-5 and 9), 3.35 (app. s, 2H, H-5 and 9), 1.92 – 1.43 (m, 6H, H-6, 7 and 8). ^{13}C NMR (101 MHz, Chloroform-*d*) δ 170.03, 159.59, 137.84, 129.51, 118.85, 115.23, 112.14, 55.34, 24.60. LCMS *m/z* calc. for $\text{C}_{13}\text{H}_{17}\text{NO}_2$ $[\text{M}]^+$: 219.3, found 219.7 with t_{R} 2.64 min, purity > 95%.

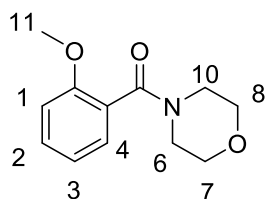


Reaction code: Liu211-159

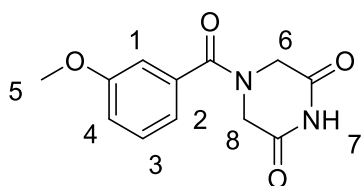
(3-Fluorophenyl)(morpholino)methanone (116) was prepared according to general procedure **8** using **132** (0.20 g, 1.43 mmol) and morpholine (0.15 g, 1.71 mmol). The crude product was purified by column chromatography (eluent PET/EtOAc 3:1) to give a yellow oily product (0.29 g, 98%). ^1H NMR (400 MHz, Chloroform-*d*) δ 7.48 – 7.34 (m, 1H, H-2), 7.19 (dt, $J = 1.3, 7.6$ Hz, 1H, H-1), 7.13 (app. ddd, $J = 2.6, 4.9, 8.8$ Hz, 2H, H-3 and 4), 3.60 (m, 8H, H-5, 6, 7 and 8). ^{13}C NMR (101 MHz, Chloroform-*d*) δ 168.92 (d, $J = 2.4$ Hz), 162.57 (d, $J = 248.4$ Hz, $^1\text{J}_{\text{CF}}$), 137.37 (d, $J = 6.9$ Hz), 130.43 (d, $J = 8.0$ Hz, $^3\text{J}_{\text{CF}}$), 122.73 (d, $J = 3.2$ Hz), 116.94 (d, $J = 21.1$ Hz, $^2\text{J}_{\text{CF}}$), 114.42 (d, $J = 22.8$ Hz, $^2\text{J}_{\text{CF}}$), 66.83. LCMS *m/z* calc. $\text{C}_{11}\text{H}_{12}\text{FNO}_2$ $[\text{M}+\text{H}]^+$: 210.3, found 210.0 with t_{R} 2.27 min, purity > 95%.

**Reaction code: Liu211-165**

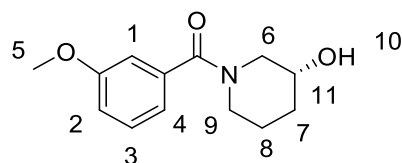
4-(3-Methoxybenzoyl)piperazin-2-one (119f) was prepared according to general procedure **8** using 3-methoxybenzoic acid (**128**) (0.10 g, 0.66 mmol) and piperazin-2-one (0.079 g, 0.79 mmol). The crude product was purified by column chromatography (eluent MeOH/DCM 1:10) to give a white solid (0.077 g, 50%). ¹H NMR (400 MHz, DMSO-*d*₆) δ 8.13 (s, 1H, H-9), 7.38 (dd, *J* = 7.6, 8.7 Hz, 1H, H-4), 7.09 – 7.02 (m, 1H, H-2), 6.99 (app. dt, *J* = 1.6, 7.1 Hz, 2H, H-3 and 5), 4.07 (s, 1H, H-6), 3.90 (s, 1H, H-6), 3.79 (s, 3H, H-10), 3.79-3.64 (broad, 1H, H-7), 3.61-3.37 (s, 1H, H-7), 3.23 (s, 2H, H-8). ¹³C NMR (101 MHz, DMSO-*d*₆) δ 169.18, 166.41, 159.62, 137.23, 130.21, 119.37, 116.02, 112.74, 55.72, 46.20, 44.32. LCMS *m/z* calc. C₁₂H₁₄N₂O₃ [M]⁺: 234.3, found 234.9 with *t*_R 1.96 min, purity > 95%.

**Reaction code: Liu211-169**

(2-Methoxyphenyl)(morpholino)methanone (127) was prepared according to general procedure **8** using 2-methoxybenzoic acid (**129**) (0.20 g, 1.32 mmol) and morpholine (0.137 g, 1.58 mmol). The crude product was purified by column chromatography (eluent EA/PET 1:1) to give a yellow oil (0.319 g, 92%). ¹H NMR (400 MHz, Methanol-*d*₄) δ 7.42 (ddd, *J* = 1.7, 7.4, 8.4 Hz, 1H, H-2), 7.23 (dd, *J* = 1.8, 7.5 Hz, 1H, H-4), 7.07 (dd, *J* = 0.9, 8.4 Hz, 1H, H-1), 7.02 (td, *J* = 0.9, 7.5 Hz, 1H, H-3), 3.85 (s, 3H, H-11), 3.82 – 3.68 (m, 4H, H-6 and 10), 3.67 – 3.53 (m, 2H, H-7 and 8), 3.37 – 3.14 (m, 2H, H-7 and 8). ¹³C NMR (101 MHz, Methanol-*d*₄) δ 168.79, 155.39, 130.94, 127.65, 124.62, 120.70, 111.01, 66.43, 54.81, 42.10. LCMS *m/z* calc. C₁₂H₁₅NO₃ [M]⁺: 221.3, found 221.9 with *t*_R 2.22 min, purity > 95%.

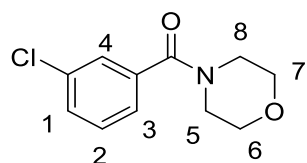
**Reaction code: Liu211-237**

4-(3-Methoxybenzoyl)piperazine-2,6-dione (119g) was prepared according to general procedure **8** using 3-methoxybenzoic acid (**128**) (0.20 g, 1.32 mmol) and piperazine-2,6-dione (0.150 g, 1.2 mmol). The crude product was purified by column chromatography (eluent MeOH/DCM 1:10) to give a yellow solid (156 mg, 48%). ¹H NMR (400 MHz, DMSO-*d*₆) δ 11.45 (s, 1H, H-7), 7.40 (t, *J* = 8.1 Hz, 1H, H-2), 7.09 (ddd, *J* = 1.1, 2.5, 8.3 Hz, 1H, H-3), 7.03 – 6.98 (m, 2H, H-4 and 1), 3.79 (s, 3H, H-5). ¹³C NMR (101 MHz, DMSO-*d*₆) δ 169.49, 165.06, 159.65, 135.92, 130.33, 119.69, 116.66, 113.08, 55.76. LCMS *m/z* calc. C₁₂H₁₂N₂O₄ [M+H]⁺: 249.2, found 249.0 with *t*_R 2.15min, purity > 95%.



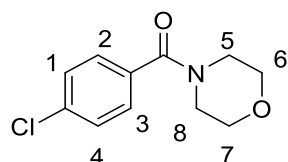
Reaction code: **Liu211-239**

(R)-(3-hydroxypiperidin-1-yl)(3-methoxyphenyl)methanone (119e) was prepared according to general procedure **8** using 3-methoxybenzoic acid (**128**) (0.20 g, 1.32 mmol) and (*R*)-piperidin-3-ol (0.18 g, 1.32 mmol). The crude product was purified by column chromatography (eluent EA/PET 1:1) to give a white solid (0.297 g, 97%). ¹H NMR (400 MHz, Chloroform-*d*) δ 7.32 (dd, *J* = 8.9, 7.3 Hz, 1H, H-3), 7.08 – 6.87 (m, 3H, H-2, 3, 4), 3.83 (s, 3H, H-5), 4.41-3.05 (m, 4H, H-6 and 9), 2.61 (s, 1H, H-11), 2.22 – 1.75 (m, 2H, H-7), 1.73 – 1.38 (m, 2H, H-8). ¹³C NMR (101 MHz, Methanol-*d*₄) δ 171.35, 159.83, 137.08, 129.51, 118.50 (d, *J* = 32.9 Hz), 115.12, 112.18, 65.56 (d, *J* = 21.5 Hz), 54.53, 53.94, 42.18, 32.05, 22.87. LCMS *m/z* calc. C₁₃H₁₈NO₃[M]⁺: 235.3, found 235.9 with *t*_R 2.24 min, purity > 95%.

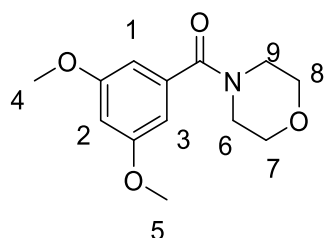


Reaction code: **Liu211-247**

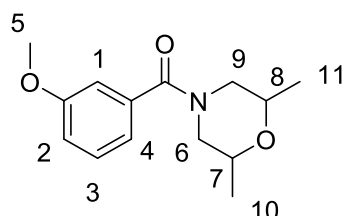
(3-Chlorophenyl)(morpholino)methanone (115) was prepared according to general procedure **8** using 3-chlorobenzoic acid (**130**) (0.10 g, 0.64 mmol) and morpholine (0.057 g, 0.64 mmol). The crude product was purified by column chromatography (eluent EA/PET 1:1) to give a white solid (0.082 g, 53%). ¹H NMR (400 MHz, Chloroform-*d*) δ 7.45 – 7.34 (m, 3H, H-1, 3 and 4), 7.29 (dt, *J* = 1.3, 7.4 Hz, 1H, H-2), 3.61 (m, 8H, H- 5, 6, 7 and 8). ¹³C NMR (101 MHz, Chloroform-*d*) δ 168.84, 137.05, 134.72, 130.05, 129.98, 127.31, 125.17, 66.84. LCMS *m/z* calc. C₁₁H₁₁ClNO₂ [M]⁺: 225.7, found 225.7 with *t*_R 2.44 min, purity > 95%.

**Reaction code: Liu211-249**

(4-Chlorophenyl)(morpholino)methanone (116) was prepared according to general procedure **8** using 4-chlorobenzoic acid (**130**) (0.10 g, 0.64 mmol) and morpholine (0.057 g, 0.64 mmol). The crude product was purified by column chromatography (eluent EA/PET 1:1) to give a white solid (0.072 g, 47%). ^1H NMR (400 MHz, $\text{DMSO-}d_6$) δ 7.57 – 7.49 (m, 2H, H-2 and 3), 7.49 – 7.34 (m, 2H, H-1 and 4), 3.45 (m, 8H, H-5, 6, 7, and 8). ^{13}C NMR (101 MHz, $\text{DMSO-}d_6$) δ 168.48, 134.84, 134.74, 129.53, 129.00, 66.49. LCMS m/z calc. $\text{C}_{11}\text{H}_{13}\text{ClNO}_2$ $[\text{M}]^+$: 225.7, found 225.9 with t_{R} 2.46 min, purity > 95%.

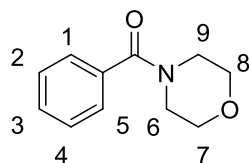
**Reaction code: Liu211-251**

(3,5-dimethoxyphenyl)(morpholino)methanone (125) was prepared according to general procedure **8** using 3,5-dimethoxybenzoic acid (**134**) (0.10 g, 0.55 mmol) and morpholine (0.047 g, 0.55 mmol). The crude product was purified by column chromatography (eluent EA/PET 1:1) to give a white foaming compound (0.256 g, 53%). ^1H NMR (400 MHz, $\text{DMSO-}d_6$) δ 6.56 (t, $J = 2.3$ Hz, 1H, H-2), 6.51 (app. d, $J = 2.3$ Hz, 2H, H-1 and 3), 3.77 (app. s, 6H, H-4 and 5), 3.58 (s broad, 4H, H-6 and 9), 2.51 (app. p, $J = 1.8$ Hz, 4H, H-7 and 8). ^{13}C NMR (101 MHz, $\text{DMSO-}d_6$) δ 169.02, 160.89, 138.18, 105.16, 101.59, 55.86, 55.38, 38.72. LCMS m/z calc. $\text{C}_{13}\text{H}_{17}\text{NO}_4$ $[\text{M}]^+$: 251.3, found 251.9 with t_{R} 2.37 min, purity > 95%.

**Reaction code: Liu225-261/273/211-275**

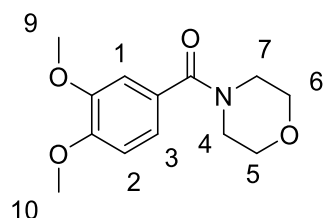
(2,6-dimethylmorpholino)(3-methoxyphenyl)methanone (119d) was prepared according to general procedure **8** using 3-methoxybenzoic acid (**128**) (0.30 g, 1.97

mmol) and morpholine (0.227 g, 1.97 mmol). The crude product was purified by column chromatography (eluent EA/PET 4:1) to give a colorless oil (0.092 g, 19 %). ^1H NMR (400 MHz, Chloroform-*d*) δ 7.30 (td, $J = 1.0, 8.0$ Hz, 1H, H-4), 7.02 – 6.87 (m, 3H, H-1, 2 and 3), 4.65 – 4.43 (m, 1H, H-6), 3.81 (d, $J = 0.9$ Hz, 3H, H-5), 3.71 – 3.57 (m, 1H, H-7), 3.70 – 3.38 (m, 2H, H-6 and 9), 2.77 (s, 1H, H-8), 2.52 (m, 2H, H-6 and 9), 1.34 – 1.15 (m, 3H, H-10), 1.08 (s, 3H, H-11). ^{13}C NMR (101 MHz, CDCl_3) δ 169.83, 159.69, 136.88, 129.66, 119.06, 118.75, 115.57, 115.51, 112.51, 71.95, 55.34, 53.22, 47.50, 18.67. LCMS m/z calc. $\text{C}_{14}\text{H}_{19}\text{NO}_4$ $[\text{M}+\text{H}]^+$: 250.3, found 250.1 with t_{R} 2.53 min, purity > 95%.



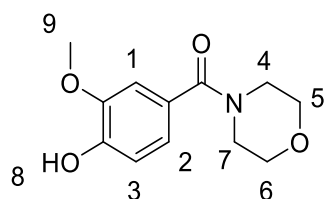
Reaction code: Liu211-273

morpholino(phenyl)methanone (113) was prepared according to general procedure **8** using benzoic acid (**136**) (0.20 g, 1.39 mmol) and morpholine (0.121 g, 1.39 mmol). The crude product was purified by column chromatography (eluent EA/PET 2:1) to give a colorless oil (0.296 g, >100%). ^1H NMR (400 MHz, $\text{DMSO}-d_6$) δ 7.54 – 7.28 (m, 5H, H-1, 2, 3, 4 and 5), 3.76– 3.47 (s, broad, 6H, H-6, 9, 7 and 8), 3.43 (s broad, 2H, H-7 and 8). ^{13}C NMR (101 MHz, $\text{DMSO}-d_6$) δ 169.54, 136.07, 130.05, 128.90, 127.46, 66.55, 38.71. LCMS m/z calc. $\text{C}_{11}\text{H}_{13}\text{NO}_2$ $[\text{M}]^+$: 191.3 found 191.2 with t_{R} 1.95 min, purity > 95%.

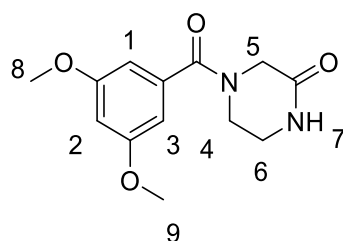


Reaction code: Liu225-13

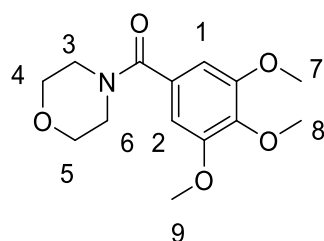
(3,4-dimethoxyphenyl)(morpholino)methanone (124) was prepared according to general procedure **8** using 3,4-dimethoxybenzoic acid (**133**) (0.10 g, 0.55 mmol) and morpholine (0.048g, 0.55 mmol). The crude product was purified by column chromatography (eluent EA/PET 1:1) to give a white solid (0.121 g, 88%). ^1H NMR (400 MHz, $\text{DMSO}-d_6$) δ 7.21 – 6.78 (m, 3H, H-1, 2 and 3), 3.79 (s, 3H, H-10), 3.78 (s, 3H, H-9), 3.60 (app. d, $J = 9.7$ Hz, 8H, H-4, 5, 6, and 7). ^{13}C NMR (101 MHz, $\text{DMSO}-d_6$) δ 169.47, 150.33, 148.91, 128.10, 120.49, 111.60, 111.52, 66.58, 56.03. LCMS m/z calc. $\text{C}_{13}\text{H}_{17}\text{NO}_4$ $[\text{M}]^+$: 251.3, found 251.7 with t_{R} 2.16 min, purity > 95%.

**Reaction code: Liu225-15**

(4-hydroxy-3-methoxyphenyl)(morpholino)methanone (123) was prepared according to general procedure **8** using 4-hydroxy-3-methoxybenzoic acid (0.10 g, 0.59 mmol) and morpholine (0.052g, 0.59 mmol). The crude product was purified by column chromatography (eluent EA/PET 1:1) to give a white solid (0.121 g, 86%). ¹H NMR (400 MHz, DMSO-*d*₆) δ 9.43 (s, 1H, H-8), 6.97 (d, *J* = 1.9 Hz, 1H, H-1), 6.86 (dd, *J* = 1.9, 8.1 Hz, 1H, H-2), 6.80 (d, *J* = 8.0 Hz, 1H, H-3), 3.79 (s, 3H, H-9), 3.59 (app. t, *J* = 4.8 Hz, 4H, H-4 and 7), 3.50 (app. d, *J* = 4.7 Hz, 4H, H-5 and 6). ¹³C NMR (101 MHz, DMSO-*d*₆) δ 169.72, 148.55, 147.75, 126.56, 120.97, 115.34, 112.22, 66.61, 56.12. LCMS *m/z* calc. C₁₂H₁₅NO₄ [M]⁺: 237.3 found 237.7 with *t*_R 1.95 min, purity > 95%.

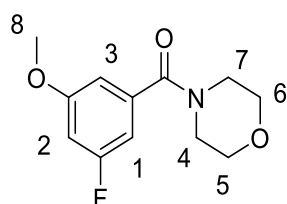
**Reaction code: Liu225-17**

4-(3,5-dimethoxybenzoyl)piperazin-2-one was prepared according to general procedure **8** using 3,5-dimethoxybenzoic acid (**134**) (0.10 g, 0.66 mmol) and piperazin-2-one (0.066g, 0.65 mmol). The crude product was purified by column chromatography (eluent MeOH/DCM 1:10) to give a white solid (0.127 g, 88%). ¹H NMR (400 MHz, DMSO-*d*₆) δ 8.10 (s, 1H, H-7), 6.56 (t, *J* = 2.3 Hz, 1H, H-2), 6.53 (app. d, *J* = 2.3 Hz, 2H, H-1 and 3), 4.04 (s broad, 2H, H-5), 3.75 (app. s, 6H, H-8, 9), 3.54–3.37 (m, 2H, H-4), 3.28 (s broad, 2H, H-6). ¹³C NMR (101 MHz, DMSO-*d*₆) δ 169.02, 166.49, 160.92, 138.00, 105.12, 101.93, 55.89, 46.42, 44.23. LCMS *m/z* calc. C₁₂H₁₆N₂O₄ [M+H]⁺: 265.3 found 265.0 with *t*_R 2.15 min, purity > 95%.

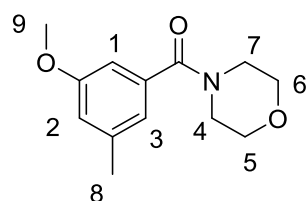


Reaction code: Liu225-21

morpholino(3,4,5-trimethoxyphenyl)methanone (126) was prepared according to general procedure **8** using 3,4,5-trimethoxybenzoic acid (**135**) (0.10 g, 0.47 mmol) and morpholine (0.049, 0.56 mmol). The crude product was purified by column chromatography (eluent MeOH/DCM 1:20) to give a white solid (0.156 g, 90%). ¹H NMR (400 MHz, Chloroform-*d*) δ 6.70 – 6.56 (m, 2H, H-1 and 2), 3.90 – 3.85 (m, 9H, H-7, 8 and 9), 3.71 (app. s, 8H, H-3, 4, 5 and 6). ¹³C NMR (101 MHz, Chloroform-*d*) δ 170.19, 153.39, 139.36, 130.66, 104.40, 66.91, 60.90, 56.28. LCMS *m/z* calc. C₁₄H₁₉NO₅ [M+H]⁺: 282.3 found 281.9 with *t_R* 2.24 min, purity > 95%.

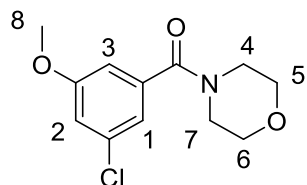
**Reaction code: Liu225-23**

(3-fluoro-5-methoxyphenyl)(morpholino)methanone (120) was prepared according to general procedure **8** using 3-fluoro-5-methoxybenzoic acid (0.10 g, 0.59 mmol) and morpholine (0.061 g, 0.71 mmol). The crude product was purified by column chromatography (eluent MeOH/DCM 1:20) to give a white solid (0.156 g, 90%). ¹H NMR (400 MHz, Chloroform-*d*) δ 6.75 (t, *J* = 1.8 Hz, 1H, H-3), 6.73 – 6.65 (m, 2H, H- 2 and 1), 3.84 (s, 3H, H-8), 3.83 – 3.29 (m, 8H, H- 4, 5, 6 and 7). ¹³C NMR (101 MHz, DMSO-*d*₆) δ 167.92, 164.38, 161.95, 161.22, 138.87, 109.40, 106.27 (d, *J* = 23.2 Hz, ²*J*_{CF}), 102.98 (d, *J* = 25.0 Hz, ²*J*_{CF}), 66.42, 56.31. LCMS *m/z* calc. C₁₂H₁₄FNO₃ [M]⁺: 239.3 found 239.7 with *t_R* 2.39 min, purity > 95%.

**Reaction code: Liu225-33**

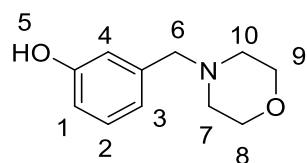
(3-methoxy-5-methylphenyl)(morpholino)methanone (122) was prepared according to general procedure **8** using 3-methoxy-5-methylbenzoic acid (0.10 g, 0.59 mmol) and morpholine (0.062 g, 0.71 mmol). The crude product was purified by column chromatography (eluent MeOH/DCM 1:20) to give a white solid (0.108 g, 77%). ¹H NMR (400 MHz, Chloroform-*d*) δ 6.79 – 6.73 (m, 2H, H-1 and 3), 6.71 (t, *J* = 2.0 Hz, 1H, H-2), 3.79 (s, 3H, H-9), 3.78 – 3.30 (m, 8H, H- 4, 5, 6 and 7), 2.33 (s, 3H, H-8). ¹³C NMR (101 MHz, Chloroform-*d*) δ 170.36, 159.64, 140.06, 136.47, 119.87,

116.25, 109.48, 66.93, 55.34, 21.51. LCMS m/z calc. $C_{13}H_{17}NO_3$ $[M]^+$: 235.3 found 235.9 with t_R 2.42 min, purity > 95%.



Reaction code: Liu225-49

Preparation of (3-chloro-5-methoxyphenyl)(morpholino)methanone (121). 3-chloro-5-methoxybenzoic acid (0.200 g, 1.072 mmol) was dissolved in PhMe in the presence of catalytic amount of DMF (0.01 equiv.) followed by addition of $SOCl_2$ (0.255 g, 2.14 mmol) under N_2 . The reaction mixture was allowed to heat up to $70^\circ C$ for 2 hours. The reaction was monitored by TLC and once the reaction finished, solvent was removed under vacuum and the crude product was used directly without further purification. The crude product was diluted with dry DCM and morpholine (0.279 g, 3.22 mmol) was added at room temperature. The mixture was allowed to stir at room temperature for overnight. The reaction was monitored by TLC and quenched by addition of water. The reaction mixture was stirred for 5 minutes and diluted with water and was extracted by EtOAc three times and the combined organic layers were combined and washed with brine and dried over Na_2SO_4 . The crude product was purified by column chromatography (eluent MeOH/DCM 1:30) to give a white solid (0.073 g, 27%). 1H NMR (400 MHz, Chloroform- d) δ 6.98 – 6.91 (m, 2H, H-1 and 3), 6.85 – 6.78 (m, 1H, H-2), 3.81 (s, 3H, H-8), 3.80 – 3.32 (m, 8H, H-4, 5, 6 and 7). ^{13}C NMR (101 MHz, Chloroform- d) δ 168.67, 160.45, 137.69, 135.28, 119.16, 115.69, 111.32, 66.80, 55.70. LCMS m/z calc. $C_{12}H_{14}ClNO_3$ $[M+H]^+$: 256.7 found 257.9 with t_R 2.52 min, purity > 95%.

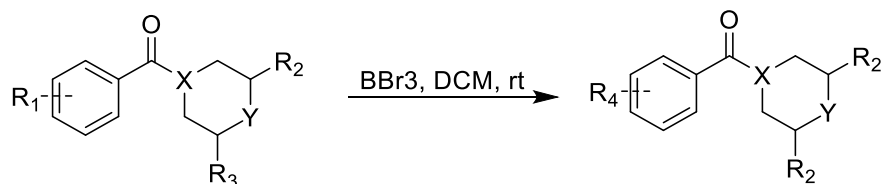


Reaction code: Liu211-141

Preparation of 3-(morpholinomethyl)phenol (141). Benzaldehyde **142** (0.10 g, 0.82 mmol), morpholine (0.071, 0.82 mmol) and HOAc (cat. 0.01 equiv) were dissolved in THF under N_2 and stirred at rt for 8 h followed by addition of $NaBH(OAc)_3$ (0.87 g, 4.1 mmol). The reaction mixture was allowed to stir at room temperature for overnight. The reaction was monitored by TLC and quenched by addition of Sat. $NaHCO_3$. The reaction mixture was stirred for 5 minutes and diluted with water and was extracted by EtOAc three times and the combined organic layers were combined and washed with brine and dried over Na_2SO_4 . The crude product was purified by column

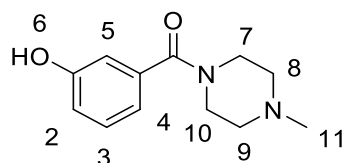
chromatography (eluent MeOH/DCM 1:10) to give a yellow solid (0.098 g, 62%). ^1H NMR (400 MHz, DMSO- d_6) δ 9.28 (s, 1H, H-5), 7.09 (t, J = 7.8 Hz, 1H, H-2), 6.77 – 6.67 (m, 2H, H-3 and 4), 6.67 – 6.58 (m, 1H, H-1), 3.56 (app. t, J = 4.6 Hz, 4H, H-8 and 9), 3.36 (s, 2H, H-6), 2.32 (app. t, J = 4.6 Hz, 4H, H-7 and 10). ^{13}C NMR (101 MHz, DMSO- d_6) δ 157.75, 129.54, 119.92, 116.05, 114.39, 66.68, 62.96, 53.67. LCMS m/z calc. $\text{C}_{11}\text{H}_{15}\text{NO}_2$ $[\text{M}]^+$: 221.3 found 221.8 with t_{R} 2.29 min, purity > 95%.

Preparation of (3-hydroxyphenyl)(4-methylpiperazin-1-yl)methanones 114, 118a-c



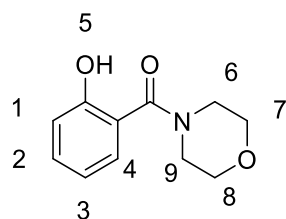
General procedure 9

Methoxyphenylmethanones (1 equiv) was dissolved in DCM followed by addition of excessive amount of BBr_3 at 0°C under inert gas. The reaction mixture was then slowly warm up to room temperature. The reaction was monitored by TLC and quenched by addition of water. The reaction mixture was stirred for 5 minutes and the diluted with water and was extracted by EtOAc three times and the combined organic layers were combined and dried over Na_2SO_4 . The crude product was purified by column chromatography.



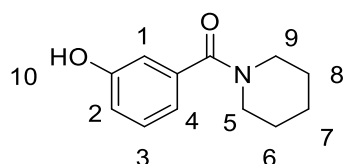
Reaction code: Reaction code 211-143

(3-hydroxyphenyl)(4-methylpiperazin-1-yl)methanone (118b) was prepared according to general procedure 9 using **119b** (0.068 g, 0.4 mmol) and BBr_3 (4 mmol). The crude product was purified by column chromatography (eluent MeOH/DCM 1:10) to give white solid (10.2 mg, 16%). ^1H NMR (400 MHz, Chloroform- d) δ 7.18 (t, J = 7.8 Hz, 1H, H-3), 6.87 (dd, J = 1.5, 2.5 Hz, 1H, H-5), 6.85 – 6.78 (m, 2H, H-2 and 4), 3.81 (m, 2H, H-7 and 10), 3.46 (m, 2H, H-7 and 10), 2.52 (m, 2H, H-8 and 9), 2.33 (m, 5H, H-8 and 9, H-11). ^{13}C NMR (101 MHz, Chloroform- d) δ 170.75, 157.12, 136.15, 129.71, 117.95, 117.55, 114.51, 45.81. LCMS m/z calc. $\text{C}_{12}\text{H}_{16}\text{N}_2\text{O}_2$ $[\text{M}]^+$: 220.3, found 220.8 with t_{R} 0.32 min, purity > 95%.



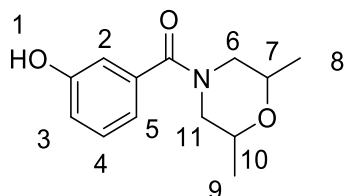
Reaction code: Liu211-231 and 225-267

(2-hydroxyphenyl)(morpholino)methanone (114) was prepared according to general procedure **9** using **127** (0.075 g, 0.34 mmol) and BBr_3 (5 mmol). The crude product was purified by column chromatography (eluent EA/PET 1:1) to give white solid (22 mg, 31%). ^1H NMR (400 MHz, Methanol- d_4) δ 7.45 – 7.14 (m, 2H, H-2 and 4), 7.03 – 6.73 (m, 2H, H-1 and 3), 3.71 (app. s, 8H, H-6~9). ^{13}C NMR (101 MHz, Methanol- d_4) δ 169.39, 167.52, 153.50, 133.35, 130.73, 130.49, 127.90, 122.67, 119.39, 117.32, 115.33, 66.43. LCMS m/z calc. $\text{C}_{11}\text{H}_{13}\text{NO}_3$ $[\text{M}]^+$: 208.2, found 208.1 with t_{R} 0.79 min, purity > 95%.



Reaction code: Liu211-235

(3-hydroxyphenyl)(piperidin-1-yl)methanone (118c) was prepared according to general procedure **9** using **119c** (0.05 g, 0.22 mmol) and BBr_3 (0.5 mmol). The crude product was purified by column chromatography (eluent EA/PET 1:2) to give white solid (39 mg, 84%). ^1H NMR (400 MHz, $\text{DMSO}-d_6$) δ 9.64 (s, 1H, H-10), 7.22 (t, J = 7.8 Hz, 1H, H-3), 6.87 – 6.78 (m, 1H, H-2), 6.78 – 6.69 (m, 2H, H1 and 4), 3.70 – 3.38 (m, 2H, H-5 and 9), 3.27 (s, 2H, H-5 and 9), 1.61 (app. dp, J = 3.0, 3.9, 6.7 Hz, 2H, H-6 and 8), 1.50 (d, J = 25.3 Hz, 4H, H-6 and 7 and 8). ^{13}C NMR (101 MHz, $\text{DMSO}-d_6$) δ 169.22, 157.71, 138.28, 129.97, 117.41, 116.56, 113.79, 24.53. LCMS m/z calc. $\text{C}_{11}\text{H}_{15}\text{NO}_2$ $[\text{M}+\text{H}]^+$: 206.2, found 207.0 with t_{R} 2.37 min, purity > 95%.

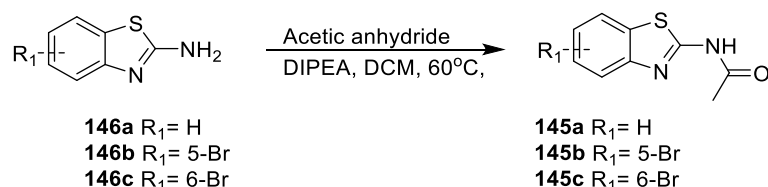


Reaction code: Liu 247-11

(2,6-dimethylmorpholino)(3-hydroxyphenyl)methanone (118d) was prepared according to general procedure **9** using **119d** (0.106 g, 0.43 mmol) and BBr_3 (2.12 mmol). The crude product was purified by column chromatography (eluent EA/PET

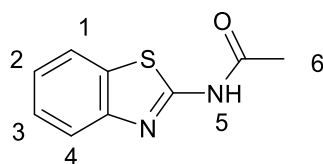
1:2) to give white solid (58 mg, 57%). ^1H NMR (400 MHz, $\text{DMSO-}d_6$) δ 9.68 (s, 1H, H-1), 7.23 (t, $J = 7.8$ Hz, 1H, H-4), 6.93 – 6.71 (m, 3H, H-3, 2, 5), 4.34 (s, 1H, H-7), 3.53 (app. d, $J = 6.5$ Hz, 3H, H-10 and 6, 11), 2.95 – 2.58 (m, 1H, H-6), 2.45 (s, 1H, H-11), 1.45 – 0.70 (m, 6H, H-8 and 9). ^{13}C NMR (101 MHz, $\text{DMSO-}d_6$) δ 169.16, 157.77, 137.43, 130.04, 117.83, 116.97, 114.23, 71.67, 52.96, 47.31, 18.96. LCMS m/z calc. $\text{C}_{13}\text{H}_{17}\text{NO}_3$ $[\text{M}]^+$: 235.3, found 235.9 with t_{R} 2.30 min, purity > 95%.

Preparation of *N*-(benzo[*d*]thiazol-2-yl)acetamides (**145a-c**)



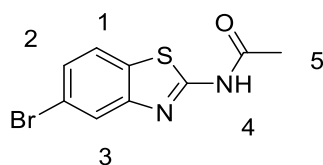
General procedure 10

benzo[*d*]thiazol-2-amines (**146a-c**) (1 equiv.) was dissolved in DCM followed by addition of acetic anhydride (1.1 equiv.) and the mixture was allowed to heat up to 40~60 °C under N_2 . The reaction was monitored by TLC and the crude product was purified by column chromatography.



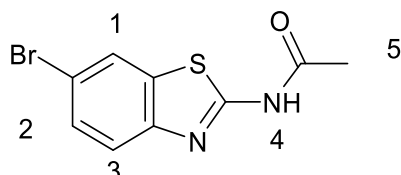
Reaction code: Liu225-135

***N*-(benzo[*d*]thiazol-2-yl)acetamide (**145a**)** was prepared according to general procedure **10** using **146a** (0.10 g, 0.4 mmol) and acetic anhydride (0.5 g, 0.5 mmol). The crude product was purified by column chromatography (eluent EA/PET 1:2) to give a white solid (0.108 g, 80%). ^1H NMR (400 MHz, $\text{DMSO-}d_6$) δ 12.17 (broad, 1H, H-5), 7.95 (d, $J = 7.9$ Hz, 1H, H-4), 7.73 (d, $J = 8.1$ Hz, 1H, H-1), 7.42 (td, $J = 1.4, 7.2, 7.8$ Hz, 1H, H-3), 7.29 (t, $J = 7.5$ Hz, 1H, H-2), 2.20 (s, 3H, H-6). ^{13}C NMR (101 MHz, $\text{DMSO-}d_6$) δ 172.47, 169.86, 167.47, 158.40, 148.99, 131.88, 126.51, 123.90, 122.12, 120.94, 23.24. LCMS m/z calc. $\text{C}_9\text{H}_8\text{N}_2\text{OS}$ $[\text{M}]^+$: 192.4 found 192.8 with t_{R} 2.18 min, purity > 95%.



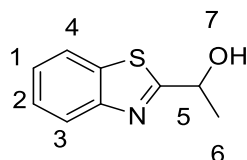
Reaction code: Liu225-137

***N*-(5-bromobenzo[*d*]thiazol-2-yl)acetamide (145b)** was prepared according to general procedure **10** using **146b** (0.20 g, 0.87 mmol) and acetic anhydride (0.174 g, 1.74 mmol). The crude product was purified by column chromatography (eluent EA/PET 1:2) to give a white solid (0.199 g, 84%). ¹H NMR (400 MHz, DMSO-*d*₆) δ 12.47 (s, 1H, H-4), 8.18 – 7.83 (m, 2H, H-1 and 3), 7.44 (dd, *J* = 2.0, 8.4 Hz, 1H, H-2), 2.20 (s, 3H, H-5). ¹³C NMR (101 MHz, DMSO-*d*₆) δ 170.12, 160.12, 150.55, 131.15, 126.52, 124.03, 123.31, 119.28, 23.24. LCMS *m/z* calc. C₉H₆BrN₂OS [M]⁺: 270.3 found 270.0 with *t*_R 2.39 min, purity > 95%.



Reaction code: Liu225-139

***N*-(6-bromobenzo[*d*]thiazol-2-yl)acetamide (145c)** was prepared according to general procedure **10** using **146c** (0.10 g, 0.4 mmol) and acetic anhydride (0.5 g, 0.5 mmol). The crude product was purified by column chromatography (eluent EA/PET 1:2) to give a brown solid (0.21 g, 81%). ¹H NMR (400 MHz, DMSO-*d*₆) δ 12.42 (s, 1H, H-4), 8.24 (d, *J* = 2.5 Hz, 1H, H-1), 7.67 (d, *J* = 8.6 Hz, 1H, H-3), 7.57 (dd, *J* = 2.2, 8.3 Hz, 1H, H-2), 2.21 (s, 3H, H-5). ¹³C NMR (101 MHz, DMSO-*d*₆) δ 172.48, 170.11, 167.47, 159.23, 148.18, 134.11, 129.54, 124.69, 122.55, 115.81, 23.21. LCMS *m/z* calc. C₉H₆BrN₂OS [M]⁺: 271.3 found 272.2 with *t*_R 2.35 min, purity > 95%.



Reaction code: Liu211-265

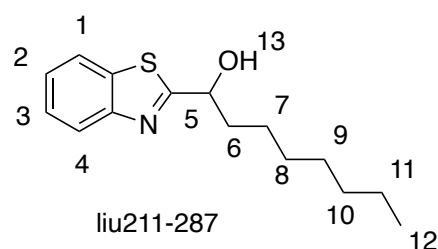
Preparation of 1-(benzo[*d*]thiazol-2-yl)ethan-1-ol (143). The Grignard reagent methylmagnesium bromide (2M solution, 0.35 mmol) was added dropwise to a solution of benzo[*d*]thiazole-2-carbaldehyde (0.048 g, 0.294 mmol) in anhydrous THF under N₂ at 0 °C and stirred for 30 min and warm up to rt and stirred 6 h. The mixture was quenched by Sat. NH₄Cl and the diluted with water. The mixture was extracted by EtOAc three times and the combined organic layers were combined and washed with brine and dried over Na₂SO₄. The crude product was purified by column chromatography (eluent EA/PET 1:4) to give a yellow oil (0.039 g, 75%). ¹H NMR (400 MHz, DMSO-*d*₆) δ 8.10 – 8.06 (m, 1H, H-3), 7.94 (dt, *J* = 1.1, 8.1 Hz, 1H, H-4), 7.49 (ddd, *J* = 1.3, 7.2, 8.2 Hz, 1H, H-2), 7.40 (ddd, *J* = 1.3, 7.2, 8.3 Hz, 1H, H-1), 6.32 (d, *J* = 5.2 Hz, 1H, H-7), 5.07 (qd, *J* = 5.0, 6.5 Hz, 1H, H-5), 1.54 (d, *J* = 6.5 Hz, 3H, H-6).

^{13}C NMR (101 MHz, $\text{DMSO-}d_6$) δ 180.04, 153.65, 134.87, 126.38, 125.14, 122.83, 122.71, 67.55, 24.33. LCMS m/z calc. $\text{C}_9\text{H}_9\text{NOS}$ $[\text{M}]^+$: 179.0 found 179.7 with t_{R} 2.34 min, purity > 95%.

General procedure 11 Preparation of 1-(benzo[d]thiazol-2-yl)-1-ols 148a-d

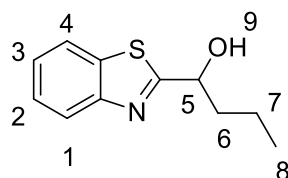
Magnesium turnings (1.4 equiv) and a single chip of I_2 were added to a Schlenk flask under N_2 . The reaction flask was gently heated with a heat gun to initiate the reaction. Once the flask was full of the I_2 gas, anhydrous THF was added and the solution was gently heated for a few minutes. Alkyl bromide (1.0 equiv) was then added and the reaction mixture was then refluxed for an hour until the full consumption of the Mg turnings.

Benzothiazole-2-carboxaldehyde (1 equiv) was dissolved in anhydrous THF and added dropwise the reaction mixture under ice bath. The reaction was slowly warm up to room temperature and stirred overnight. Once the reaction finished, Sat. NH_4Cl was added and the aqueous layer was extracted by EtOAc three times. The combined organic layers were combined and washed with brine and dried over Na_2SO_4 . The crude product was purified by column chromatography.

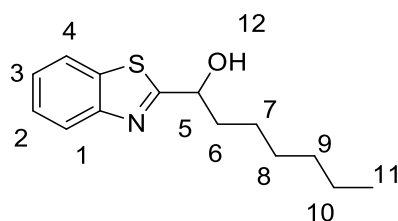


Reaction code: Liu211-287

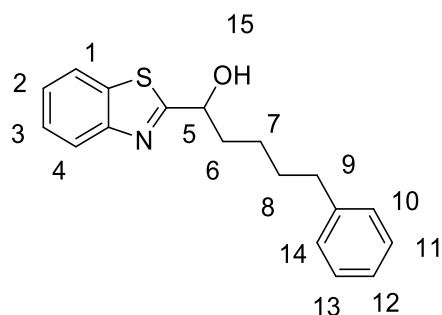
1-(benzo[d]thiazol-2-yl)octan-1-ol (148c) was prepared according to general procedure 11 using **150c** (0.082 g, 0.50 mmol), Mg (0.019 g, 0.78 mmol), and benzo[d]thiazole-2-carbaldehyde **151** (0.10 g, 0.56 mmol). The crude product was purified by column chromatography (eluent EA/PET 1:4) to give a white solid (0.97 g, 66%). ^1H NMR (400 MHz, $\text{DMSO-}d_6$) δ 8.07 (dd, $J = 8.1, 1.3$ Hz, 1H, H-4), 7.98 – 7.88 (m, 1H, H-1), 7.48 (ddd, $J = 8.1, 7.2, 1.3$ Hz, 1H, H-3), 7.40 (td, $J = 7.6, 1.2$ Hz, 1H, H-2), 6.30 (d, $J = 5.3$ Hz, 1H, H-13), 4.90 (dt, $J = 7.8, 4.9$ Hz, 1H, H-5), 2.01 – 1.83 (m, 1H, H-6), 1.83 – 1.68 (m, 1H, H-6), 1.53 – 1.38 (m, 2H, H-7), 1.27 (app. dq, $J = 10.9, 6.0, 4.3$ Hz, 8H, H-8-11), 0.91 – 0.77 (m, 3H, H-12). ^{13}C NMR (101 MHz, Chloroform- d) δ 176.45, 152.79, 134.82, 126.07, 125.00, 122.86, 121.84, 72.39, 38.16, 31.78, 29.37, 29.17, 25.16, 22.63, 14.09. LCMS m/z calc. $\text{C}_{15}\text{H}_{21}\text{NOS}$ $[\text{M}]^+$: 263.4, found 263.8 with t_{R} 3.15 min, purity > 95%.

**Reaction code: Liu225-203**

1-(benzo[d]thiazol-2-yl)butan-1-ol (148a) was prepared using propylmagnesium chloride (0.303 mmol) and benzo[d]thiazole-2-carbaldehyde (0.050 g, 0.303 mmol). The crude product was purified by column chromatography (eluent EA/PET 1:4) to give a white solid (0.40 g, 64%). ^1H NMR (400 MHz, Methanol- d_4) δ 7.96 (dt, $J = 7.9$, 0.9 Hz, 1H, H-1), 7.93 – 7.86 (m, 1H, H-4), 7.48 (ddd, $J = 8.3$, 7.2, 1.3 Hz, 1H, H-2), 7.39 (ddd, $J = 8.3$, 7.2, 1.2 Hz, 1H, H-3), 4.99 (dd, $J = 8.1$, 4.7 Hz, 1H, H-5), 3.34 (s, 1H, H-9), 2.08 – 1.73 (m, 2H, H-6), 1.63 – 1.41 (m, 2H, H-7), 0.98 (t, $J = 7.4$ Hz, 3H, H-8). ^{13}C NMR (101 MHz, Methanol- d_4) δ 179.58, 152.84, 134.39, 125.82, 124.72, 121.82, 121.66, 71.28, 48.24, 48.03, 47.81, 47.60, 47.39, 47.18, 46.96, 39.74, 18.10, 12.75. Purity > 95%.

**Reaction code: Liu225-201**

1-(benzo[d]thiazol-2-yl)heptan-1-ol (148b) was prepared according to general procedure 11 using **150b** (0.100 g, 0.61 mmol), Mg (0.021 g, 0.91 mmol), and benzo[d]thiazole-2-carbaldehyde **151** (0.10 g, 0.56 mmol). The crude product was purified by column chromatography (eluent EA/PET 1:4) to give a white solid (0.40 g, 41%). ^1H NMR (400 MHz, DMSO- d_6) δ 8.07 (d, $J = 7.9$ Hz, 1H, H-1), 7.93 (d, $J = 8.1$ Hz, 1H, H-4), 7.54 – 7.44 (m, 1H, H-2), 7.44 – 7.29 (m, 1H, H-3), 6.30 (d, $J = 5.3$ Hz, 1H, H-12), 4.90 (dt, $J = 7.8$, 4.9 Hz, 1H, H-5), 1.90 (dtd, $J = 13.0$, 7.8, 4.6 Hz, 1H, H-6), 1.77 (dq, $J = 14.6$, 7.5 Hz, 1H, H-6), 1.42 (app. p, $J = 7.3$ Hz, 2H, H-7), 1.35 – 1.13 (m, 6H, H-7, 8 and 9), 0.92 – 0.75 (m, 3H, H-11). ^{13}C NMR (101 MHz, DMSO- d_6) δ 179.62, 153.63, 134.77, 126.35, 125.10, 122.82, 122.68, 71.14, 37.89, 31.68, 28.96, 25.06, 22.50, 14.40. LCMS m/z calc. $\text{C}_{14}\text{H}_{19}\text{NOS}$ $[\text{M}+\text{H}]^+$: 250.3, found 250.3 with t_R 3.05 min, purity > 95%.

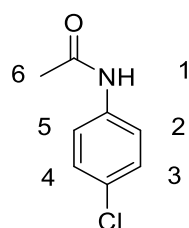


Reaction code: Liu225-197

1-(benzo[d]thiazol-2-yl)-5-phenylpentan-1-ol (148d) was prepared according to general procedure **11** using **150d** (0.10 g, 0.47 mmol), Mg (0.016 g, 0.66 mmol), and benzo[d]thiazole-2-carbaldehyde **151** (0.68 g, 0.042 mmol). The crude product was purified by column chromatography (eluent EA/PET 1:4) to give a white solid (0.50 g, 36%). ¹H NMR (400 MHz, Chloroform-*d*) δ 8.01 (d, *J* = 8.1 Hz, 1H, H-4), 7.91 (dd, *J* = 8.0, 1.2 Hz, 1H, H-1), 7.50 (ddd, *J* = 8.3, 7.1, 1.3 Hz, 1H, H-3), 7.41 (td, *J* = 7.6, 7.2, 1.2 Hz, 1H, H-2), 7.33 – 7.24 (m, 2H, H-10 and 14), 7.19 (app. td, *J* = 6.2, 1.7 Hz, 3H, H-11, 12 and 13), 5.12 (dt, *J* = 7.5, 3.4 Hz, 1H, H-15), 3.18 (d, *J* = 4.7 Hz, 1H, H-5), 2.65 (t, *J* = 7.6 Hz, 2H, H-9), 2.16 – 2.04 (m, 1H, H-6), 1.98 (dddd, *J* = 13.6, 9.7, 8.0, 5.5 Hz, 1H, H-6), 1.72 (dddd, *J* = 11.7, 10.4, 6.1, 2.7 Hz, 2H, H-7), 1.67 – 1.51 (m, 2H, H-8). ¹³C NMR (101 MHz, Chloroform-*d*) δ 176.01, 152.82, 142.38, 134.87, 128.40, 128.30, 126.12, 125.72, 125.05, 122.91, 121.86, 72.34, 38.00, 35.77, 31.23, 24.82. LCMS *m/z* calc. C₁₈H₁₉NOS [M+H]⁺: 298.4, found 298.5 with *t_R* 3.03 min, purity > 95%.

General procedure 12 Preparation of *N*-phenylacetamides 152a-c

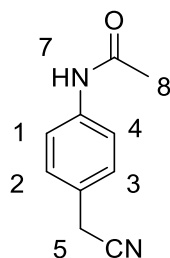
Substituted anilines (**153a-b**, **74**) (1 equiv.) was dissolved in DCM followed by addition of acetic anhydride (3.0 equiv.) and the mixture was heated up to 40~60 °C under N₂. The reaction was monitored by TLC and the crude product was purified by column chromatography.



Reaction code: Liu247-23/225-235

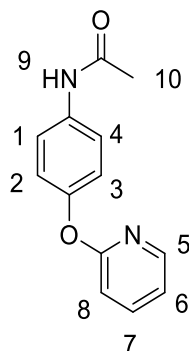
***N*-(4-chlorophenyl)acetamide (152a)** was prepared according to general procedure **12** using **153a** (0.10 g, 0.79 mmol) and acetic anhydride (0.098 g, 0.94 mmol). The crude product was purified by column chromatography (eluent EA/PET 1:2) to give a white solid (0.10g, 75%). ¹H NMR (400 MHz, DMSO-*d*₆) δ 10.06 (s, 1H, H-1), 7.64 – 7.49 (m, 2H, H-2 and 5), 7.49 – 7.23 (m, 2H, H-3 and 4), 2.05 (s, 3H, H-6). ¹³C NMR

(101 MHz, DMSO- d_6) δ 168.89, 138.74, 129.00, 126.97, 120.93, 24.44. LCMS m/z calc. C_8H_8ClNO $[M+H]^+$: 170.6, found 170.2 with t_R 2.50 min, purity > 95%.



Reaction code: Liu211-283

***N*-(4-(cyanomethyl)phenyl)acetamide (152b)** was prepared according to general procedure **12** using **153b** (0.30 g, 0.79 mmol) and acetic anhydride (0.069 g, 0.81 mmol). The crude product was purified by column chromatography (eluent EA/PET 1:2) to give a yellow solid (0.32 g, 81%). 1H NMR (400 MHz, DMSO- d_6) δ 9.99 (s, 1H, H-7), 7.59 (app. d, J = 8.2 Hz, 2H, H-1 and 4), 7.26 (app. d, J = 8.3 Hz, 2H, H-2 and 3), 3.96 (s, 2H, H-5), 2.04 (s, 3H, H-8). ^{13}C NMR (101 MHz, DMSO- d_6) δ 168.81, 139.22, 128.90, 125.92, 119.85, 119.80, 24.45, 22.28. LCMS m/z calc. $C_{10}H_{10}N_2O$ $[M+H]^+$: 175.2, found 175.1 with t_R 2.12 min, purity > 95%.

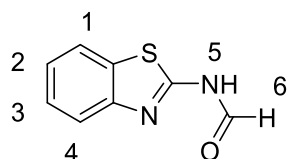


Reaction code: Liu225-37

***N*-(4-(pyridin-2-yloxy)phenyl)acetamide (152c)** was prepared according to general procedure **12** using **74** (0.050 g, 0.224 mmol) and acetic anhydride (0.069 g, 0.67 mmol). The crude product was purified by column chromatography (eluent EA/PET 1:1) to give a white solid (0.32g, 63%). 1H NMR (400 MHz, DMSO- d_6) δ 9.97 (s, 1H, H-9), 8.14 (dd, J = 2.0, 5.0 Hz, 1H, H-5), 7.83 (ddd, J = 2.0, 7.3, 8.8 Hz, 1H, H-7), 7.66 – 7.54 (m, 2H, H-1 and 4), 7.11 (dd, J = 4.9, 7.2 Hz, 1H, H-6), 7.08 – 7.03 (m, 2H, H-2 and 3), 6.98 (d, J = 8.3 Hz, 1H, H-8), 2.05 (s, 3H, H-10). ^{13}C NMR (101 MHz, DMSO- d_6) δ 168.57, 163.80, 149.42, 147.85, 140.53, 136.43, 121.97, 120.72, 119.25, 111.62, 24.38. LCMS m/z calc. $C_{13}H_{12}N_2O_2$ $[M]^+$: 228.3, found 228.7 with t_R 2.37 min, purity > 95%.

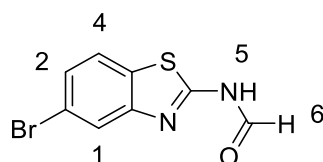
General procedure 13 Preparation of *N*-(benzo[*d*]thiazol-2-yl)formamides 155a-b

The mixture of acetic anhydride (8.0 equiv.) and formic acid (6.0 equiv) were heated at 60°C for 2 hours and cooled to room temperature. Benzothiazolamines (1.0 equiv) was added portionwise and the temperature was kept under 40°C. The reaction mixture was stirred at room temperature for overnight. Once the reaction finished, solvent was removed under vacuum and the crude product was purified by column chromatography.



Reaction code: Liu195-189

***N*-(benzo[*d*]thiazol-2-yl)formamide (155a)** was prepared according to general procedure 13 using **146a** (0.10 g, 0.67 mmol), acetic anhydride (0.54 g, 5.33 mmol) and formic acid (0.18 g, 4.00 mmol). The crude product was purified by column chromatography (eluent EA/PET 1:2) to give a white solid (0.108 g, 93%). ¹H NMR (400 MHz, DMSO-*d*₆) δ 12.44 (s, 1H, H-5), 8.59 (s, 1H, H-6), 7.98 (dd, *J* = 1.3, 8.0 Hz, 1H, H-4), 7.77 (d, *J* = 8.0 Hz, 1H, H-1), 7.44 (ddd, *J* = 1.3, 7.2, 8.2 Hz, 1H, H-3), 7.32 (td, *J* = 1.2, 7.6 Hz, 1H, H-2). ¹³C NMR (101 MHz, DMSO-*d*₆) δ 161.01, 156.72, 148.85, 132.04, 126.72, 124.29, 122.28, 121.24. LCMS *m/z* calc. C₈H₆N₂OS [M+H]⁺: 179.2, found 179.3 with *t*_R 2.46 min, purity > 95%.

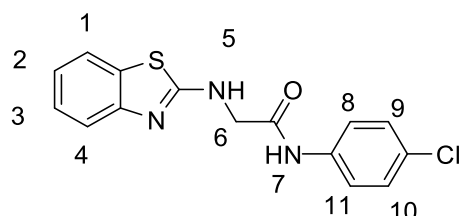


Reaction code: Liu195-201

***N*-(5-bromobenzo[*d*]thiazol-2-yl)formamide (155b)** was prepared according to general procedure 13 using **146b** (0.20 g, 0.87 mmol), acetic anhydride (0.92 g, 6.98 mmol) and formic acid (0.24 g, 5.23 mmol). The crude product was purified by column chromatography (eluent EA/PET 1:2) to give a white solid (0.137 g, 61%). ¹H NMR (400 MHz, DMSO-*d*₆) δ 12.58 (s, 1H, H-5), 8.62 (s, 1H, H-6), 8.08 – 7.78 (m, 2H, H-1 and 4), 7.48 (dd, *J* = 1.9, 8.5 Hz, 1H, H-2). ¹³C NMR (101 MHz, DMSO-*d*₆) δ 161.31, 131.30, 126.94, 124.20, 123.62, 119.49. LCMS *m/z* calc. C₈H₅BrN₂OS [M]⁺: 257.1, found 257.0 with *t*_R 2.70 min, purity > 95%.

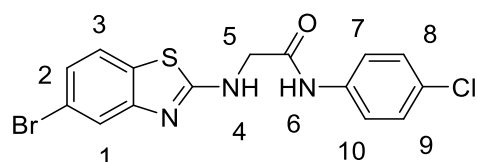
General procedure 14 Preparation of 2-(benzo[*d*]thiazol-2-ylamino)-*N*-(4-chlorophenyl)acetamides 154a-b

N-(benzo[*d*]thiazol-2-yl)formamides (1.0 equiv) was dissolved in DMF and NaH (1.2 equiv) was added under the protection of inert N₂ under ice bath. The reaction mixture was allowed to stir 1 hour before the addition of **91** (1.0 equiv). The reaction was monitored by TLC and quenched by addition of Sat. NH₄Cl. The reaction mixture was stirred for 5 minutes and the diluted with water and was extracted by EtOAc three times and the combined organic layers were combined and washed with brine and dried over Na₂SO₄. The crude product was purified by column chromatography.



Reaction code: Liu195-193/221

2-(benzo[*d*]thiazol-2-ylamino)-*N*-(4-chlorophenyl)acetamide (154a) was prepared according to general **procedure 14** using *N*-(benzo[*d*]thiazol-2-yl)formamides **155a** (0.050 g, 0.28 mmol) and **91** (0.076 g, 0.31 mmol). The crude product was purified by column chromatography (eluent EA/PET 1:2) to give a white solid (0.49 g, 55%). ¹H NMR (400 MHz, DMSO-*d*₆) δ 10.29 (s, 1H, H-7), 8.39 (t, *J* = 5.9 Hz, 1H, H-5), 7.72 – 7.68 (m, 1H, H-4), 7.68 – 7.61 (m, 2H, H-8 and 11), 7.41 – 7.34 (m, 3H, H-1, 9 and 10), 7.22 (ddd, *J* = 1.3, 7.3, 8.1 Hz, 1H, H-3), 7.04 (td, *J* = 1.2, 7.5 Hz, 1H, H-2), 4.25 (d, *J* = 5.9 Hz, 2H, H-6). ¹³C NMR (101 MHz, DMSO-*d*₆) δ 168.38, 166.73, 152.57, 138.33, 131.16, 129.19, 125.99, 121.64, 121.49, 121.09, 118.65, 47.51. LCMS *m/z* calc. C₁₅H₁₂ClN₃OS [M]⁺: 317.8, found 317.9 with *t*_R 5.32 min, purity > 95%.



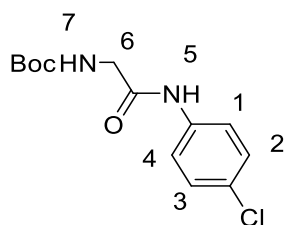
Reaction code: Liu195-227

2-((5-bromobenzo[*d*]thiazol-2-yl)amino)-*N*-(4-chlorophenyl)acetamide (154b) was prepared according to general **procedure 14** using *N*-(5-bromobenzo[*d*]thiazol-2-yl)formamide **155b** (0.050g, 0.19 mmol) and **91** (0.058 g, 0.0.23 mmol). The crude product was purified by column chromatography (eluent EA/PET 1:2) to give a white solid (0.09 g, 12%). ¹H NMR (400 MHz, DMSO-*d*₆) δ 10.29 (s, 1H, H-6), 8.59 (t, *J* = 5.8 Hz, 1H, H-4), 7.69 – 7.59 (m, 3H, H-1, H7 and 10), 7.52 (d, *J* = 1.9 Hz, 1H, H-3), 7.40 – 7.34 (m, 2H, H-8 and 9), 7.18 (dd, *J* = 2.0, 8.4 Hz, 1H, H-2), 4.25 (d, *J* = 5.8 Hz, 2H, H-5). ¹³C NMR (126 MHz, DMSO-*d*₆) δ 174.56, 168.06, 154.17, 149.8, 138.17, 131.83, 130.47, 129.21, 127.33, 124.05, 123.20, 121.09, 120.91, 118.78, 47.49.

LCMS m/z calc. $C_{15}H_{11}BrClN_3OS^+[M+H]^+$: 397.7, found 397.9 with t_R 2.92 min, purity > 95%.

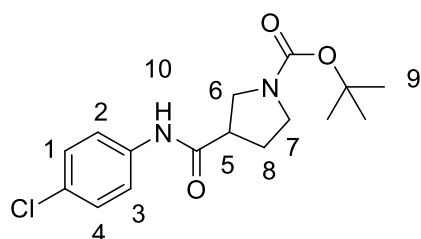
General procedure 15 Preparation of 157a-c

4-chloroaniline **172** (1 equiv), HATU (1.5 equiv), DMAP (0.1 equiv) and Boc-AA (1 equiv) were dissolved in 1mL/mmol anhydrous NMP and stirred at room temperature for 5 minutes before addition of DIPEA (3 equiv). The mixture stirred at room temperature for overnight. The reaction was monitored by TLC and quenched by addition of water. The reaction mixture was stirred for 5 minutes and the diluted with water and was extracted by EtOAc three times and the combined organic layers were combined and washed with Sat. $NaHCO_3$ and brine and dried over Na_2SO_4 . The crude product was purified by column chromatography.



Reaction code: Liu195-207

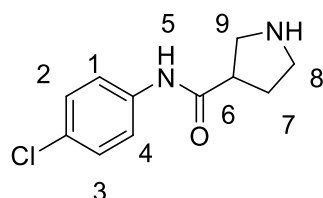
tert-butyl (2-((4-chlorophenyl)amino)-2-oxoethyl)carbamate (157a) was prepared according to general procedure **15** using 4-chloroaniline **153a** (0.17 g, 1.14 mmol), HATU (0.65 g, 1.71 mmol), DMAP (0.014 g, 0.11 mmol) and Boc-Gly-OH (0.2 g, 1.14 mmol). The crude product was purified by column chromatography (eluent EA/PET 1:2) to give a white solid (0.24 g, 74%). 1H NMR (400 MHz, $DMSO-d_6$) δ 10.02 (s, 1H, H-5), 7.68 – 7.49 (m, 2H, H-1 and 4), 7.44 – 7.29 (m, 2H, H- 2 and 3), 7.03 (t, J = 6.1 Hz, 1H, H-7), 3.68 (d, J = 6.1 Hz, 2H, H-6), 1.36 (s, 9H, H-Boc). ^{13}C NMR (101 MHz, $DMSO-d_6$) δ 168.88, 156.40, 138.38, 129.12, 127.14, 121.06, 78.55, 44.25, 38.72, 28.67, 24.57.



Reaction code: Liu195-155/liu225-285

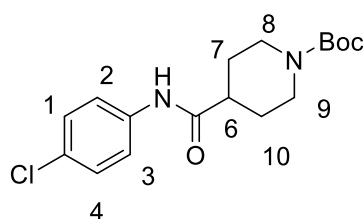
tert-butyl 3-((4-chlorophenyl)carbamoyl)pyrrolidine-1-carboxylate (157b) was prepared according to general procedure **15** using 4-chloroaniline **153a** (0.10 g, 0.78 mmol), HATU (0.45g, 1.7 mmol), DMAP (0.009 g, 0.08mmol) and Boc-Pro-OH (0.17g, 0.78 mmol). The crude product was purified by column chromatography (eluent

EA/PET 1:2) to give a yellow oil (0.25 g, 98%). ^1H NMR (400 MHz, Chloroform-*d*) δ 7.54 – 7.40 (m, 2H, H-2 and 3), 7.26 (app. d, $J = 8.7$ Hz, 2H, H-1 and 4), 3.80 – 3.49 (m, 3H, H-5, and 6), 3.35 (app. dt, $J = 7.9, 10.8$ Hz, 1H, H-7), 2.98 (app. d, $J = 7.4$ Hz, 1H, H-7), 2.15 (ddd, $J = 4.9, 8.8, 12.8$ Hz, 2H, H-8), 1.46 (s, 9H, H-9). ^{13}C NMR (101 MHz, DMSO-*d*₆) δ 138.49, 129.08, 127.26, 121.21, 78.82, 65.39, 38.72, 28.64, 24.57, 15.64. LCMS m/z calc. $\text{C}_{16}\text{H}_{21}\text{ClN}_2\text{O}_3$ $[\text{M}+\text{H}]^+$: 325.8, found 325.1 with t_{R} 2.91 min, purity > 95%.



Reaction code Liu195-159

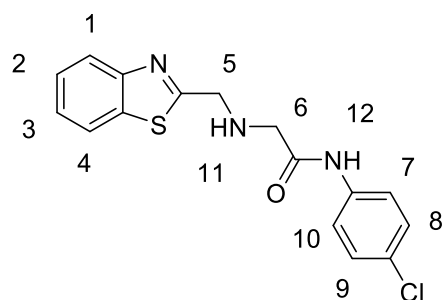
Preparation of *N*-(4-chlorophenyl)pyrrolidine-3-carboxamide (158b). **157b** (0.25 g, 0.76 mmol) was dissolved in 5 mL of DCM followed by addition of excessive 4N HCl at room temperature. The reaction mixture was stirred at room temperature for overnight to give a white solid (0.24 g, >100%). ^1H NMR (400 MHz, DMSO-*d*₆) δ 10.62 (s, 1H, H-5), 7.79 – 7.53 (m, 2H, H1 and 4), 7.50 – 7.27 (m, 2H, H2 and 3), 3.39 (app.d, $J = 4.9$ Hz, 1H, H-6), 3.37 – 3.26 (m, 2H, H-8 and 9), 3.19 (app. tq, $J = 5.6, 9.9$ Hz, 2H, H-8 and 9), 2.24 (app. dq, $J = 7.1, 13.8$ Hz, 1H, H-7), 2.03 (app. dq, $J = 7.3, 14.0$ Hz, 1H, H-7). ^{13}C NMR (101 MHz, DMSO-*d*₆) δ 170.87, 138.38, 129.10, 127.49, 121.30, 47.15, 45.19, 43.54, 29.34. LCMS m/z calc. $\text{C}_{11}\text{H}_{13}\text{ClN}_2\text{O}$ $[\text{M}+\text{H}]^+$: 225.6, found 225.5 with t_{R} 1.21 min, purity > 95%.



Reaction code: Liu195-167/ 225-287

***tert*-Butyl 4-((4-chlorophenyl)carbamoyl)piperidine-1-carboxylate (158c)** was prepared according to general procedure **15** using 4-chloroaniline **153a** (0.24 g, 1.95 mmol), HATU (1.11 g, 2.93 mmol), DMAP (0.023 g, 0.19 mmol) and 1-(*tert*-butoxycarbonyl)piperidine-4-carboxylic acid (0.45g, 1.9 mmol). The crude product was purified by column chromatography (eluent EA/PET 1:2) to give a white solid (0.145 g, 22%). ^1H NMR (400 MHz, Chloroform-*d*) δ 7.53 – 7.45 (m, 2H, H-2 and 3), 7.32 – 7.25 (m, 2H, H-1 and 4), 4.19 (m, 2H, H-8 and 9), 2.77 (m, 2H, H-8 and 9), 2.40 (tt, $J = 3.8, 11.5$ Hz, 1H, H-6), 1.99 – 1.83 (m, 2H, H-7 and 10), 1.85 – 1.61 (m, 2H, H-7 and 10), 1.48 (s, 9H, H-Boc). ^{13}C NMR (101 MHz, Chloroform-*d*) δ 172.72, 154.70, 136.41,

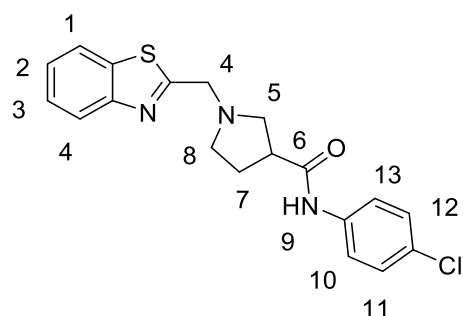
129.34, 129.02, 121.13, 79.84, 44.27, 38.65, 28.58, 28.45. LCMS m/z calc. $C_{17}H_{23}ClN_2O_3$ $[M+H]^+$: 339.8, found 339.0 with t_R 2.95 min, purity > 95%.



Reaction code: Liu195-225

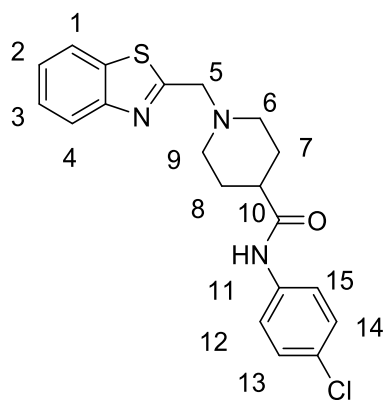
Preparation of 2-((benzo[d]thiazol-2-ylmethyl)amino)-N-(4-chlorophenyl)acetamide 156a.

157a (0.085 g, 0.31 mmol) was dissolved in DCM followed by addition of excessive amount of 4N HCl in dioxane. Reaction mixture was stirred at room temperature for overnight and solvent was removed under vacuum and the crude product of **184** was used directly for the next step without further purification. benzo[d]thiazole-2-carbaldehyde (0.050 g, 0.31 mmol) and **158a** (0.057 g, 0.31 mmol) were dissolved in anhydrous THF at room temperature under the protection of inert N_2 atmosphere, catalytic amount of HOAc was added and the mixture was stirred at room temperature for 6 hours followed by addition of $NaBH(OAc)_3$ (0.33 g, 1.53 mmol). The mixture stirred at room temperature for overnight. The reaction was monitored by TLC and quenched by addition of Sat. $NaHCO_3$. The reaction mixture was stirred for 5 minutes and the diluted with Sat. $NaHCO_3$ and was extracted by EtOAc three times and the combined organic layers were combined and washed with brine and dried over Na_2SO_4 . The crude product was purified by column chromatography (eluent EA/PET 1:1) to give a yellow oily product (0.10 g, 10%). 1H NMR (400 MHz, Chloroform- d) δ 9.28 (s, 1H, H-12), 8.03 – 7.96 (m, 1H, H-1), 7.90 (dt, J = 0.9, 8.0 Hz, 1H, H-4), 7.60 – 7.55 (m, 2H, H-7 and 10), 7.50 (ddd, J = 1.3, 7.2, 8.3 Hz, 1H, H-2), 7.44 – 7.36 (m, 1H, H-3), 7.32 – 7.27 (m, 2H, H-8 and 9), 4.32 (s, 2H, H-5), 3.58 (s, 2H, H-6). ^{13}C NMR (101 MHz, DMSO- d_6) δ 175.04, 170.44, 153.59, 138.21, 135.10, 129.14, 127.27, 126.38, 125.20, 122.72, 122.69, 121.13, 52.37, 50.98. LCMS m/z calc. $C_{16}H_{14}ClN_3OS$ $[M+H]^+$: 332.8, found 332.0 with t_R 2.49 min, purity > 95%.



Reaction code: Liu195-177

1-(Benzo[d]thiazol-2-ylmethyl)-N-(4-chlorophenyl)pyrrolidine-3-carboxamide(156b). Benzo[d]thiazole-2-carbaldehyde (0.023 g, 0.14 mmol) and **158b** (0.034 g, 0.14 mmol) were dissolved in anhydrous THF at room temperature under the protection of inert N₂ atmosphere, catalytic amount of HOAc was added and the mixture was stirred at room temperature for 6 hours followed by addition of NaBH(OAc)₃ (0.045 g, 0.21 mmol). The mixture stirred at room temperature for overnight. The reaction was monitored by TLC and quenched by addition of Sat. NaHCO₃. The reaction mixture was stirred for 5 minutes and the diluted with Sat. NaHCO₃ and was extracted by EtOAc three times and the combined organic layers were combined and washed with brine and dried over Na₂SO₄. The crude product was purified by column chromatography (eluent EA/PET 1:1) to give a white solid (0.007 g, 13%). ¹H NMR (400 MHz, Methanol-*d*₄) δ 8.01 – 7.87 (m, 2H, H-1 and 4), 7.62 – 7.54 (m, 2H, H-10 and 13), 7.50 (ddd, *J* = 1.3, 7.2, 8.3 Hz, 1H, H-3), 7.42 (ddd, *J* = 1.2, 7.2, 8.3 Hz, 1H, H-2), 7.35 – 7.24 (m, 2H, H-11 and 12), 4.25 – 4.02 (m, 2H, H-4), 3.25 – 3.05 (m, 2H, H-5), 2.94 (ddt, *J* = 3.6, 5.6, 10.1 Hz, 2H, H-8), 2.85 (td, *J* = 6.7, 8.5 Hz, 1H, H-6), 2.34 – 1.98 (m, 2H, H-7). ¹³C NMR (101 MHz, Methanol-*d*₄) δ 173.91, 172.43, 152.47, 137.41, 135.01, 128.52, 128.36, 125.90, 125.00, 121.95, 121.67, 121.12, 57.07, 56.57, 53.77, 48.25, 48.04, 47.82, 47.61, 47.40, 47.18, 46.97, 44.20, 28.30. LCMS *m/z* calc. C₁₉H₁₈ClN₃OS [M+H]⁺: 372.8, found 372.0 with *t_R* 2.95 min, purity > 95%.

**Reaction code: Liu195-161/247-15**

1-(Benzo[d]thiazol-2-ylmethyl)-N-(4-chlorophenyl)piperidine-4-carboxamide (156c). **157b** (0.25 g, 0.25 mmol) was dissolved in DCM followed by addition of excessive amount of 4N HCl in dioxane. Reaction mixture was stirred at room temperature for overnight and solvent was removed under vacuum and the crude product of **158c** was used directly for the next step without further purification. benzo[d]thiazole-2-carbaldehyde (0.042 g, 0.26 mmol) and **158c** (0.067 g, 0.26 mmol) were dissolved in anhydrous THF at room temperature under the protection of inert N₂ atmosphere, catalytic amount of HOAc was added and the mixture was stirred at room temperature for 6 hours followed by addition of NaBH(OAc)₃ (0.082 g, 0.39 mmol).

The mixture stirred at room temperature for overnight. The reaction was monitored by TLC and quenched by addition of Sat. NaHCO₃. The reaction mixture was stirred for 5 minutes and diluted with Sat. NaHCO₃ and was extracted by EtOAc three times and the combined organic layers were combined and washed with brine and dried over Na₂SO₄. The crude product was purified by column chromatography (eluent EA/PET 1:1) to give a white solid (0.050 g, 52%). ¹H NMR (400 MHz, Chloroform-*d*) δ 7.97 (d, *J* = 8.1 Hz, 1H, H-4), 7.92 – 7.85 (m, 1H, H-1), 7.50 – 7.46 (m, 2H, H-12 and 15), 7.46 – 7.34 (m, 2H, H-3 and 2), 7.31 – 7.27 (m, 2H, H-13 and 14), 3.97 (s, 2H, H-5), 3.11 (app. dd, *J* = 5.7, 9.2 Hz, 2H, H-6 and 9), 2.40 – 2.19 (m, 3H, H-6 and 9 and 10), 2.04 – 1.83 (m, 4H, H-7 and 8). ¹³C NMR (101 MHz, DMSO-*d*₆) δ 174.02, 173.45, 153.42, 138.78, 135.34, 129.02, 126.98, 126.34, 125.31, 122.80, 122.71, 121.09, 121.00, 60.11, 53.40, 42.93, 28.98. LCMS *m/z* calc. C₂₀H₂₀ClN₃OS [M+H]⁺: 386.9, found 386.20 with *t*_R 2.31 min, purity > 95%.

Reference

- (1) Khan, H. A.; Ahmad, A.; Mehboob, R. Nosocomial Infections and Their Control Strategies. *Asian Pacific Journal of Tropical Biomedicine* **2015**, *5* (7), 509–514. <https://doi.org/10.1016/j.apjtb.2015.05.001>.
- (2) Abdulhaq, N.; Nawaz, Z.; Zahoor, M. A.; Siddique, A. B. Association of Biofilm Formation with Multi Drug Resistance in Clinical Isolates of *Pseudomonas Aeruginosa*. *EXCLI J* **2020**, *19*, 201–208. <https://doi.org/10.17179/excli2019-2049>.
- (3) Sou, T.; Kukavica-Ibrulj, I.; Levesque, R. C.; Friberg, L. E.; Bergström, C. A. S. Model-Informed Drug Development in Pulmonary Delivery: Semimechanistic Pharmacokinetic–Pharmacodynamic Modeling for Evaluation of Treatments against Chronic *Pseudomonas Aeruginosa* Lung Infections. *Mol. Pharmaceutics* **2020**, *17* (5), 1458–1469. <https://doi.org/10.1021/acs.molpharmaceut.9b00968>.
- (4) Oliver, A.; Cantón, R.; Campo, P.; Baquero, F.; Blázquez, J. High Frequency of Hypermutable *Pseudomonas Aeruginosa* in Cystic Fibrosis Lung Infection. *Science* **2000**, *288* (5469), 1251–1253. <https://doi.org/10.1126/science.288.5469.1251>.
- (5) Mok, N.; Yuen Chan, S.; Yang Liu, S.; Lin Chua, S. Vanillin Inhibits PqsR-Mediated Virulence in *Pseudomonas Aeruginosa*. *Food & Function* **2020**, *11* (7), 6496–6508. <https://doi.org/10.1039/D0FO00046A>.
- (6) Brindhadevi, K.; LewisOscar, F.; Mylonakis, E.; Shanmugam, S.; Verma, T. N.; Pugazhendhi, A. Biofilm and Quorum Sensing Mediated Pathogenicity in *Pseudomonas Aeruginosa*. *Process Biochemistry* **2020**, *96*, 49–57. <https://doi.org/10.1016/j.procbio.2020.06.001>.
- (7) Zhao, X.; Yu, Z.; Ding, T. Quorum-Sensing Regulation of Antimicrobial Resistance in Bacteria. *Microorganisms* **2020**, *8* (3), 425. <https://doi.org/10.3390/microorganisms8030425>.
- (8) Saeki, E. K.; Kobayashi, R. K. T.; Nakazato, G. Quorum Sensing System: Target to Control the Spread of Bacterial Infections. *Microbial Pathogenesis* **2020**, *142*, 104068. <https://doi.org/10.1016/j.micpath.2020.104068>.
- (9) Piewngam, P.; Chiou, J.; Chatterjee, P.; Otto, M. Alternative Approaches to Treat Bacterial Infections: Targeting Quorum-Sensing. *Expert Review of Anti-infective Therapy* **2020**, *18* (6), 499–510. <https://doi.org/10.1080/14787210.2020.1750951>.
- (10) García-Reyes, S.; Soberón-Chávez, G.; Cocotl-Yanez, M. The Third Quorum-Sensing System of *Pseudomonas Aeruginosa*: *Pseudomonas* Quinolone Signal and the Enigmatic PqsE Protein. *Journal of Medical Microbiology*, **2020**, *69* (1), 25–34. <https://doi.org/10.1099/jmm.0.001116>.

- (11) Ilangovan, A.; Fletcher, M.; Rampioni, G.; Pustelny, C.; Rumbaugh, K.; Heeb, S.; Cámara, M.; Truman, A.; Chhabra, S. R.; Emsley, J.; Williams, P. Structural Basis for Native Agonist and Synthetic Inhibitor Recognition by the *Pseudomonas Aeruginosa* Quorum Sensing Regulator PqsR (MvfR). *PLOS Pathogens* **2013**, *9* (7), e1003508. <https://doi.org/10.1371/journal.ppat.1003508>.
- (12) Soheili, V.; Tajani, A. S.; Ghodsi, R.; Bazzaz, B. S. F. Anti-PqsR Compounds as next-Generation Antibacterial Agents against *Pseudomonas Aeruginosa*: A Review. *European Journal of Medicinal Chemistry* **2019**, *172*, 26–35. <https://doi.org/10.1016/j.ejmech.2019.03.049>.
- (13) Soukarieh, F.; Liu, R.; Romero, M.; Roberston, S. N.; Richardson, W.; Lucanto, S.; Oton, E. V.; Qudus, N. R.; Mashabi, A.; Grossman, S.; Ali, S.; Sou, T.; Kukavica-Ibrulj, I.; Levesque, R. C.; Bergström, C. A. S.; Halliday, N.; Mistry, S. N.; Emsley, J.; Heeb, S.; Williams, P.; Cámara, M.; Stocks, M. J. Hit Identification of New Potent PqsR Antagonists as Inhibitors of Quorum Sensing in Planktonic and Biofilm Grown *Pseudomonas Aeruginosa*. *Front. Chem.* **2020**, *8*, 204. <https://doi.org/10.3389/fchem.2020.00204>.
- (14) Lister, P. D.; Wolter, D. J.; Hanson, N. D. Antibacterial-Resistant *Pseudomonas Aeruginosa*: Clinical Impact and Complex Regulation of Chromosomally Encoded Resistance Mechanisms. *Clin Microbiol Rev* **2009**, *22* (4), 582–610. <https://doi.org/10.1128/CMR.00040-09>.
- (15) Wagner, S.; Sommer, R.; Hinsberger, S.; Lu, C.; Hartmann, R. W.; Empting, M.; Titz, A. Novel Strategies for the Treatment of *Pseudomonas Aeruginosa* Infections. *J. Med. Chem.* **2016**, *59* (13), 5929–5969. <https://doi.org/10.1021/acs.jmedchem.5b01698>.
- (16) Stewart, P. S. Mechanisms of Antibiotic Resistance in Bacterial Biofilms. *International Journal of Medical Microbiology* **2002**, *292* (2), 107–113. <https://doi.org/10.1078/1438-4221-00196>.
- (17) Jolly, A. L.; Takawira, D.; Oke, O. O.; Whiteside, S. A.; Chang, S. W.; Wen, E. R.; Quach, K.; Evans, D. J.; Fleiszig, S. M. J. *Pseudomonas Aeruginosa*-Induced Bleb-Niche Formation in Epithelial Cells Is Independent of Actinomyosin Contraction and Enhanced by Loss of Cystic Fibrosis Transmembrane-Conductance Regulator Osmoregulatory Function. *mBio* **2015**, *6* (2). <https://doi.org/10.1128/mBio.02533-14>.
- (18) Sean, Y.T.; Song-Lin, C.; Yicai, C.; Scott, R.; Staffan, K.; Thomas, N.; Liang, Y.; Michael, G. Identification of Five Structurally Unrelated Quorum-Sensing Inhibitors of *Pseudomonas aeruginosa* from a Natural-Derivative Database. *Antimicrobial Agents and Chemother.* **2013**, *57* (11). <https://aac.asm.org/content/57/11/5629.short>.
- (19) Diggle, S. P.; Winzer, K.; Chhabra, S. R.; Worrall, K. E.; Cámara, M.; Williams, P. The *Pseudomonas Aeruginosa* Quinolone Signal Molecule Overcomes the Cell Density-Dependency of the Quorum Sensing Hierarchy, Regulates Rhl-Dependent Genes at the Onset of Stationary Phase and Can Be Produced in

- the Absence of LasR. *Molecular Microbiology* **2003**, *50* (1), 29–43. <https://doi.org/10.1046/j.1365-2958.2003.03672.x>.
- (20) Lami, R. Chapter 3 - Quorum Sensing in Marine Biofilms and Environments. In *Quorum Sensing*; Tommonaro, G., Ed.; Academic Press, 2019; pp 55–96. <https://doi.org/10.1016/B978-0-12-814905-8.00003-4>.
- (21) Abedon, S. T.; Duffy, S.; Turner, P. E. Bacteriophage Ecology. In *Encyclopedia of Microbiology (Third Edition)*; Schaechter, M., Ed.; Academic Press: Oxford, 2009; pp 42–57. <https://doi.org/10.1016/B978-012373944-5.00022-5>.
- (22) Peterson, J. W. Bacterial Pathogenesis. In *Medical Microbiology*; Baron, S., Ed.; University of Texas Medical Branch at Galveston: Galveston (TX), 1996.
- (23) Ahmed, E.; Holmström, S. J. M. Siderophores in Environmental Research: Roles and Applications. *Microbial Biotechnology* **2014**, *7* (3), 196–208. <https://doi.org/10.1111/1751-7915.12117>.
- (24) Raines, D. J.; Sanderson, T. J.; Wilde, E. J.; Duhme-Klair, A.-K. Siderophores. In *Reference Module in Chemistry, Molecular Sciences and Chemical Engineering*; Elsevier, 2015. <https://doi.org/10.1016/B978-0-12-409547-2.11040-6>.
- (25) Page, M. G. P. The Role of Iron and Siderophores in Infection, and the Development of Siderophore Antibiotics. *Clin Infect Dis* **2019**, *69* (Suppl 7), S529–S537. <https://doi.org/10.1093/cid/ciz825>.
- (26) Hall, S.; McDermott, C.; Anoopkumar-Dukie, S.; McFarland, A. J.; Forbes, A.; Perkins, A. V.; Davey, A. K.; Chess-Williams, R.; Kiefel, M. J.; Arora, D.; Grant, G. D. Cellular Effects of Pyocyanin, a Secreted Virulence Factor of *Pseudomonas Aeruginosa*. *Toxins* **2016**, *8* (8), 236. <https://doi.org/10.3390/toxins8080236>.
- (27) Ortiz-Castro, R.; Pelagio-Flores, R.; Méndez-Bravo, A.; Ruiz-Herrera, L. F.; Campos-García, J.; López-Bucio, J. Pyocyanin, a Virulence Factor Produced by *Pseudomonas Aeruginosa*, Alters Root Development through Reactive Oxygen Species and Ethylene Signaling in *Arabidopsis*. *Mol Plant Microbe Interact* **2014**, *27* (4), 364–378. <https://doi.org/10.1094/MPMI-08-13-0219-R>.
- (28) Castañeda-Tamez, P.; Ramírez-Peris, J.; Pérez-Velázquez, J.; Kuttler, C.; Jalalimanesh, A.; Saucedo-Mora, M. Á.; Jiménez-Cortés, J. G.; Maeda, T.; González, Y.; Tomás, M.; Wood, T. K.; García-Contreras, R. Pyocyanin Restricts Social Cheating in *Pseudomonas Aeruginosa*. *Front. Microbiol.* **2018**, *9*. <https://doi.org/10.3389/fmicb.2018.01348>.
- (29) Zhu, Y.; Li, J. J.; Reng, J.; Wang, S.; Zhang, R.; Wang, B. Global Trends of *Pseudomonas Aeruginosa* Biofilm Research in the Past Two Decades: A Bibliometric Study. *MicrobiologyOpen* **2020**, *9* (6), e1021. <https://doi.org/10.1002/mbo3.1021>.
- (30) Rumbaugh, K. P.; Sauer, K. Biofilm Dispersion. *Nature Reviews Microbiology* **2020**, 1–16. <https://doi.org/10.1038/s41579-020-0385-0>.

- (31) Pang, Z.; Raudonis, R.; Glick, B. R.; Lin, T.-J.; Cheng, Z. Antibiotic Resistance in *Pseudomonas Aeruginosa*: Mechanisms and Alternative Therapeutic Strategies. *Biotechnology Advances* **2019**, *37* (1), 177–192. <https://doi.org/10.1016/j.biotechadv.2018.11.013>.
- (32) Karami, P.; Khaledi, A.; Mashoof, R. Y.; Yaghoobi, M. H.; Karami, M.; Dastan, D.; Alikhani, M. Y. The Correlation between Biofilm Formation Capability and Antibiotic Resistance Pattern in *Pseudomonas Aeruginosa*. *Gene Reports* **2020**, *18*, 100561. <https://doi.org/10.1016/j.genrep.2019.100561>.
- (33) Whiteley, M.; Bangera, M. G.; Bumgarner, R.E.; Parsek, M. R.; Teitzel, G. M.; Lory, S.; Greenberg, E. P. Gene expression in *Pseudomonas aeruginosa* biofilms. *Nature*. **2001**. 413(6858). <https://www.nature.com/articles/35101627> (accessed Aug 8, 2020).
- (34) Stover, C.K.; Pham, X. Q.; Erwin, A. L.; Mizoguchi, S. D.; Hickey, M. J.; Brinkman, F. S.; Hufnagle, W. O.; Kowalik, D. J.; Lagrou, M.; Garber, R. L.; Goltry, L.; Tolentino, E.; Westbrook-Wadman, S.; Yuan, Y.; Brody, L. L.; Coulter, S. N.; Folger, K. R.; Kas, A.; Larbig, K.; Lim, R.; Smith, K.; Spencer, D.; Wong, G. K.; Wu, Z.; Paulsen, I. T.; Reizer, J.; Saier, M. H.; Hancock, R. E.; Lory, S.; Olson, M. V. Complete genome sequence of *Pseudomonas aeruginosa* PAO1, an opportunistic pathogen. *Nature*. 2000. 406 (6799):947-8
- (35) Yoshimura, F.; Nikaido, H. Permeability of *Pseudomonas Aeruginosa* Outer Membrane to Hydrophilic Solutes. *Journal of Bacteriology* **1982**, *152* (2), 636–642.
- (36) Sugawara, E.; Nagano, K.; Nikaido, H. Alternative Folding Pathways of the Major Porin OprF of *Pseudomonas Aeruginosa*. *The FEBS Journal* **2012**, *279* (6), 910–918. <https://doi.org/10.1111/j.1742-4658.2012.08481.x>.
- (37) Nikaido, H.; Nikaido, K.; Harayama, S. Identification and Characterization of Porins in *Pseudomonas Aeruginosa*. *Journal of Biological Chemistry* **1991**, *266* (2), 770–779. [https://doi.org/10.1016/S0021-9258\(17\)35239-0](https://doi.org/10.1016/S0021-9258(17)35239-0).
- (38) Clatworthy, A. E.; Romano, K. P.; Hung, D. T. Whole-Organism Phenotypic Screening for Anti-Infectives Promoting Host Health. *Nature Chemical Biology* **2018**, *14* (4), 331–341. <https://doi.org/10.1038/s41589-018-0018-3>.
- (39) Megan, G.; Sebastian, L.; Matthew, B. Chemical Strategies To Target Bacterial Virulence. *Chem Rev.* **2017**. 117 (5):4422-4461. <https://pubs.acs.org/doi/abs/10.1021/acs.chemrev.6b00676>.
- (40) Rahul, S.M.; I, Atri, T.; Ritam, S.; Nagaraja, T.; Anirban, G.; Mohsina, T.; Anirban, B.; Hemanta, K.; Santasabuj, D. Ribavirin suppresses bacterial virulence by targeting LysR-type transcriptional regulators. *Nature*. **2016**. 39454 <https://www.nature.com/articles/srep39454>
- (41) González-Bello, C. Antibiotic Adjuvants – A Strategy to Unlock Bacterial Resistance to Antibiotics. *Bioorganic & Medicinal Chemistry Letters* **2017**, *27* (18), 4221–4228. <https://doi.org/10.1016/j.bmcl.2017.08.027>.

- (42) Viducic, D.; Murakami, K.; Amoh, T.; Ono, T.; Miyake, Y. RpoN Modulates Carbapenem Tolerance in *Pseudomonas Aeruginosa* through Pseudomonas Quinolone Signal and PqsE. *Antimicrobial Agents and Chemotherapy* **2016**, *60* (10), 5752–5764. <https://doi.org/10.1128/AAC.00260-16>.
- (43) Allen, R. C.; Popat, R.; Diggle, S. P.; Brown, S. P. Targeting Virulence: Can We Make Evolution-Proof Drugs? *Nature Reviews Microbiology* **2014**, *12* (4), 300–308. <https://doi.org/10.1038/nrmicro3232>.
- (44) Colleen T.O’Loughlin; Laura, C. M; Albert, S.; Knut, D.; Martin F. S.; Bonnie L. B. A quorum-sensing inhibitor blocks *Pseudomonas aeruginosa* virulence and biofilm formation. *Pnas.* **2013**, *110* (44). <https://www.pnas.org/content/110/44/17981>.
- (45) Lynette, C.; Garland R. M.; Gary R. E.; Scott J. H. The biology and future prospects of antivirulence therapies. *Nat Rev Microbiol.* **2008**, *6*(1): 17-27. <https://www.nature.com/articles/nrmicro1818>
- (46) Lee, J.; Zhang, L. The Hierarchy Quorum Sensing Network in *Pseudomonas Aeruginosa*. *Protein Cell* **2015**, *6* (1), 26–41. <https://doi.org/10.1007/s13238-014-0100-x>.
- (47) Mühlen, S.; Dersch, P. Anti-Virulence Strategies to Target Bacterial Infections. *Curr. Top. Microbiol. Immunol.* **2016**, *398*, 147–183. https://doi.org/10.1007/82_2015_490.
- (48) Bacterial Quorum Sensing: Its Role in Virulence and Possibilities for Its Control <http://perspectivesinmedicine.cshlp.org/content/2/11/a012427.short> (accessed Jul 16, 2020).
- (49) Ng, W.-L.; Bassler, B. L. Bacterial Quorum-Sensing Network Architectures. *Annual Review of Genetics.* **2009**, *43* (1), 197–222. <https://doi.org/10.1146/annurev-genet-102108-134304>.
- (50) Breah, L.; Michael, J. F. Exploiting Quorum Sensing to Confuse Bacterial Pathogens. *Microbiol Mol Biol Rev.* **2013**, *77*, 73-111. <https://mmbr.asm.org/content/77/1/73>.
- (51) Catherine, G.; Mélanie, T.; Solange, M.; Yves, D.; Denis, F. Quorum quenching: role in nature and applied developments. *FEMS Microbiology Reviews.* 2015, *40* (1):86-116. <https://academic.oup.com/femsre/article/40/1/86/2467695>.
- (52) Cheng, J.; Indrajeet, S.; Debarshi, P.; Lynn, H.; Damien, M.; Tezcan, G.; Laurence, R.; Everett, C. P.; James, P. C.; Derek, S. T.; Designed Small-Molecule Inhibitors of the Anthranilyl-CoA Synthetase PqsA Block Quinolone Biosynthesis in *Pseudomonas aeruginosa*. *ACS Chem. Biol.* 2016, *11* (11): 3061-3067. <https://pubs.acs.org/doi/abs/10.1021/acschembio.6b00575>.
- (53) Stephen, M.; Dana, S. W.; Everett, C. P. Dueling quorum sensing systems in *Pseudomonas aeruginosa* control the production of the *Pseudomonas* quinolone signal (PQS). *FEMS Microbiol. Lett.* **2004**, *230* (1):27-34. <https://academic.oup.com/femsle/article/230/1/27/765008>.

- (54) Dana, S. W.; Worth, C.; Edson R. Ra.; Elizabeth, A. L.; Elana, E.; James P. C.; Everett C. P. Regulation of Pseudomonas Quinolone Signal Synthesis in Pseudomonas aeruginosa. *J. Bacteriol*, **2005**, 187(13):4372-4280. <https://jb.asm.org/content/187/13/4372>.
- (55) Pol, N. J.; Gudrun, K.; Jessica A. T.; Karina, B. X.; Robbert, H. C.; Wim, J. Q.; The Multiple Signaling Systems Regulating Virulence in Pseudomonas aeruginosa. *Microbiol. Mol. Biol. Rev*, **2012**, 76(1):46-65. DOI: 10.1128/MMBR.05007-11
- (56) Larry, A. G.; Susan, L. M.; Marina, S. K.; Everett, C. P.; Colin M. Functions Required for Extracellular Quinolone Signaling by Pseudomonas aeruginosa. *J. Bacteriol*, **2002**, 184(23):6472-6480. <https://jb.asm.org/content/184/23/6472>.
- (57) Shen, Y.; Vanessa, J.; Janine, S.; Ingo, F.; Stefan, W.; Erik, S.; Susanne, H.; Wulf B. Structure Elucidation and Preliminary Assessment of Hydrolase Activity of PqsE, the Pseudomonas Quinolone Signal (PQS) Response Protein. *Biochemistry*, **2009**, 48 (43):10298-307. <https://pubs.acs.org/doi/abs/10.1021/bi900123j>.
- (58) Pesci, E. C.; Pearson, J. P.; Seed, P. C.; Iglewski, B. H. Regulation of las and rhl quorum sensing in Pseudomonas aeruginosa. *J. Bacteriol*, **1997**, 179 (10):3127-32. <https://jb.asm.org/content/179/10/3127>.
- (59) Wagner, V. E.; Gillis, R. J.; Iglewski, B. H. Transcriptome Analysis of Quorum-Sensing Regulation and Virulence Factor Expression in Pseudomonas Aeruginosa. *Vaccine* **2004**, 22, S15–S20. <https://doi.org/10.1016/j.vaccine.2004.08.011>.
- (60) Gaoping, X.; Eric, D.; Jianxin, H.; François, L.; Biliiana, L.; Marie-Hélène, C.; Sylvain, M.; Anastasia, P. T.; Scott, E. S.; Laurence, G. R. MvfR, a key Pseudomonas aeruginosa pathogenicity LTTR-class regulatory protein, has dual ligands. *Mol Microbiol*, **2006**, 62(6):1689-99. <https://onlinelibrary.wiley.com/doi/full/10.1111/j.1365-2958.2006.05462.x>.
- (61) Kitao, T.; Lepine, F.; Babloui, S.; Walte, F.; Steinbacher, S.; Maskos, K.; Blaesse, M.; Negri, M.; Pucci, M.; Zahler, B.; Felici, A.; Rahme, L. G. Molecular Insights into Function and Competitive Inhibition of Pseudomonas Aeruginosa Multiple Virulence Factor Regulator. *mBio* **2018**, 9 (1). <https://doi.org/10.1128/mBio.02158-17>.
- (62) Florian, B.; Manfred, N.; Victor, W.; Michael, M.; Rolf, M.; Susanne, H. Biosynthetic Pathway of Pseudomonas aeruginosa 4-Hydroxy-2-Alkylquinolines. *J. Bacteriol*. **2005**, 187(11):3630–3635. <https://jb.asm.org/content/187/11/3630>.
- (63) Stephan, B.; Christian, P.; Christiane, R.; Birgit, K.; Franz, N.; Susanne, H. The PqsR and RhlR Transcriptional Regulators Determine the Level of Pseudomonas Quinolone Signal Synthesis in Pseudomonas aeruginosa by Producing Two Different pqsABCDE mRNA Isoforms. *J Bacteriol*. **2014**, 196(23):4163-71. doi: 10.1128/JB.02000-14.

- (64) Eric, D.; Suresh, G.; Anastasia, P. T.; François, L.; Katie, E. P.; Maude, S.; Gaoping, X.; Laurence G R.. The contribution of MvfR to *Pseudomonas aeruginosa* pathogenesis and quorum sensing circuitry regulation: multiple quorum sensing-regulated genes are modulated without affecting lasRI, rhlRI or the production of N-acyl- L-homoserine lactones. *Mol Microbiol.* **2005**, 55(4):998-1014. <https://onlinelibrary.wiley.com/doi/full/10.1111/j.1365-2958.2004.04448.x> (accessed Jul 16, 2020).
- (65) Déziel, E.; Lépine, F.; Milot, S.; He, J.; Mindrinos, M. N.; Tompkins, R. G.; Rahme, L. G. Analysis of *Pseudomonas Aeruginosa* 4-Hydroxy-2-Alkylquinolines (HAQs) Reveals a Role for 4-Hydroxy-2-Heptylquinoline in Cell-to-Cell Communication. *PNAS* **2004**, 101 (5), 1339–1344. <https://doi.org/10.1073/pnas.0307694100>.
- (66) Schertzer, J. W.; Brown, S. A.; Whiteley, M. Oxygen Levels Rapidly Modulate *Pseudomonas Aeruginosa* Social Behaviours via Substrate Limitation of PqsH. *Molecular Microbiology* **2010**, 77 (6), 1527–1538. <https://doi.org/10.1111/j.1365-2958.2010.07303.x>.
- (67) Bredenbruch, F.; Geffers, R.; Nimtz, M.; Buer, J.; Häussler, S. The *Pseudomonas Aeruginosa* Quinolone Signal (PQS) Has an Iron-Chelating Activity. *Environmental Microbiology* **2006**, 8 (8), 1318–1329. <https://doi.org/10.1111/j.1462-2920.2006.01025.x>.
- (68) Welch, M.; Hodgkinson, J. T.; Gross, J.; Spring, D. R.; Sams, T. Ligand Binding Kinetics of the Quorum Sensing Regulator PqsR. *Biochemistry* **2013**, 52 (25), 4433–4438. <https://doi.org/10.1021/bi400315s>.
- (69) Masanori, T.; Toshiaki, N.; Hiroo U.; Nobuhiko, N. The Effect of a Cell-to-cell Communication Molecule, *Pseudomonas* Quinolone Signal (PQS), Produced by *P. aeruginosa* on Other Bacterial Species. *Microbes Environ.* **2010**, 25(1):1-7. https://www.jstage.jst.go.jp/article/jsme2/advpub/0/advpub_ME09156/_article/-char/ja.
- (70) Lee, J.; Wu, J.; Deng, Y.; Wang, J.; Wang, C.; Wang, J.; Chang, C.; Dong, Y.; Williams, P.; Zhang, L.-H. A Cell-Cell Communication Signal Integrates Quorum Sensing and Stress Response. *Nat Chem Biol* **2013**, 9 (5), 339–343. <https://doi.org/10.1038/nchembio.1225>.
- (71) Lu, C.; Maurer, C. K.; Kirsch, B.; Steinbach, A.; Hartmann, R. W. Overcoming the Unexpected Functional Inversion of a PqsR Antagonist in *Pseudomonas Aeruginosa*: An in Vivo Potent Antivirulence Agent Targeting Pqs Quorum Sensing. *Angew Chem Int Ed Engl* **2014**, 53 (4), 1109–1112. <https://doi.org/10.1002/anie.201307547>.
- (72) Passador, L.; Tucker, K. D.; Guertin, K. R.; Journet, M. P.; Kende, A. S.; Iglewski, B. H. Functional Analysis of the *Pseudomonas Aeruginosa* Autoinducer PAI. *J Bacteriol* **1996**, 178 (20), 5995–6000.
- (73) Maura, D.; Rahme, L. G. Pharmacological Inhibition of the *Pseudomonas Aeruginosa* MvfR Quorum-Sensing System Interferes with Biofilm Formation

- and Potentiates Antibiotic-Mediated Biofilm Disruption. *Antimicrobial Agents and Chemotherapy* **2017**, *61* (12). <https://doi.org/10.1128/AAC.01362-17>.
- (74) Mayr, L. M.; Fuerst, P. The Future of High-Throughput Screening. *J Biomol Screen* **2008**, *13* (6), 443–448. <https://doi.org/10.1177/1087057108319644>.
- (75) Benet, L. Z.; Hosey, C. M.; Ursu, O.; Oprea, T. I. BDDCS, the Rule of 5 and Drugability. *Adv Drug Deliv Rev* **2016**, *101*, 89–98. <https://doi.org/10.1016/j.addr.2016.05.007>.
- (76) Bajorath, J. Integration of Virtual and High-Throughput Screening. *Nature Reviews Drug Discovery* **2002**, *1* (11), 882–894. <https://doi.org/10.1038/nrd941>.
- (77) Joseph-McCarthy, D.; Campbell, A. J.; Kern, G.; Moustakas, D. Fragment-Based Lead Discovery and Design. *J. Chem. Inf. Model.* **2014**, *54* (3), 693–704. <https://doi.org/10.1021/ci400731w>.
- (78) Erlanson, D. A.; Fesik, S. W.; Hubbard, R. E.; Jahnke, W.; Jhoti, H. Twenty Years on: The Impact of Fragments on Drug Discovery. *Nature Reviews Drug Discovery* **2016**, *15* (9), 605–619. <https://doi.org/10.1038/nrd.2016.109>.
- (79) Kirsch, P.; Hartman, A. M.; Hirsch, A. K. H.; Empting, M. Concepts and Core Principles of Fragment-Based Drug Design. *Molecules* **2019**, *24* (23). <https://doi.org/10.3390/molecules24234309>.
- (80) Lamoree, B.; Hubbard, R. E. Current Perspectives in Fragment-Based Lead Discovery (FBLD). *Essays in Biochemistry* **2017**, *61* (5), 453–464. <https://doi.org/10.1042/EBC20170028>.
- (81) Price, A. J.; Howard, S.; Cons, B. D. Fragment-Based Drug Discovery and Its Application to Challenging Drug Targets. *Essays in Biochemistry* **2017**, *61* (5), 475–484. <https://doi.org/10.1042/EBC20170029>.
- (82) Carr, R. A. E.; Congreve, M.; Murray, C. W.; Rees, D. C. Fragment-Based Lead Discovery: Leads by Design. *Drug Discovery Today* **2005**, *10* (14), 987–992. [https://doi.org/10.1016/S1359-6446\(05\)03511-7](https://doi.org/10.1016/S1359-6446(05)03511-7).
- (83) Rees, D. C.; Congreve, M.; Murray, C. W.; Carr, R. Fragment-Based Lead Discovery. *Nat Rev Drug Discov* **2004**, *3* (8), 660–672. <https://doi.org/10.1038/nrd1467>.
- (84) Keserű, G. M.; Makara, G. M. Hit Discovery and Hit-to-Lead Approaches. *Drug Discovery Today* **2006**, *11* (15), 741–748. <https://doi.org/10.1016/j.drudis.2006.06.016>.
- (85) Erlanson, D. A. Introduction to Fragment-Based Drug Discovery. In *Fragment-Based Drug Discovery and X-Ray Crystallography*; Davies, T. G., Hyvönen, M., Eds.; Topics in Current Chemistry; Springer: Berlin, Heidelberg, 2012; pp 1–32. https://doi.org/10.1007/128_2011_180.
- (86) Murray, C. W.; Rees, D. C. The Rise of Fragment-Based Drug Discovery. *Nature Chem* **2009**, *1* (3), 187–192. <https://doi.org/10.1038/nchem.217>.

- (87) Erlanson, D. A.; de Esch, I. J. P.; Jahnke, W.; Johnson, C. N.; Mortenson, P. N. Fragment-to-Lead Medicinal Chemistry Publications in 2018. *J. Med. Chem.* **2020**, *63* (9), 4430–4444. <https://doi.org/10.1021/acs.jmedchem.9b01581>.
- (88) Yang, H.; Chennamaneni, L. R.; Ho, M. W. T.; Ang, S. H.; Tan, E. S. W.; Jeyaraj, D. A.; Yeap, Y. S.; Liu, B.; Ong, E. H.; Joy, J. K.; Wee, J. L. K.; Kwek, P.; Retna, P.; Dinie, N.; Nguyen, T. T. H.; Tai, S. J.; Manoharan, V.; Pendharkar, V.; Low, C. B.; Chew, Y. S.; Vuddagiri, S.; Sangthongpitag, K.; Choong, M. L.; Lee, M. A.; Kannan, S.; Verma, C. S.; Poulsen, A.; Lim, S.; Chuah, C.; Ong, T. S.; Hill, J.; Matter, A.; Nacro, K. Optimization of Selective Mitogen-Activated Protein Kinase Interacting Kinases 1 and 2 Inhibitors for the Treatment of Blast Crisis Leukemia. *J. Med. Chem.* **2018**, *61* (10), 4348–4369. <https://doi.org/10.1021/acs.jmedchem.7b01714>.
- (89) Reich, S. H.; Sprengeler, P. A.; Chiang, G. G.; Appleman, J. R.; Chen, J.; Clarine, J.; Eam, B.; Ernst, J. T.; Han, Q.; Goel, V. K.; Han, E. Z. R.; Huang, V.; Hung, I. N. J.; Jemison, A.; Jessen, K. A.; Molter, J.; Murphy, D.; Neal, M.; Parker, G. S.; Shaghafi, M.; Sperry, S.; Staunton, J.; Stumpf, C. R.; Thompson, P. A.; Tran, C.; Webber, S. E.; Wegerski, C. J.; Zheng, H.; Webster, K. R. Structure-Based Design of Pyridone–Aminal EFT508 Targeting Dysregulated Translation by Selective Mitogen-Activated Protein Kinase Interacting Kinases 1 and 2 (MNK1/2) Inhibition. *Journal of Medicinal Chemistry* **2018**. <https://doi.org/10.1021/acs.jmedchem.7b01795>.
- (90) Schulz, M. N.; Hubbard, R. E. Recent Progress in Fragment-Based Lead Discovery. *Current Opinion in Pharmacology* **2009**, *9* (5), 615–621. <https://doi.org/10.1016/j.coph.2009.04.009>.
- (91) Hajduk, P. J.; Greer, J. A Decade of Fragment-Based Drug Design: Strategic Advances and Lessons Learned. *Nature Reviews Drug Discovery* **2007**, *6* (3), 211–219. <https://doi.org/10.1038/nrd2220>.
- (92) Chilingaryan, Z.; Yin, Z.; Oakley, A. J. Fragment-Based Screening by Protein Crystallography: Successes and Pitfalls. *Int J Mol Sci* **2012**, *13* (10), 12857–12879. <https://doi.org/10.3390/ijms131012857>.
- (93) Drinkwater, N.; Vu, H.; Lovell, K. M.; Criscione, K. R.; Collins, B. M.; Prisinzano, T. E.; Poulsen, S.-A.; McLeish, M. J.; Grunewald, G. L.; Martin, J. L. Fragment-Based Screening by X-Ray Crystallography, MS and Isothermal Titration Calorimetry to Identify PNMT (Phenylethanolamine N-Methyltransferase) Inhibitors. *Biochem J* **2010**, *431* (1), 51–61. <https://doi.org/10.1042/BJ20100651>.
- (94) Schulz, M. N.; Landström, J.; Bright, K.; Hubbard, R. E. Design of a Fragment Library That Maximally Represents Available Chemical Space. *J Comput Aided Mol Des* **2011**, *25* (7), 611. <https://doi.org/10.1007/s10822-011-9461-x>.
- (95) Congreve, M.; Chessari, G.; Tisi, D.; Woodhead, A. J. Recent Developments in Fragment-Based Drug Discovery. *J. Med. Chem.* **2008**, *51* (13), 3661–3680. <https://doi.org/10.1021/jm8000373>.

- (96) Erlanson, D. A.; McDowell, R. S.; O'Brien, T. Fragment-Based Drug Discovery. *J. Med. Chem.* **2004**, *47* (14), 3463–3482. <https://doi.org/10.1021/jm040031v>.
- (97) Lipinski, C. A. Lead- and Drug-like Compounds: The Rule-of-Five Revolution. *Drug Discovery Today: Technologies* **2004**, *1* (4), 337–341. <https://doi.org/10.1016/j.ddtec.2004.11.007>.
- (98) Giménez, B. G.; Santos, M. S.; Ferrarini, M.; Fernandes, J. P. S.; Fernandes, J. P. S. Evaluation of Blockbuster Drugs under the Rule-of-Five. *Die Pharmazie - An International Journal of Pharmaceutical Sciences* **2010**, *65* (2), 148–152. <https://doi.org/10.1691/ph.2010.9733>.
- (99) Zhang, M.-Q.; Wilkinson, B. Drug Discovery beyond the 'Rule-of-Five.' *Current Opinion in Biotechnology* **2007**, *18* (6), 478–488. <https://doi.org/10.1016/j.copbio.2007.10.005>.
- (100) Meenakshi Singh; Benjamin Tam; Barak Akabayov. NMR-Fragment Based Virtual Screening: A Brief Overview. *Molecules* **2018**, *23* (2), 233. <https://doi.org/10.3390/molecules23020233>.
- (101) Congreve, M.; Carr, R.; Murray, C.; Jhoti, H. A 'Rule of Three' for Fragment-Based Lead Discovery? *Drug Discovery Today* **2003**, *8* (19), 876–877. [https://doi.org/10.1016/S1359-6446\(03\)02831-9](https://doi.org/10.1016/S1359-6446(03)02831-9).
- (102) de Souza Neto, L. R.; Moreira-Filho, J. T.; Neves, B. J.; Maidana, R. L. B. R.; Guimarães, A. C. R.; Furnham, N.; Andrade, C. H.; Silva, F. P. In Silico Strategies to Support Fragment-to-Lead Optimization in Drug Discovery. *Front. Chem.* **2020**, *8*, 93. <https://doi.org/10.3389/fchem.2020.00093>.
- (103) Jhoti, H.; Williams, G.; Rees, D. C.; Murray, C. W. The "rule of Three" for Fragment-Based Drug Discovery: Where Are We Now? *Nat Rev Drug Discov* **2013**, *12* (8), 644–644. <https://doi.org/10.1038/nrd3926-c1>.
- (104) Baker, M. Fragment-Based Lead Discovery Grows Up. *Nature Reviews Drug Discovery* **2013**, *12* (1), 5–7. <https://doi.org/10.1038/nrd3926>.
- (105) Keeley, A.; Petri, L.; Ábrányi-Balogh, P.; Keserű, G. M. Covalent Fragment Libraries in Drug Discovery. *Drug Discovery Today* **2020**. <https://doi.org/10.1016/j.drudis.2020.03.016>.
- (106) Hubbard, R. E.; Murray, J. B. Chapter Twenty - Experiences in Fragment-Based Lead Discovery. In *Methods in Enzymology*; Kuo, L. C., Ed.; Fragment-Based Drug Design; Academic Press, 2011; Vol. 493, pp 509–531. <https://doi.org/10.1016/B978-0-12-381274-2.00020-0>.
- (107) Hanby, A. R.; Troelsen, N. S.; Osberger, T. J.; Kidd, S. L.; Mortensen, K. T.; Spring, D. R. Fsp3-Rich and Diverse Fragments Inspired by Natural Products as a Collection to Enhance Fragment-Based Drug Discovery. *Chem. Commun.* **2020**, *56* (15), 2280–2283. <https://doi.org/10.1039/C9CC09796A>.
- (108) Lam, K. S. New Aspects of Natural Products in Drug Discovery. *Trends in Microbiology* **2007**, *15* (6), 279–289. <https://doi.org/10.1016/j.tim.2007.04.001>.

- (109) Morrison, N. C.; Prosser, K. E.; Stokes, R. W.; Cordes, A.; Metzler-Nolte, N.; M. Cohen, S. Expanding Medicinal Chemistry into 3D Space: Metallofragments as 3D Scaffolds for Fragment-Based Drug Discovery. *Chemical Science* **2020**, *11* (5), 1216–1225. <https://doi.org/10.1039/C9SC05586J>.
- (110) Morley, A. D.; Pugliese, A.; Birchall, K.; Bower, J.; Brennan, P.; Brown, N.; Chapman, T.; Drysdale, M.; Gilbert, I. H.; Hoelder, S.; Jordan, A.; Ley, S. V.; Merritt, A.; Miller, D.; Swarbrick, M. E.; Wyatt, P. G. Fragment-Based Hit Identification: Thinking in 3D. *Drug Discovery Today* **2013**, *18* (23–24), 1221–1227. <https://doi.org/10.1016/j.drudis.2013.07.011>.
- (111) Davis, B. J.; Roughley, S. D. Fragment-Based Lead Discovery. In *Annual Reports in Medicinal Chemistry*; Elsevier, 2017; Vol. 50, pp 371–439. <https://doi.org/10.1016/bs.armc.2017.07.002>.
- (112) Davis, B. J.; Hubbard, R. E. Fragment-Based Ligand Discovery. In *Structural Biology in Drug Discovery*; Renaud, J., Ed.; Wiley, 2020; pp 79–98. <https://doi.org/10.1002/9781118681121.ch4>.
- (113) Scott, D. E.; Coyne, A. G.; Hudson, S. A.; Abell, C. Fragment-Based Approaches in Drug Discovery and Chemical Biology. *Biochemistry* **2012**, *51* (25), 4990–5003. <https://doi.org/10.1021/bi3005126>.
- (114) Murray, C. W.; Blundell, T. L. Structural Biology in Fragment-Based Drug Design. *Current Opinion in Structural Biology* **2010**, *20* (4), 497–507. <https://doi.org/10.1016/j.sbi.2010.04.003>.
- (115) O'Brien, R.; Markova, N.; Holdgate, G. A. Thermodynamics in Drug Discovery. In *Applied Biophysics for Drug Discovery*; John Wiley & Sons, Ltd, 2017; pp 7–28. <https://doi.org/10.1002/9781119099512.ch2>.
- (116) Tellinghuisen, J. Isothermal Titration Calorimetry at Very Low c. *Analytical Biochemistry* **2008**, *373* (2), 395–397. <https://doi.org/10.1016/j.ab.2007.08.039>.
- (117) Ladbury, J. E.; Klebe, G.; Freire, E. Adding Calorimetric Data to Decision Making in Lead Discovery: A Hot Tip. *Nature Reviews Drug Discovery* **2010**, *9* (1), 23–27. <https://doi.org/10.1038/nrd3054>.
- (118) Fattori, D.; Squarcia, A.; Bartoli, S. Fragment-Based Approach to Drug??Lead Discovery: Overview and Advances in Various Techniques. *Drugs in R & D* **2008**, *9* (4), 217–227. <https://doi.org/10.2165/00126839-200809040-00002>.
- (119) Davis, A.; Ward, S. E. *The Handbook of Medicinal Chemistry: Principles and Practice*; Royal Society of Chemistry, 2015.
- (120) Wermuth, C. G. *The Practice of Medicinal Chemistry*; Academic Press, 2011.
- (121) Gao, K.; Oerlemans, R.; Groves, M. R. Theory and Applications of Differential Scanning Fluorimetry in Early-Stage Drug Discovery. *Biophys Rev* **2020**, *12* (1), 85–104. <https://doi.org/10.1007/s12551-020-00619-2>.

- (122) Wakayama, R.; Uchiyama, S.; Hall, D. Ionic Liquids and Protein Folding—Old Tricks for New Solvents. *Biophys Rev* **2019**, *11* (2), 209–225. <https://doi.org/10.1007/s12551-019-00509-2>.
- (123) Lo, M.-C.; Aulabaugh, A.; Jin, G.; Cowling, R.; Bard, J.; Malamas, M.; Ellestad, G. Evaluation of Fluorescence-Based Thermal Shift Assays for Hit Identification in Drug Discovery. *Analytical Biochemistry* **2004**, *332* (1), 153–159. <https://doi.org/10.1016/j.ab.2004.04.031>.
- (124) Joe, C.; Reto, W. Applied Biophysical Methods in Fragment-Based Drug Discovery. *SLAS Discovery*, **2020**, *25*(5) 471–490 <https://journals.sagepub.com/doi/abs/10.1177/2472555220916168>.
- (125) Ciulli, A.; Abell, C. Fragment-Based Approaches to Enzyme Inhibition. *Current Opinion in Biotechnology* **2007**, *18* (6), 489–496. <https://doi.org/10.1016/j.copbio.2007.09.003>.
- (126) Ferenczy, G. G.; Keserű, G. M. Thermodynamic Profiling for Fragment-Based Lead Discovery and Optimization. *Expert Opinion on Drug Discovery* **2020**, *15* (1), 117–129. <https://doi.org/10.1080/17460441.2020.1691166>.
- (127) Makraki, E.; Darby, J. F.; Carneiro, M. G.; Firth, J. D.; Heyam, A.; Ab, E.; O'Brien, P.; Siegal, G.; Hubbard, R. E. Fragment-Derived Modulators of an Industrial β -Glucosidase. *Biochem J* **2020**, *477* (22), 4383–4395. <https://doi.org/10.1042/BCJ20200507>.
- (128) William, P. J. Screening Technologies for Small Molecule Discovery: The State of the Art. *Chem. Biol.* **2014**, *21*(9):1162-1170 <https://doi.org/10.1016/j.chembiol.2014.07.015>
- (129) Renaud, J.-P.; Chung, C.; Danielson, U. H.; Egner, U.; Hennig, M.; Hubbard, R. E.; Nar, H. Biophysics in Drug Discovery: Impact, Challenges and Opportunities. *Nat Rev Drug Discov* **2016**, *15* (10), 679–698. <https://doi.org/10.1038/nrd.2016.123>.
- (130) Ma, R.; Wang, P.; Wu, J.; Ruan, K. Process of Fragment-Based Lead Discovery—A Perspective from NMR. *Molecules* **2016**, *21* (7), 854. <https://doi.org/10.3390/molecules21070854>.
- (131) Silvestre, H. L.; Blundell, T. L.; Abell, C.; Ciulli, A. Integrated Biophysical Approach to Fragment Screening and Validation for Fragment-Based Lead Discovery. *PNAS* **2013**, *110* (32), 12984–12989. <https://doi.org/10.1073/pnas.1304045110>.
- (132) Erlanson, D. A.; Davis, B. J.; Jahnke, W. Fragment-Based Drug Discovery: Advancing Fragments in the Absence of Crystal Structures. *Cell Chemical Biology* **2019**, *26* (1), 9–15. <https://doi.org/10.1016/j.chembiol.2018.10.001>.
- (133) Maveyraud, L.; Mourey, L. Protein X-Ray Crystallography and Drug Discovery. *Molecules* **2020**, *25* (5), 1030. <https://doi.org/10.3390/molecules25051030>.

- (134) Wiene-Schmidt, B.; Oebbeke, M.; Ngo, K.; Heine, A.; Klebe, G. Two Methods, One Goal: Structural Differences between Cocrystallization and Crystal Soaking to Discover Ligand Binding Poses. *ChemMedChem* **2021**, *16* (1), 292–300. <https://doi.org/10.1002/cmdc.202000565>.
- (135) Alexander W. Protein crystallography: alive and well. **2021**, *The FEBS Journal*. <https://febs.onlinelibrary.wiley.com/doi/full/10.1111/febs.15822>.
- (136) Smyth, M. S.; Martin, J. H. J. X Ray Crystallography. *Mol Pathol* **2000**, *53* (1), 8–14.
- (137) Xuhan L.; Adriaan P. I.; Gerard J. P. v. W. Computational Approaches for De Novo Drug Design: Past, Present, and Future. *Artificial Neural Networks*, **2020**, pp 139-165. https://link.springer.com/protocol/10.1007/978-1-0716-0826-5_6.
- (138) Sliwoski, G.; Kothiwale, S.; Meiler, J.; Lowe, E. W. Computational Methods in Drug Discovery. *Pharmacol Rev* **2014**, *66* (1), 334–395. <https://doi.org/10.1124/pr.112.007336>.
- (139) Abbass, J.; Nebel, J.-C. Enhancing Fragment-Based Protein Structure Prediction by Customising Fragment Cardinality According to Local Secondary Structure. *BMC Bioinformatics* **2020**, *21* (1), 170. <https://doi.org/10.1186/s12859-020-3491-0>.
- (140) Bissaro, M.; Sturlese, M.; Moro, S. The Rise of Molecular Simulations in Fragment-Based Drug Design (FBDD): An Overview. *Drug Discovery Today* **2020**. <https://doi.org/10.1016/j.drudis.2020.06.023>.
- (141) Marchand, J.-R.; Caflich, A. In Silico Fragment-Based Drug Design with SEED. *European Journal of Medicinal Chemistry* **2018**, *156*, 907–917. <https://doi.org/10.1016/j.ejmech.2018.07.042>.
- (142) McInnes, C. Virtual Screening Strategies in Drug Discovery. *Current Opinion in Chemical Biology* **2007**, *11* (5), 494–502. <https://doi.org/10.1016/j.cbpa.2007.08.033>.
- (143) A. Srinivas Reddy; S. Priyadarshini Patil; P. Praveen Kumar; H.N. Pradeep; G. Narahari Sastry. Virtual Screening in Drug Discovery - A Computational Perspective. *Current Protein and Peptide Science* **2007**, *8* (4), 329–351. <https://doi.org/10.2174/138920307781369427>.
- (144) Cheng, T.; Li, Q.; Zhou, Z.; Wang, Y.; Bryant, S. H. Structure-Based Virtual Screening for Drug Discovery: A Problem-Centric Review. *AAPS J* **2012**, *14* (1), 133–141. <https://doi.org/10.1208/s12248-012-9322-0>.
- (145) Lionta, E.; Spyrou, G.; K. Vassilatis, D.; Cournia, Z. Structure-Based Virtual Screening for Drug Discovery: Principles, Applications and Recent Advances. *Current Topics in Medicinal Chemistry* **2014**, *14* (16), 1923–1938.
- (146) Hou, T.; Xu, X. Recent Development and Application of Virtual Screening in Drug Discovery: An Overview. *Current Pharmaceutical Design* **2004**, *10* (9), 1011–1033. <https://doi.org/10.2174/1381612043452721>.

- (147) Kitchen, D. B.; Decornez, H.; Furr, J. R.; Bajorath, J. Docking and Scoring in Virtual Screening for Drug Discovery: Methods and Applications. *Nature Reviews Drug Discovery* **2004**, *3* (11), 935–949. <https://doi.org/10.1038/nrd1549>.
- (148) Bancet, A.; Raingeval, C.; Lomberget, T.; Le Borgne, M.; Guichou, J.-F.; Krimm, I. Fragment Linking Strategies for Structure-Based Drug Design. *J. Med. Chem.* **2020**. <https://doi.org/10.1021/acs.jmedchem.0c00242>.
- (149) Tron, A. E.; Belmonte, M. A.; Adam, A.; Aquila, B. M.; Boise, L. H.; Chiarparin, E.; Cidado, J.; Embrey, K. J.; Gangl, E.; Gibbons, F. D.; Gregory, G. P.; Hargreaves, D.; Hendricks, J. A.; Johannes, J. W.; Johnstone, R. W.; Kazmirski, S. L.; Kettle, J. G.; Lamb, M. L.; Matulis, S. M.; Nooka, A. K.; Packer, M. J.; Peng, B.; Rawlins, P. B.; Robbins, D. W.; Schuller, A. G.; Su, N.; Yang, W.; Ye, Q.; Zheng, X.; Secrist, J. P.; Clark, E. A.; Wilson, D. M.; Fawell, S. E.; Hird, A. W. Discovery of Mcl-1-Specific Inhibitor AZD5991 and Preclinical Activity in Multiple Myeloma and Acute Myeloid Leukemia. *Nature Communications* **2018**, *9* (1), 5341. <https://doi.org/10.1038/s41467-018-07551-w>.
- (150) Zhu, P.-J.; Yu, Z.-Z.; You, Q.-D.; Jiang, Z.-Y. Myeloid Cell Leukemin-1 Inhibitors: A Growing Arsenal for Cancer Therapy. *Drug Discovery Today* **2020**. <https://doi.org/10.1016/j.drudis.2020.07.021>.
- (151) Bruncko, M.; Wang, L.; Sheppard, G. S.; Phillips, D. C.; Tahir, S. K.; Xue, J.; Erickson, S.; Fidanze, S.; Fry, E.; Hasvold, L.; Jenkins, G. J.; Jin, S.; Judge, R. A.; Kovar, P. J.; Madar, D.; Nimmer, P.; Park, C.; Petros, A. M.; Rosenberg, S. H.; Smith, M. L.; Song, X.; Sun, C.; Tao, Z.-F.; Wang, X.; Xiao, Y.; Zhang, H.; Tse, C.; Leverson, J. D.; Elmore, S. W.; Souers, A. J. Structure-Guided Design of a Series of MCL-1 Inhibitors with High Affinity and Selectivity. *J. Med. Chem.* **2015**, *58* (5), 2180–2194. <https://doi.org/10.1021/jm501258m>.
- (152) Zender, M.; Witzgall, F.; Kiefer, A.; Kirsch, B.; Maurer, C. K.; Kany, A. M.; Xu, N.; Schmelz, S.; Börger, C.; Blankenfeldt, W.; Empting, M. Flexible Fragment Growing Boosts Potency of Quorum-Sensing Inhibitors against *Pseudomonas Aeruginosa* Virulence. *ChemMedChem* **2020**, *15* (2), 188–194. <https://doi.org/10.1002/cmdc.201900621>.
- (153) Fleitas Martínez, O.; Cardoso, M. H.; Ribeiro, S. M.; Franco, O. L. Recent Advances in Anti-Virulence Therapeutic Strategies With a Focus on Dismantling Bacterial Membrane Microdomains, Toxin Neutralization, Quorum-Sensing Interference and Biofilm Inhibition. *Front Cell Infect Microbiol* **2019**, *9*. <https://doi.org/10.3389/fcimb.2019.00074>.
- (154) Klockgether, J.; Munder, A.; Neugebauer, J.; Davenport, C. F.; Stanke, F.; Larbig, K. D.; Heeb, S.; Schöck, U.; Pohl, T. M.; Wiehlmann, L.; Tümmler, B. Genome Diversity of *Pseudomonas Aeruginosa* PAO1 Laboratory Strains. *Journal of Bacteriology* **2010**, *192* (4), 1113–1121. <https://doi.org/10.1128/JB.01515-09>.
- (155) Harrison, E. M.; Carter, M. E. K.; Luck, S.; Ou, H.-Y.; He, X.; Deng, Z.; O'Callaghan, C.; Kadioglu, A.; Rajakumar, K. Pathogenicity Islands PAPI-1 and PAPI-2 Contribute Individually and Synergistically to the Virulence of

- Pseudomonas Aeruginosa* Strain PA14. *IAI* **2010**, 78 (4), 1437–1446. <https://doi.org/10.1128/IAI.00621-09>.
- (156) Fletcher, M. P.; Diggle, S. P.; Cámara, M.; Williams, P. Biosensor-Based Assays for PQS, HHQ and Related 2-Alkyl-4-Quinolone Quorum Sensing Signal Molecules. *Nat Protoc* **2007**, 2 (5), 1254–1262. <https://doi.org/10.1038/nprot.2007.158>.
- (157) Rahim, M. I.; Szafranski, S. P.; Ingendoh-Tsakmakidis, A.; Stiesch, M.; Mueller, P. P. Evidence for Inoculum Size and Gas Interfaces as Critical Factors in Bacterial Biofilm Formation on Magnesium Implants in an Animal Model. *Colloids and Surfaces B: Biointerfaces* **2020**, 186, 110684. <https://doi.org/10.1016/j.colsurfb.2019.110684>.
- (158) Zaborin, A.; Gerdes, S.; Holbrook, C.; Liu, D. C.; Zaborina, O. Y.; Alverdy, J. C. *Pseudomonas Aeruginosa* Overrides the Virulence Inducing Effect of Opioids When It Senses an Abundance of Phosphate. *PLOS ONE* **2012**, 7 (4), e34883. <https://doi.org/10.1371/journal.pone.0034883>.
- (159) Fletcher, M.; Cámara, M.; Barrett, D. A.; Williams, P. Biosensors for Qualitative and Semiquantitative Analysis of Quorum Sensing Signal Molecules. In *Pseudomonas Methods and Protocols*; Filloux, A., Ramos, J.-L., Eds.; Methods in Molecular Biology; Springer: New York, NY, 2014; pp 245–254. https://doi.org/10.1007/978-1-4939-0473-0_20.
- (160) Kumar, R.; Singh, T.; Singh, H.; Jain, S.; Roy, R. K. Design, Synthesis and Anticonvulsant Activity of Some New 6,8-Halo-Substituted-2h-[1,2,4]Triazino[5,6-b]Indole-3(5h)-One/-Thione and 6,8-Halo-Substituted 5-Methyl-2h-[1,2,4]Triazino[5,6-b]Indol-3(5h)-One/-Thione. *EXCLI J* **2014**, 13, 225–240.
- (161) Gladych, J. M. Z.; Hornby, R.; Hunt, J. H.; Jack, D.; Boyle, J. J.; Ferlauto, R. J.; Haff, R. F.; Kormendy, C. G.; Stanfield, F. J.; Stewart, R. C. Antiviral Agents. 5H-as-Triazino[5,6-b]Indoles. *J. Med. Chem.* **1972**, 15 (3), 277–281. <https://doi.org/10.1021/jm00273a017>.
- (162) Kgokong, J. L.; Smith, P. P.; Matsabisa, G. M. 1,2,4-Triazino-[5,6b]Indole Derivatives: Effects of the Trifluoromethyl Group on in Vitro Antimalarial Activity. *Bioorganic & Medicinal Chemistry* **2005**, 13 (8), 2935–2942. <https://doi.org/10.1016/j.bmc.2005.02.017>.
- (163) Gupta, L.; Sunduru, N.; Verma, A.; Srivastava, S.; Gupta, S.; Goyal, N.; Chauhan, P. M. S. Synthesis and Biological Evaluation of New [1,2,4]Triazino[5,6-b]Indol-3-Ylthio-1,3,5-Triazines and [1,2,4]Triazino[5,6-b]Indol-3-Ylthio-Pyrimidines against *Leishmania Donovanii*. *European Journal of Medicinal Chemistry* **2010**, 45 (6), 2359–2365. <https://doi.org/10.1016/j.ejmech.2010.02.015>.
- (164) Al Osaimi, A. G.; Ali, R. S.; Saad, H. A.; El Sayed Aly, M. R. Synthesis and Antimicrobial Activity of Novel Fused [1,2,4]Triazino[5,6-b]Indole Derivatives. *Russ J Gen Chem* **2017**, 87 (6), 1246–1255. <https://doi.org/10.1134/S1070363217060202>.

- (165) Hassan, S. Y. Synthesis, Antibacterial and Antifungal Activity of Some New Pyrazoline and Pyrazole Derivatives. *Molecules* **2013**, *18* (3), 2683–2711. <https://doi.org/10.3390/molecules18032683>.
- (166) Sharma, R.; Pandey, A. K.; Shivahare, R.; Srivastava, K.; Gupta, S.; Chauhan, P. M. S. Triazino Indole–Quinoline Hybrid: A Novel Approach to Antileishmanial Agents. *Bioorganic & Medicinal Chemistry Letters* **2014**, *24* (1), 298–301. <https://doi.org/10.1016/j.bmcl.2013.11.018>.
- (167) Hlaváč, M.; Kováčiková, L.; Prnová, M. Š.; Šramel, P.; Addová, G.; Májeková, M.; Hanquet, G.; Boháč, A.; Štefek, M. Development of Novel Oxotriazinoindole Inhibitors of Aldose Reductase: Isosteric Sulfur/Oxygen Replacement in the Thioxotriazinoindole Cemtirestat Markedly Improved Inhibition Selectivity. *J. Med. Chem.* **2020**, *63* (1), 369–381. <https://doi.org/10.1021/acs.jmedchem.9b01747>.
- (168) Hamid, H. M. A. Functionalised 1,2,4-Triazino[5,6-b]Indoles. *Journal of Chemical Research* **2004**, *2004* (3), 183–185. <https://doi.org/10.3184/0308234041640735>.
- (169) Sareen, S.; Mathew, G.; Joseph, L. Improvement in Solubility of Poor Water-Soluble Drugs by Solid Dispersion. *Int J Pharm Investig* **2012**, *2* (1), 12–17. <https://doi.org/10.4103/2230-973X.96921>.
- (170) Davis, B. J.; Hubbard, R. E. Fragment-Based Ligand Discovery. In *Structural Biology in Drug Discovery*; John Wiley & Sons, Ltd, 2020; pp 79–98. <https://doi.org/10.1002/9781118681121.ch4>.
- (171) Osborne, J.; Panova, S.; Rapti, M.; Urushima, T.; Jhoti, H. Fragments: Where Are We Now? *Biochemical Society Transactions* **2020**, *48* (1), 271–280. <https://doi.org/10.1042/BST20190694>.
- (172) Zender, M.; Klein, T.; Henn, C.; Kirsch, B.; Maurer, C. K.; Kail, D.; Ritter, C.; Dolezal, O.; Steinbach, A.; Hartmann, R. W. Discovery and Biophysical Characterization of 2-Amino-Oxadiazoles as Novel Antagonists of PqsR, an Important Regulator of *Pseudomonas aeruginosa* Virulence. *J. Med. Chem.* **2013**, *56* (17), 6761–6774. <https://doi.org/10.1021/jm400830r>.
- (173) Klein, T.; Henn, C.; Jong, J. C. de; Zimmer, C.; Kirsch, B.; Maurer, C. K.; Pistorius, D.; Müller, R.; Steinbach, A.; Hartmann, R. W. Identification of Small-Molecule Antagonists of the *Pseudomonas aeruginosa* Transcriptional Regulator PqsR: Biophysically Guided Hit Discovery and Optimization <https://pubs.acs.org/doi/pdf/10.1021/cb300208g> (accessed Jul 12, 2020). <https://doi.org/10.1021/cb300208g>.
- (174) S. Cremosnik, G.; Liu, J.; Waldmann, H. Guided by Evolution: From Biology Oriented Synthesis to Pseudo Natural Products. *Natural Product Reports* **2020**. <https://doi.org/10.1039/D0NP00015A>.
- (175) Moningka, R.; Romero, F. A.; Hastings, N. B.; Guo, Z.; Wang, M.; Di Salvo, J.; Li, Y.; Trusca, D.; Deng, Q.; Tong, V.; Terebetski, J. L.; Ball, R. G.; Ujjainwalla,

- F. Fragment-Based Lead Discovery of a Novel Class of Small Molecule Antagonists of Neuropeptide B/W Receptor Subtype 1 (GPR7). *Bioorganic & Medicinal Chemistry Letters* **2020**, *30* (23), 127510. <https://doi.org/10.1016/j.bmcl.2020.127510>.
- (176) Li, Q. Application of Fragment-Based Drug Discovery to Versatile Targets. *Front Mol Biosci* **2020**, *7*. <https://doi.org/10.3389/fmolb.2020.00180>.
- (177) Hansen, B. B.; Jepsen, T. H.; Larsen, M.; Sindet, R.; Vifian, T.; Burhardt, M. N.; Larsen, J.; Seitzberg, J. G.; Carnerup, M. A.; Jerre, A.; Mølck, C.; Lovato, P.; Rai, S.; Nasipireddy, V. R.; Ritzén, A. Fragment-Based Discovery of Pyrazolopyridones as JAK1 Inhibitors with Excellent Subtype Selectivity. *J. Med. Chem.* **2020**, *63* (13), 7008–7032. <https://doi.org/10.1021/acs.jmedchem.0c00359>.
- (178) Canning, P.; Birchall, K.; Kettleborough, C. A.; Merritt, A.; Coombs, P. J. Fragment-Based Target Screening as an Empirical Approach to Prioritising Targets: A Case Study on Antibacterials. *Drug Discovery Today* **2020**. <https://doi.org/10.1016/j.drudis.2020.09.003>.
- (179) Wei, W.; Cherukupalli, S.; Jing, L.; Liu, X.; Zhan, P. Fsp3: A New Parameter for Drug-Likeness. *Drug Discovery Today* **2020**, *25* (10), 1839–1845. <https://doi.org/10.1016/j.drudis.2020.07.017>.
- (180) Dutta, A. K.; Rösgen, J.; Rajarathnam, K. Using Isothermal Titration Calorimetry to Determine Thermodynamic Parameters of Protein–Glycosaminoglycan Interactions. *Methods Mol Biol* **2015**, *1229*, 315–324. https://doi.org/10.1007/978-1-4939-1714-3_25.
- (181) Su, H.; Xu, Y. Application of ITC-Based Characterization of Thermodynamic and Kinetic Association of Ligands With Proteins in Drug Design. *Front. Pharmacol.* **2018**, *9*. <https://doi.org/10.3389/fphar.2018.01133>.
- (182) Chodera, J. D.; Mobley, D. L. Entropy-Enthalpy Compensation: Role and Ramifications in Biomolecular Ligand Recognition and Design. *Annu Rev Biophys* **2013**, *42*, 121–142. <https://doi.org/10.1146/annurev-biophys-083012-130318>.
- (183) Davis, B. J.; Hubbard, R. E. Fragment-Based Ligand Discovery. In *Structural Biology in Drug Discovery*; John Wiley & Sons, Ltd, 2020; pp 79–98. <https://doi.org/10.1002/9781118681121.ch4>.
- (184) Hodgkinson, J.; Bowden, S. D.; Galloway, W. R. J. D.; Spring, D. R.; Welch, M. Structure-Activity Analysis of the Pseudomonas Quinolone Signal Molecule. *J Bacteriol* **2010**, *192* (14), 3833–3837. <https://doi.org/10.1128/JB.00081-10>.
- (185) Diggle, S. P.; Matthijs, S.; Wright, V. J.; Fletcher, M. P.; Chhabra, S. R.; Lamont, I. L.; Kong, X.; Hider, R. C.; Cornelis, P.; Cámara, M.; Williams, P. The Pseudomonas Aeruginosa 4-Quinolone Signal Molecules HHQ and PQS Play Multifunctional Roles in Quorum Sensing and Iron Entrapment. *Chemistry & Biology* **2007**, *14* (1), 87–96. <https://doi.org/10.1016/j.chembiol.2006.11.014>.

- (186) Fletcher, M. P.; Diggle, S. P.; Crusz, S. A.; Chhabra, S. R.; Cámara, M.; Williams, P. A Dual Biosensor for 2-Alkyl-4-Quinolone Quorum-Sensing Signal Molecules. *Environ Microbiol* **2007**, *9* (11), 2683–2693. <https://doi.org/10.1111/j.1462-2920.2007.01380.x>.
- (187) Tamaian, R.; Moț, A.; Silaghi-Dumitrescu, R.; Ionuț, I.; Stana, A.; Oniga, O.; Nastasă, C.; Benedec, D.; Tipericiuc, B. Study of the Relationships between the Structure, Lipophilicity and Biological Activity of Some Thiazolyl-Carbonyl-Thiosemicarbazides and Thiazolyl-Azoles. *Molecules* **2015**, *20* (12), 22188–22201. <https://doi.org/10.3390/molecules201219841>.
- (188) Pajouhesh, H.; Lenz, G. R. Medicinal Chemical Properties of Successful Central Nervous System Drugs. *NeuroRx* **2005**, *2* (4), 541–553.
- (189) Constantinescu, T.; Lungu, C. N.; Lung, I. Lipophilicity as a Central Component of Drug-Like Properties of Chalcones and Flavonoid Derivatives. *Molecules* **2019**, *24* (8). <https://doi.org/10.3390/molecules24081505>.
- (190) Ramos, A. F.; Woods, D. F.; Shanahan, R.; Cano, R.; McGlacken, G. P.; Serra, C.; O’Gara, F.; Reen, F. J. A Structure-Function Analysis of Interspecies Antagonism by the 2-Heptyl-4-Alkyl-Quinolone Signal Molecule from *Pseudomonas Aeruginosa*. *Microbiology*, **2020**, *166* (2), 169–179. <https://doi.org/10.1099/mic.0.000876>.
- (191) Nam, S.; Ham, S.-Y.; Kwon, H.; Kim, H.-S.; Moon, S.; Lee, J.-H.; Lim, T.; Son, S.-H.; Park, H.-D.; Byun, Y. Discovery and Characterization of Pure RhIR Antagonists against *Pseudomonas Aeruginosa* Infections. *J. Med. Chem.* **2020**, *63* (15), 8388–8407. <https://doi.org/10.1021/acs.jmedchem.0c00630>.
- (192) Motbainor, H.; Bereded, F.; Mulu, W. Multi-Drug Resistance of Blood Stream, Urinary Tract and Surgical Site Nosocomial Infections of *Acinetobacter Baumannii* and *Pseudomonas Aeruginosa* among Patients Hospitalized at Felegehiwot Referral Hospital, Northwest Ethiopia: A Cross-Sectional Study. *BMC Infect Dis* **2020**, *20* (1), 92. <https://doi.org/10.1186/s12879-020-4811-8>.
- (193) Starkey, M.; Lepine, F.; Maura, D.; Bandyopadhaya, A.; Lesic, B.; He, J.; Kitao, T.; Righi, V.; Milot, S.; Tzika, A.; Rahme, L. Identification of Anti-Virulence Compounds That Disrupt Quorum-Sensing Regulated Acute and Persistent Pathogenicity. *PLOS Pathogens* **2014**, *10* (8), e1004321. <https://doi.org/10.1371/journal.ppat.1004321>.
- (194) Fundamentals of Medicinal Chemistry | Wiley <https://www.wiley.com/en-us/Fundamentals+of+Medicinal+Chemistry-p-9780470871690> (accessed Jan 19, 2021).
- (195) O’Boyle, N. M.; Boström, J.; Sayle, R. A.; Gill, A. Using Matched Molecular Series as a Predictive Tool To Optimize Biological Activity. *J. Med. Chem.* **2014**, *57* (6), 2704–2713. <https://doi.org/10.1021/jm500022q>.
- (196) Jorge, S. D.; Palace-Berl, F.; Masunari, A.; Cechinel, C. A.; Ishii, M.; Pasqualoto, K. F. M.; Tavares, L. C. Novel Benzofuroxan Derivatives against Multidrug-

- Resistant *Staphylococcus Aureus* Strains: Design Using Topliss' Decision Tree, Synthesis and Biological Assay. *Bioorganic & Medicinal Chemistry* **2011**, *19* (16), 5031–5038. <https://doi.org/10.1016/j.bmc.2011.06.034>.
- (197) Wilder, C. N.; Diggle, S. P.; Schuster, M. Cooperation and Cheating in *Pseudomonas Aeruginosa*: The Roles of the Las, Rhl and Pqs Quorum-Sensing Systems. *ISME J* **2011**, *5* (8), 1332–1343. <https://doi.org/10.1038/ismej.2011.13>.
- (198) Rampioni, G.; Falcone, M.; Heeb, S.; Frangipani, E.; Fletcher, M. P.; Dubern, J.-F.; Visca, P.; Leoni, L.; Cámara, M.; Williams, P. Unravelling the Genome-Wide Contributions of Specific 2-Alkyl-4-Quinolones and PqsE to Quorum Sensing in *Pseudomonas Aeruginosa*. *PLoS Pathog* **2016**, *12* (11). <https://doi.org/10.1371/journal.ppat.1006029>.
- (199) Gallagher, L. A.; McKnight, S. L.; Kuznetsova, M. S.; Pesci, E. C.; Manoil, C. Functions Required for Extracellular Quinolone Signaling by *Pseudomonas Aeruginosa*. *Journal of Bacteriology* **2002**, *184* (23), 6472–6480. <https://doi.org/10.1128/JB.184.23.6472-6480.2002>.
- (200) Thomann, A.; de Mello Martins, A. G. G.; Brengel, C.; Empting, M.; Hartmann, R. W. Application of Dual Inhibition Concept within Looped Autoregulatory Systems toward Antivirulence Agents against *Pseudomonas Aeruginosa* Infections. *ACS Chem. Biol.* **2016**, *11* (5), 1279–1286. <https://doi.org/10.1021/acschembio.6b00117>.
- (201) Inhibition of the pqsABCDE and pqsH in the pqs quorum sensing system and related virulence factors of the *Pseudomonas aeruginosa* PAO1 strain by farnesol | Elsevier Enhanced Reader <https://reader.elsevier.com/reader/sd/pii/S0964830520301876?token=EE7929ED33D254832F810EA107D8B5B8379AAE20E319A818DEC905C80FA7C219B8DB6E91F30C36F266B4A91936598A74> (accessed Jan 21, 2021). <https://doi.org/10.1016/j.ibiod.2020.104956>.
- (202) Shaker, B.; Ahmad, S.; Thai, T. D.; Eyun, S.; Na, D. Rational Drug Design for *Pseudomonas Aeruginosa* PqsA Enzyme: An in Silico Guided Study to Block Biofilm Formation. *Front Mol Biosci* **2020**, *7*. <https://doi.org/10.3389/fmolb.2020.577316>.
- (203) Alcalde-Rico, M.; Olivares-Pacheco, J.; Alvarez-Ortega, C.; Cámara, M.; Martínez, J. L. Role of the Multidrug Resistance Efflux Pump MexCD-OprJ in the *Pseudomonas Aeruginosa* Quorum Sensing Response. *Front. Microbiol.* **2018**, *9*, 2752. <https://doi.org/10.3389/fmicb.2018.02752>.